

ISSN number 0971 - 9709



The Journal of Indian Geophysical Union

VOLUME 22, ISSUE 3 | MAY 2018

AN OPEN ACCESS BIMONTHLY JOURNAL OF IGU



Journal of Indian Geophysical Union Editorial Board	Indian Geophysical Union Executive Council
Chief Editor P.R. Reddy (Geosciences), Hyderabad	President Prof. Shailesh Nayak, Distinguished Scientist, MoES, New Delhi
Associate Editors B.V.S. Murthy (Exploration Geophysics), Hyderabad D. Srinagesh (Seismology), Hyderabad Nandini Nagarajan (Geomagnetism & MT), Hyderabad M.R.K. Prabhakara Rao (Ground Water Geophysics), Hyderabad	Vice-Presidents Dr. Satheesh C. Sheno, Director, INCOIS, Hyderabad Prof. Talat Ahmad, VC, JMI, New Delhi Dr. V.M. Tiwari, Director, CSIR-NGRI, Hyderabad Dr. Sunil K. Singh, Director, CSIR-NIO, Goa
Editorial Team Solid Earth Geosciences: Vineet Gahlaut (Seismology), New Delhi B. Venkateswara Rao (Water resources Management), Hyderabad N.V. Chalapathi Rao (Geology, Geochemistry & Geochronology), Varanasi V.V. Sessa Sai (Geology & Geochemistry), Hyderabad Marine Geosciences: K.S.R. Murthy (Marine Geophysics), Visakhapatnam M.V. Ramana (Marine Geophysics), Goa Rajiv Nigam (Marine Geology), Goa Atmospheric and Space Sciences: Ajit Tyagi (Atmospheric Technology), New Delhi Umesh Kulshrestha (Atmospheric Sciences), New Delhi P. Sanjeeva Rao (Agrometeorology & Climatoplogy), New Delhi U.S. De (Meteorology), Pune Archana Bhattacharya (Space Sciences), Mumbai Editorial Advisory Committee: Walter D Mooney (Seismology & Natural Hazards), USA Manik Talwani (Marine Geosciences), USA T.M. Mahadevan (Deep Continental Studies & Mineral Exploration), Ernakulum D.N. Avasthi (Petroleum Geophysics), New Delhi Larry D Brown (Atmospheric Sciences & Seismology), USA Alfred Kroener (Geochronology & Geology), Germany Irina Artemieva (Lithospheric Structure), Denmark R.N. Singh (Theoretical & Environmental Geophysics), Ahmedabad Rufus D Catchings (Near Surface Geophysics), USA Surjalal Sharma (Atmospheric Sciences), USA H. J. Kumpel (Geosciences, App. Geophysics, Theory of Poroelasticity), Germany Saulwood Lin (Oceanography), Taiwan Jong-Hwa Chun (Petroleum Geosciences), South Korea Xiujuan Wang (Marine Geology & Environment), China Jiro Nagao (Marine Energy and Environment), Japan Information & Communication: B.M. Khanna (Library Sciences), Hyderabad	Hon. Secretary Dr. Kalachand Sain, CSIR-NGRI, Hyderabad Joint Secretary Dr. O.P. Mishra, MoES, New Delhi Org. Secretary Dr. ASSSRS Prasad, CSIR-NGRI, Hyderabad Treasurer Md. Rafique Attar, CSIR-NGRI, Hyderabad Members Prof. Rima Chatterjee, ISM, Dhanbad Prof. P. Rama Rao, Andhra Univ., Visakhapatnam Prof. S.S. Teotia, Kurukshetra Univ., Kurukshetra Mr. V. Rama Murty, GSI, Hyderabad Prof. B. Madhusudan Rao, Osmania Univ., Hyderabad Prof. R.K. Mall, BHU, Varanasi Dr. A.K. Chaturvedi, AMD, Hyderabad Mr. Sanjay Jha, Omni Info, NOIDA Mr. P.H. Mane, ONGC, Mumbai Dr. Rahul Dasgupta, OIL, NOIDA Dr. M. Ravi Kumar, ISR, Gujarat Prof. Surjalal Sharma, Univ. of Maryland, USA Dr. P. Sanjeeva Rao, Advisor, SERB, DST, New Delhi Dr. N. Satyavani, CSIR-NGRI, Hyderabad Prof. Devesh Walia, North Eastern Hills Univ., Shillong
EDITORIAL OFFICE Indian Geophysical Union, NGRI Campus, Uppal Road, Hyderabad- 500 007 Telephone: +91 -40-27012799; 27012734; Telefax: +91-04-27171564 E. mail: jigu1963@gmail.com, website: www.j-igu.in	
The Open Access Journal with six issues in a year publishes articles covering Solid Earth Geosciences; Marine Geosciences; and Atmospheric, Space and Planetary Sciences.	
Annual Subscription Individual ₹ 1000 per issue and Institutional ₹ 5000 for six issues Payments should be sent by DD drawn in favour of "The Treasurer, Indian Geophysical Union", payable at Hyderabad, Money Transfer/NEFT/RTGS (Inter-Bank Transfer), Treasurer, Indian Geophysical Union, State Bank of India, Habsiguda Branch, Habsiguda, Uppal Road, Hyderabad- 500 007 A/C: 52191021424, IFSC Code: SBIN0020087, MICR Code: 500002318, SWIFT Code: SBININBBHO9. For correspondence, please contact, Hon. Secretary, Indian Geophysical Union, NGRI Campus, Uppal Road, Hyderabad - 500 007, India; Email: igu123@gmail.com; Ph: 040 27012799, 272012734	

CONTENTS

Editorial

S No.	Title	Authors	Pg. No:
1	Efficacy of Integrated Geophysical Techniques in Delineating Groundwater Potential Zones in the Deccan Basalt Region of Maharashtra	Ram Raj Mathur and Kadari Srinivas Rao	257
2	Site characterisation using Multi-channel Analysis of Surface Waves at various locations in Kumaon Himalayas, India	Anand Joshi and Parul Bhardwaj	265
3	Application of Crosshole Seismic technique and MASW at Heavy Engineering Site, near Mahabalipuram, Tamilnadu.	K. Satish Kumar, P. Pavan Kishore, G.S. Srinivas, P. Prabhakara Prasad and T. Sheshunarayana.	279
4	Application of Shallow Seismic Studies for Civil Engineering Applications: A case study from Chennai city, Tamilnadu.	G.S. Srinivas, P.Shiva Shankar, K. Satish Kumar, S. Trupti, P. Pavan Kishore, K.N.S.S.Srinivas and T. Seshunarayana	286
5	Evaluation of Percolation Tank Efficiency on Groundwater Recharge: A Case Study for Karnampettai Percolation Pond, India.	L.Surinaidu, A. Raviraj and R. Rangarajan	292
6	Hydrochemical Signatures for Identification of Fresh and Saline Water Resources, along Visakhapatnam-Bhimunipatnam Corridor.	P. Padmavathi Devi	306
7	Estimation of Total and Unit Stream power along Bhagirathi River, Uttarakhand, India.	Satya Prakash and Rajesh Kumar	316
8	Petrology, mineral chemistry and geochemistry of the chromian muscovite bearing quartzite in the Neoproterozoic Veligallu schist belt, eastern Dharwar craton, India.	Tarun C. Khanna and V.V. Sesha Sai	325
9	Long range forecast and development of a weak southwest monsoon during 2017- Pt. II: Development.	Onkari Prasad, O. P.Singh and K. Prasad	333
10	Severe cyclonic storm JAL, air-sea interaction perspectives and floods along Andhra Pradesh-Tamilnadu coast.	G.R. Chinthalu, T. Dharmaraj, M.N. Patil, A.R. Dhakate, S.D. Pawar and Siingh.D	341
11	Meteorological conditions for development of heat wave over Coastal Andhra Pradesh and Telangana.	Charan Singh and S.V.J. Kumar	349
12	FORTTRAN code to convert resistivity Vertical Electrical Sounding data to RES2DINV format	R. Rajesh and R.K.Tiwari	359
	Endeavours in seismic monitoring of oceans through drifting network with development of a New Generation Mobile Earthquake Recorder in Marine Areas by Independent Divers---The Son-o-Mermaid--- Technical Note	Raja Acharya	363

Editorial

I took leave from all through March editorial. I never expected that I would be writing May issue's editorial, as official term of my editorship continues only till 31st March (this editorial has been written in February). Since final edited versions of papers need to be published on time to make the contributors happy and as the incoming editor officially takes charge only from 1st April, to avoid delay in releasing the May issue I have completed basic structuring of the issue before end of February and continued pre publication procedures. After sending the galley proofs of all the articles for correction by respective authors I proceeded to US on 15th March to spend 3 months with my son, daughter and couple of my friends. The responsibility of sending the corrected galley proofs to publisher, after correcting any errors was entrusted to Dr. A.S.S.R.S. Prasad, Org. Secretary of IAGU, who is well versed with such procedures. Due to the concerted efforts of many well wishers of IAGU the May issue was released on time. The next issue in July will be processed and published by the new editor Dr. O.P. Pandey. I wish him success in enhancing the quality of the journal.

For this issue I selected a topic that is relevant to motivate talented female earth scientists.

Gender bias in Earth science research

In one of the most detailed breakdowns yet of gender bias in scholarly publishing, the American Geophysical Union (AGU) in Washington DC has found that its female members submit fewer papers, and are asked to be peer reviewers less frequently, than men. The effect holds across all age ranges, from scientists in their twenties to those in their seventies (*P.S: I have noticed similar effect even in India. Random statistical evaluation of IAGU publications shows prevalence of similar trend*).

The AGU began the study at the request of Marcia McNutt, the former editor-in-chief of *Science* who is now president of the US National Academy of Sciences

in Washington DC. Lerback and Hanson of AGU examined information from 97,431 people, cross-referencing their e-mail addresses with the editorial databases of the 19 AGU journals that existed at the time. About 29% of the society's members are women. Between 2012 and 2015, women who published in AGU journals as first authors had submitted about 1.8 papers each, compared with 2.1 papers for men in the corresponding situation. And women served as peer-reviewers just 18% of the time. The gender differences persisted across age groups, with the greatest discrepancy for the youngest scientists, in their twenties. When asked for the names of possible peer reviewers, female first authors suggested female reviewers 20% of the time, whereas male first authors suggested women 15% of the time. Women also declined invitations to serve as peer reviewers at higher rates than men, completing an average of 3.65 reviews each, compared with 4.34 for men. Scientists who miss out on the chance to participate in peer review are also missing opportunities to develop their reputation and professional skills, says Hanson. "Reviewing is a way to impress people," he notes. Dan Lovegrove, a geology publisher for Amsterdam-based publishing group Elsevier, stated that although 30% of contributions to Elsevier's Earth and planetary science journals come from women, only 13% of its journal editors are female. He says that the company has launched a pilot project to encourage gender equality in recruitment for its editorial boards. (**Source:***Nature* doi:10.1038/nature.2016.20708).

I have selected the topic cited above for this issue's editorial after reading an excellent article by Dr. Kusala Rajendran, a renowned Seismologist working as Professor at IISc, Bengaluru. She has mentioned in an essay recalling the events, influences, and challenges that have shaped her professional life that the India of her childhood did not encourage girls to reach their full potential. She recalls how Indian society of her childhood (and perhaps even now) has remained profoundly patriarchal. With a strong resolve to do well in academics she joined

Roorkee University to pursue her post graduate studies in Geophysics. She recalls that out of nine students admitted that year, she was the only woman in the batch of 1976. There had been no women in the two senior years either. She recalls that she often found herself feeling lonely and isolated as a result, especially during field trips. After completing her education she joined as a junior scientist at CESS (Trivandrum) and got married to C.P. Rajendran. Subsequently she went on a study leave to the US, where she did her PhD under the supervision of Prof. Pradirep Talwani, at the University of South Carolina. After she returned to India 1993, she along with her husband, carried out significant studies in Latur, Kutch, and the Himalaya. Their papers have received considerable attention and are well cited and as a geologist-seismologist duo, they have achieved a degree of recognition. Despite the recognition, she recalls how she often found herself feeling professionally isolated, which motivated her decision to move to IISC where she helped to establish the centre for Earth sciences.

Some points in her recollections are thought provoking and deserves attention and discussion. For example, she notes that limited female representation at top positions in Indian science establishments could well be a factor that inhibits rightful representation and recognition for deserving female candidates. Although she finds the national science academies in India relatively better in this regard, she remains unconvinced that individuals are being judged solely on intellectual merit. She also makes an interesting observation on the conflicts that women of her generation, who are inextricably bound to the cultural and social values face in their professional life. Thus, one has to remain subservient in the family sphere, where as higher-level administrative or leadership positions demand leadership. Many other women in command-driven and male-dominated professions seem to share this view point. A unique challenge she has faced as an earthquake scientist is participating in field work at remote locations, which in her case was made possible through the collaborative research with her husband. Her recollections touch on the experiences of a few female scientists whose

professional ambitions could not be fully achieved due to such constraints. (Source: An Indian Geophysicist Reflects–Kusala Rajendran). *Our grateful thanks are due to Dr. Hortense Marcelin, Managing Editor, Inference: International Review of Science (Quarterly Email Newsletter) Paris, France, for permitting us to publish the bio-sketch of Kusala Rajendran in JIGU.* (For more details visit www.inference-review.com).

Prof. Kusala Rajendran tells the story of her journey as a Geophysicist that started in the mid-70s. Sure, it was an uncommon choice of study for a girl at that time. Societies and establishments have changed since then. There seems to be some improvement in the recent times as evidenced by equal number of girls compared to boys at the Post graduate level in the Geophysics department of Andhra University, Visakhapatnam and good number of research fellows in the research institutes like CSIR-NGRI. Let us hope for a much improved status for young women researchers. But whether there are equal opportunities for both genders, whether the women can fearlessly move about and do field work in remote areas and whether their families would treat it as normal for a woman professional to be travelling to distant areas are issues that would remain as deterrents at least in the path of some female researchers. For significant improvement in the quality of our research pursuits, it is extremely essential for us to eradicate the gender bias and encourage women scientists to be self sufficient in every respect. Rajendran's story asserts every woman that they are no less in their talents and that they too can do it. Such an assertion is supported by significant works carried out by many female scientists. As I was concluding this subsection of my editorial I came across a write up (Physics Today, 1 January, 2018, PP 46-52) on 1834 mathematician Mary Somerville. She published "On the Connexion of the Physical Sciences", a work that was instrumental in the making of modern physics as a discipline. Apart from receiving rare appreciation from her male contemporaries "Connexion" also posed key questionsCould women excel at science? Were the scientific writings of a woman inherently different from those of a man? Cambridge

philosopher William Whewell in his review of "Connexion" believed that in the rare circumstance when a woman wrote from deep knowledge, she could do so not with a concern for grubby industrial utility but with lucid metaphysical clarity. Female authorship offered the possibility of direct insight into the laws of nature. Somerville wrote because she believed in the importance of what she had to say and in her significance as a symbol of self education, liberalism, and woman's rights. She realized that the most powerful way of communicating her message was through the story of her own life. Dr. Kusala Rajendran probably believed similarly and brought out her Bio-Sketch. It is clear from the details given above that gender bias existed since time immemorial,

but, a female scientist of either 19th century or 21st century could excel if there is a profound resolve to excel against many odds. I do hope that our young female earth scientists will follow in the footsteps of Dr. Kusala Rajendran and break all the barriers that inhibit their growth as excellent scientists.

In this Issue:

In this issue there are 12 research articles and one Technical note, apart from the editorial.

I profoundly thank the Editorial team and IGU management for achieving a significant level of quality to JIGU.

P.R.Reddy

Efficacy of Integrated Geophysical Techniques in Delineating Groundwater Potential Zones in the Deccan Basalt Region of Maharashtra

Ram Raj Mathur^{*1} and Kadari Srinivas Rao²

¹Centre of Exploration Geophysics, Osmania University, Hyderabad, India

²Groundwater Surveys and Development Agency, Maharashtra, India

*Corresponding Author: ramrajmathur@gmail.com

ABSTRACT

We developed a methodology to study the depth and aerial extent of aquifers in the Dhotra-Jahangir area of Washim District, Maharashtra to yield better results with more reliability. The area was selected as a model to solve existing groundwater problems due to the droughts of 2013 and 2016 in Maharashtra.

The 2-D interpretation of the data helped to delineate the groundwater horizons, their thickness and orientation for identifying dug-cum-borehole sites. The higher values of real and imaginary component in the VLF-EM profile indicate a low resistive zone which can be attributed to weathered or fractured basalt. The Dug well at the suggested site revealed the static water level at 3.8 m during April 2013. Thus, the integration of resistivity and VLF-EM methods proved to be effective in locating the sources of groundwater with a yield of about 9500 lph which successfully addressed the problem for drinking and cultivation purposes during the entire year.

Key words: Deccan Basalts, Dhotra Maharashtra, Gradient Resistivity Profiling, VLF-EM method, Vertical Electrical Sounding..

INTRODUCTION

The Deccan Lavas are mostly alkali basalts with many irregular flows dipping in different directions (Agashe and Gupte, 1971). They also represent variable morphology, structure and texture depicting thick extensive flows of compact basalt, flows of amygdaloidal basalts and thin irregular flows of vesicular basalts (Karmakar, 1978; Adyalkar and Mani, 1971). The lateral extent of individual flows is of the order of 20 to 160 km (Bean et al., 1986; Choubey, 1973). The Deccan Trap region which comprises of the continental flood basalt with a variety of compositions and many trace elements (Mahoney, 1988) offers a challenge to Earth Scientists to understand the occurrence of groundwater.

The occurrence of groundwater in this region though is not scanty; the source finding becomes challenging as the source is unevenly distributed and controlled by faults, fractures, joints etc., and the weathered layer (Singhal, 1997; Deolankar, 1980; Dhokariker, 1991; Ghosh et al., 2006; Limaye, 2010). Hence, the areas with extensive agriculture activity faced acute scarcity due to the unscientific source finding.

In Maharashtra, the Groundwater Surveys and Development Agency (GSDA, 1974; 2001; 2008; 2010) under the Water Supply and Sanitation Department is the primary agency involved in solving the drinking water and irrigation problems in rural and urban areas. The initial study in such areas includes study of aerial photos, geo-hydrological data and existing bore well data.

Integrated geophysical studies have proved to be effective in delineating the prospective aquifer zones in the Deccan Basalt region (Deshpande and Sen Gupta, 1956; Bose and Ramakrishna, 1978; Nishat Ahmad, 2001; Shettigara and Adams, 1989; Kulkarni et al., 2004).

A rectangular area of length 600 m and width 180 m in Gat No. 29 (Figure 1) was chosen to conduct the geophysical surveys for the present study in the basaltic rock terrain within the Tapi Basin. Hydro-geological study of the area revealed that majority of the region is dry and not suitable for groundwater extraction. The only sources of groundwater in this area are one dug well (6 m deep) and one bore well (120 m deep) which were reported to be dry during all seasons affecting drinking and irrigation requirements.

To address the above issue, detailed geo-hydrological and geophysical surveys comprising Resistivity and VLF-EM surveys were conducted in the study area to suggest new sources for drilling based on the interpreted results. The present study clearly demonstrates the efficacy of integration of different methods in delineating pockets of groundwater potential in the basaltic terrain which could be adopted in similar virgin areas to address the scarcity of water for drinking and irrigation purposes.

STUDY AREA

The Study area, Gat No. 29 (Figure 1) is located due northwest at about 2.5 km distance of Dhotra-Jahangir village settlement (Govtan), Taluka Karanja, District

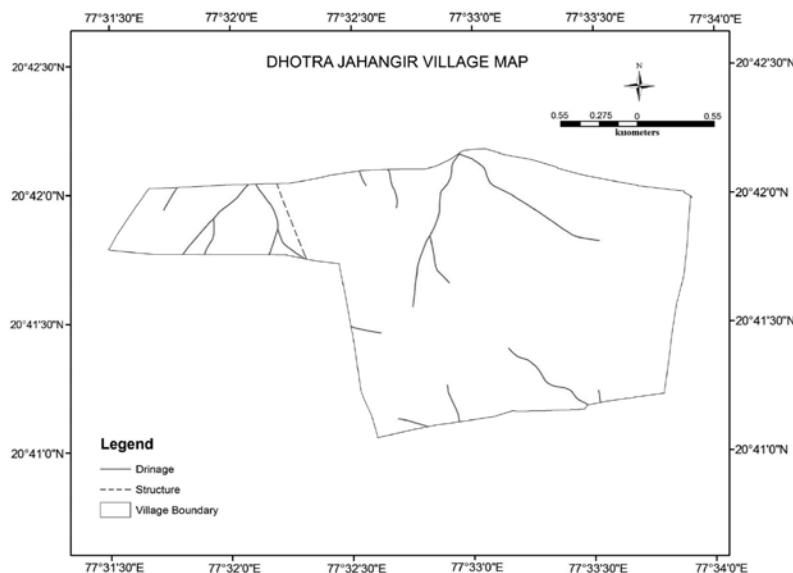


Figure 1. Location, Lineament and Drainage Pattern map of Gat No.29 Dhotra-Jahangir Village, Maharashtra

Washim, Maharashtra, India. The area falls in the SE quadrant of Survey of India Toposheet No 55 H (1:250,000 scale) and the elevation is 336 m above mean sea level (MSL).

The study area falling under the Tapi Basin and designated as Watershed PTU-2 is covered by a normal to undulating topography with a gentle slope towards the southern part of the area. The streams flow from northeast to southwest direction. The drainage pattern is dendritic to sub-dendritic and all streams are seasonal (Figure 1). The area receives a rainfall of about 702 mm. during the southwest monsoon.

Geological and geo-hydrological study

The geo-hydrological surveys comprise of the observations of the well sections of 6 dug wells and 8 bore wells in the area. The Deccan Traps formed due to fissure type volcanic eruption activity during upper cretaceous to lower Eocene periods encompass the entire area under investigation. The delineated aquifers are mostly situated in weathered, vesicular, or fractured basalt underlain by compact basalt. The dug wells with depths ranging from about 6 to 7 m go dry during the summer months starting from March while the bore wells with depths between 60 and 150 m show a reduced yield. Three different layers viz., top soil cover between 1 to 1.5m depth, a middle layer from 1.5 to 5.5 m followed by compact massive basalt were observed from the dug well sections.

Geophysical study

Geo-electrical profiling and sounding were earlier carried out to decipher both lateral and depth variations of

resistivity covered by different geological formations (Telford et al., 1976; Yadav and Singh, 2007). The Very Low Frequency (VLF) electromagnetic method (Paterson and Ronka, 1971) has been proved to be a fast and easy tool for locating fractures in hard rock terrain for groundwater exploration (McNeill, J.D., 1991; Sharma, and Baranwal, 2005; Sundararajan et al., 2007).

VLF-EM and Electrical resistivity data were acquired along 9 traverses (Figure 2). The VLF-EM survey was conducted using ABEM-VLF Wadi equipment and the resistivity profiling was conducted with a McOHM Resistivity meter. The real and imaginary components were obtained using the VLF Wadi equipment along the profiles. The McOHM resistivity meter is a digital stacking instrument with the transmitter and receiver completely housed in a case and is controlled by an 8-bit CPU. The maximum output of the transmitter is 400 V peak to peak and 200 mA from an inbuilt battery or external 12V battery through a pressure boosting circuit.

The profile lengths range from 500 to 600 m. The observation interval is 10 m and the profile interval is 20 m. Further, based on the VLF-EM and Gradient Resistivity Profiling (GRP) surveys, which were conducted along nine parallel profiles, Vertical Electrical Resistivity Sounding (VES) were conducted at locations as shown in Figure 2. The results along the profiles 9010W, 9050W and 9090W show the utility of the geophysical surveys in successfully differentiating between the groundwater bearing zones and dry zones.

Analysis of VLF-EM and Electrical Gradient Profiles

The VLF-EM data was interpreted using RAMAG software of ABEM and the current density cross-sections were

Efficacy of Integrated Geophysical Techniques in Delineating Groundwater Potential Zones in the Deccan Basalt Region of Maharashtra

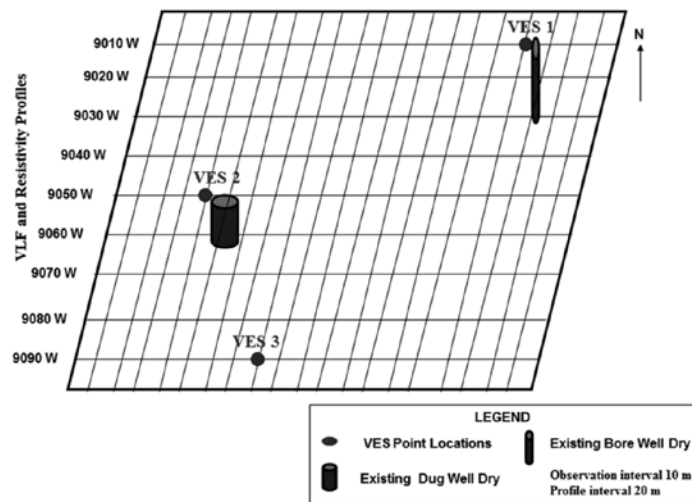


Figure 2. Profile Layout for VLF-EM and Resistivity Profiling surveys (not to scale)

interpreted. The analysis of three profiles that were interpreted for the delineation of the aquifer zones in the area are discussed in this section.

The profile P 9010W is 600 m in length and the existing dry bore well is situated at 440 m along this profile (Figure 2). The VLF-EM in-phase and quadrature components (Figure 3a) clearly demarcate the areas of weathered and fractured basalts depicted by high and low values.

The low values of the in-phase and quadrature components at 60 and 460 m observation points along this profile (Figure 3a) indicate the formation to be moderately weathered as lower current density values correspond to higher resistivity. The current density cross-section (Figure 3b) is computed using Karous and Hjelt filter (Karous and Hjelt, 1983) from the in-phase component (Figure 3a) of the VLF-EM data. The higher current density values at 500 m observation point indicate a low resistive zone which can be attributed to a weathered or fractured basalt and more likely possibility of the presence of an aquifer zone in the area. Conductive zones at 70, 450 and 490 m distances of the profile P 9010W with a dip from northeast to southwest are observed from the pseudo depth section (Figure 3b) and are interpreted as weathered to fractured basalt. These were also observed in well section with a thickness of about 4 to 6 m (GSDA, 2010). The resistivity of weathered to fractured basalt in the area is about 10 to 15 ohm m (GSDA, 2010). The conductive zones observed from 0 to 50 m along profile P 9010W are a part of the weathered to fractured basalt formations discussed earlier. The GRP data along the P 9010W profile (Figure 4) reveals a low resistivity anomaly between 440-450 m and 500-520 m of the profile indicating the formation to be moderately weathered basalt, which coincides with the conductive zones observed in the VLF pseudo depth section at 450 and 490 m. At distances beyond 500 m, the current density

concentration (Figure 3b) shows a high value of 10-15%. Also, the negative peak of in-phase does not correspond to a positive peak in the quadrature component or vice-versa, which is considered as a characteristic behaviour for the detection of conductive bodies in the VLF-EM method (Paterson and Ronka, 1971) as is observed at a distance beyond 520 m (Figure 3a) hence not considered for further investigation.

The profile P 9050W (Figure 2) traverses the existing dry dug well at 140 m observation point. A low current density concentration observed between 100 to 140 m along the profile P 9050W (Figure 5b) indicates a high resistivity zone. This phenomenon is also observed from the GRP data (Figure 6). As inferred from VES 2 (Table 2) the resistivity of this formation is approximately 100 ohm m with a thickness of about 10 to 14 m, which is massive basalt and is oriented in a northwest to southeast direction.

The profile P 9090W (Figure 2) traverses along the existing and yielding dug well at 230 m observation point. High current density anomalies are observed at 70 and 230 m along this profile (Figure 7b) indicating weaker zones, which could be weathered, vesicular and/or fractured basalt coinciding with low resistivity zone at this location in GRP data (Figure 8). The GRP data (Figure 8) shows lows at 70, 230, 450 and 500 m. At 70, 450 and 500 m, the VLF data did not indicate higher in-phase or quadrature components (Figure 7a) or high current density anomalies corresponding to that at 230 m (Figure 7b). Also, the quadrature component is clearly marked with an out-of-phase behaviour with respect to the in-phase VLF component (Figure 7a). Hence, for these reasons, a sounding (VES3) was conducted at 230 m distance (Table 2) which revealed a low resistivity layer of about 30 ohm m with a thickness of about 10-15 m implying it to be a weak zone corresponding to weathered, vesicular to

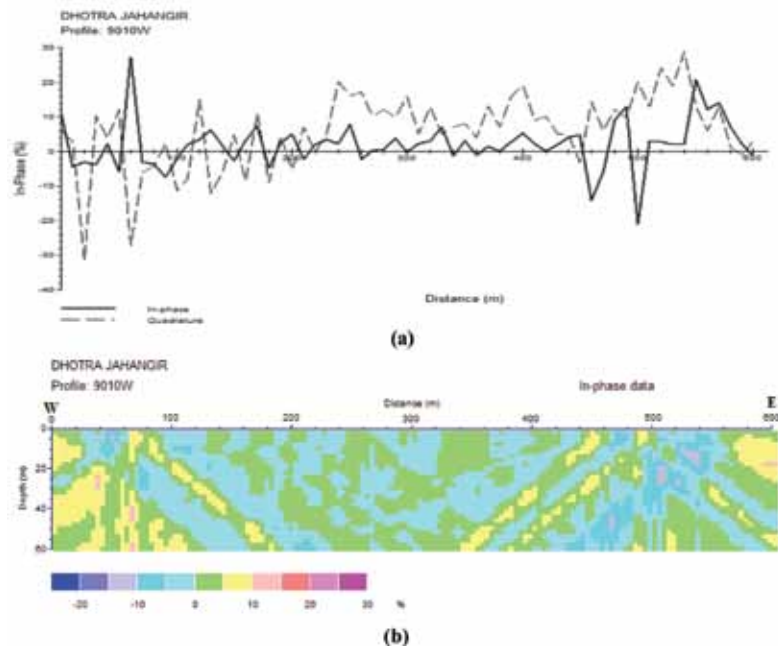


Figure 3. VLF-EM Profile 9010W (a) Real and Imaginary components (b) Pseudo-depth section.

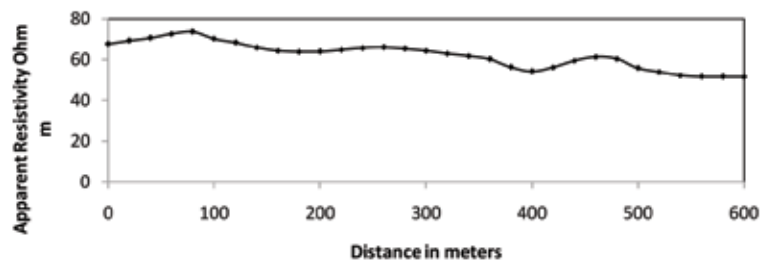


Figure 4. Gradient Resistivity Profile along P 9010W.

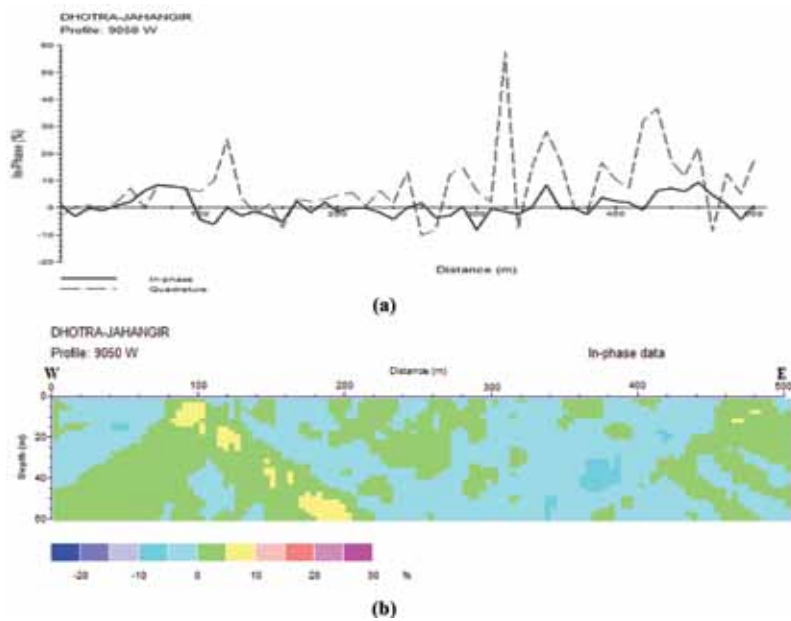


Figure 5. VLF-EM Profile 9050W (a) Real and Imaginary components (b) Pseudo-depth section.

Efficacy of Integrated Geophysical Techniques in Delineating Groundwater Potential Zones in the Deccan Basalt Region of Maharashtra

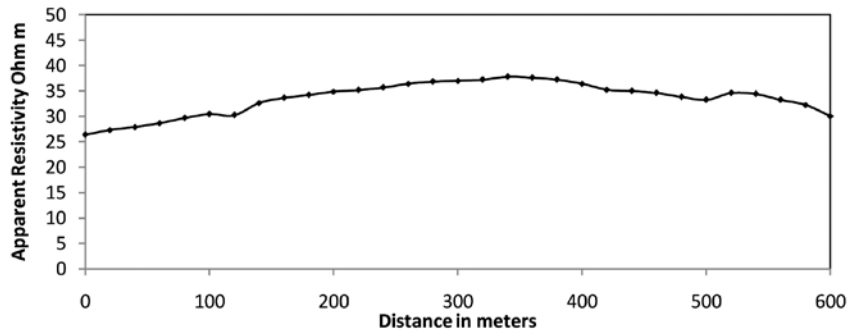


Figure 6. Gradient Resistivity Profile along P 9050W.

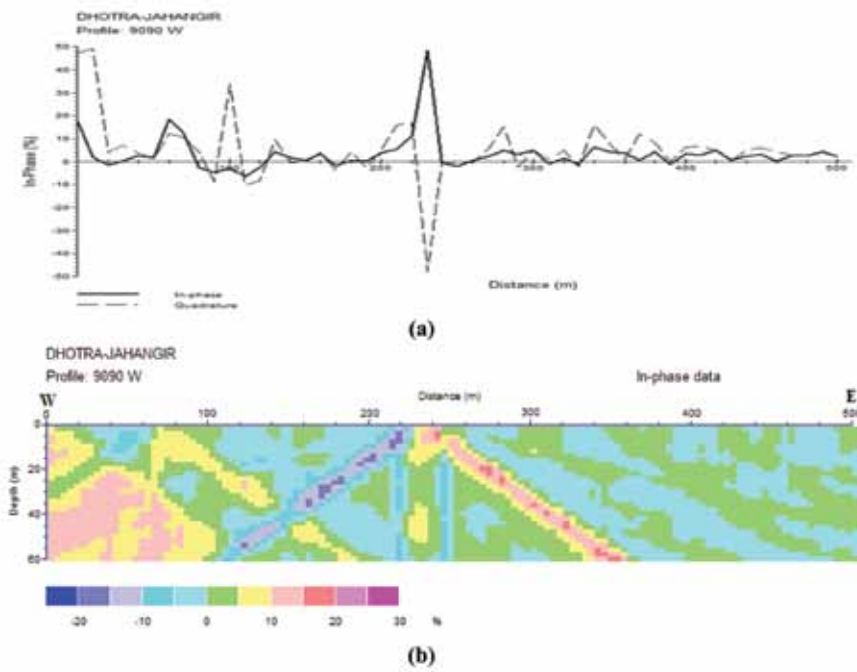


Figure 7. VLF-EM Profile 9090W (a) Real and Imaginary components (b) Pseudo-depth section

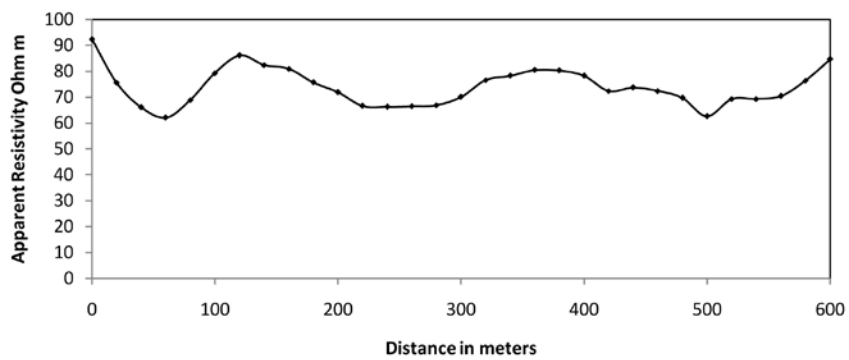


Figure 8. Gradient Resistivity Profile along P 9090W.

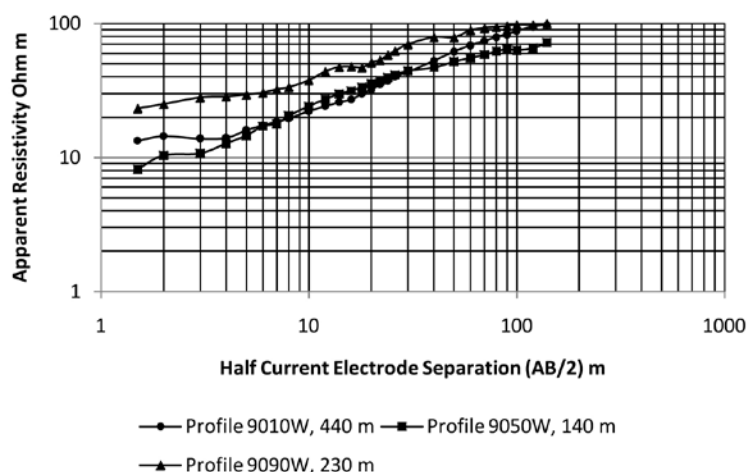


Figure 9. VES on profiles 9010W at 440 m, 9050W at 140 m and 9090W at 230 m observation points.

fractured basalt, oriented from northwest to southeast direction (Figure 7b).

RESULTS AND ANALYSIS

Based on the earlier studies (GSDA, 2010) and comparison of resistivity of different layers with well sections the following resistivity ranges are assumed for different formations.

Figure 9 shows the three Schlumberger Vertical Electrical Resistivity (VES) soundings carried out with maximum current electrode separation of 140 m. VES1, 2

and 3 were carried out on the profile P 9010W at 440 m (near an existing dry bore well), profile P 9050W at 140 m (near an existing dry dug well) and profile 9090W at 230 m observation point respectively (Figure 2). Encouraged by a 53 meter thick low resistive layer of 60 ohm m corresponding to the fractured basalt, a new dug-cum-bore well upto 60 m was suggested at the third location. The interpretation of the VES curves is shown in Table 2.

It can be observed from Table 2 that along VES1 and VES2 the weathered/fractured basalt formations show a resistivity of about 45 ohm m at depths of about 2-10 m, while at VES3 the weathered vesicular basalt of 30-40

Table 1. Resistivity ranges for different formations based on well sections and earlier studies (GSDA, 2010)

Type of Formation	Range of Resistivity
Top soil cover	10-20 ohm m
Weathered basalt	30-45 ohm m
Weathered to Massive basalt	40- 90 ohm m
Compact massive basalt	90-130 ohm m
Fractured basalt	60-90 ohm m
Compact massive basalt	> 130 ohm m

Table 2. Interpreted Results of VES along profiles 9010W, 9050W and 9090W.

Layer No	Interpreted geological formation	VES 1 P 9010W 440 m		VES 2 P 9050W 140 m		VES 3 P 9090W 230 m	
		Resistivity ohm m	Depth m	Resistivity ohm m	Depth m	Resistivity ohm m	Depth m
1	Top soil cover	8	1.2	10	1.5	23	2
2	Weathered Basalt	45	2.5	45	3	32	10
3	Weathered/Massive basalt	96	8.5	96	9	40	14.5
4	Compact massive basalt	145	37	145	21.5	90	23
5	Fractured basalt	73	54.5	93	39	60	53
6	Compact massive basalt	122		122		120	

ohm m was observed between 10 to 25 m depth. This can also be observed at 230 m distance in the VLF-EM pseudo depth section with the weathered basalt corresponding to a current density of 20-25% as dipping towards southeast (Figure 7b). Further, the bore well along near VES1 drilled up to 60 m in a vertical direction went dry as it did not pierce through the length of the aquifer due to its dipping nature. Based on this interpretation, a dug-well upto a depth of 14 m with a 6 m diameter and further a well bore to a depth of 46 m with a 160 mm diameter was recommended to exploit the total aquifer zones corresponding to the deeper horizons to cater to the needs of drinking and irrigation. The static water level during the summer month of April 2014 was observed to be 3.8 m at this location, which was very encouraging. Thus, the integration of VLF-EM and VES surveys has resulted in successful delineation of aquifer zones in the complex hydrogeological trap terrain.

CONCLUSIONS

Groundwater problems associated with the complex geology of the Deccan Basalt region can be resolved by integrating different geophysical approaches. The overlapping ranges of resistivity values of weathered basalt, vesicular basalt and fractured basalt even in closer proximities and their dipping nature in the subsurface lead to confusion in recommending well sites in trap terrain. The VLF-EM method in combination with the resistivity gradient profiling technique can help to resolve this issue and locate the aquifer zones. Never the less identifying of the direction of weathered or fractured zones is vital for groundwater exploitation in such a region. The failure of dug well or bore wells should not be attributed to non-availability of groundwater in the region, but drilling the bore wells in the direction of the weathered and fractured layers is also necessary. This methodology can be successfully applied in similar hard rock basaltic regions to address the existing drought situation to some extent.

ACKNOWLEDGMENTS

The authors are grateful to Dr. Praveen Gedam, Director, Groundwater Surveys and Development Agency (GSDA) under Water Supply and Sanitation Department, Government of Maharashtra for permitting and supporting the geophysical work carried out in this area. The authors are thankful to Shri C.S.N Murthy, Chief Geophysicist GSDA Pune, Shri N.G. Baskar, Senior Geophysicist GSDA Amravati, Shri Nishat Ahmad Senior Geophysicist, GSDA, Pune for their valuable suggestions and fruitful discussions during the interpretation of the geophysical data. The authors are also thankful to Shri Gajanan Devesing Jadav for constructing a dug-cum-bore-well as per the interpreted

results. The authors thank the reviewer Dr. M. R. K. Prabhakara Rao and Dr. P. R. Reddy for improving the quality and understanding of the concept presented in the paper that has societal relevance to solve groundwater problems in drought affected areas.

Compliance with Ethical Standards

The authors declare that they have no conflict of interest and adhere to copyright norms.

REFERENCES

- Adyalkar P.G., and Mani, V.V.S., 1971. Paleogeography, geomorphological setting and groundwater possibilities in the Deccan Traps of Western Maharashtra, *Bull. Volcanology*, v.35, pp: 696-708.
- Agashe, L.V., and Gupte, R.B., 1971. Mode of eruption of Deccan Traps basalts, *Bulletin Volcanology*, v.35, pp: 591-601.
- Bean, J.E., Turner, C.A., Hooper, P.R., Subbarao, K.V., and Walsh, J.N., 1986. Stratigraphy, composition and form of the Deccan basalts, Western Ghats, India, *Bull Volcanology*, v.48, pp: 61-83.
- Bose, R.N., and Ramkrishna, T.S., 1978. Electrical resistivity surveys for groundwater in the Deccan trap country of Sangli District, Maharashtra. *J. Hydrol*, v.38, pp: 209-221
- Choubey, V.D., 1973. Long-distance correlation of Deccan basalt flow, central India, *Journal Geological Soc America*, v.84, pp: 2785-2790.
- Deolankar, S.B., 1980. The Deccan basalts of Maharashtra state, India: their potential as aquifers. *Ground Water*, v.18, no.5, pp: 434-437.
- Deshpande, B.G., and Sen Gupta, S.N., 1956. Geology and groundwater in the Deccan traps and the application of geophysical methods, *Bull Series B Geol Surv Ind*, v.8, pp: 26.
- Dhokarikar, B.G., 1991. Groundwater resource development in basaltic rock terrain of Maharashtra. Water Industry Publications, Pune.
- Ghosh, P., Sayeed, M.R.G., Islam, R., and Hundekari, S.M., 2006. Inter-basaltic clay (bole-bed) horizons from Deccan traps of India: Implications for palaeo-climate during Deccan trap volcanism. *Palaeogr, Palaeoclimatol., Palaeoecol.*, v.242, pp: 90-109.
- GSDA, 1974. GSDA Task Force Report GSDA, Maharashtra.
- GSDA, 2001. Consolidated Geophysical Survey Report, Groundwater Surveys and Development Agency year 1995-96 to 2000-2001.
- GSDA, 2008. A Report. Geophysical Investigations for Identification of Seepages in Sawangi Minor Irrigation Tank, Village Sawangi, Taluka Warud, District Amravati, State Maharashtra. Report No. 1921.
- GSDA, 2010. Report of Washim District General Point, Groundwater Surveys and Development Agency, 2010.

- Karmakar, B.M., 1978. The Deccan Trap basalt flows of the Borghat sector of Central Railways, Jour. Geological Soc. India, v.19, pp: 106-114.
- Karous, M., and Hjelt, S.E., 1983. Linear Filter of VLF Dip-Angle Measurements, Geophysical Prospecting, v.31, pp: 782-794.
- Kulkarni, H., Shankar, P.S.V., Deolankar, S.B., and Shah, M., 2004. Groundwater demand management at local scale in rural areas of India: a strategy to ensure water well sustainability based on aquifer diffusivity and community participation. Hydrogeol J., v.12, no.2, pp: 184-196.
- Limaye, S.D., 2010. Groundwater development and management in the Deccan traps (basalts) of western India. Hydrogeol. J., v.18, no.3, pp: 543-558.
- Mahoney, J.J., 1988. Deccan Traps, In: Macdougall, J.D., (Ed.) Continental Flood Basalts, Dordrecht: Kluwer Academic, pp: 151-194.
- McNeill, J.D., 1991. Advances in electromagnetic methods for groundwater studies, Geoexploration, v.27, no.1-2, pp: 65-80.
- Nishat Ahmad, 2001. Geophysical Technique a reliable tool in designing the cost effective layout for unconventional measures to strengthen the source well: A case study of village Aware, Taluka Uran, District Raigad, State Maharashtra. Seminar on 'An Integrated Approach for Strengthening and Protecting Drinking Water Sources'. September 27-28, 2001, pp: 415- 424.
- Paterson, N.R., and Ronka, V., 1971. Five Years of Surveying with the Very Low Frequency Electromagnetics Method, Geoexploration, v.9, pp: 7-26.
- Sharma, S.P., and Baranwal, V.C., 2005. Delineation of groundwater-bearing fracture zones in a hard rock area integrating Very Low Frequency Electromagnetic and Resistivity data. Journal of Applied Geophysics, v.57, pp: 155-166.
- Shettigara, V.K., and Adams, W.M., 1989. Detection of lateral variations in geological structures using electrical resistivity gradient profiling, Geophysical Prospecting, v.37, no.3, pp: 293-310.
- Singhal, B.B.S., 1997. Hydrogeological characteristics of Deccan trap formations of India. In Hard Rock Hydrosystems, Proceeding of Rabat Symposium, IAHS Publ. no.241, pp: 75-80.
- Sundararajan, N., Nandakumar, G., Chary, M.N., Raman, K., and Srinivas, Y., 2007. VES and VLF – An Application to Groundwater Exploration, Khammam, India. The Leading Edge, pp: 708-716.
- Telford, W.M., Geldart, L.P., Sheriff, R.E. and Keys, D.A., 1976. Applied Geophysics, Oxford & IBH, pp: 860.
- Yadav, G.S., and Singh, S.K., 2007. Integrated resistivity surveys for delineation of fractures for groundwater exploration in hard rock areas. J. Appl. Geophys., v.62, pp: 301-312.

Received on: 20.12.17; Revised on: 24.1.18; Re-revised on: 11.2.18; Accepted on: 14.2.18

Site characterisation using Multi-channel Analysis of Surface Waves at various locations in Kumaon Himalayas, India

Anand Joshi¹ and Parul Bhardwaj²

¹Department of Earth Science, Indian Institute of Technology Roorkee, Roorkee, India 247667

²KDMIPE, Oil & Natural Gas Corporation Ltd., Dehradun, India 248195

*Corresponding Author: parul1611pandit@gmail.com

ABSTRACT

Local site amplification is greatly influenced by the top 30 m soil column. Rayleigh waves in top soil, acquired by Multi-channel Analysis of Surface Wave (MASW) technique, are helpful in local site amplification studies. In this paper, the acquired data in Kumaon Himalayas are processed for noise elimination and signal enhancement and also for the estimation of shear wave velocity by using "Seisimager" software. We estimated 2D shear wave velocity (V_{s30}) down to 30 m depth in Kumaon region. Average V_{s30} is found to be in the range of 120 - 712 ms^{-1} and average predominant frequency in the range of 1.01 - 5.94 Hz. Estimated average shear wave velocity is used for site classification, which can be used for geotechnical characterization of shallow subsurface formations.

Key words: Shear wave velocity, Predominant frequency, MASW, Kumaon Himalayas

INTRODUCTION

The earthquake ground motions are affected by the source processes, propagation of seismic waves in the medium, and the site characteristics. The study of effects of local site conditions is one of the most vital areas of earthquake engineering. For site classification, V_{s30} , shear wave velocity down to 30 m depth, is a key parameter that characterizes earthquake strong ground motion. The strong ground motion plays an important role in evaluation of seismic hazards in a region. Since 30 m is a typical depth of borings and detailed site characterization in engineering site investigation, most of the site-effect studies in earthquake ground motions are based on the properties in the upper 30 m (Anderson et al., 1996).

The V_{s30} estimate is used to suggest the possible amplification and de-amplification of sites (Dobry et al., 2000). National Earthquake Hazards Reduction Program (NEHRP) provides guidelines for grouping sites into different classes (Borcherdt, 1994; Shafiee et al., 2005; Wen et al., 2008). The current NEHRP approach categorizes soils into A, B, C, D, E and F based on V_{s30} profile, thickness and liquefaction potential (Thitimakorn et al., 2012). The present paper presents a study for estimating the V_{s30} in Kumaon region. MASW method is used to acquire the field data and "Seisimager" software is used for processing and interpretation.

Seismotectonics of the Region

The Kumaon Himalayas lie in the state of Uttarakhand, India and shares its border with Nepal. It falls in the seismic zone V, as per the Seismic Zoning map of India

(BIS, 2002). Himalayan fold thrust movement causes high seismic activity in this region. Robust wraps and recurrence of many former faults and thrusts during Quaternary are evident in this region. It falls between the Eurasian plate and Indo-Australian plate, where the stress is constantly getting accumulated giving indications of a potential major earthquake ($M > 8$). Considering the historical earthquakes across these two plates, Kumaon Himalayas are in the central seismic gap. Hence, the shallow subsurface imaging is important for this region.

The location map of this area of study is shown in Figure 1. It also shows location of the broad band stations. Seven stations are tabulated as per the generalised stratigraphy and lithology in Table 1 (Valdiya, 1980).

METHODOLOGY AND DATA

MASW is a non-invasive, non-destructive, and continuous profiling method which efficiently deals with many difficulties related to earthquake engineering. It is widely used for the micro-zonation and site studies. This seismic method is generally utilized for geotechnical characterization of shallow subsurface formations (Park et al., 1999; Xia et al., 1999; Miller et al., 1999). MASW studies have been carried out by several Indian scientists across various parts of India including Jabalpur, Delhi, Ahmedabad and Bangalore (Seshunarayana et al., 2004; Satyam and Rao, 2010; Anbazhagan and Sitharam, 2006; Trivedi et al., 2009). Ariffin et al., (2015) have shown that a combination of active and passive MASW method gives improved results.

In this study, data has been acquired using McSEIS-SX 24 channel digital engineering seismograph with 4.5 Hz geophone array. Geophones are arranged vertically in a

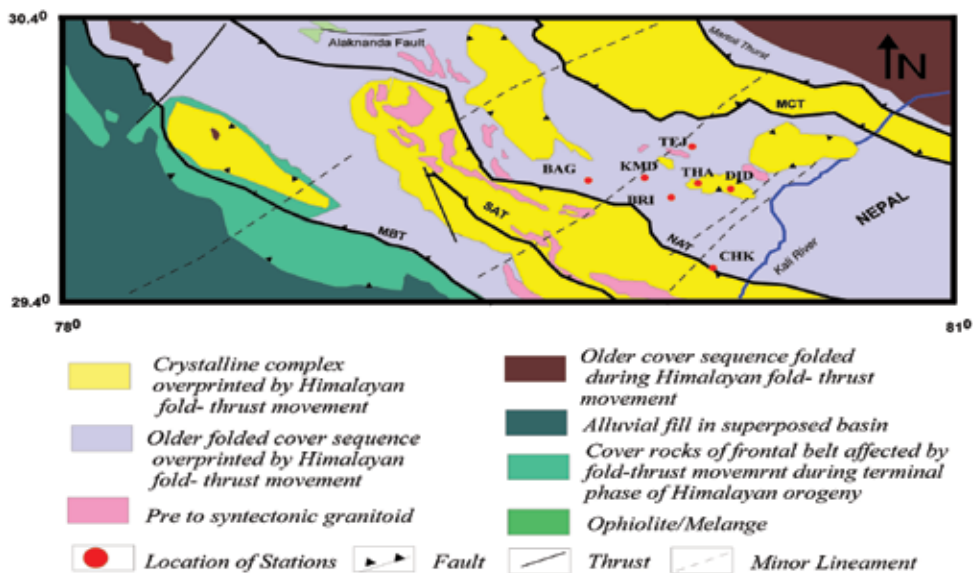


Figure 1. The present area of study belongs to the Kumaon and Garhwal Himalayas, India. MBT = Main Boundary Thrust, MCT = Main Central Thrust, and NAT = North Almora Thrust. Red circles show the location of the stations. Source of the tectonics and geology of the region is as per GSI (2000).

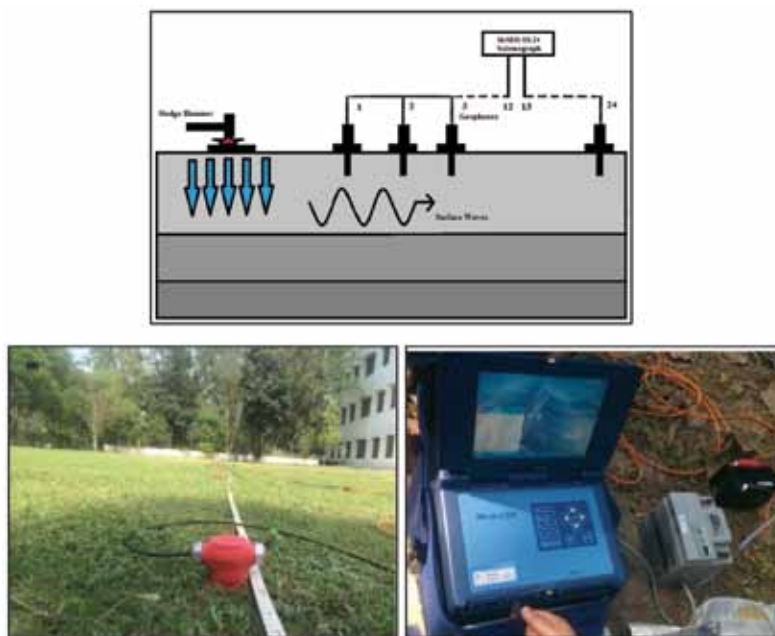


Figure 2. Schematic layout used for data acquisition with McSEIS-SX.

horizontal ground spread. The receiver spacing represents the shortest generated wavelength, which determines the minimum depth to be used in the investigation. In contrast, the spread length of the receiver represents the longest wavelength, which determines the maximum depth to be used in the investigation (Ariffin et al., 2015). During the acquisition, equal geophone and source spacing is considered. The 4.5 Hz geophones are coupled to the seismograph through fixing cables. Seismic waves are generated using mechanical source (hammer 11 kg) and data is recorded in a multi-channel seismograph recorder.

The information of the fundamental mode of Rayleigh waves is used for the generation of dispersion curves by picking the highest energy portion in spectrum to draw curve, which represents the relationship between Rayleigh wave phase velocity and frequency. Raw data for every position is recorded and protected in the apparatus. The raw waveform data obtained has been analysed and processed by the software “Seisimager”. Average V_{s30} is estimated using generated 2D shear wave velocity models for all the stations. A schematic layout for data acquisition is shown in Figure 2.

Table 1: Generalised stratigraphy with lithology and age of the locations in Kumaon Himalayas.

Station name	Formation	Lithology	Stratigraphy units	Age
Chaukori	Askot Crystalline	Granite Gneiss, Quartzite, mica-schist and amphibolite	Askot Crystalline	Mesoproterozoic
Kameri Devi	Berinag	Quartzite	Jaunsar Group	Neo-Proterozoic
Tejam	Deoban	Quartzite, Dolomite	Tejam Group	Middle Riphean-Upper Riphean
Thal	Mandhali	Slate, Phyllite and Limestone, Dolomite	Tejam Group	Upper Riphean-Early Vendian
Didihat	Askot Crystalline	Granite Gneiss, Quartzite, mica-schist and amphibolite	Askot Crystalline	Mesoproterozoic
Berinag	Berinag	Quartzite	Jaunsar Group	Neo-Proterozoic
Bhageshwar	Berinag	Quartzite	Jaunsar Group	Neo-proterozoic

Table 2. Name, Code and acquisition parameters of the stations

Station name	Latitude (in degree)	Longitude (in degree)	Station code	Geophone spacing (m)	Source spacing (m)	Spread length (m)
Chaukori	29.52N	80.19E	CHK	2.5	2.5	60
Kameri Devi	29.84N	79.96E	KMD	2.5	2.5	60
Tejam	29.95N	80.12E	TEJ	1	1	24
Thal	29.82N	80.14E	THA	2	2	48
Didihat	29.80N	80.25E	DID	3	3	72
Berinag	29.77N	80.05E	BRI	2.5	2.5	60
Bageshwar	29.83N	79.77E	BAG	2.5	2.5	60

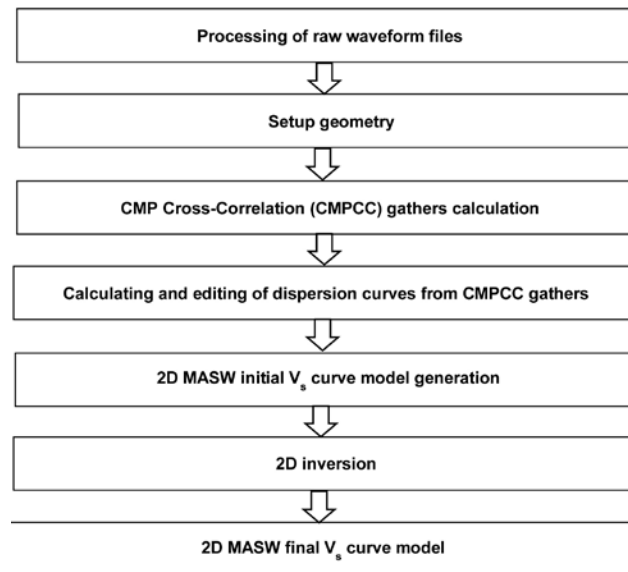


Figure 3. Flowchart depicting the processing steps.

MASW method is applied at various stations in the tough and rocky Kumaon Himalayas, India. The conventional CMP rolling method with 0.01 msec sampling interval has been used. The number of hammering stacks is three and the recording length is 800 msec. 24 geophones were active during the entire survey. Data acquisition parameters of the seven stations are given in Table 2. Geophone spacing varies from 1m to 3m depending on the availability of flat terrain at various stations. Since the said

geographical region is highly rugged and rocky, therefore, it is very tough to find a large flat area for the survey. And hence, the survey is conducted on the playgrounds of schools in various localities. This gives an idea about the velocity profile of below mentioned schools.

The creation of dispersion curve is one of the most critical steps for attaining correct shear wave velocity model. 1D shear wave velocity models are calculated using the dispersion curves by using the Least Square Method

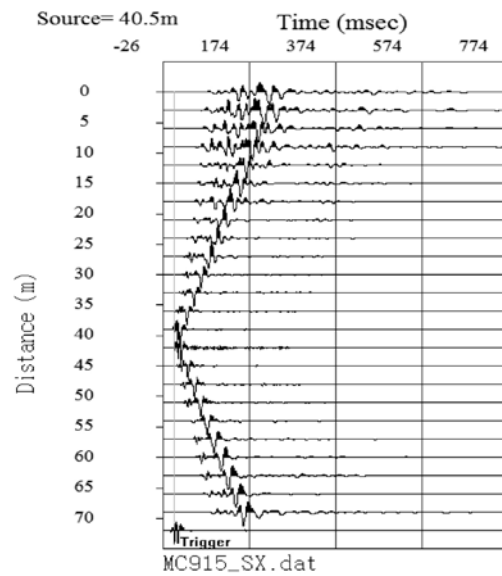


Figure 4. Multi-channel Records (shot gather) in Kumaon Himalayas.

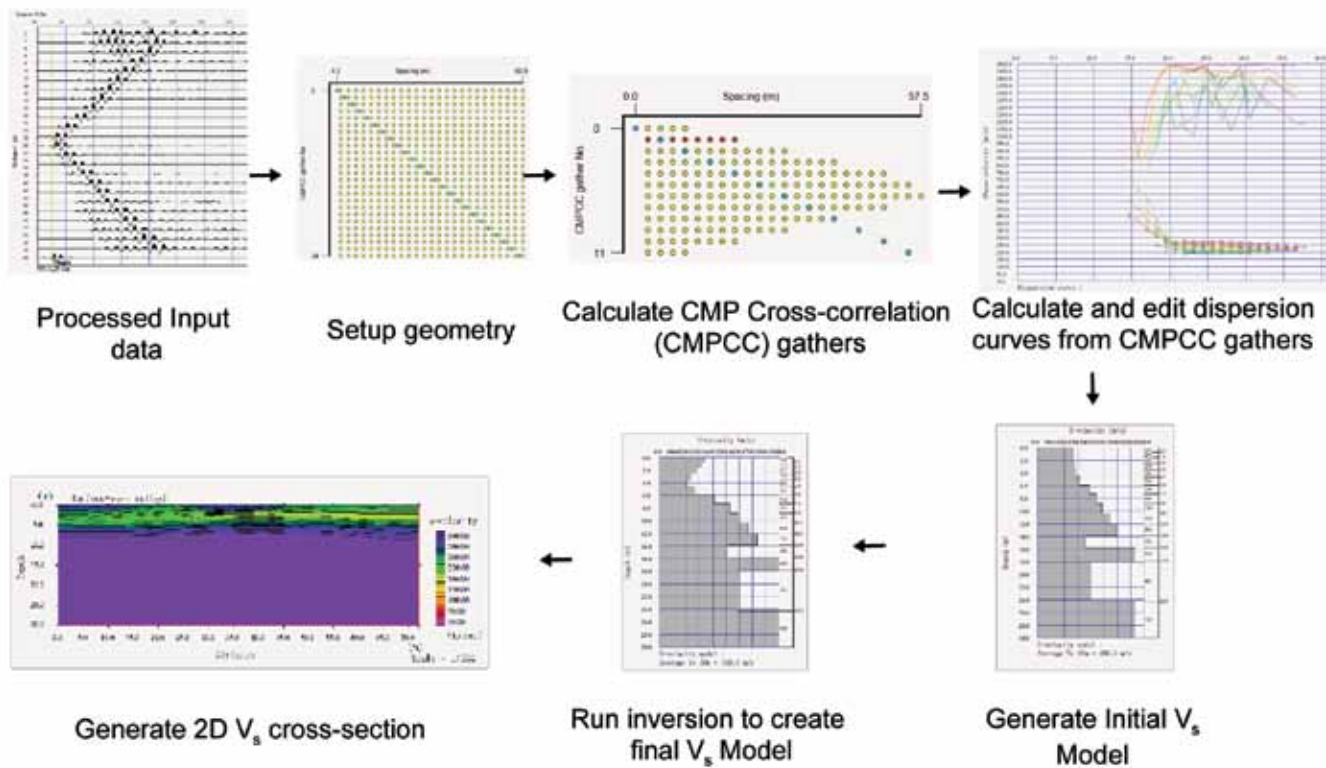


Figure 5. General processing steps used for MASW technique at Didihat Station.

(LSM). As a result, 2D V_{s30} map is constructed. 2D shear wave velocity map is generated using kriging algorithm of interpolation. Flowchart showing the steps of data processing is given in Figure 3 and Figure 5. The raw seismic waveform data is shown in Figure 4.

Common Mid-Point (CMP) gathers and corresponding dispersion curves with initial and final 1D shear wave

velocity models at source spacing 0 m, 6 m, 12 m, 18 m, 24 m, 30 m, 36 m, 42 m, 48 m, 54 m, 60 m, 66 m and 72 m are generated for Didihat. The spread length of Didihat is 72 m. This detailed procedure is followed for each station during processing. An example is shown in Figure 6 for source spacing 30 m at Didihat station. Following equation is used to estimate average value of V_{s30} .

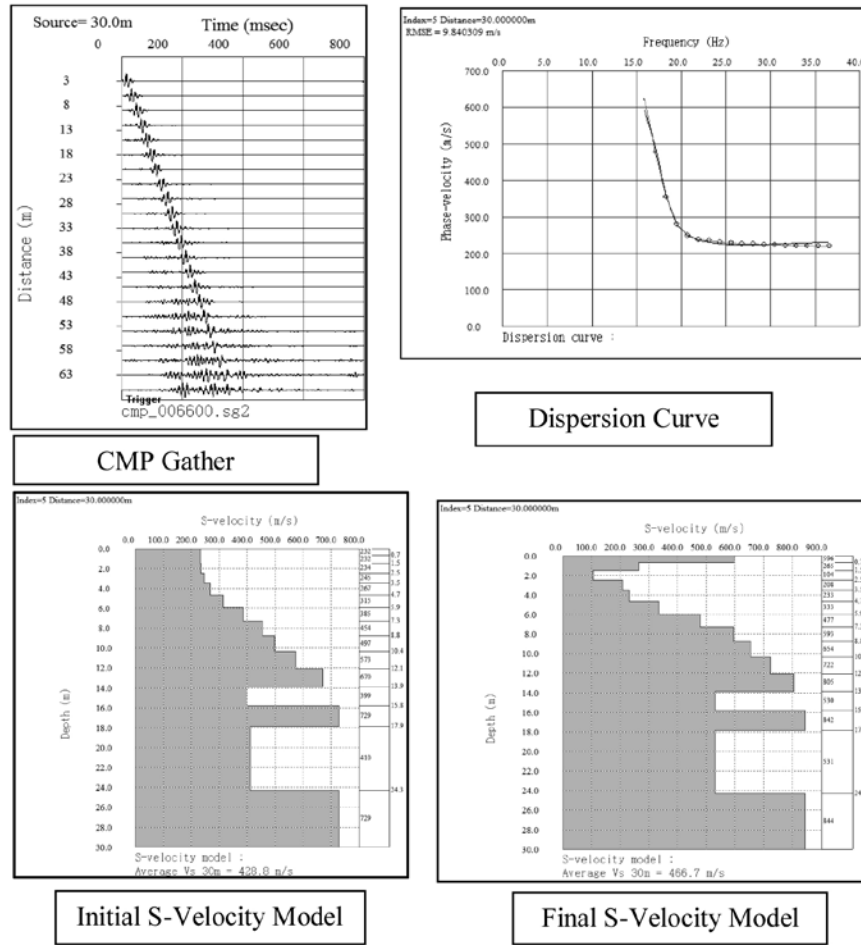


Figure 6. CMP gathers and corresponding Dispersion curve with initial and 2D Shear Wave Velocity Model at Source = 30m for Didihat.

$$V_{s30} = \frac{30}{\sum_{i=1}^n \left[\frac{h_i}{v_i} \right]} \quad (\text{Eq. 1})$$

Where, h_i is the thickness of the i^{th} soil layer in metres; v_i is the shear wave velocity for the i^{th} layer in ms^{-1} , and n is the no. of layers above 30 m.

The predominant frequency is defined as frequency corresponding to the highest value in amplitude spectrum of soil column. It can also be estimated by the following equation:

$$F_p = \frac{V_{s30}}{4h} \quad (\text{Eq. 2})$$

Where, F_p is the predominant frequency of the soil column in Hz, V_{s30} is shear wave velocity of the soil column in ms^{-1} and h is the thickness of the soil column i.e. 30 m. The average V_{s30} and predominant frequency of 30 m soil column along with the Root Mean Square Error (RMSE) at various stations in Kumaon Himalayas is tabulated in Table 3.

The RMSE is calculated using following equation

$$RMSE = \sqrt{\frac{1}{N} \left(\sum_{i=1}^N (d_i^M - d_i^T)^2 \right)} \quad (\text{Eq. 3})$$

Where N is the total number of data points and d_i^T and d_i^M are phase velocity of theoretical and measured dispersion curve, respectively. With the successive iterations, the RMSE for shear wave velocity model decreases as shown in Table 3. The RMSE is plotted against the number of iterations for all the stations - depicting the accuracy of the Shear wave velocity profiles generated as shown in Figure 7.

RESULTS AND DISCUSSION

The dispersion curves are extracted by keeping 4.50 Hz as minimum frequency. After processing the dispersion curves, the variation of phase velocity with respect to frequency is calculated. For Didihat, based on phase velocity data

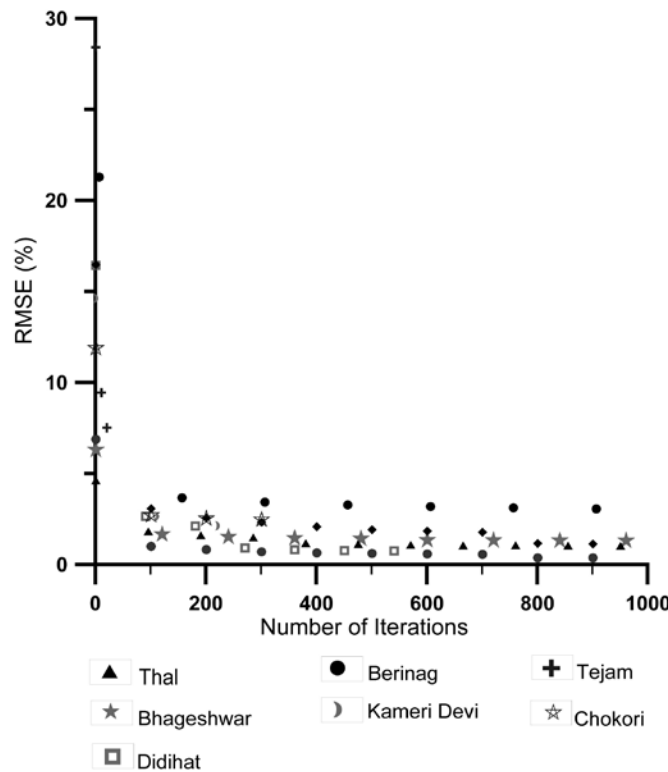


Figure 7. Root Mean Square Error (RMSE) plot against number of iterations at the stations in Kumaon Himalayas.

Table 3. Average Predominant Frequency (PF) of soil column estimated after inversion at various locations in Kumaon Himalayas

Station name	RMSE				Average V_{s30} m	Average PF
	Initial model error		Final model error			
	Velocity (m/s)	RMSE (%)	Velocity (m/s)	RMSE (%)		
Chaukori	99.40	29.00	20.70	2.30	470	3.92
Kameri Devi	42.90	18.40	4.30	1.02	380	3.17
Tejam	27.80	35.80	5.02	7.20	121	1.01
Thal	40.30	6.80	5.40	0.90	524	4.37
Didihat	58.40	18.30	3.60	0.74	486	4.05
Berinag	86.90	15.45	13.75	1.70	712	5.94
Bhageshwar	33.00	7.20	4.60	1.18	409	3.41

obtained in frequency domain, the frequency range is within 14.6 - 37.8 Hz with phase velocity in 200-700 ms^{-1} range. Similarly, the frequency range for Berinag, Tejam, Bageshwar, Kameri Devi, Thal and Chaukori varies from 25.62 - 39.04 Hz, 15.20 - 29.60 Hz, 7.32 - 39.04 Hz, 10.98 - 35.38 Hz, 8.54 - 39.04 Hz and 15.80 - 39.04 Hz and phase velocity varies from 307 - 772 ms^{-1} , 45 - 155 ms^{-1} , 278 - 441 ms^{-1} , 157 - 476 ms^{-1} , 446 - 576 ms^{-1} and 121 - 631 ms^{-1} , respectively.

The results including dispersion curves, 1D velocity models and 2D velocity model are shown for the seven stations in Kumaon Himalayas from Figure 8 to Figure 14. It is observed that geological setting and lithology

of the area play a major role on predominant frequency. Estimated predominant frequencies, derived using equation 2, vary from 3.92 - 4.05 Hz for the granitic and gneissic rocks, 3.17 - 5.94 Hz for the quartzite rocks, 1.01 Hz for quartzite along with dolomite rocks and 4.37 Hz for the slates, phyllites along with limestones and dolomite.

High-rise buildings typically have low natural frequency as compared to small buildings. Kumaon region is mostly populated with small to medium buildings. It is observed that Predominant Frequency in this region varies from 1.01 to 5.94 Hz indicating a wide range of damaging pattern to various structures in the region. Estimated Predominant Frequency is 1.01 Hz at Tejam, which corresponds to

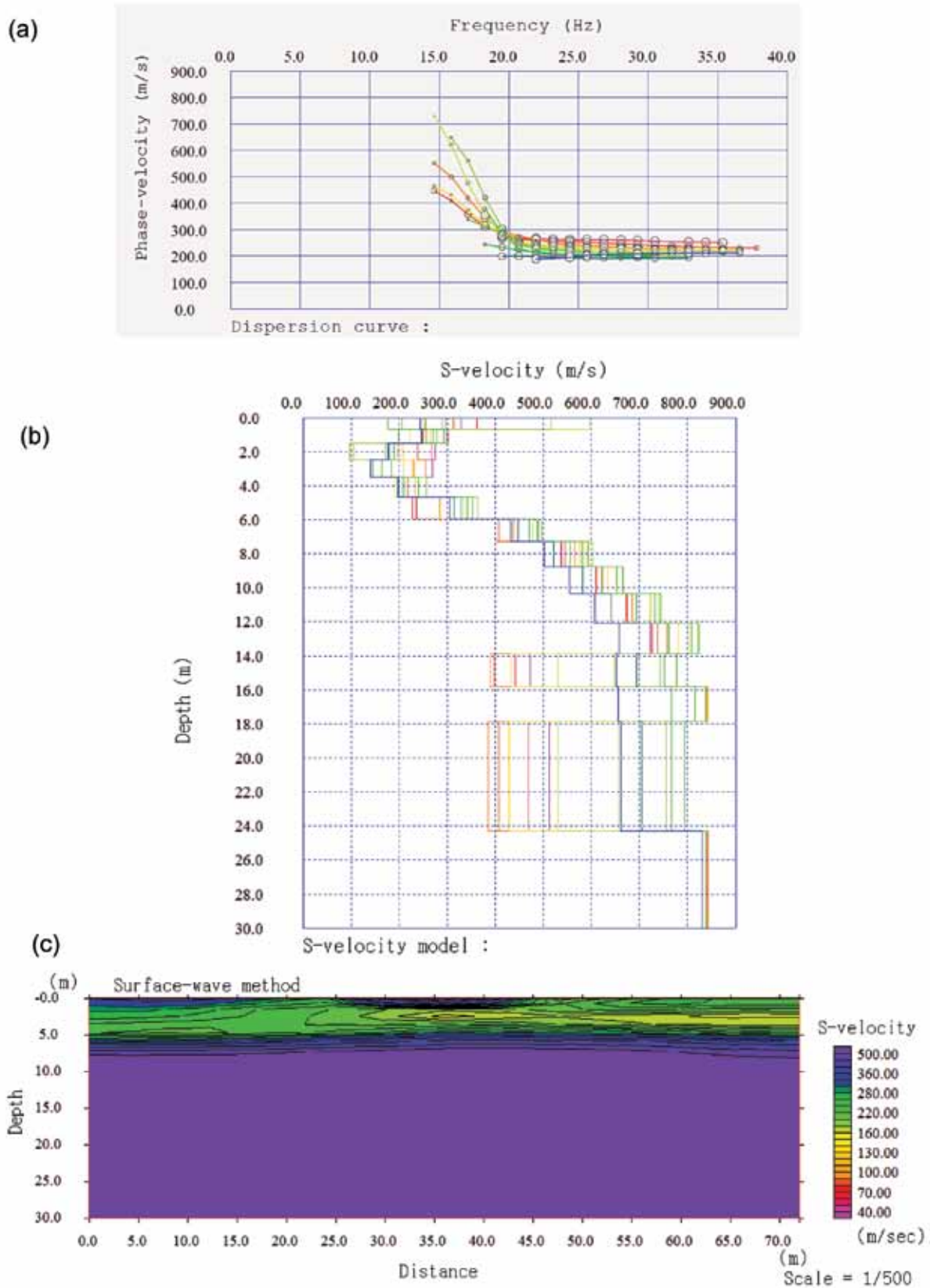


Figure 8. The results obtained at Didihat station (a) dispersion curve obtained from processed record, (b) 1D Shear Wave Velocity Model inverted using trends in (a), and (c) 2D Shear Wave Velocity Model.

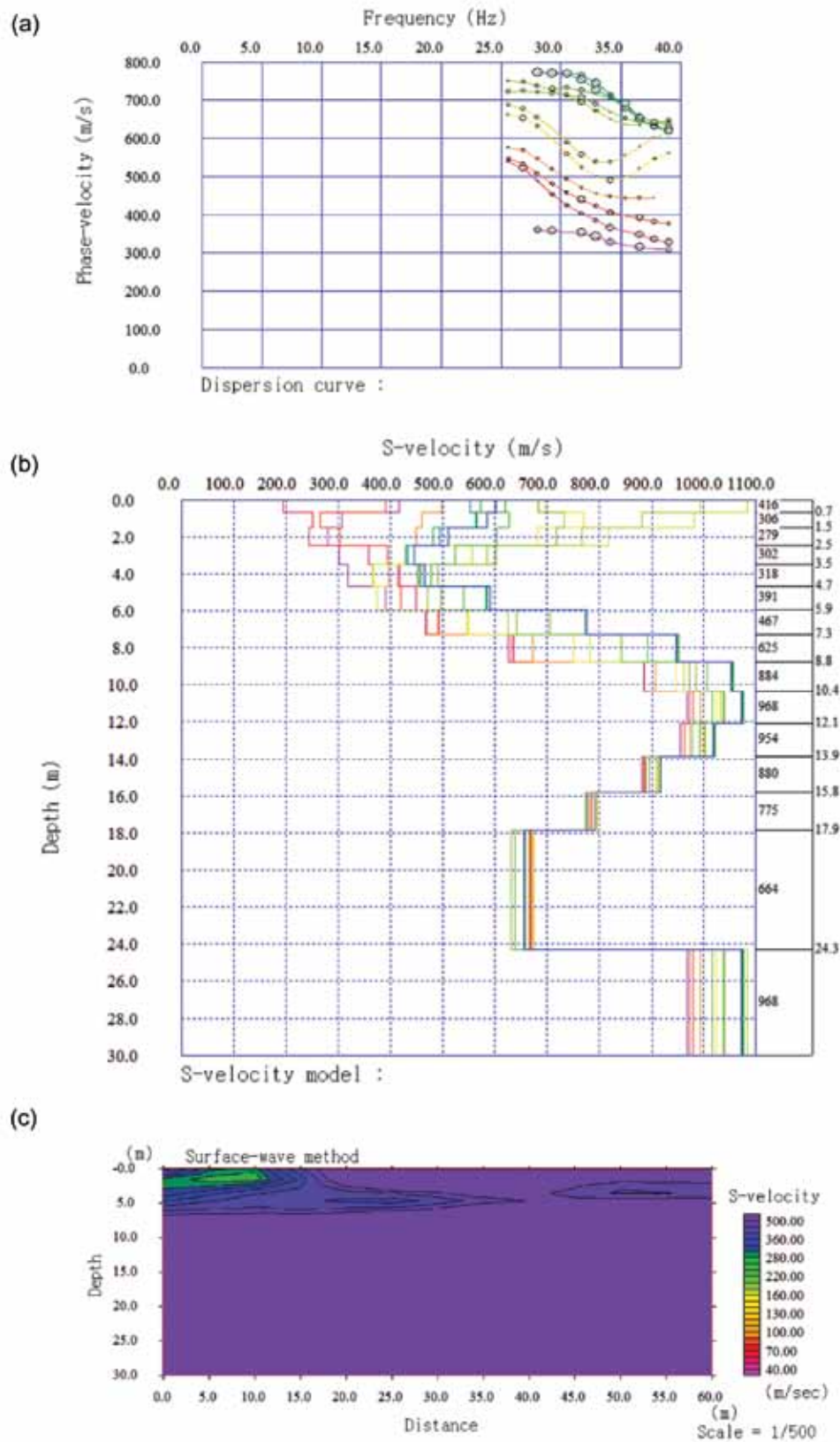


Figure 9. The results obtained at Berinag station (a) dispersion curve obtained from processed record, (b) 1D Shear Wave Velocity Model inverted using trends in (a), and (c) 2D Shear Wave Velocity Model.

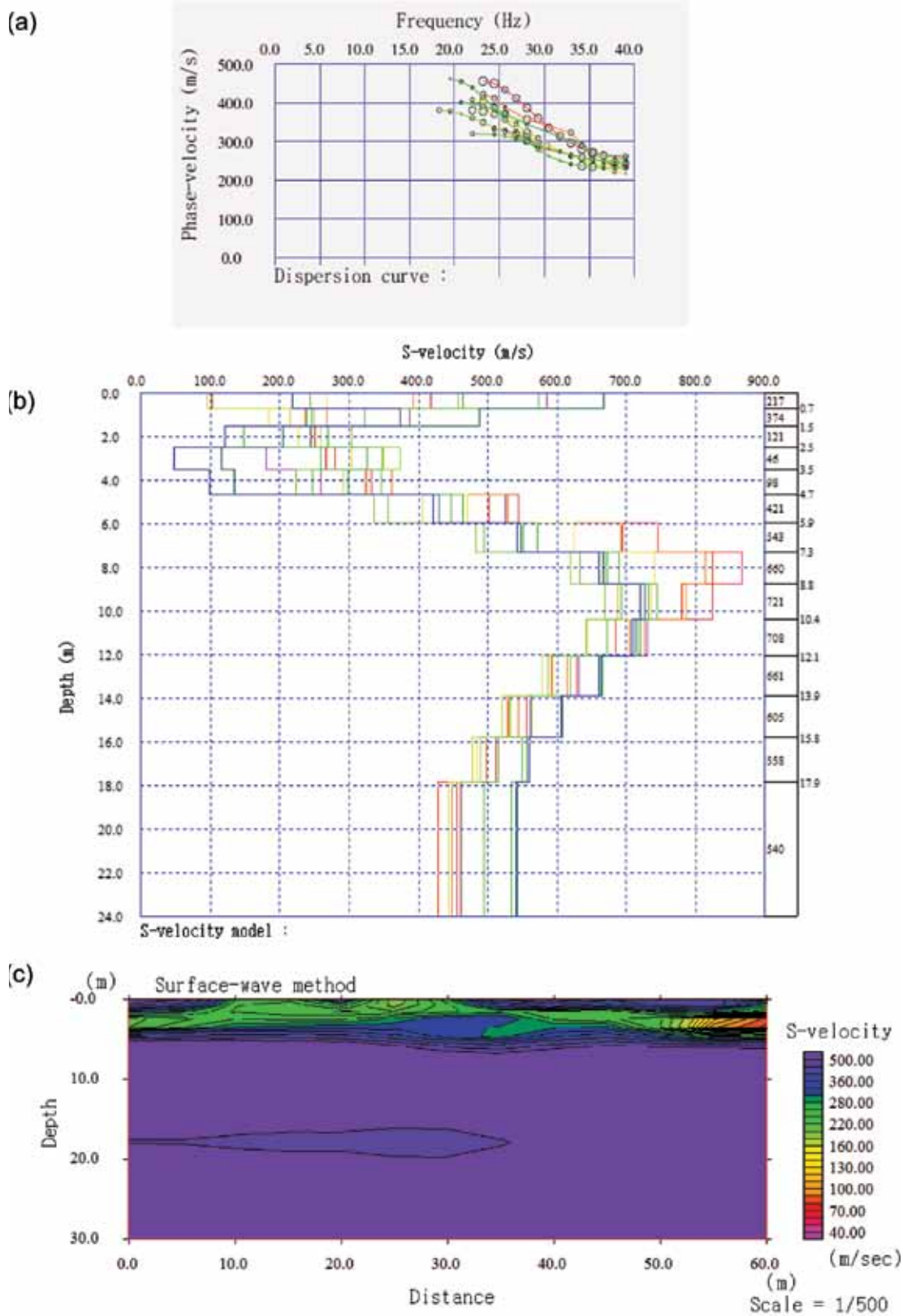


Figure 10. The results obtained at Chaukori station (a) dispersion curve obtained from processed record, (b) 1D Shear Wave Velocity Model inverted using trends in (a), and (c) 2D Shear Wave Velocity Model.

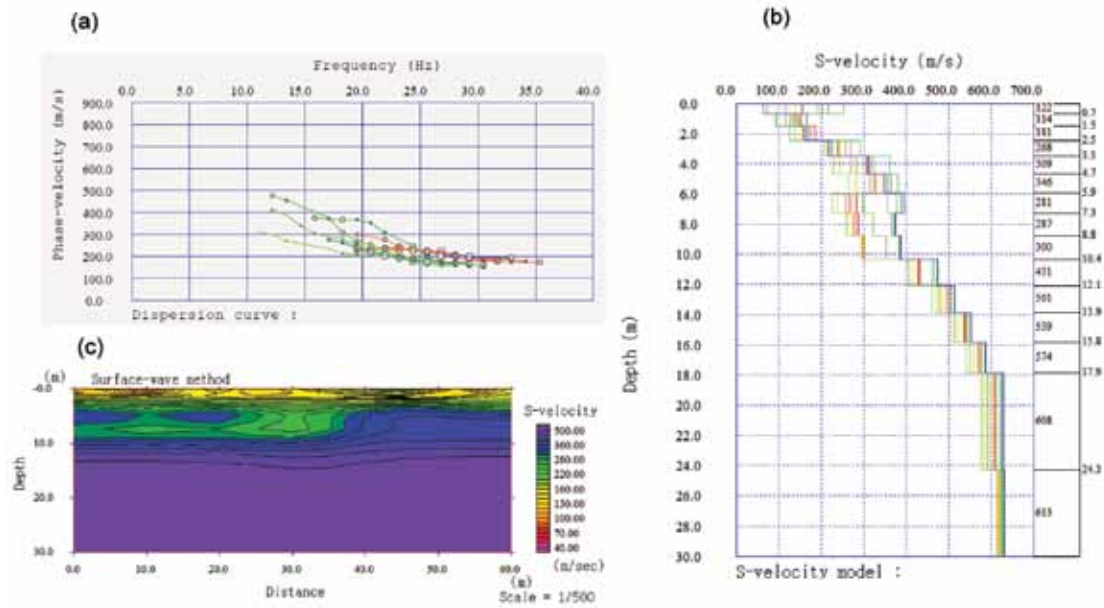


Figure 11. The results obtained at Kameri Devi station (a) dispersion curve obtained from processed record, (b) 1D Shear Wave Velocity Model inverted using trends in (a), and (c) 2D Shear Wave Velocity Model.

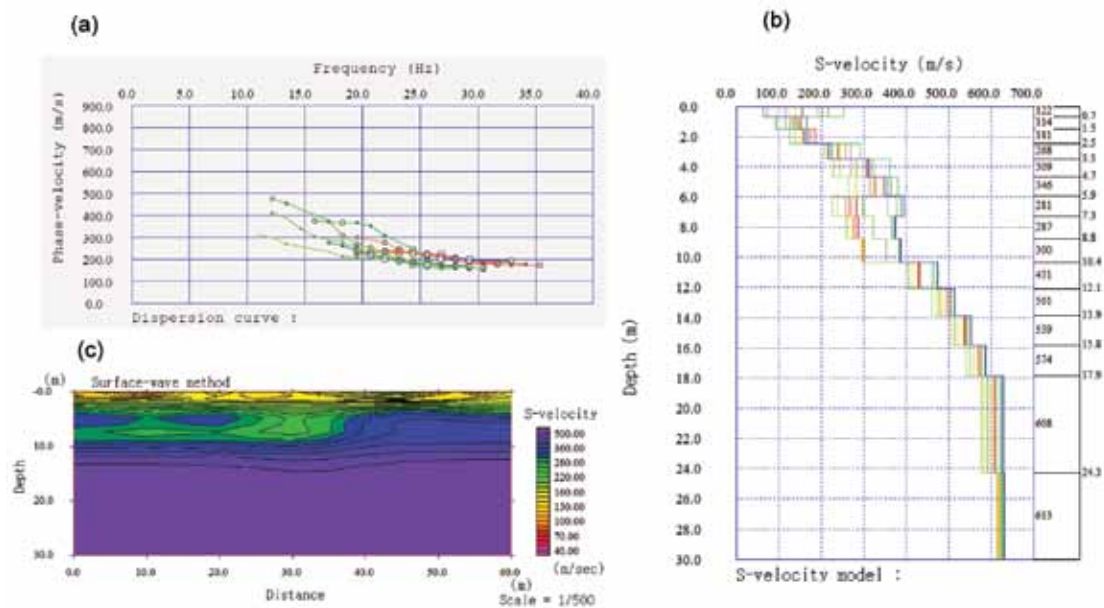


Figure 12. The results obtained at Bhageshwar station (a) dispersion curve obtained from processed record, (b) 1D Shear Wave Velocity Model inverted using trends in (a), and (c) 2D Shear Wave Velocity Model.

Proterozoic crystalline formations containing quartzite and dolomitic limestones with bands and intercalations of limestones. The estimated Predominant Frequency is 5.94 Hz at Berinag, which corresponds to quartzite rocks. The higher estimated Predominant Frequency at various locations is hazardous to small buildings.

Chaukori village is located in Berinag tehsil of Pithoragarh district of Uttarakhand. It is 86 Km away from district Pithoragarh at an elevation of ± 2010 m.

Stratigraphically, it falls in Askot Crystalline. The Askot Crystalline consists of granite and gneisses. Based on the phase velocity data obtained in frequency domain; the estimated frequency range is within 15.80 - 39.04 Hz and the range of phase velocity is 121-631 ms^{-1} . The average shear wave velocity of Chaukori is 470 ms^{-1} , hence it can be classified as class C i.e. very hard soil and soft rock category. Its estimated average predominant frequency is 4 Hz.

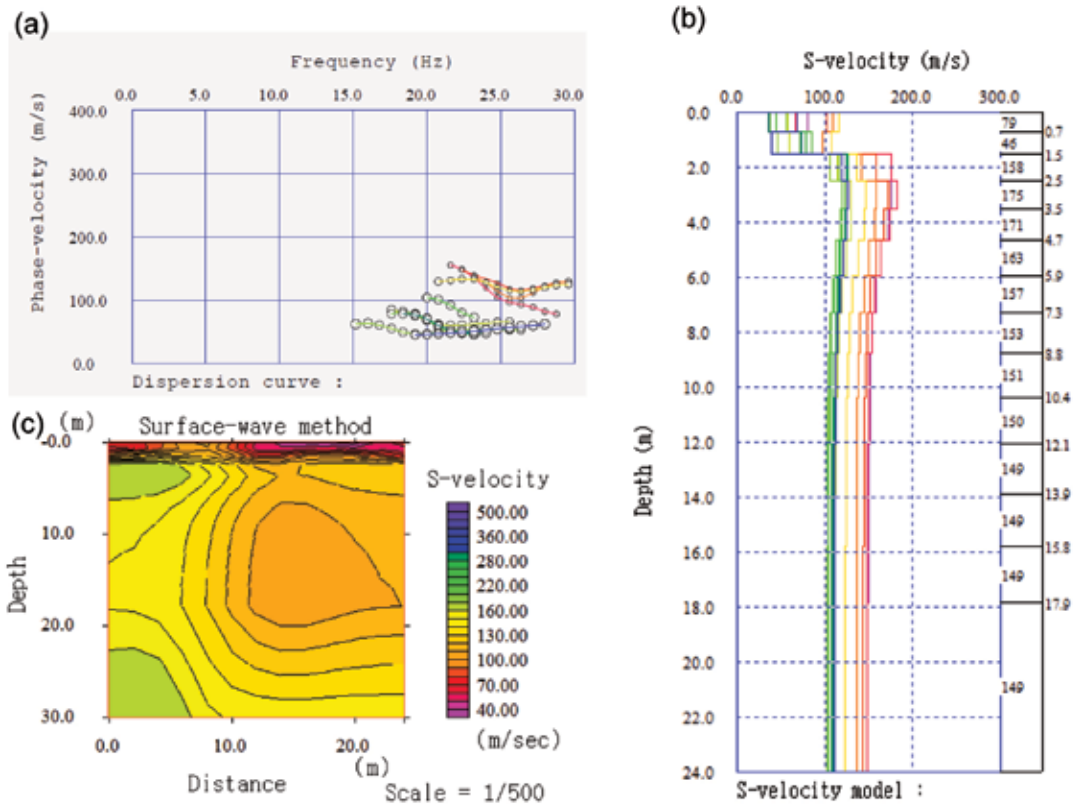


Figure 13. The results obtained at Tejam station (a) dispersion curve obtained from processed record, (b) 1D Shear Wave Velocity Model inverted using trends in (a), and (c) 2D Shear Wave Velocity Model.

Granite and gneisses are moderately suited for high rise structures such as dams and multi-storey buildings and the site is more appropriate for low height buildings e.g. schools, primary health centers etc.

Kamedidevi is famous for the temple of goddess Shakti, situated in Bhageshwar district of Uttarakhand. Stratigraphically, it forms the part of Berinag Formation of Jaunsar Group having quartzite as lithological unit. Based on the phase velocity data obtained in frequency domain; the estimated frequency range is within 11.0 - 35.0 Hz and the range of phase velocity is 157 - 476 ms^{-1} . The average shear wave velocity of Kamedidevi is 380 ms^{-1} , hence it can be classified as class C i.e. very hard soil and soft rock category. Its estimated average predominant frequency is 3 Hz.

Quartzite type of rocks was profiled in this study and significant differences were found in near-surface velocity. This explains part of the measured differences in site amplification. The rock sites are located in average shear wave velocity of 380 ms^{-1} , which are quite significant for low rise buildings rather than high rise buildings.

Tejam village is located in Munsiri tehsil, 74 km away from district Pithoragarh. Stratigraphically it forms the part of Deoban Formation of Tejam Group having quartzite and dolomite as lithological units. Based on the phase

velocity data obtained in frequency domain; the estimated frequency range is within 15.0 – 29.5 Hz and the range of phase velocity is 45 - 155 ms^{-1} . The average shear wave velocity of Tejam is 121 ms^{-1} , hence it can be classified as class E i.e. soft clay category. Its estimated average predominant frequency is 1 Hz. The results reveal that the quartzite inter-bedded with dolomite is not good for high rise structures and multi-storey buildings, however the site is more suited for low rise buildings e.g. weirs, barrages etc.

Thal village lies in Pithoragarh district of Uttarakhand at an elevation of 784 m above mean sea level. It is located 245 km from the state capital Dehradun. It belongs to Mandhali Formation of Tejam Group. The rocks exposed are slate, phyllite, limestone and dolomite. Based on the phase velocity data obtained in frequency domain; the estimated frequency range is within 8.5 - 39.0 Hz and the range of phase velocity is 446 – 576 ms^{-1} . The average shear wave velocity of Thal is 524 ms^{-1} hence it can be classified as class C i.e. very hard soil and soft rock category. Its estimated average predominant frequency is 4 Hz.

Didihat is a busy township in Pithoragarh and is situated at the hill top plains of Digtarh-Bhadigad with Charamgad River flowing below the town. Stratigraphically it falls in Askot Crystalline. The Askot Crystalline is mainly composed of granite and gneisses with some traces of mica-

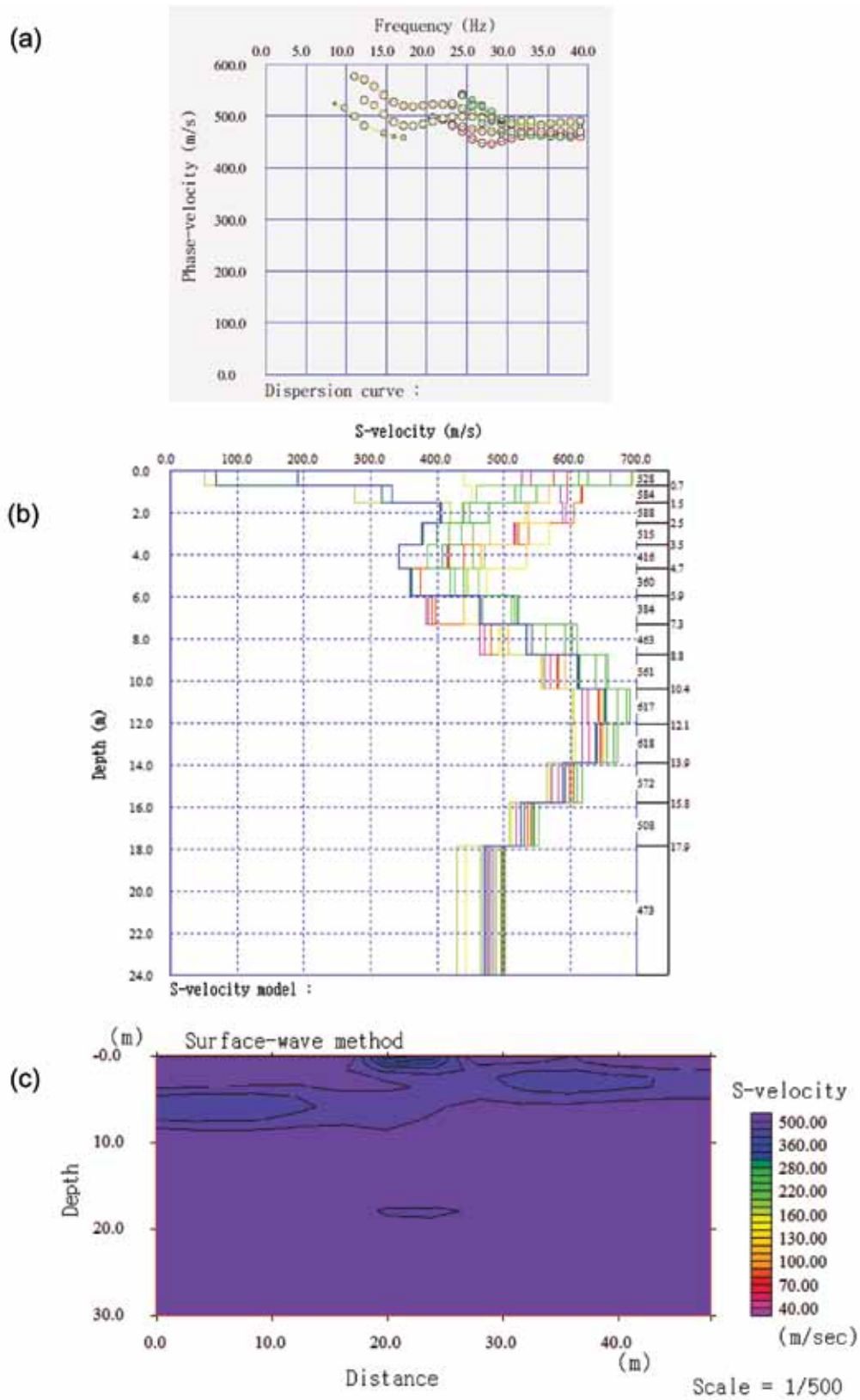


Figure 14. The results obtained at Thal station (a) dispersion curve obtained from processed record, (b) 1D Shear Wave Velocity Model inverted from trends in (a), and (c) 2D Shear Wave Velocity Model.

Table 4. NEHRP site classes (BSSC, 2003)

Site classification	Description	Average shear wave velocity up to 30 m (V_{s30})
A	Very hard rocks	>1500
B	Rocks	$760 < V_{s30} < 1500$
C	Very hard soil and soft rock	$360 < V_{s30} < 760$ Or $N > 50, S_u > 100$ Kpa
D	Hard soil (sands, clays and gravels)	$180 < V_{s30} < 360$ or $50 > N > 15, 100 > S_u > 50$ Kpa
E	Soft clay of thickness about H in site profiles	$V_{s30} < 180$ or $H > 3m(PI > 20), w > 40\%, S_u < 25$ Kpa
F	Soils requiring site – specific evaluations	

H: Thickness, S_u : Undrained Shear Strength, N: Standard Penetration Test Blow Count PI: Plasticity Index, w: Water Content

schist and amphibolite. It is located at an elevation of 1725 m. Based on the phase velocity data obtained in frequency domain; the estimated frequency range is within 14.5 - 38.0 Hz and the range of phase velocity is 200-700 ms^{-1} . The average shear wave velocity of Didihat is 486 ms^{-1} , hence it can be classified as class C i.e. very hard soil and soft rock category. Its estimated average predominant frequency is 4 Hz. The results reveal that the lithology like granite and gneisses with some traces of mica-schist and amphibolite is not good for high rise structures and multi-storey buildings without proper strengthening of material, however the site is more suited for low rise buildings e.g. weirs, barrages etc.

Berinag is situated 160 km from Nainital in Pithoragarh district, Uttarakhand. It gets its name from temple situated at the top of Berinag hill. It is located at an elevation of 1860 m from mean sea level. Stratigraphically it falls in Berinag Formation of Jaunsar Group. The rock exposed is mostly quartzite of Neo-Proterozoic age. Based on the phase velocity data obtained in frequency domain; the estimated frequency range is within 26 - 39 Hz and the range of phase velocity is 307 – 772 ms^{-1} . The average shear wave velocity of Berinag is 712 ms^{-1} , hence it can be classified as class C i.e. very hard soil and soft rock category. Its estimated average predominant frequency is 6.0 Hz.

This type of lithology mostly having quartzite is suitable for the construction of high rise structures such as dams and buildings, however the site is perfectly suitable for moderately to low height buildings e.g. schools, primary health centers etc.

Bhageshwar is well known for its scenic beauty, glaciers, rivers and temples. It is located on the confluence of Sarju and Gomati rivers. It is having rocks of Berinag Formation of Jaunsar Group. Quartzite of Neo Proterozoic age is exposed in this area. Based on the phase velocity data obtained in frequency domain; the estimated frequency range is within 7.0 - 39.0 Hz and phase velocity is within the range of 278 -441 ms^{-1} .

The average shear wave velocity of Bhageshwar is 409 ms^{-1} , hence it can be classified as class C i.e. very hard soil and soft rock category. Its estimated average predominant frequency is 3.0 Hz. This type of lithology mostly having quartzite is averagely suited for construction of high rise structures such as dams and buildings, however the site is perfectly suited for moderately to low rise buildings e.g. schools, primary health centers etc.

According to the site classification by NEHRP, the stations lie in C and E classes as shown in Table 4. Bageshwar, Chaukori, Thal, Berinag, Kameri Devi and Didihat lie in class C with hard to very hard soil category. Tejam with shear wave velocity 120 ms^{-1} is categorised under class E of soft clay category.

CONCLUSION

MASW technique is a non-destructive method to measure shear wave velocity and is useful to measure shear wave velocity in an urban region. This technique gives a 2D shear wave velocity model with depth, which can easily be interpreted. This seismic experiment has given an important information about the velocity model of the various localities in Kumaon Himalayas. Attained 1D and 2D velocity models help in the soil classification in terms of Predominant Frequencies, average shear wave velocities and depth of various layered units. Shear wave velocity increases with depth due to greater degree of compaction and central crystalline formation present in the region. Soil classification is carried out on the basis of the results obtained in terms of average shear wave velocity; showing the importance of study in geotechnical engineering studies. Such analysis could be done for other sites of the Himalayas as well, to obtain the better image of the subsurface structure. Velocity information is also important for simulation of earthquake strong ground motions.

ACKNOWLEDGEMENTS

The authors place on record their sincere thanks to Director (Exploration), ONGC, for his kind permission to publish this work. The authors are thankful to Mr. S.K. Das, Ex-Executive Director, ONGC and Dr. Dinesh Kumar, Professor, Kurukshetra University, Kurukshetra for their valuable suggestions and constructive comments. The views expressed in this work are solely of the authors and do not necessarily reflect the views of ONGC. The work presented in this paper is an outcome of the sponsored project from Department of Science and Technology (DST), Government of India with project reference no. SR/S4/ES-596/2011 and SER-1136-ESD/17-18. Thanks are due to Dr. B.K. Rastogi for useful suggestions. The authors thankfully acknowledge for final refinement and editing by Dr.P.R.Reddy.

Compliance with Ethical Standards

The authors declare that they have no conflict of interest and adhere to copyright norms.

REFERENCE

- Anbazhagan, P, and Sitharam, T.G., 2006. Evaluation of Dynamic Properties and Ground Profiles using MASW: Correlation between Vs and N60, 13th symposium of Earthquake Engineering, Indian Institute of Technology, Roorkee, Paper No. 2008.
- Anderson, J.G., Lee, Y., Zeng, Y. and Day, S., 1996. Control of Strong Motion by the Upper 30 Meters, Bulletin of the Seismological Society of America, v.86, pp: 1749-1759.
- Ariffin, J., Ismail, M.A.M., Tan, C.G., and Murtadza, N.M., 2015. Site Characterization of Marine Clay Deposits in South Seberang Prai, Penang using Combined Active and Passive Multichannel Analysis of Surface Wave (MASW). Soft Soil Engineering International Conference 2015 (SEIC2015) IOP Conf. Series: Materials Science and Engineering, doi:10.1088/1757-899X/136/1/012032.
- B.I.S., 2002. Indian standard criteria for earthquake resistant design of structures, IS 1893: (Part 1) 2002, Part 1 General Provisions and Buildings (Fifth Revision), Bureau of Indian Standards, New Delhi.
- Borcherdt, R.D., 1994. Estimates of site-dependent response spectra for design (methodology and justification). Earthquake Spectra v.10, pp: 617– 653.
- Building Seismic Safety Council, 2003. NEHRP Recommended Provisions for seismic Regulations for New buildings and other Structures, Part1: Provisions, FEMA 368, Federal Emergency Management Agency, Washington, D.C.
- Dobry, R., Borcherdt, R.D., Crouse, C.B., Idriss, I.M., Joyner, W.B., Martin, G.R., Power, M.S., Rinne, E.E. and Seed, R.B., 2000. New site coefficients and site classification system used in recent building seismic code provisions. Earthquake Spectra, v.16, pp: 41- 67.
- Miller, R.D., Xia, J., Park, C.B., and Inanov, J.M., 1999. Using MASW to map bedrock in Olathe, Kansas. Society Exploration Geophysics., pp: 433-436.
- Park, C.B., Miller, R.D., and Xia, J., 1999. Multichannel analysis of surface waves (MASW).Geophysics, v.64, pp: 800–808.
- Satyam, D.N., and Rao, K.S., 2010. Multi-Channel Analysis of Surface Wave (MASW) testing for Dynamic site characterization of Delhi region, 5th International Conference on Recent Advances in Geotechnical Earthquake Engineering and soil dynamics, San Diego, California, I, pp: 327-330.
- Seshunarayana, T, and Sundararajan, N., 2004. Evaluation of 5th Conference & Exposition on Petroleum Geophysics. Hyderabad-2004, India, pp: 642-646.
- Shafiee, A., and Azadi, A., 2006. Shear-wave velocity characteristics of geological units throughout Tehran City, Iran. Journal of Asian Earth Sciences.
- Thitimakorn, T, and Channoo, S., 2012. Shear Wave Velocity of Soils and NEHRP Site Classification Map of Chiangrai City, Northern Thailand. Electronic Journal of Geotechnical Engineering, v.17, pp: 2891-2894.
- Trivedi, S.S., Rao, K.S., Gupta, K.K., and Rathod, G.W., 2009. Mapping average shear wave velocity for Ahmedabad soil sites: A case study. IGC, Guntur, India.
- Valdiya, K.S., 1980. Geology of Kumaun Lesser Himalaya, Interim Record: Dehradun. Wadia Institute of Himalayan Geology, pp: 289.
- Wen, R., Shi, D., and Ren, Y., 2008. Site Classification based on Geological Genesis and its application. The 14th World Conference on Earthquake Engineering, Beijing, China.
- Xia, J., Miller, R.D., and Park, C.B., 1999. Estimation of near-surface shear wave velocity by inversion of Rayleigh waves. Geophysics, v.64, pp: 691-700.

Received on: 23.10.17; Revised on: 19.1.18; Re revised on: 2.2.18; Accepted on: 10.2.18

Application of Crosshole Seismic technique and MASW at Heavy Engineering Site, near Mahabalipuram, Tamilnadu

K. Satish Kumar*, P. Pavan Kishore, G.S. Srinivas, P. Prabhakara Prasad and T. Seshunarayana

CSIR-NGRI, Uppal Road, Hyderabad 500007

*Corresponding Author: satish_marine777@yahoo.co.in

ABSTRACT

Seismic velocities (V_p and V_s) of the subsurface play a vital role in designing the engineering parameters for major civil engineering structures. A case history is presented from the charnockite province in east coast of India near Mahabalipuram, Tamilnadu. As a part of the feasibility study Crosshole seismic and Multi Channel Analysis of Surface waves (MASW) surveys were conducted near a heavy engineering construction site. V_p and V_s are determined up to 55 m depth with an interval of 1.5 m. Dynamic elastic constants, average shear wave velocity, predominant frequency and amplification of the area were calculated. Velocity data reveals that soil cover composition varies with depth, namely, highly weathered, moderately weathered and fresh Charnockite occur successively from top to bottom in the subsurface. Dynamic elastic constants, average shear wave velocity, predominant frequency, and amplification are estimated.

Key words: V_p and V_s , crosshole seismics, MASW and Charnockites

INTRODUCTION

Estimation of elastic moduli and seismic velocities in hard rock terrain is essential to analyze the foundation vibrations, earthquake resistance and geotechnical problems at heavy civil engineering structure sites. Usually, these constants are calculated with the help of engineering methods (Cone Penetration test, Soil Penetration test etc.), geophysical methods (Seismic downhole, Seismic uphole, Seismic Refraction, Crosshole Seismics, etc.) and laboratory methods (ultrasonic Pulse Transmission). Compared to engineering and laboratory methods, the geophysical techniques have been proved to be more reliable, non-destructive and cost-effective (Hassani et al., 1997; Turesson, 2006). Laboratory methods have certain limitations (core samples are free from the overburden stress, and core samples are too small as compared to relative rock heterogeneity) to determine the seismic velocities and elastic moduli of rock mass (Swain, 1962). The cross-hole seismic technique provides good results compared to laboratory methods in certain cases (Young, 1961). Estimation of seismic velocities using Crosshole method yielded best results at heavy engineering structure sites (Dobecki, 1979). This technique/ method also provide attenuation properties of the rock mass, which play a key role in determining the quality of the rock (Balakrishna et al., 1981). In view of the above, Crosshole seismic technique was employed at Mahabalipuram, Tamilnadu (Figure 1) to estimate the in situ seismic velocities and elastic moduli of the Charnockite basement and estimating the weathering profile of the subsurface. This study was carried out in one set of boreholes, which includes one-

shot hole (BH-S) and two receiver holes (BH-R1 & BH-R2). The P & S wave velocities are calculated up to 55 m depth with an interval of 1.5 m. The laboratory estimated density values are used to calculate the elastic moduli (Rao et al., 2006). The MASW test (Park et al., 1999; Miller et al., 1999; Seshunarayan et al., 2008; Seshunarayan et al., 2008; Satish Kumar et al., 2010) was also conducted to know the shear wave velocities of top layers at places where cross-hole technique was not possible to conduct due to the presence of borehole casing. In this paper, P&S wave velocities, Dynamic elastic constants, average shear wave velocity, predominant frequency, and amplification of the area were calculated.

GEOLOGICAL SETTING

The study area is located in Eastern Dharwar Craton and consists of Tonalite-Trondhjemite-Granodiorite (TTG) gneisses, Charnockites, schist belts and younger granites (Rogers, 1986). The present study area is characterized by Charnockite rocks containing quartz, feldspar, hypersthene, garnet, and mica (Holland, 1990). The Charnockite rock samples collected from the excavated portions indicates, they are inter-layered and contain garnet, biotite, muscovite, pyrites and phlogopite mica. Three different shades of Charnockites are seen in this area such as blue, gray and black, and they are particularly medium grained (Elango et al., 2004). The Charnockite rocks exposed in the area are fresh with slight weathering. Although altered materials are also seen mostly along the fractures, it is mainly due to weathering and leaching (Figure 1).

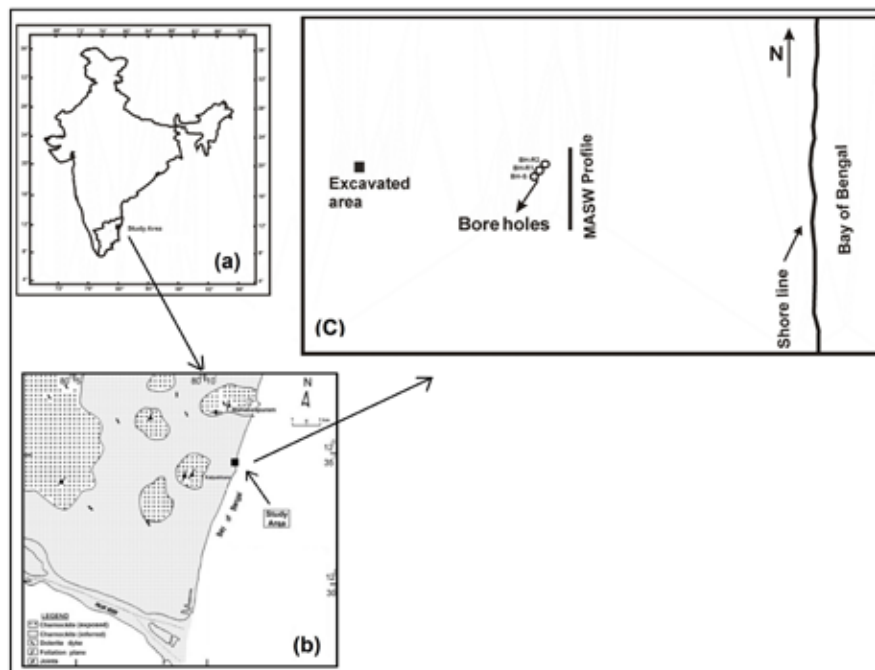


Figure 1. shows (a) Location of the study area, b) Regional Geological map of the study area (after Rao et al., 2006), c) Location of three borehole, MASW profile, and excavated area.

The lithological information obtained from the drill logs named BH-S, BH-R1 and BH-R2 correspond to alluvium, moderately weathered Charnockite and fresh Charnockite occurs successively from top to bottom (Figure 4).

METHODOLOGY

Cross-hole seismic survey was conducted across three boreholes BH-S, BH-R1 & BH-R2. Each borehole has an inner diameter of three inches and three meters of horizontal separation between two holes. Due to collapsing nature of the upper sandy alluvium layer, these boreholes have been iron cased up to the depth of 16.5 m. Explosives with “seismic” detonator have been lowered in to TBH-S borehole and detonated for generation of elastic waves. Shooting was conducted from the depth of 55.5 m to 16.5 m with an interval of 1.5 m in BH-S. 10 Hz three component geophones for generation of P, SV, and SH waves are used as receivers in other two boreholes (BH-R1 & BH-R2). Seismic data have been acquired using a 24 channel engineering Seismograph (Strata View, manufactured by Geometrics Inc, USA). In this survey, seismic energy is generated at the desired depth of one borehole and the time for that energy to travel to another borehole through the subsurface layer is measured at the same depth level. From the borehole spacing and travel time, the velocity of the seismic wave (P & S) is computed (Woods, 1978; Woods, 1994; Seshunarayana et al., 2001; Seshunarayana et al., 2005; Crice, 2002; ASTM, 2000).

Inline geometry technique has been adopted to eliminate the errors caused by the inherent delay associated with the electrical detonator, (Butler et al., 1981). Moving the source and the receivers to different depths, the travel time of the wave between the source and receivers are recorded (Seshunarayana et al., 2001). To calculate the elastic properties, laboratory mean density value of 2.722 gm/cc is taken as reference (Rao et al., 2006). Elastic constants are calculated from the velocity data of Crosshole seismic survey using standard relations (Timoshenko and Goodier, 1970; Sharma 1986, Crice, 2002).

The shear wave (S-wave) velocity section was obtained by modeling the Multichannel Analysis of Surface Waves (MASW) data (Park et al., 1999; Miller et al., 1999). Rayleigh wave data (rich in ground-roll) has been recorded using an engineering Seismograph (Strata View, manufactured by Geometrics Inc, USA) and 24 low-frequency vertical geophones with a natural frequency of 4.5 Hz, placed at 1 m interval. Acoustic energy was generated using a 10-kg sledgehammer hit on a metal plate. The 5 m near offset was chosen depending upon the site condition (Xu and Butt, 2006). The acquired surface wave data was processed using the Standard procedures by the Surfseis software. Each set of Rayleigh wave data (shot gather) was transformed from time domain to frequency domain to generate dispersion curves (frequency vs. phase velocity), which have been further transformed into S-wave velocity-depth profile through an inversion process. Each set of velocity-depth profiles was arranged in sequential

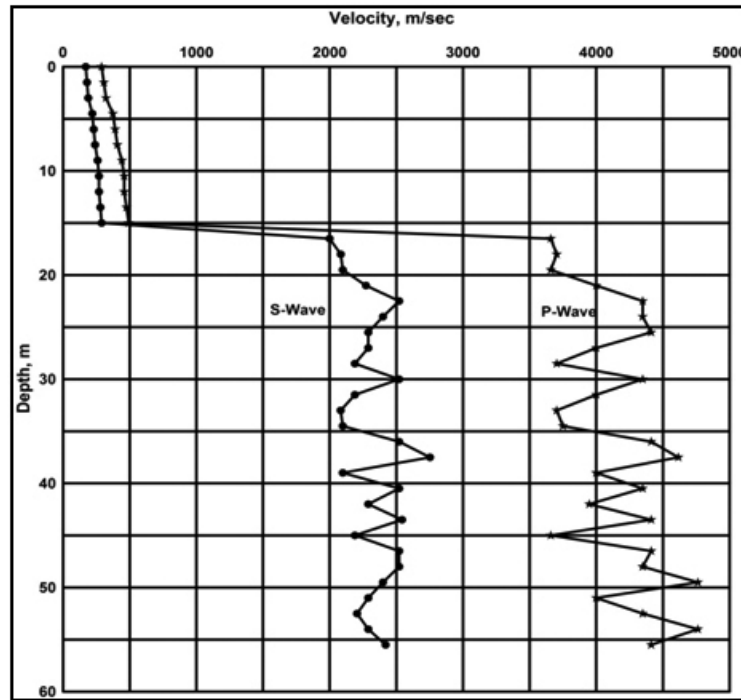


Figure 2. Shows the plot of calculated P & S wave velocities of the subsurface concerning depth. (m/s: meter/second).

order from the first shot station to form a 2-D shear wave velocity field. The depth-velocity results of the MASW are commonly found to be in good agreement with the borehole velocity measurements (Xia et al., 2002). Probing depth of the MASW investigation, in this study is 15 m, which is dependent on the energy source parameters (e.g., frequency) and the mechanical properties of subsurface materials. P- wave velocity of 15 m column was obtained by the standard relation of V_p and V_s .

Shear wave velocity is known to be an important parameter to access the dynamic properties of the site. The National Earthquake Hazard Reduction Program (NEHRP) provision (BSSC, 1994) and new 1997 uniform building code classify the sites depending on the average shear wave velocity of the site (example: Velocity column up to 30 m) (Dobry et al., 2000; Kanli et al., 2006). The classification of sites based on harmonic mean shear wave velocity is given by Federal Emergency Management Agency, (FEMA, 1997). This classification is applicable in determining the seismic coefficients for earthquake resistant structure design. Average shear wave velocity of the site using MASW test was calculated as follows.

$$V_s^{Average} = \frac{\sum_{i=1}^n d_i}{\sum_{i=1}^n d_i / V_{si}}$$

Where,

i is a layer between 1 to n

d_i is a thickness of a layer

V_{si} is an S-wave velocity in m/s of a layer

The average shear wave velocity up to top 30 m of the area computed using MASW and crosshole data is 410 m/s.

Amplification and Predominant Frequency

Local amplification of the ground is often controlled by the soft surface layer which leads to trapping of seismic energy due to the impedance contrast between the soft surface soils and the underlying bedrock. The soil properties and thicknesses of surface layers play a key role in influencing the ground motion. The amplification depends on the resonance between the frequency content of the earthquake waves and the natural period(s) of the ground layers. The predominant frequency and amplification are proportional to the layer thickness and impedance contrast, respectively. Shima (1978) found that the analytically calculated amplification factor is linearly related to the ratio of shear wave velocity of the surface layer to that of bedrock. The period of vibration corresponding to the fundamental frequency is called characteristic site period. The value indicates a period of vibration at which the most significant amplification would occur. Borchardt, et al., (1991) proposed relation between the average shear wave velocity of surficial layers and the relative amplification as given in equation.

$$AHSA = 700/V_s^{30}$$

AHSA is the average horizontal spectral amplification, V_s^{30} is the average shear wave velocity (m/s) over a depth of 30m.

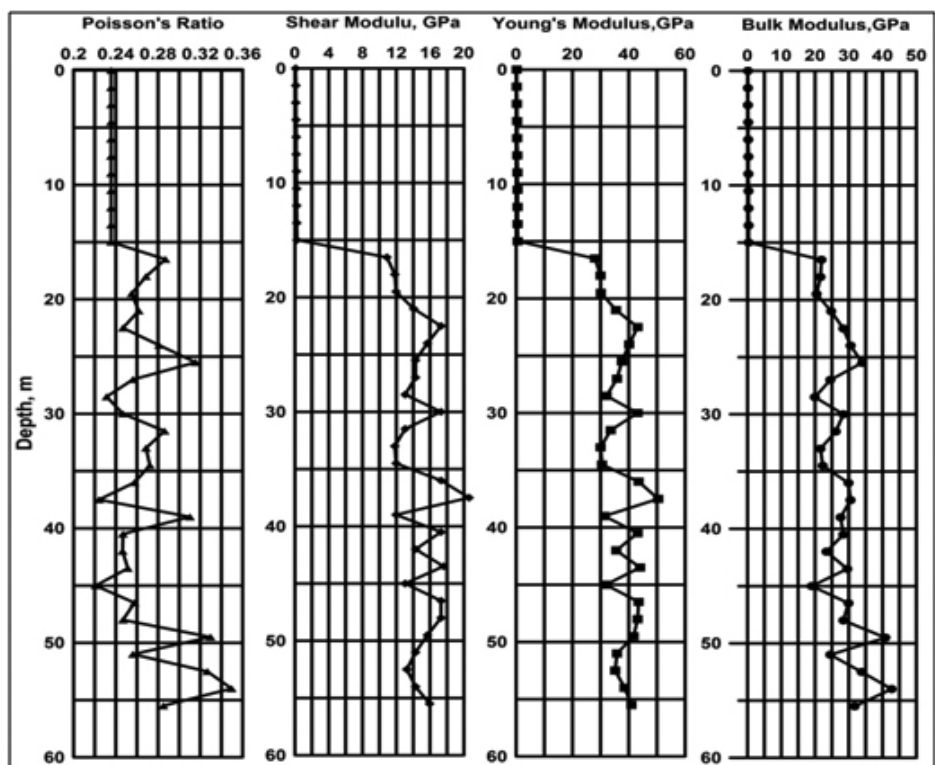


Figure 3. Shows the plot of calculated elastic moduli ((GPa: Giga Pascal)).

The calculated horizontal spectral amplification of the site is 1.7.

The fundamental site period (T_s) corresponds to the first mode of vibration of the soil deposit. It is one of the parameters for seismic microzonation. It is governed by the thickness and the shear wave velocity of the soil layer and is calculated by using the expression given by Kramer (1996). The period of vibration corresponding to the fundamental frequency is called the characteristic site period. We have estimated the frequencies at which the seismic waves are expected to resonate in the soil column of 30 m depth.

The predominant frequencies at which the seismic waves are expected to resonate in the soil column of 30 m depth are computed by using the frequency-shear wave velocity relationships (Kandpal et al., 2009; Trupti et al., 2013). To estimate the frequencies at which the seismic waves are expected to resonate in the soil column of 30 m depth, the simple relationship between the shear wave velocity (β) of the sediment column (30 m), is

$$f = \beta/4H$$

Where, β is the average shear wave velocity,

H is the thickness of the sediments.

The estimated predominant frequency of the area is 3.42 Hz.

RESULTS

The velocity model prepared based on the field studies is shown in Figure 2. P-wave and corresponding S-wave

velocities of the formation are calculated by using interval times of the two receivers and distance between the boreholes. The calculated P- wave velocity (V_p) is in the range of 3660 m/s to 4750 m/s, and the S wave velocities (V_s) vary in the range of 2000m/s to 2600m/s. The calculated elastic constants such as $\sigma = 0.16-0.29$, $E = 28.02\text{GPa}-42.8\text{GPa}$, $G = 10.89\text{GPa}-18.4\text{GPa}$ and $k = 20.28\text{GPa}-24.81\text{GPa}$ of the Charnockites are shown in Figure 3. V_p and V_s velocity in alluvium, are estimated. From the surface and bore hole studies it is inferred that the alluvial soils are upto depth of about 16 m and moderately weathered Charnockite are up to about 20 m depth. Beyond 20 m depth it is fresh Charnockite rock (Figure 2) from MASW data (Figure 4). It is interpreted from Figure 2. Moderately weathered Charnockite is characterized by 2000 to 3600 m/sec P-wave velocities and fresh charnockite range between $\sim 3660 - 4750$ m/sec. The thickness of this layer is 1.5m. Fresh Charnockite present from 21 m to 55.5 m depth has V_p and V_s velocities of ~ 4000 m/sec to 4750 m/sec and ~ 2270 m/sec to 2600 m/sec, respectively. Minor fractures or deviations in the borehole are characterized by low velocities (both V_p & V_s) within the higher velocities as shown in Figure 2. A 50-m-long (N-S oriented) shear wave velocity section of the study area is shown in Figure 5. It is inferred from this section, that the soil cover and weathering cap of varying consolidation are characterized by S-wave velocities of approximately $\sim 160-240$ m/s, and $\sim 240-350$ m/s, respectively. The soil cover and highly

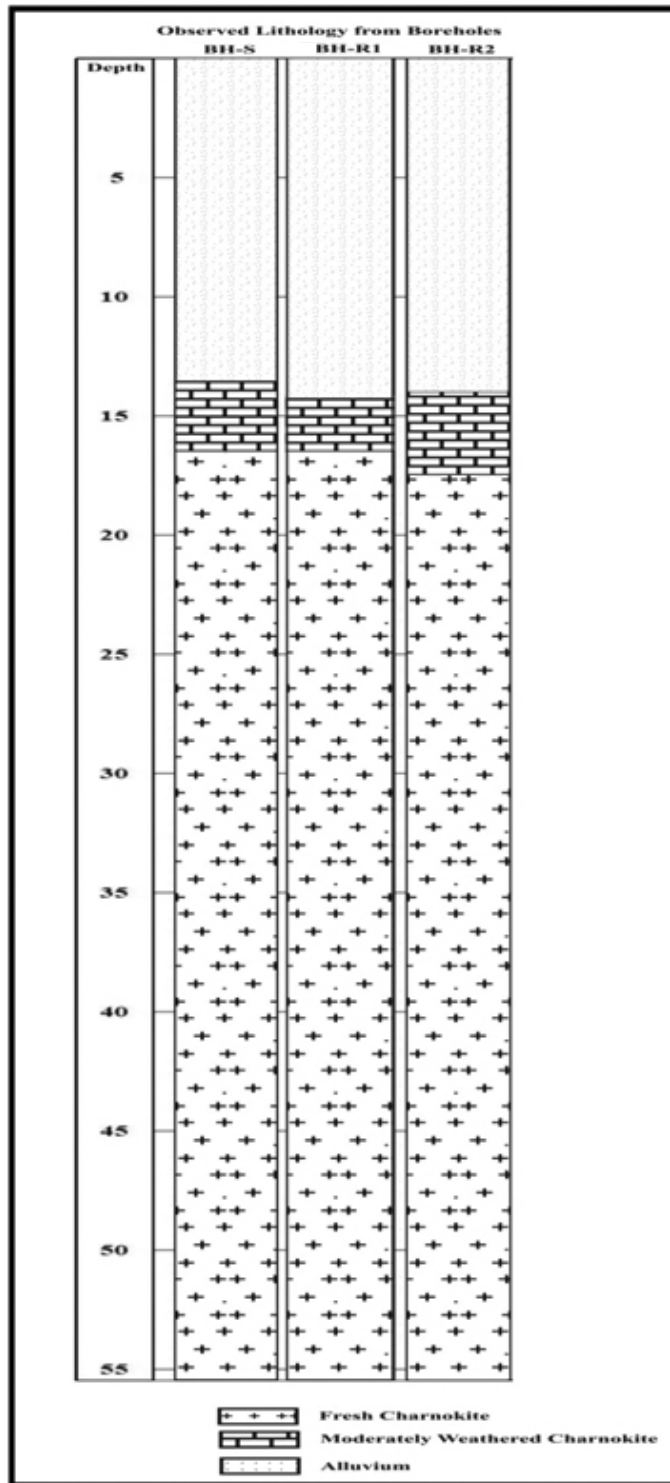


Figure 4. shows the observed lithology from core log data and Interpreted lithology from MASW and Crosshole survey. (BH-S: Source Borehole, BH-R1: Receiver Borehole one, BH-R2: Receiver Borehole two).

weathered Charnockite occur successively from top to bottom. The thickness of soil cover varies from surface to 7 m depth, and the highly weathered cap is present from

7 m to 15 m. The average shear wave velocity of site up to 30 m is 410 m/sec, whereas amplification and predominant frequency of the area are 1.7 and 3.42 Hz, respectively.

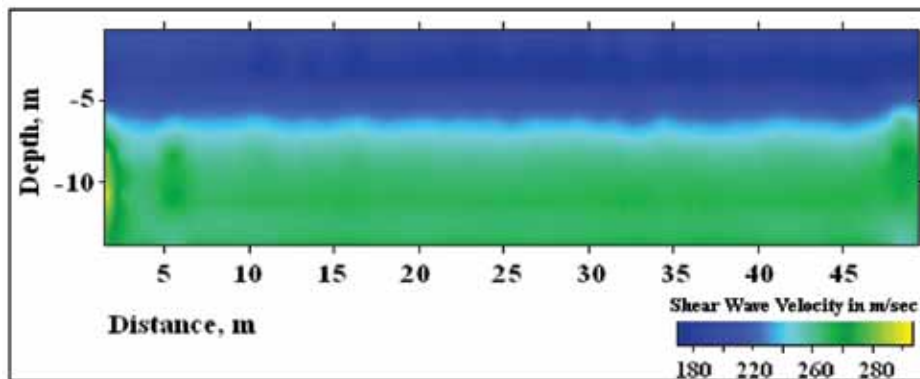


Figure 5. Shows the Shear wave velocity field consists of two velocity layers. It is interpreted that the soil cover and weathering cap of varying consolidation are characterized by an S-wave velocity of $\sim 160\text{-}240$ m/s, and $\sim 240\text{-}350$ m/s, respectively.

CONCLUSION

It is observed from Crosshole seismic and MASW studies that the present study area occupied by alluvium up to the depth of 15 m is underlain by a weathered and hard Charnockitic rocks. Dynamic elastic constants, average shear wave velocity, predominant frequency, and amplification are estimated through field studies.

ACKNOWLEDGEMENTS

The authors are grateful to Director, CSIR-NGRI for the support at various stages of the work. In the course of the project formulation, execution and for writing this paper, various persons of the Engineering Geophysics Division of NGRI unreservedly rendered their help, which is gratefully acknowledged. Authors express sincere thanks to D.B.Mahajan, M/s DBM Geotechnics and Constructions Pvt. Ltd., for sponsoring the project. This study has been supported by CSIR-NGRI Fast Track Translatory (FTT) Project. Thanks are due to Dr.P.R.Reddy for apt reviewing and final editing.

Compliance with Ethical Standards

The authors declare that they have no conflict of interest and adhere to copyright norms.

REFERENCES

American Society of Testing and Materials (ASTM)., 2000. Standard test methods for Crosshole seismic testing, Designated 4428/D4428M-84 report.

Balakrishna, S., Ramana,Y.V., Varadarajan, G., Seshunarayana, T., Subrahmanyam, K., and Prabhakara Prasad, P., 1981. Propagation velocity of rocks of Panchpatmani region by laboratory and field geophysical methods, un published NGRI Tech.Report.No.81-184 and 185.

Borcherdt, R.D., Wentworth, C.M., Glassmoyer, G., Fumal, T., Mork, P and Gibbs, J., 1991. On the Observation,

Characterization, and Predictive GIS Mapping of Ground Response in the San Francisco Bay Region, California, Proc 4th International Conference on Seismic Zonation, Stanford, California, v.3, pp: 545-552.

Building Seismic Safety Council (BSSC), 1994. NEHRP Recommended provisions for the development of seismic regulations for new buildings, part I: Provisions, developed for the Federal Emergency Management Agency, Washington D.C.

Butler, D.K., Joseph, R. and Curro, J.R., 1981. Crosshole seismic testing-procedures and pitfalls, v.46, no.1, pp: 23-29.

Crice Doug., 2002. Borehole shear wave surveys for engineering site investigations, open document of Geostuff, pp: 1-14, available in <http://www.geostuff.com/shearwave2.pdf>.

Dobecki, T.L., 1979. Measurement of in-situ dynamic properties in relation to geological conditions: in reviews in engineering geology, Geological Society of America, v.4, pp: 201ff.

Dobry, R., Borchedt, R.D., Crouse, C.B., Idriss, I.M., Joyner, W.B., Martin, G.R., Power, M.S., Rinne and Seed, R.B., 2000. New site coefficients and site classification system used in recent building seismic code provisions, Earthquake Spectra, v.16, no.1, pp: 41-67.

Elango, L., Sanjeevi, S., Nagendra, R., and Selvan, T.A., 2004. A report on geological mapping of PFBR project site at Mahabalipuram, Tamilnadu. un published report of Anna University, Chennai.

Federal Emergency Management Agency (FEMA)., 1997. Multi Hazard Identification and Assessment. FEMA. Washington, D.C.

Hassani, F.P, Guevremont, P., Momayezl, M., Sadril, A., Saleh, K., 1997. Application of nondestructive evaluation techniques on concrete dams, Int. J. Rock Mech. & Min. Sci. v. 34, no.3-4, pp: 125.

Holland, T.H., 1900. The Charnokite series, a group of Achaean hypersthene rocks in peninsular India, Mem.Geol.Surv. India, v. 28, pp: 182-249.

Kandpal G.C., John, B., Joshi, K.C., 2009. Geotechnical Studies in relation to Seismic Microzonation of Union Territory of Chandigarh. J.Ind.Geophys.Union, v.13, no.2, pp: 75-83.

Kanli, A.I., Tildy, P., Pronay, Z., Pinar, A., and Hemann, L., 2006. V_s^{30} mapping and soil classification for site effect evaluation

Application of Crosshole Seismic technique and MASW at Heavy Engineering Site,
near Mahabalipuram, Tamilnadu

- in Dinar region, SW Turkey, *Geophysics J.Int.*, v.165, pp: 223-235.
- Kramer, S.L., 1996. *Geotechnical earthquake engineering*. Prentice Hall Publishers, Englewood Cliffs, New Jersey.
- Miller, R.D., Xia, J., Park, C.B., and Ivanov, J., 1999. Multichannel analysis of surface waves to map bedrock, *The Leading Edge*, v.18, pp: 1392-1396.
- Park, C.B., Miller, R.D., and Xia, J., 1999. Multi-channel analysis of surface waves, *Geophysics*, v.64, pp: 800-808.
- Rao, M.V.M.S., Prasanna Lakshmi, K.J., Sarma, L.P., and Chary, K.B., 2006. Elastic properties of granulite facies rocks of Mahabalipuram, Tamil Nadu, India, *J. Earth Syst. Sci.*, v.115, no.6, pp: 673-683.
- Rogers, J.J.W., 1986. Dharwar Craton and assembly of Peninsular India. *Jour.Geol.* v.94, pp: 129-143.
- Satish Kumar, K., Senthil Kumar, P., Prabhakara Prasad, P., Srinivas, K.N.S.S.S. Mysaiah.D and Seshunarayana, T., 2010. Proceedings of ASCE, GeoFlorida, 2010. *Advances in Analysis, Modeling & Design*, edited by dante Fratta, pp: 140.
- Seshunarayana, T., Prabhakara Prasad, P., Prasad Rao, S.V.V., Subrahmanyam, K., and Varadarajan, G., 2001. Crosshole velocity measurement to assess the nature of rock mass on which to erect a heavy Buddha statue in Hyderabad. *Geol. Soc. India*, v.58, pp: 65-68.
- Seshunarayana, T., Prabhakara Prasad, P., Satish Kumar, K., and Kiran Kumar Reddy., 2005. Crosshole seismic survey near Mamallapuram, Tamilnadu, unpublished report of NGRI, Hyderabad, T.R.No.NGRI-2005-EXP-497. 13.
- Seshunarayana, T., Satish Kumar, K., Deenanadh, S., Rama Mohan Rao, Y., and Senthil Kumar, P., 2008. Subsurface imaging of dykes in Hyderabad granite terrain using multichannel analysis of surface waves, in: *Indian Dykes*, edited by R.K.Srivastava, Ch. Sivaji and N.V.Chalapathi Rao, Narosa Publishing House, New Delhi, 8 pages.
- Seshunarayana, T., Senthil Kumar, P., Sampath Rao, V., Mysaiah, D., Satish Kumar, K., and Pavan Kishore, P., 2008. Multichannel Analysis of Surface Waves Reveals Shear Zones and Fractures in a Shallow Granite Basement: Wailapally Watershed Near Hyderabad. *Journal of Geol. Soc. India* v.71, pp: 261-265.
- Sharma P.V., 1986. *Geophysical Methods in Geology*, Elsevier Science Publishers, 2nd edition, pp: 442.
- Shima, E., 1978. Seismic Microzonation Map of Tokyo, Proc. 2nd International Conference on Microzonation, v.1, pp: 433-443.
- Swain, R.J., 1962. Recent techniques for determination of "in-situ" elastic properties and measurement of motion amplification in layered media. *Geophysics*, v.27, no.2, pp: 237-241.
- Timoshenko S.P., and Goodier J.N., 1970. *In Theory of Elasticity*, McGraw-Hill, New York, 3rd edition.
- Trupti, S., Goverdhan, K., Srinivas, K.N.S.S.S., Prabhakar Prasad, P., and Seshunarayana, T., 2013. Site classification of Pondicherry using shear-wave velocity and horizontal-to-vertical spectral ratio, *Natural Hazards*, v.69, pp: 953-964. DOI:10.1007/s11069-013-0746-3.
- Turesson, A., 2006. A comparison of methods for the analysis of Compressional, shear, and surface wave seismic data, and determinant of shear modulus. *Journal of Applied Geophysics*, v.61, no.2, pp: 83-91.
- Woods, R.D., 1978. *Measurement of Dynamic Soil Properties, State of the Art Report: Proceedings of the ASCE Geotechnical Engineering Division Specialty Conference, Earthquake Engineering and Soil Dynamics*, Pasadena, CA, v.1, pp: 91-178.
- Woods, R.D., 1994. *Borehole Methods in Shallow Seismic Exploration: Geophysical Characterization of Sites*, Volume prepared by ISSMFE, Technical Committee # 10, XIII ICSMFE, New Delhi, India, Richard Woods, Editor, pp: 91-100.
- Xia, J., Miller, R.D., Park, C.B., and Tian, G., 2002. Determining Q of near-surface materials from Rayleigh waves, *J. Applied Geophysics*, v.51, pp: 121-129.
- Xu, C., and Butt, S.D., 2006. Evaluation of MASW techniques to image steeply dipping cavities in laterally inhomogeneous terrain, *J. Applied Geophysics*, v.59, pp: 106-116.
- Young, D.D., 1961. *In-situ measurements of elastic properties: University of California Lawrence Radiation Laboratory Report UCR L-6477*.

Received on: 4.1.18; Revised on: 19.1.18; Re revised on: 15.2.18; Accepted on: 18.2.18

Application of Shallow Seismic Studies for Civil Engineering Applications: A case study from Chennai city, Tamilnadu

G.S. Srinivas, P.Shiva Shankar, K. Satish Kumar*, S.Trupti, P.Pavan Kishore,
K.N.S.S.Srinivas and T. Seshunarayana

CSIR-NGRI, Uppal Road, Hyderabad-500007, India.

*Corresponding Author: satish_marine777@yahoo.co.in

ABSTRACT

Shear wave (V_s) and P-wave (V_p) velocities were estimated for the evaluation of the sub-surface structure along four profiles at CSIR-SERC Campus in Chennai city to aid in the structural design for a proposed high rise building. These velocities are essential parameters for determining the dynamic properties of soil in the shallow subsurface. Dynamic properties, thickness of soil, depth to basement and the associated in-homogeneities such as fractures, joints, voids and shear zones, play a very important role in design and construction of civil structures. Multichannel analysis of surface waves (MASW) and refraction methods were used for the estimation of V_s and V_p respectively to decipher the subsurface structure in detail. From the Seismic velocity-depth sections, the near surface distribution of rocks, soils and their physical properties were determined to characterize the site conditions. The results indicate a three layered structure with P-wave velocities of 400-500 m/s, 2700-3100 m/s and 5300-5500 m/s and S-wave velocities of >200 m/s, 200 to 300 m/s and >400 m/s up to a depth of 30 m. The obtained results are well correlating with the available borehole lithological data. These results are helpful in civil engineering applications in estimation of elastic properties, depth to bedrock and useful in planning of high rise structures.

Key words: Shear wave velocity, P wave velocity, bedrock, MASW and Structures.

INTRODUCTION

Several geophysical methods have been suggested for shallow near-surface characterization and in-situ measurement of P- and S- wave velocities using different configurations, processing techniques and inversion algorithms. The frequently used techniques are seismic refraction, spectral analysis of surface waves (SASW) and multichannel analysis of surface waves (MASW). MASW is a non-destructive and economical geophysical method, mostly used in geotechnical engineering for the measurement of shear wave velocity, evaluation of dynamic properties, subsurface structure and related studies. (Park et al., 1998,1999; Xia et al., 1999, 2000, 2002; Miller et al., 1999; Kanli et al., 2006).

Damage due to seismic waves depends on local ground conditions/soil type and its thickness apart from the type of constructions. The soft deposits (clay and sands along the coast and rivers) generally amplify ground motion thereby increasing the damage during an earthquake. Hence, the geotechnical characteristics of (V_p and V_s of soils, rocks and pavement) shallow material and its impact on seismic wave propagation are of great importance in groundwater, geo technical engineering, seismic hazard assessment and microzonation studies. The most challenging part of these investigations is to collect the data needed with the minimum expenditure and time (Oyedele et al., 2012).

The primary objective of this study is the identification of bedrock depth, which is the solid rock that lies below

loose material, such as sand, top soil, gravel, or clay. It is very much essential to identify the bedrock depth, in order to estimate the impact of local site conditions in the event of an earthquake. In general, the soil cover over the bedrock may attenuate or amplify the earthquake motion depending upon geotechnical characteristics, their depth and composition of the soil. Usually the younger soft soil tends to amplify the ground motion as compared to the older, more competent soils or bedrock. The P wave Seismic refraction method is used to decipher the structure of the underlying bedrock. In refraction, seismic wave velocity is computed based on the first arrival times. These velocities can assist in the interpretation of geological layers as well as estimation of bed rock. Seismic refraction is a quantitative technique to determine the bedrock depth and lithological characteristics. MASW is very effective in delineation of subsurface features, any stratigraphic changes as well as the top rock and the associated features. In the present study, seismic refraction and MASW methods are used for the identification of bedrock depth and characterize the subsurface.

GEOLOGY OF THE AREA

The study area falls between 12° 59' 12.12"N to 12° 59' 13.37"N latitude and 80° 14' 44.24"N to 80° 14' 46.18"N longitude along the SE coast of India and in the NE corner of Tamil Nadu. The sea coast is flat and comprises of sandy structures for about one kilometre from the shore. Many

parts of the city in the east and southern regions comprise of shallow bedrock (which is crystalline in nature) while some other areas towards west and north have Gondwana deposits below the alluvium (Ballukraya and Ravi, 1994). Most of the area is covered by Pleistocene/Recent alluvium, which has been deposited by the two rivers in the area, Coovum and Adyar. The alluvium mostly comprises of clay, sand, sandy clay and boulder/gravel zones occasionally. In general, sand is found along the river banks and coasts. The southern part of the study area has occurrences of Igneous / metamorphic rocks. The eastern and northern parts of the study area have marine sediments comprising of clay-silt sands and charnockites. The western part of the area is seen to be having alluvium and sedimentary rocks, along with a thin layer of laterite at some locations. Small boulders and rounded pebbles are seen at several locations at different depths. Thus, in general, It is observed that, the eastern side of the coastal zone is predominantly sandy, while the north western side is predominantly clayey in nature (Boominathan et al., 2008).

DATA ACQUISITION AND PROCESSING

Seismic refraction survey and MASW tests were conducted along four profiles. Two profiles (No-1 & 2) were laid in "E-W" another two profiles (No-3 & 4) were laid in "S-N" direction. The data was acquired using 24-channel seismograph with the following acquisition parameters:

For refraction survey, number 4.5 Hz geophones; 24; Geophone interval: 5m; spread length:115m; number of shots:5 (all in line shots, 2 far offset shots at 30m on either side, 2 near offset shots at 5m on either side and 1 shot at the middle of the spread); Sampling interval: 0.25m sec; Record length: 0.5sec.

The data processing involves picking the first arrival times from the time traces recorded from all shot points. From these arrival times the Time-Distance Curve is generated for each profile. The Time-Term inversion method, a standard inversion iterative method is a linear Least-Squares approach to determine the best discrete-layer solution to the data set (Bath, 1978). The time term inversion technique is applied to the travel time to estimate the velocities of different layers and the corresponding depths of the layers. It is a simple travel-time inversion enveloped by Scheidegger and Willmore (1957) and has been used widely for seismic refraction studies in the 1960-70s (Willmore and Bancroft, 1960; Berry and West, 1966; Meru, 1966; Yoshii and Asano, 1972).

MASW data was processing using "SurSeis software package" (Kansas Geological Society Make). The data has been subjected to following standard processing steps: (i) conversion of the field (SEG-2) data of Kansas Geological Society data format (ii) removal of bad traces through

muting procedure (iii) generation of dispersive curve from filtered data (iv) extraction of dispersive curve (vii) Inversion of each dispersion curve for 1D shear wave velocity and finally staking of each 1D shear wave velocity curves for 2D shear wave velocity with depth.

RESULTS

The obtained P- and S- wave velocities with depth of four profiles are presented in Figure 1 to 4. P- and S- wave velocity depth sections of profile 1 in E-W direction shown in Figure 1. The P-wave velocity depth section of profile 1 shows the three (Figure 1a) different velocity layers. The average thickness of first layer is 3 m with a velocity of 500 m/s, the second layer is spreading between 3 m to 11 m with a velocity of 2700 m/s and the third layer velocity is 5400 m/s. It is also inferred from that the shear wave velocity depth section (Figure 1b), that the thickness of top layer is around 3 m with a velocity of < 200 m/s, depth to the second layer is 3 m with a velocity of 200 m/s to 500 m/s and depth to the third layer is 12 m with a velocity of >500 m/s.

It is observed from the P- and S- wave velocity depth sections of profile 1, top soil is present up to a depth of 3 m below that weathered charnockite is presented up to the depth of 12 m. Moderately weathered charnockite is extended up to the depth of 30 m. Further, fractured/moderately the weathered charnockite is also seen (Figure 1b) from the shear wave velocity section.

Figure 2 shows the P- and S- wave velocity depth sections of profile 2 in E-W direction. The P-wave velocity depth section of profile 2 is also showing the three layers (Figure 2a). The average thickness of first layer is around 4 m with a velocity of 500 m/s, the second layer is between 4 m to 12 m with a velocity of 3100 m/s and the third layer velocity is 5500 m/s. It is also inferred from the shear wave velocity depth section (Figure 2b), that the thickness of top layer is around 5 m with a velocity of < 200 m/s, depth to the second layer is 5 m and extending up to the depth of 20 m with a velocity of 200 m/s to 500 m/s and third layer is extended up the depth of 30 m with a velocity of >500 m/s, which may be moderately weathered charnockite.

It is observed from the P- and S- wave velocity depth sections of profile 2, top soil is observed up to the depth of 4 m below that weathered charnockite is seen up to the depth of 20 m. It is observed from the shear wave velocity section moderately/fractured weathered charnockite is present in some parts up to the depth of 30 m.

It is inferred from the E-W profiles that the top soil, weathered charnockite and fractured/moderately charnockite extended up to the depth of 30 m sequentially. Further fractured/moderately weathered charnockite is seen in some part of the profiles.

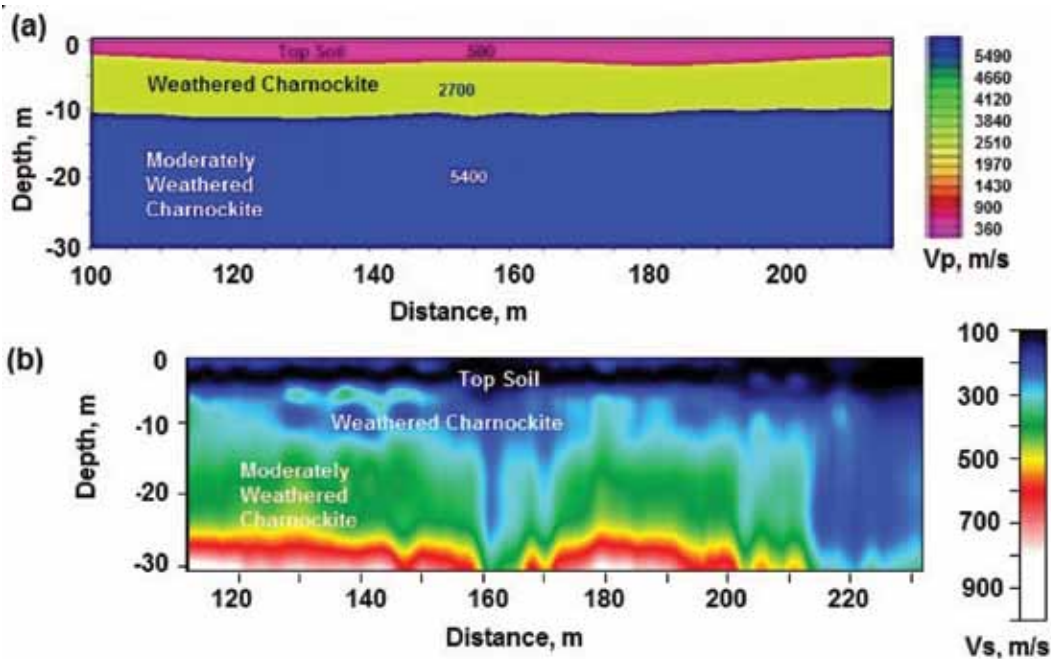


Figure 1. shows a) P-wave velocity depth section of profile 1, b) Shear wave velocity depth section of profile 1.

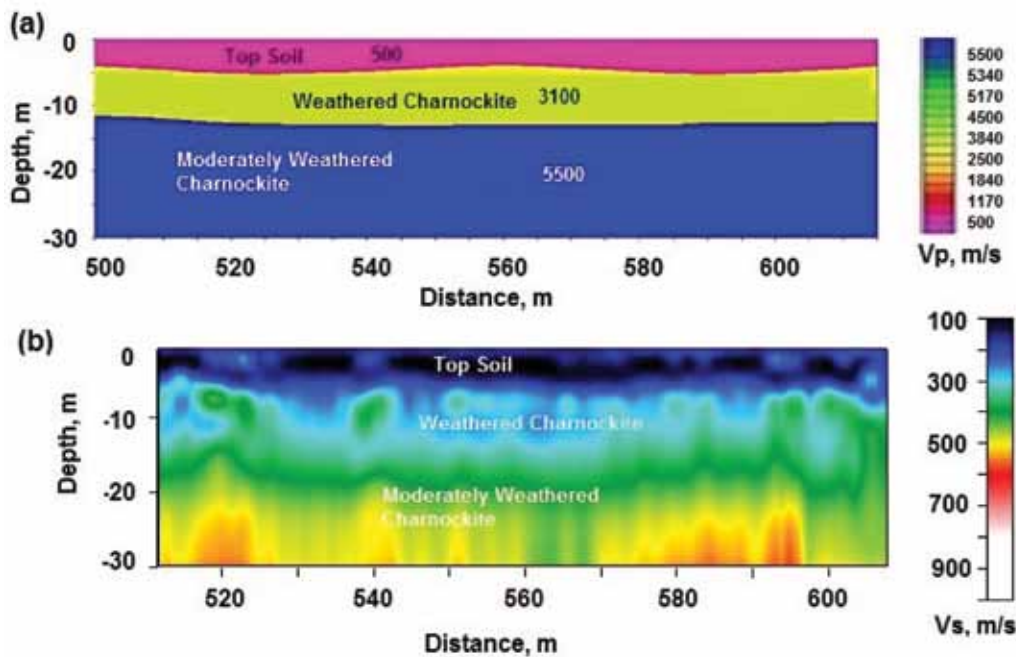


Figure 2. shows a) P-wave velocity depth section of profile 2, b) Shear wave velocity depth section of profile 2.

Figure 3 shows the P- and S- wave velocity depth sections of profile 3 in N-S direction. The P-wave velocity depth section of profile 2 is also showing the three layers (Figure 3a). The average thickness of first layer is around 3 m with a velocity of 400 m/s, the second layer is seen between 4 m to 11 m with a velocity of 2800 m/s and is third layer velocity is 5500 m/s. It is also inferred from the shear wave velocity depth section (Figure 3b), the average

thickness of top layer is around 3 m with a velocity of < 200 m/s, depth to the second layer is 3 m and extending up to the depth of 18 m with a velocity of 200 m/s to 500 m/s and third layer is extended up the depth of 30 m with a velocity of >500 m/s.

It is observed from the P- and S- wave velocity depth sections of profile 3, top soil is present at up to the depth of 3 m below that weathered charnockite is presented

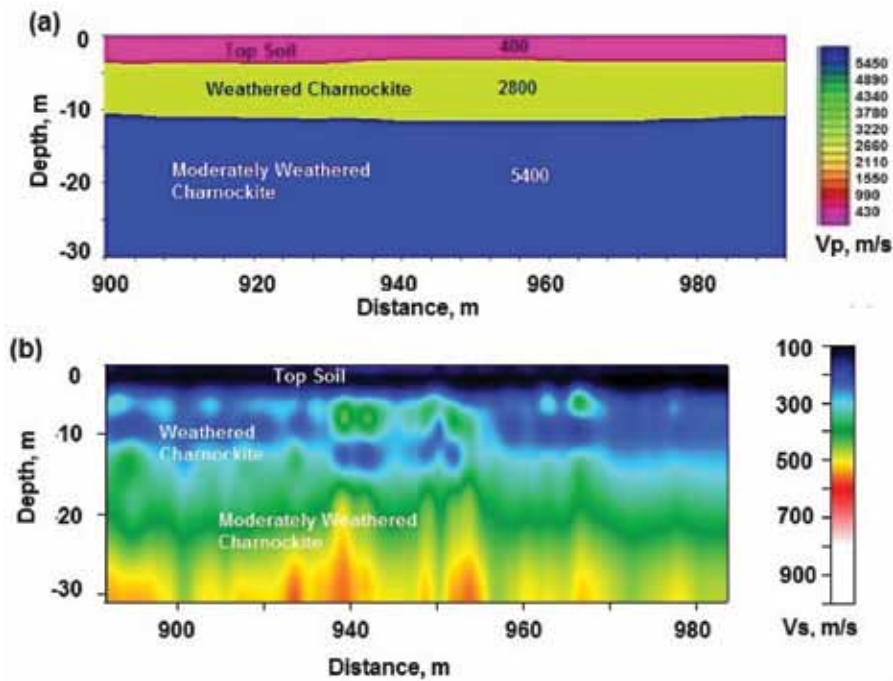


Figure 3. shows a) P-wave velocity depth section of profile 3, b) Shear wave velocity depth section of profile 3.

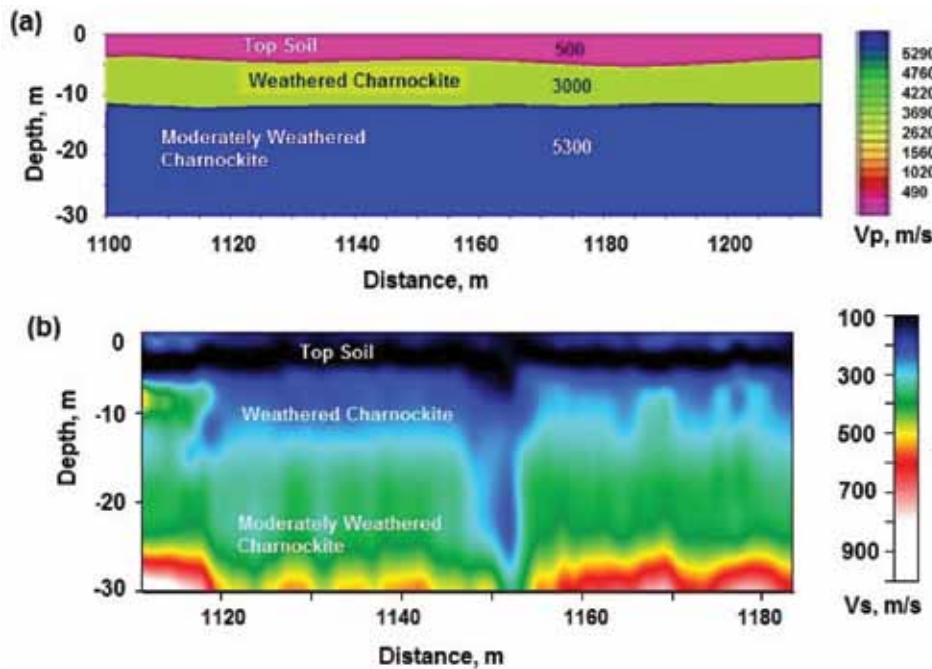


Figure 4. shows a) P-wave velocity depth section of profile 4, b) Shear wave velocity depth section of profile 4.

up to the depth of 18 m. The depth to the fractured/moderately weathered charnockite is 18 m. Further, a patch of fractured/moderately weathered charnockite is seen in the central portion of the profile at a depth of 5 m (Figure 3b).

Figure 4 shows the P- and S- wave velocity depth sections of profile 4 in N-S direction. The P-wave velocity depth section of profile 4 shows the three layers (Figure

4a). The average thickness of first layer is around 3 m with a velocity of 500 m/s, the second layer is present between 4 m to 12 m with a velocity of 3000 m/s and depth to the bottom most layer is around 12 m with a velocity of 5300 m/s. It is also inferred from the shear wave velocity depth section (Figure 4b), the average thickness of top layer is around 3 m with a velocity of < 200 m/s, depth to the second layer is 5 m and extending up to the depth of

15 m with a velocity of 200 m/s to 500 m/s and third layer with a velocity of >500 m/s.

It is seen from the P- and S- wave velocity depth sections of profile 4, top soil is presented up to the depth of 5 m below that weathered charnockite is presented up to the depth of 15 m. The depth to the fractured/moderately weathered charnockite is 15 m. Further, a patch of fractured/moderately weathered charnockite is seen in the central portion of the profile at a depth of 5 m and extended up the depth of 30 m (Figure 4b).

It is inferred from the N-S profiles of the study area, top soil, weathered charnockite and fractured/moderately weathered charnockite extended up to the depth of 30 m sequentially. Further weathered charnockite is presented in central part of the profiles in shallow levels.

The interpreted rock strata from the present analysis are correlated with the nearby borehole information (GMCL, 2013) and it is observed from the borehole sections that soil with clay is present up to the depth of 9 m, where as highly weathered to slightly weathered Charnockitic rock is present up to the depth of 15 m. The interpreted depth strata from the present analysis are well correlated with the borehole results and provided the depth information up to the depth of 30 m in terms of P- and S- wave velocities for site evaluation for construction of high rise building at SERC complex.

CONCLUSIONS

The MASW and Seismic refraction studies at CSIR-SERC complex in Chennai city clearly shows the presence of top soil, weathered charnockite, and fresh charnockite sequentially up to the depth of 30 m.

P-wave velocities of 400-500 m/s, 2700-3100 m/s and 5300-5500 m/s are estimated for top soil, weathered charnockite, and fresh charnockite respectively using refraction technique.

S-wave velocities of >200 m/s, 200 to 300 m/s and >400 m/s are estimated for top soil, weathered charnockite, and fresh charnockite respectively using MASW technique.

Seismic velocities are obtained in the two mutually perpendicular directions with limited borehole information are provided the optimum coverage economically to understand the soils and basement characteristics. These results are helpful in civil engineering applications in estimation of elastic properties, depth to bedrock and planning of high rise structures in the study area.

ACKNOWLEDGEMENTS

The authors thank CSIR-SERC for the project proposal and support during various stages of the work. The authors are grateful to Director, CSIR-NGRI for the support during the

course of work. In the course of the project formulation, execution and for writing this paper, various persons of the Engineering Geophysics Division of NGRI unreservedly rendered their help, which is gratefully acknowledged. The authors gratefully thank Dr.P.R.Reddy for precise review of the manuscript and final editing.

This study has been supported by CSIR-NGRI Fast Track Translatory (FTT) Project. S.Trupiti acknowledges CSIR for providing Research Associate (RA).

Compliance with Ethical Standards

The authors declare that they have no conflict of interest and adhere to copyright norms.

REFERENCES

- Bâth, M., 1978. An analysis of the time term method in refraction seismology. *Tectono-physics*, v.51, no.3-4, pp: 155-169. doi:10. 1016/0040-1951(78)90238-X.
- Boominathan, A., Dodagoudar, G.R., Suganthi A., and Uma Maheswari, R., 2008. Seismic hazard assessment of Chennai city considering local site effect, *J. Earth Syst. Sci.*, v.117, no.2, pp: 853-863.
- Ballukraya, P.N., and Ravi, R., 1994. Hydrogeological environment of Madras city aquifers, *J. Appl. Hydrol.*, v.87, no.1-4, pp: 75-82.
- Berry, M.J., and West, G.F., 1966. An interpretation of the first arrival data of the Lake Superior experiment by the time-term method, *Bull. Seism. Soc. Am.* v.56, pp: 141-171.
- GMCL, 2013. Geotechnical Investigation at Proposed construction of Multistorey innovation complex building in CSIR complex Taramani, Chennai, Un published report no: GMC-CSIR-Taramani-JC-GT-323.
- Kanlı, A.I., Tildy, P., Pronay, Z., Pinar, A., and Hemann, L., 2006. Vs³⁰ mapping and soil classification for seismic site effect evaluation in Dinar region. *Geophys. J. Int. SW Turkey*, v. 165, pp: 223-235.
- Meru, R.F., 1966. An iterative method for solving the time-term equations, J.S.Steinhardt and T. J. Smith, Ed., *Geophys. Monogr.*, v.10, pp: 495-497, Am.Geophys. Union.
- Miller, R.D., Xia, J., Park, C.B., and Inanov, J.M., 1999. Multichannel analysis of surface waves to map bedrock. *The Leading Edge*, v.18, no.12, pp: 1392-1396.
- Oyedele, K.F., Oladele, S., and Okoh, C.N., 2012. Geo-assessment of subsurface conditions in Magodo brook estate, Lagos, Nigeria. *International journal of advanced scientific technical research*, v.2, no.4, pp: 733-741.
- Park Choon, B., Miller Richard, D., and Xia, Jianghai., 1999. Multichannel analysis of surface waves. *Geophysics*, v.64, no.3, pp: 800-808.
- Park, C.B., Xia, J., and Miller, R.D., 1998. Imaging dispersion curves of surface waves on multichannel record. In: 68th

Application of Shallow Seismic Studies for Civil Engineering Applications:
A case study from Chennai city, Tamilnadu

- Ann. Internat. Mtg., Society of Exploration Geophysicists (SEG). Expanded Abstracts., pp: 1377–1380.
- Scheidegger, A., and Willmore, P.L., 1957. The use of a least square method for the interpretation of data from seismic surveys, *Geophysics.*, v.22, pp: 9–22.
- Willmore, P.L., and Bancroft, A.M., 1960. The time-term method approach to refraction seismology, *Geophys. J.*, v.3, pp: 19–432.
- Xia, J., Miller, R.D, and Park, C.B., 1999. Estimation of near surface shear-wave velocity by inversion of Rayleigh wave. *Geophysics.*, v.64, no.3, pp: 691–700.
- Xia, J., Miller, R.D., Park, C.B., Hunter, J.A., and Harris, J.B., 2000. Comparing shear-wave velocity profiles from MASW with borehole measurements in unconsolidated sediments, Fraser River Delta, B.C. *J. Environ. Eng. Geophys. Canada.*, v.5, no.3, pp: 1–13.
- Xia, J., Miller, R.D., Park, C.B., Hunter, J.A., Harris, J.B., and Ivanov, J., 2002. Comparing shear-wave velocity profiles inverted from multichannel surface wave with borehole measurements. *Soil Dyn.Earthquake Eng.*, v.22, pp: 181–190.
- Yoshii, T., and Asano, S., 1972. Time-term analysis of explosion seismic data, *J. Phys. Earth.*, v. 20, pp: 47–57.

Received on: 9.2.18; Revised on: 20.2.18; Accepted on: 22.2.18

Evaluation of Percolation Tank Efficiency on Groundwater Recharge: A Case Study for Karnampettai Percolation Pond, India

L.Surinaidu¹, A. Raviraj² and R. Rangarajan^{1*}

¹CSIR-National Geophysical Research Institute (NGRI), Hyderabad- 500 007

²Water Technology Center, Tamil Nadu Agriculture University, Coimbatore - 641003

*Corresponding Author: rangarajanngr@gmail.com

ABSTRACT

Over abstraction of groundwater when compared to less amount of rainfall recharge throughout India is mainly due to increasing demands for irrigated agriculture causing severe groundwater depletion. Such an alarming situation is increasing unabated in spite of massive water harvesting measures that are implemented through watershed development programs (WDP). In order to improve the artificial percolation efficiency some new developmental programs are being implemented through managed aquifer recharge (MAR) (mainly percolation tanks and check dams). Keeping in view the well known Water Development Programs limitations due to the increasing number of recharging structures and huge cost involved in their construction, it has become necessary and important to evaluate and understand the MAR performance for sustainable management of groundwater resources. The present study examines the percolation efficiency of typical Karnampettai percolation tank located in Tamilnadu, South India using an integrated approach combining geophysical, hydrogeological and geotracer (radiotracer: tritium and chemical tracers: rhodamine B, bromide) investigations. The results indicated that percolation from the tank is 28 to 35 mm/day with an average percolation rate of 32 mm/day. The percolation rate is reduced progressively with a gradual decline of water level in the percolation tank. The average natural recharge (rainfed and irrigation fields) in the study area is 30 mm (8% of the rainfall). The study indicated that 65% of the total rainfall is lost due to soil moisture deficiency caused by evaporation and evapotranspiration. The study also reveals that the groundwater flow velocity near to the percolation pond is 2 m/day with effective groundwater recharge zone of 275 m.

Key words: Percolation tank, tracers, MAR, WDP, Karnampettai.

INTRODUCTION

The significant development of Indian irrigated agriculture after independence has helped to generate sufficient agriculture and horticulture output and improved food security, which supported the economic growth of the country (Tripathi and Prasad, 2009; NRAA, 2011). However, this food security has seriously hampered the sustainability of water resources (Massuel et al., 2014; Batchelor et al., 2003; Shah, 2012). Compared to river basins, coastal corridor and soft rock zones the situation is considerably precarious in the crystalline hard rock aquifer regions of India. In the hard rock areas, weathered and fractured zones play a major role in groundwater recharge and production/storage that supports the agriculture development (World Bank, 2010). In these regions groundwater is being exploited through large diameter open wells and shallow bore wells by tapping weathered zone aquifers and semi confined /fractured aquifers (Pavelic, 2012; Surinaidu et al., 2013a; CGWB, 2014).

The combined effect of overexploitation of groundwater mainly for irrigated agriculture and recurring low order of rainfall recharge has resulted in lowering and decline of water table over the years in India (CGWB, 2014). Since three decades progressively the open wells have gone dry

in early summer season itself and shallow bore wells up to 60 m depth have shown reduction in yield or drying out. Watershed development programs are being implemented through Managed Aquifer Recharge (MAR) Programmes to increase the artificial recharge by the government of India as a flagship program to boost the irrigated agriculture and there by to improve the livelihoods of the rural farming and other societal and economically back ward communities. Percolation tanks or ponds are the most common artificial recharge structures for augmenting the groundwater recharge/reserves in the western and in major part of the southern peninsular India covered by hard rocks, where the average annual rainfall is less than 700 mm and having high potential evaporation of 1500-2000 mm/year (CGWB, 2014; NRAA, 2011).

The percolation tanks generally have a storage capacity of 0.15 to 0.6 million cubic meters with command area extending to a maximum distance of 2-3 km from the tank (World Bank, 2010). The infiltration capacity of tank bed area, storativity of the weathered zone and utilization of groundwater in the command area of the tank governs the efficiency of a percolation tank. The impact of percolation tank depends on the efficiency of its percolation through its bed, its lateral movement and augmentation of the groundwater in the command area in improving the yield

of open/ shallow bore wells. The efficiency of percolation tank reduces with time due to settling of silt and forming a crust during the ponding period and increase in thickness of silt load over the years.

Limited published literature is available on water accounting (Muralidharan et al., 2005; Rolland et al., 2005; Sharda et al. 2006; Sukhija et al., 1997; Sayana et al., 2010; Abraham and Mohan, 2015). These studies in general have not focused on hydrodynamics (Massuel et al., 2014). On the other hand various researchers pointed the lack of knowledge and data for proper evaluation of artificial recharge structures (Dillon et al., 2009; Glendenning et al., 2012). Existing evaluations of large programmes show limited local impact on groundwater recharge (Kerr et al., 2002). However, focused studies taken up by some researchers have shown that mega structures have led to over-exploration of surface and groundwater water and degeneration of river basin dynamics; at places even irreversible damage to river basins (Sakthivadivel, 2007; Glendenning et al., 2012).

In such a scenario, the present study has been taken up to systematically evaluate the impact of percolation efficiency on groundwater recharge. In the present study, we have carried out integrated hydro-geological investigations that combine Electrical Resistivity Tomography (ERT), chemical tracer experiments, groundwater level and tank water level monitoring to evaluate the impact of Karnampettai percolation tank on groundwater recharge in Kodangipalayam village, Coimbatore district, Tamil Nadu, South India.

STUDY AREA AND HYDROGEOLOGY

The present study focused on Karnampettai percolation tank located in the Kodangipalayam village, Palladam taluk, Coimbatore district, South India (Figure 1). The area falls under semiarid region with an average annual rainfall of 650 mm (Indian Meteorological Department). This includes southwest monsoon from the period of June to September (26 %), northeast monsoon during the period of October to January (60 %) and summer showers from February to May (14 %). The tank is elongated in shape; water-spread area of the tank is around 0.9 ha with a storage capacity of 0.1 million cubic meters (Figure 1). The maximum water level in percolation tank is about 2 m height and above it water escapes through waste weir and flows through a stream in the command area. The catchment area for the tank is about 1.5 km².

The study area is underlain by Charnockite formations of Archaean age, covered by reddish brown soils and thin alluvium. Groundwater for agriculture in the area is mainly exploited by open wells excavated up to the maximum depth of 15 m. Thick weathered zone with vertical and horizontal fractures are observed in the open well sections. The thickness of weathered zone varies from 5-15 m.

DATA COLLECTION AND METHODOLOGY

Hydrological Data

Rainfall and evaporation is monitored by installing an automated weather station (AWS), which measures rainfall, relative humidity, solar radiation, air temperature and evaporation in the study area (Figure 1). Detailed topographic survey of the percolation tank is carried out with grid intervals of 5m x 5m, to infer the volume of water being stored. It can be calculated from the standing water level. The observation bore wells in the study area are drilled up to a maximum depth of 60 m for static water level monitoring. The lithologs of these bore wells have indicated presence of a thick weathered zone and occurrence of the potential fractured zone within the depth of 40 m. The standing water level in the percolation tank is measured once in a week. The observation bore wells (O series wells) are monitored at regular interval of time (weekly and bimonthly) for static water level measurements in order to know the influence of percolation tank structure. The open wells (K series wells) are subjected to pumping for irrigation on a regular basis. All the wells are connected to common datum plane with respect to temporary benchmark. The total storage in the percolation tank is calculated by multiplying water spread area and water level height in the percolation pond. Percolation rate from the pond is calculated using evaporation rate, rainfall and pond water level decline at two time intervals (refer table 2 and figure 5a).

The undisturbed shallow zone soil samples up to the depth of 5 cm (top soil zone) are collected from the experimental sites (8 numbers) using hand auger to find out saturated permeability coefficient (K). The samples collected in rings are loaded in the laboratory permeameter, where the samples are saturated in the container of the permeameter. The ring samples are placed in the ring holder to gradually saturate them, using the adjustable level regulator. Constant head method is used for estimating saturated permeability coefficient. The detailed procedure is well explained by Todd, 1980.

Darcy's law is used to calculate the K-factor, when applying the constant head method to determine permeability.

Darcy's law states:

$$V = K * I * A * t$$

Whereas,

V = volume of water flowing through the sample (cm³)

K = permeability coefficient or K factor (cm/d)

I = permeability rise gradient or (h/L)

L = length of the soil sample (cm)

A = cross section surface of the sample (cm²)

t = time dimension day

The permeability coefficient is calculated as, $K = (VL) / (A.t.h)$

h = water level difference inside and outside ring holder or sample cylinder (cm)

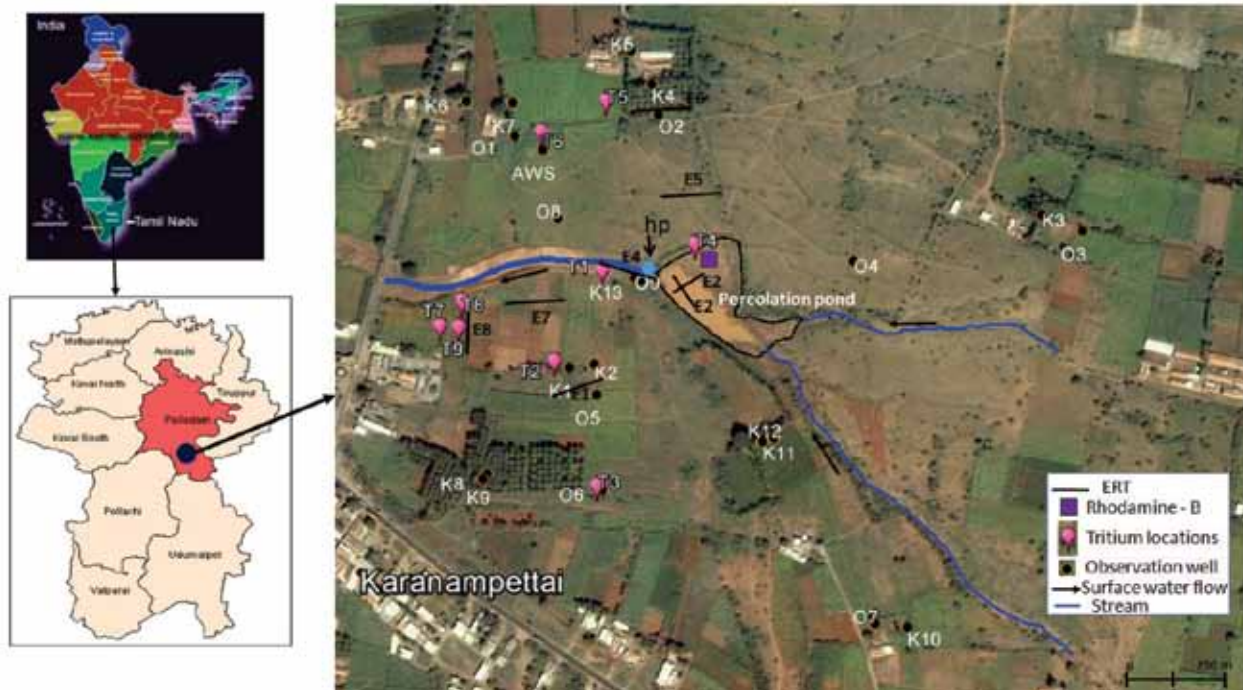


Figure 1. Location of observation wells, ERT, tracer injection and automated weather (AWS) station in the study area. Note: K Series- Open wells and O Series - Bore wells, hp-hand pump, T-Tritium injection sites.

Electrical Resistivity Tomography

Multi electrode resistivity tomography (ERT) surveys have been carried out at 8 locations (E series in figure 1) to obtain subsurface lithological information of tank storage area and also in the command area of percolation tank using ABEM multi electrode resistivity imaging system. The multi-core cable is connected to an electronic switching and transmitter unit, which is connected to a laptop computer. The data acquisition is fully automatic and sequence of measurements depends on electrode array used for the study. In the present study area, Wenner electrode configuration has been used to acquire the subsurface resistivity data. The length of the profile was selected depending on vacant space availability in the area. The measured apparent resistivity is converted in to true resistivity using RES2D.INV inversion program in order to produce the 2D resistivity cross-section image. The data inversion was carried out with the least squares inversion method (Dahlin, 1996). The ERT technique is used by many researchers for aquifer mapping, to map saline water zones, for groundwater surface water interactions and other environmental impact assessment studies (Surinaidu et al., 2012, 2013b; Chandra et al., 2011; Zarroca et al., 2011).

Tracer Studies

Borehole tracer experiments in hydrogeological studies provide information on hydraulic connectivity, velocity

and direction of groundwater flow. The tracers can be used via single and multiple well methods. In the single well method, the velocity of groundwater flow is ascertained from dilution characteristics of the same test bore hole. In the multiple well methods, the time taken by the ground water to cover a certain distance is taken in to consideration and hence the distance velocity (point to point velocity) is determined (Drost et al., 1974). Injected tritium tracer studies can be used to estimate the natural recharge caused by rainfall and bore hole tracer studies is used to measure the groundwater velocity and to determine the hydraulic connectivity within the aquifer zone. Tritium injection technique is successfully employed for rainfall-recharge measurements (Munnich, 1968; Rangarajan et al., 2009, 2014; Wu et al., 2016) and borehole tracer technique (Pitrik et al., 2007; Lin et al., 2013; Wang et al., 2008) is used for groundwater velocity measurements and also to estimate the hydraulic continuity.

In the present study both single hole and multiple well tracer methods are used. In addition, groundwater electrical conductivity is also measured, making use of tracer method to see the maximum zone of influence of a percolation tank on recharge. Tritium and chemical tracer studies have been carried out in the study area for the estimation of natural recharge caused by rainfall, to measure the groundwater velocity and also to determine the hydraulic connectivity of percolation tank.

In the study area, tritium tracer was injected at 9 sites before onset of the northeast monsoon of 2005. The

sites selected are fallow non-agricultural land, rain fed agricultural fields and supplemental irrigated fields near the observation bore holes. The tracer has been injected at the depth of 60 cm below ground level. Vertical soil samples were collected in 20 cm section up to maximum depth of 2 m using recovery pipes in the month of January 2005 after the completion of northeast monsoon. The collected depth wise samples were analyzed in the laboratory for moisture content, tracer concentration and grain size analysis.

The recharge value for each site is calculated first by determining the center of gravity of the tritium versus depth profile and the moisture content of the displaced zone. The displacement of the tracer from the depth of injection is the distance between injection depth and center of gravity or peak of the tritium concentration in the profile. The recharge is calculated by,

$$Re = M \times D$$

where,

Re = recharge in mm

M = moisture content of the displaced zone in 1 sq.mm.

D = displacement of tracer from the depth of injection

Re is the height of an imaginary water column over 1 sq.mm in the soil profile between the depth of injection and peak in tritium activity. As per the piston flow model, this amount is finally added to the groundwater as recharge. Assuming this 'Re' is due to rainfall 'R' during time 't' (period between dates of injection and soil core collection). The percentage of rainfall R contributing to the recharge is given as,

$$Re (\%) = 100 \times D \times M/R$$

In order to study the dynamic/induced movement and direction of percolated water movement from the tank, Bromide as chemical tracer and Rhodamine-B as dye tracer have been used. Bromide in the form of potassium bromide (KBr) has been injected at 45 m depth of a bore well (O9 in Figure 1) present at a distance of about 60 m from the embankment of the percolation tank. 7000 grams of Analar Grade potassium bromide, dissolved in 40 liters of the same bore well water, is transferred to the well within a period of 3 minutes and thoroughly mixed using mechanical device. Tracer has been injected on 19th December 2004, when the tank was half filled to its capacity with 3 feet of water column. The constraints faced are that the observation wells are located at far off distance from the tank and not in ideal location for tracer experiments.

20 grams of Rhodamine-B is dissolved in 5 liters of water and injected at 60 cm depth below the tank bed level at 55 locations (50 mm diameter slim holes) in a grid pattern over an area of 50 m x 50 m on 22.1.2005 (Figure 1). To achieve thorough mixing of tracer, normal water is added at all the 55 locations twice for 3 days. Water samples have been collected from tank and observation bore wells at weekly/ bimonthly interval of time. The

samples are stored in double capped polythene bottles and labeled. The samples have been analyzed in the laboratory for conductivity, Rhodamine-B and bromide concentrations. Bromide concentration in the samples has been measured using titration/specific ion electrode methods. Rhodamine concentration in water samples has been analyzed using portable Fluorimeter (Skougstad et al., 1979). The groundwater/seepage velocity (V) is estimated by dividing distance between injection well and observation wells with time (d/t).

RESULTS AND DISCUSSION

Hydrological Investigations

The total annual rainfall during 2004 and 2005 are 750 mm and 811 mm, respectively. They are excess than the average annual rainfall of 650 mm. The average annual potential evaporation computed as 1634 mm is twice the amount of annual rainfall. The pattern of rainfall shows bimodal distribution with significant summer showers of greater than 20% (Figure 2a). The pattern of rainfall shows that the seasonal precipitation occurs in pulses with large gaps between the events during the southwest monsoon and small gaps during the northeast monsoon season. Rainfall during the southwest monsoon is significantly less than the northeast monsoon. Several medium intensity rainfall events (20-40 mm/day) and few high intensity events (> 40 mm/day) have occurred during study period (Figure 2a). The monthly rainfall during the study (2004-2005) period is varying from 8 mm in February, 2005 to 204 mm in October, 2004 (Figure 2b).

The observed average evaporation during the study period from the year 2004 to 2005 is 13 mm in 2004 and 32 mm in 2005, with minimum evaporation (1.63 mm/day) in July 2004 and maximum of 7.61 mm/day in April 2004 (Figure 2b). The observed relation between rainfall pattern and water level height in the tank from January 2004 to December 2005 indicates that a single day rainfall events exceeding greater than 100 mm or group of events ranging from 20-40 mm per day can only generate runoff and fill the storage structure.

Geophysical Investigations

In order to calibrate the resistivity imaging results with a known lithological control, a site near O5 observation well and a dried dug well is selected (E1 in Figure 3) with electrode spacing of 2 m following Wenner method (E1 in Figure 3). The lithology of observation well is not available at the time of survey during June 2004. However, the cross section of dried dug well part is mapped. The topsoil is less than 30 cm followed by highly weathered granites (pink) extending to a depth of 3.5 m followed by semi-weathered

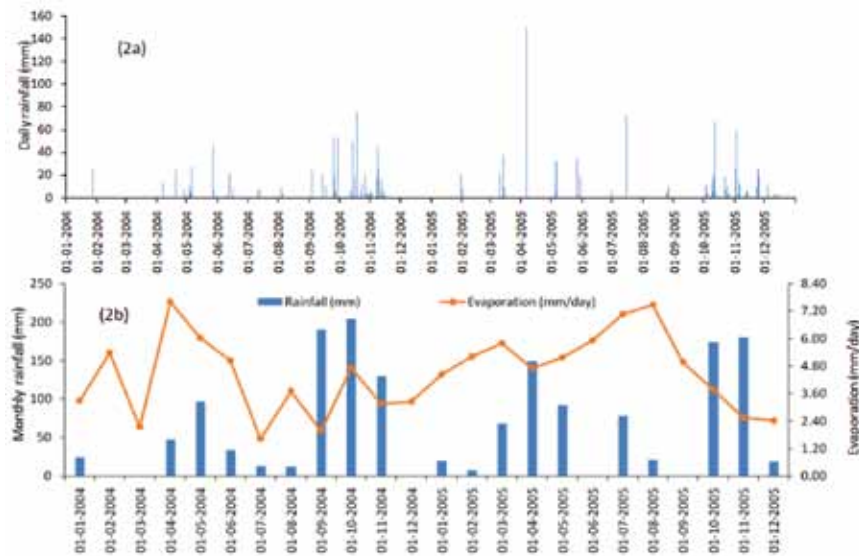


Figure 2. Daily rainfall (mm) (2a) and monthly rainfall vs. evaporation (2b) during the study period.

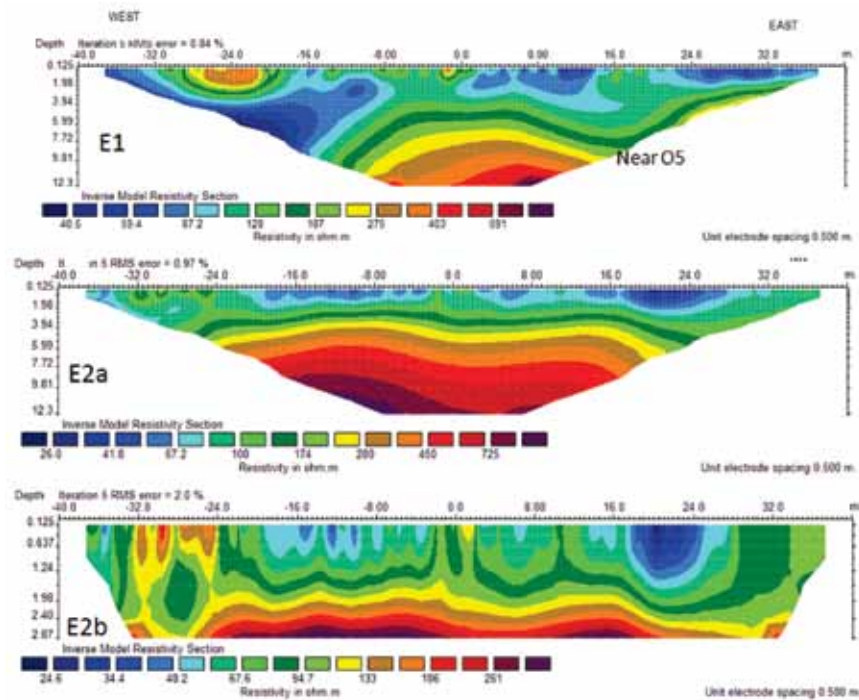


Figure 3. Vertical Electrical Resistivity tomographic cross sections carried out in the tank bed area.

formation up to the bottom well having a depth of 7 m. Since, the aim of present investigation is to know about the sub-surface formation forming the phreatic aquifer, which will be benefited from the percolation tank recharge, the adopted imaging electrode spacing of 2 m with 42 electrodes covering a profile line of 80 m length facilitated to get subsurface information of 12 m.

The resistivity image at this place has clearly indicated that the thickness of weathered zone increases towards the west away from the percolation tank. Based on the

geo-electrical nature of sub-surface at the investigated site, the subsurface can be broadly classified into two layers. The first layer with resistivity range of 40-100 Ohm.m representing the weathered zone followed by basement forming the second layer with resistivity range of 400 to more than 600 Ohm.m having a transition zone of semi-weathered zone. The depth to basement inferred from the image is about 7-8 m which is coinciding with the observation made in the dried dug well. However, the shape of the high resistive layer is having inclination

Evaluation of Percolation Tank Efficiency on Groundwater Recharge:
A Case Study for Karnampettai Percolation Pond, India

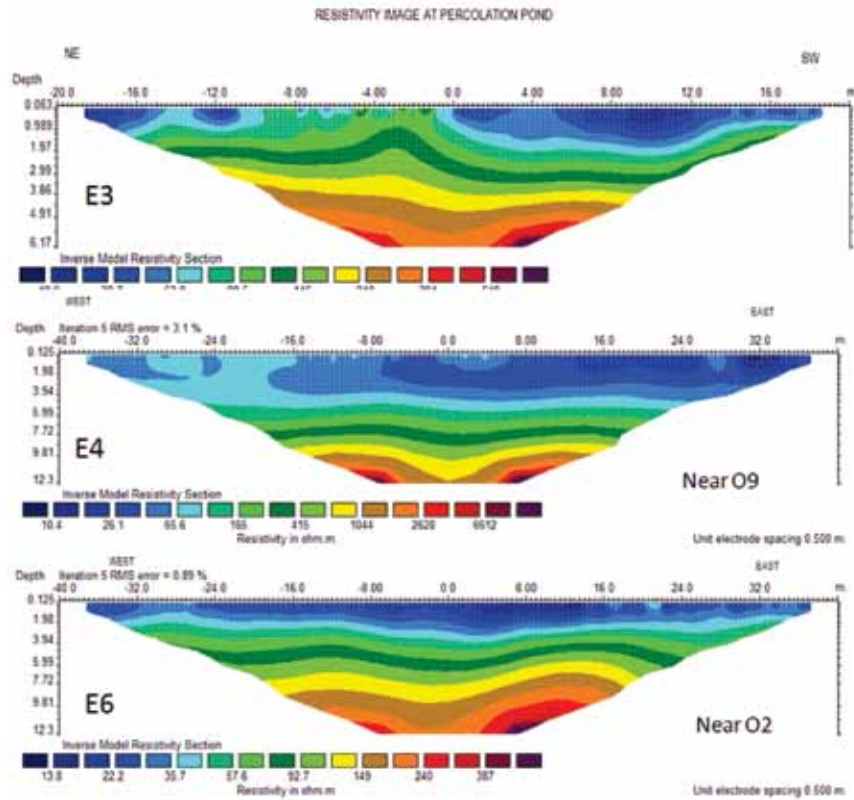


Figure 4. Vertical Electrical Resistivity tomographic cross sections in the study area

towards western part of the profile alignment. The image analysis indicates that the groundwater movement from the percolation tank towards this direction in phreatic zone might be restricted by the presence of basement rise. However, the movement of groundwater through fractures within the basement must be taking place, which is evidenced by water table response of the well O5 located nearby the investigated site (refer Figure 4).

Electrical resistivity tomography survey (E2) is conducted with a length of 80 m and 2 m electrode spacing at a distance of 40 m from the weir and along the length of the tank in NW-SE direction. It revealed sub-surface information to a depth of 12 m (E2a in Figure 3 and refer figure 1 for location). Based on the vertical distribution of resistivity ranges, the sub-surface under the profile line can be grouped into a three geo-electrical layered shallow sub surface structure. The top layer with a thickness of 2 m is more or less uniform in nature. It is represented by a resistivity that ranges from 20-40 Ohm-m, probably representing the conductive topsoil and highly weathered formation. However, these conductive formations are not of continuous nature and they are separated by some moderate resistive formation (resistivity around 100 Ohm-m) exhibiting probably the variation in degree of weathering and variable soil thickness with variable moisture content. The second geo-electric layer with a resistivity range 150-300 Ohm-m represents the

semi-weathered formation extending to a depth of 7m. The basement that follows the semi-weathered zone forms the third geo-electric layer having resistivity more than 300 Ohm-m.

In order to critically understand the composition and structure of sub-surface to a depth of 3 meters along the study profile line, the collected data (E2a) has been subjected to splicing analysis. The resultant resistivity cross section (E2b) of shallow zone under the ponding area to a depth of 3 m indicated the first geo-electric layer with resistivity range of 24 to 40 Ohm-m represents the soil and highly weathered part extending to the depth of 1.98 m or 2 m (E2b in Figure 3). However, the low order of resistivity in the NW part indicates that the area must be having high silted condition compared to the SE part. In the field it is observed that the NW part nearer to weir side is the deepest part of the tank having high silt accumulation.

A second profile (E3) is laid perpendicular to the direction to E2 keeping the center same with 40 m total length and 1 m electrode spacing following the Wenner configuration (E3 in Figure 4). The image obtained in the perpendicular direction also shows a similar geo-electric layered structure in the sub-surface. The first geo-electric layer with resistivity range of 20–30 Ohm-m indicates a maximum thickness of 2 m on the SW part, coinciding with the depression part seen as a stream channel inside the tank. In the central part, the weathering thickness is

moderate and exposures of highly jointed rocks are seen. This is being reflected in the image with a resistivity range of 50-90 Ohm-m. The second geo-electric layer following the first layer that extends to a depth of 4 m is of semi-weathered formation with resistivity range of 100 – 250 Ohm-m. The third geo-electric layer with resistivity more than 250 Ohm-m is the basement that extends to a depth beyond 4 m. The perpendicular directional investigation confirms that the tank is almost having a uniform and stratified formation of which the first geo-electric layer of 2 m thickness is the beneficiary zone of ponding.

The resistivity imaging (E4) is carried out in the downstream of the percolation tank and near to the hand pump well (E4 in Figure 4) clearly depicted a three geo-electric layered sequence of which the first layer extending to a depth of 5 m is of highly conductive nature towards the percolation tank direction (east) when compared to the western side. However, the image results indicate that the thickness of the first geo-electric layer is of uniform thickness with varying degree of weathering and saturation. The second geo-electric layer following the weathered zone represented by resistivity range of 170-400 Ohm-m is considered to be of semi-weathered nature extends to a depth of 10m. The last or bottommost geo-electric layer with more than 1000 Ohm-m is considered to be the basement. The order of resistivity range more than 2000 Ohm-m reaching a value of 6000 Ohm-m shows that the basement at this site is more compact. The water level monitoring at O9 observation well near to the investigated site has shown a fluctuation of 4 m (pre- & post-monsoon) within depth section between 2 m to 6 m below ground level. This indicates that the saturated condition varies within the first geo-electric layer with time. The collated inference brings out that the shallow zone is influenced by the percolation tank. This inference is supported by the water level response over various functional stages of percolation tank.

ERT6 is carried out inside the coconut garden on the extreme northern side of the study area (E6 in Figure 4). A dug well in the garden is being used for irrigating the coconut fields, once in ten days as reported by the farmer. The image obtained at this site clearly showed that the top layer is very thin and the maximum thickness is about 2 m only followed by thick semi-weathered formation extending to a depth of 10 m followed by basement. However, the resistivity range of the basement (250-500 Ohm-m) denote that the rock is not highly compact. It could probably indicate highly jointed basement having saturation in fractures/joints.

Percolation Tank Influence on Groundwater Recharge Dynamics

The observed relation between storage and standing water column in the tank shows exponential pattern (Figure 5a).

The percolation tank water storage was 10217.25 m³ at 2.4 m standing water level and 0.9 ha water spread area (Table 1). The minimum water storage 82.50 m³ is observed with 0.3 m standing water level and 0.05 ha water spread area during the study period. The percolation rate reduces with the progressive decline of water level in the tank (Figure 5b) over the time. The rate of peculation in the post-monsoon started with 46.8 mm/day and reduced to 15.1 mm/day during pre-monsoon season. The starting percolation rate is 42.3 mm/day and reduced to 21.8 mm/day (Table 2). The average percolation rate during 2004 and 2005 is 28 mm/day and 35 mm/day respectively. The percolation rate is very low when the water spread occupies small portion in the tank near to the bund, due to presence of 20-40 cm silt deposition (< 20 micron size particles) at this place. The estimation shows that about 92 % of the stored water (2 m head of water) percolated through the tank bed within a period of 30-40 days (Figure 5b and Table 2).

Table 1. Water column depth, storage capacity and area of Karanampettai Po.

Depth (m)	Capacity (m ³)	WSA (ha)
0.30	82.50	0.05
0.60	424.50	0.17
0.90	1097.25	0.27
1.20	2111.25	0.40
1.50	3519.00	0.53
1.80	5350.50	0.68
2.10	7609.50	0.81
2.40	10217.25	0.90

The ERT study indicates that the sub-surface formation is more or less uniformly stratified except for some minor variations at shallow depths. The infiltration rate obtained from the tank water balance equation reflects that a steady state rate of 26 mm/day (Table 2) could be taking place in the first geo-electrical layer of 2 m thickness. However, assuming an effective porosity of 20% (obtained from the tritium tracer studies in terms of volume moisture percentage, refer section 4.2) for this layer and the total area of 0.96 hectares (tank area), the water that could be accommodated within the first geo-electrical layer of 2 m thickness works out to be 3840 cubic meters or 76% of total storage of 5015 cubic meters collected in the tank during the monsoon months (November and December) of 2004. The remaining 24% of volume may be subjected to evaporation and deep percolation. The volume of water thus stored in the first geo-electric layer contributes to deeper percolation in the second geo-electric layer during the ponding period at very low rate, as the semi-weathered formations has poor permeability. The inference of less benefit in terms of groundwater augmentation is reflected in low order of water level rise of 0.67 m during this period

Evaluation of Percolation Tank Efficiency on Groundwater Recharge:
A Case Study for Karnampettai Percolation Pond, India

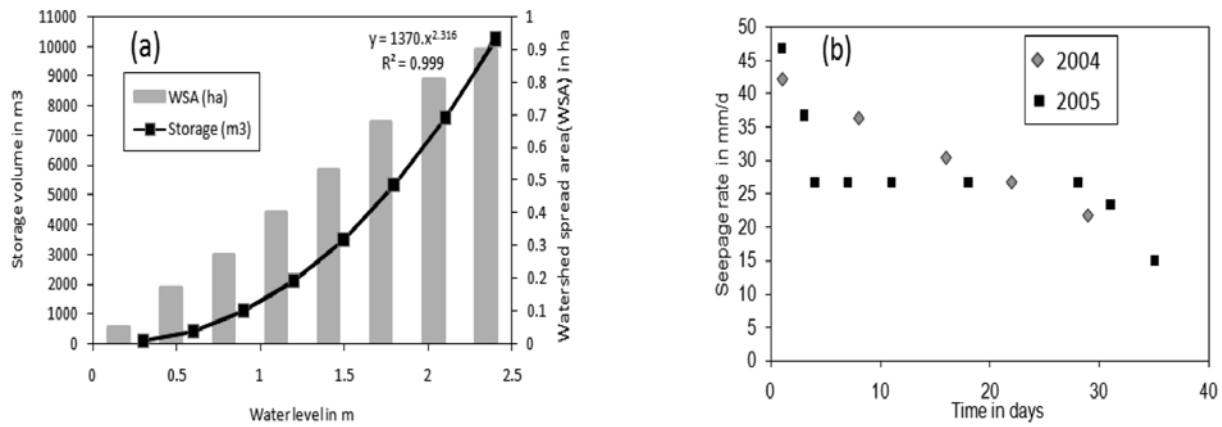


Figure 5. Water level height versus volume relationship in the percolation pond (a) and Time versus percolation rate of water (b).

Table 2. Estimated groundwater percolation from the percolation pond during the study period.

Date	Storage (m ³) (A)	Water column (m) (B)	Water loss (mm) (C=Storage difference between two time intervals)	Rainfall (mm) (D)	Evaporation (mm) (F)	Percolation (mm) (C+D-F)	Percolation (m ³ /day)	Percolation (mm/day)
26.11.04	5015	1.75						
30.11.04	3786	1.55	200	0	12.8	187.2	1150	46.8
2.12.04	3348	1.47	80	0	6.4	73.6	402	36.8
3.12.04	3192	1.44	30	0	3.2	26.8	139	26.8
6.12.04	2748	1.35	90	0	9.6	80.4	397	26.8
10.12.04	2215	1.23	120	0	12.8	107.2	476	26.8
17.12.04	1435	1.02	210	0	22.4	187.6	697	26.8
27.12.04	641	0.72	300	0	32	268	709	26.8
30.12.04	488	0.64	80	0	9.6	70.4	135	23.4
3.01.05	373	0.57	70	0	9.6	60.4	99	15.1
Total							4204	28 Average
12.04.05	6597	1.97						
4.05.05	1248	0.96	1001	0	70.4	930.6	4973	42.3
11.05.05	641	0.72	240	37.3	22.4	254.9	645	36.4
19.05.05	216	0.45	270	0	25.6	244.4	385	30.5
25.05.05	66	0.27	180	0	19.2	160.8	134	26.8
1.6.05	17	0.15	120	55.2	22.4	152.8	62	21.8
Total							6199	35 Average

in well O9 nearby the percolation tank in the downstream. The present analysis indicates that the development of water column height of 1.75 m in the percolation tank may not be adequate to induce more recharge to the groundwater. The maximum storage height of (weir level) 1.95 may also be inadequate to achieve a maximum benefit in augmenting the groundwater over the area.

In general improved groundwater levels (rise in water levels) under the influence of any recharge source can be observed in the downstream. But, in the study area significant water level rise is observed in the upstream wells located (northwest) at 275 m and 218 m from the tank (O3 and O4) due to induced hydraulic gradient and

preferential groundwater flow towards these wells resulted from regular pumping in nearby wells (figure 6b and refer figure 1 for location). The water table build up was significant in the observation bore wells located around the tank during 2004 northeast monsoon, low during summer and insignificant during southwest monsoon. The average water level rise observed in downstream area wells due to 2004 northeast monsoon is 8.5 m compared to 4.4 m in the upstream area wells (Table 3).

The rainfall events during the month of November 2004 caused storage of water in the percolation tank during the monitoring period. The O5 well has shown a rise in water table of 5.41 m. The dug well to a depth of 7 m being

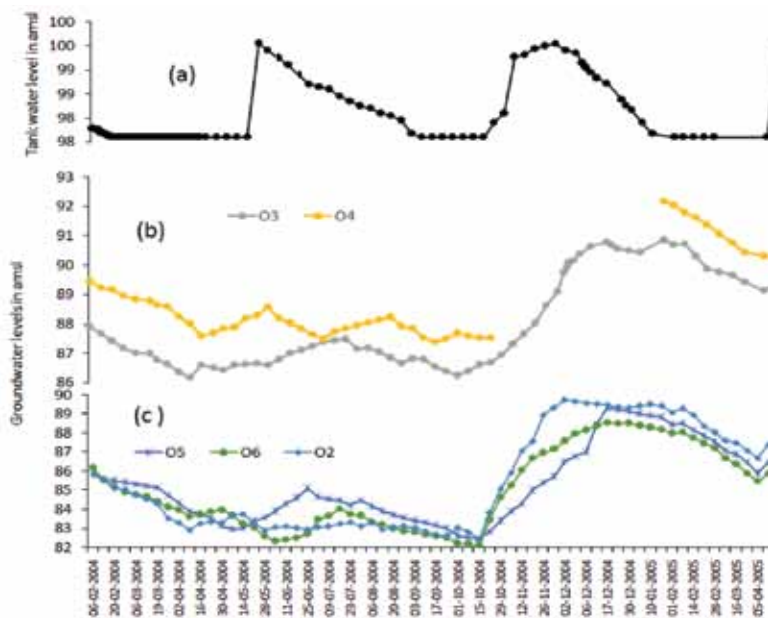


Figure 6. Percolation pond water level (a), upstream observation well water level (b) and downstream observation wells water level (c).

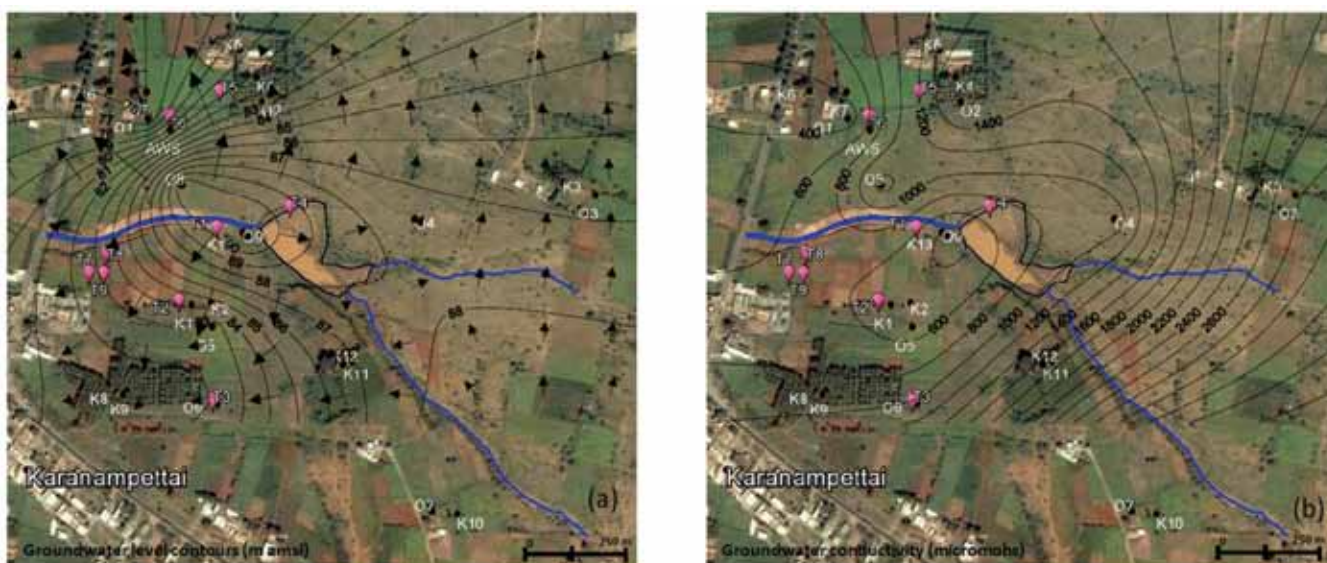


Figure 7. Groundwater contours in m amsl and arrows indicate groundwater flow direction (a), groundwater conductivity contours in micro Siemens/cm (b) in 08/12/2004.

in a dried condition throughout the observation period and borehole showing a rise in water level of the order of 5-6 m clearly indicates the movement of groundwater from recharge area through fractured zone within the basement. This is supported by a meager rise of 0.67 m in O9 well, which is just below the weir part of percolation tank. The hydrograph of O2 observation well was plotted for the calendar year of 2004 to study the influence of percolation tank towards the northern part of the area. It is surprising to note that the first cyclic filling in the tank to maximum

capacity level during the month of April-May, 2004 has not shown any influencing signature in the hydrograph. However, the wells in the downstream of percolation tank have shown the response due to ponding in terms of rise in groundwater level. The second cycling filling stage of the year has shown a rise in water level of the order of 7 m. The response of water level rise is from 15-10-04 onwards which is nearly 30 days earlier to the tank inflow and the rise reached the maximum on 3-12-04 within 21 days of maximum ponding. The hydrographs of the wells in the

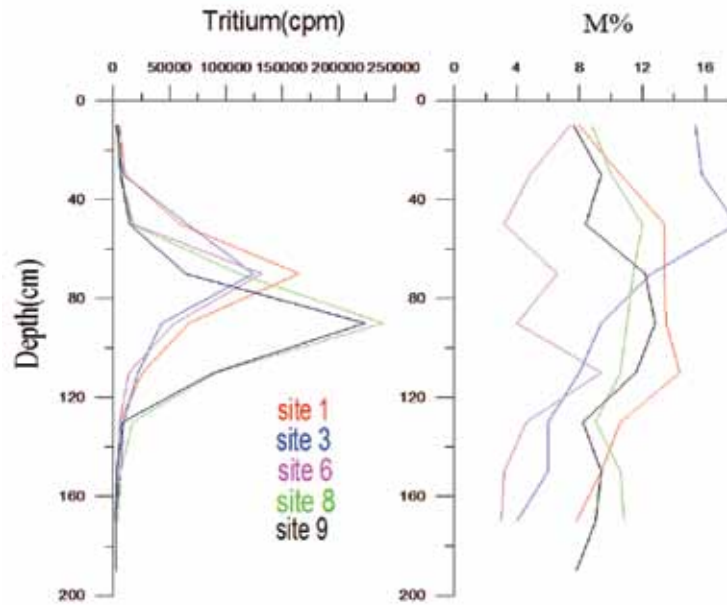


Figure 8. Tritium moisture profiles at selected rainfed and irrigated sites.

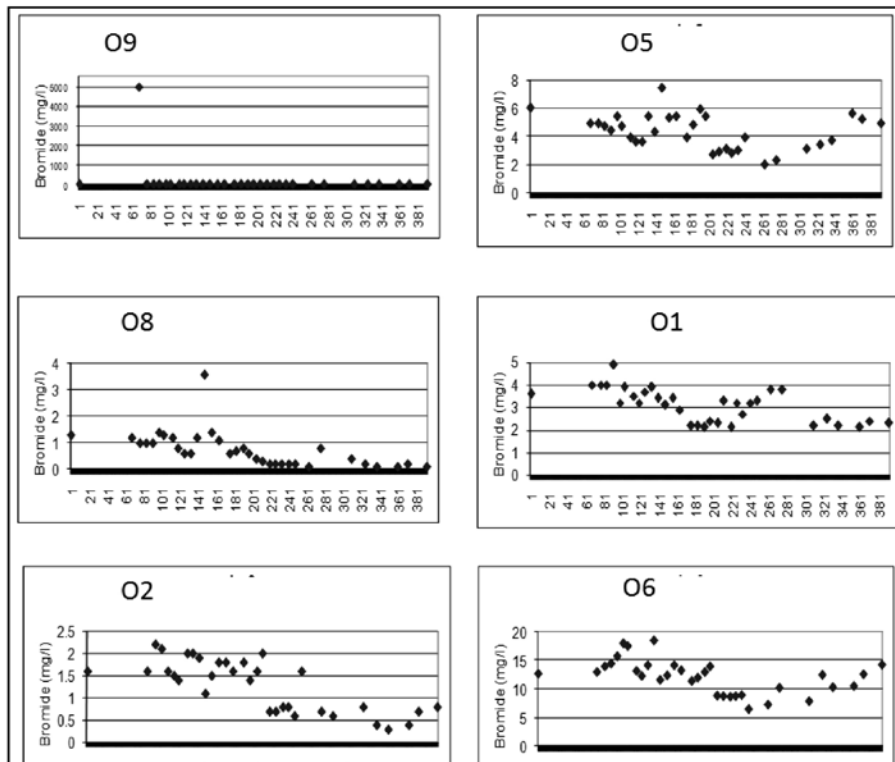


Figure 9. Bromide concentration in observation wells.

second cyclic filing depicts an immediate response of water table rise in wells with the impoundment of water in the tank (Figure 6a and Figure 6b).

The reason for groundwater flow dynamics noticed in the present study may be due to the aquifer zone in the ponding area is fully saturated with earlier ponding

water recharge and subsequently the percolated water from the tank forced the groundwater flow forward causing immediate water level rise in wells.

The water table (m amsl) contour map (Figure 7a) shows groundwater flow caused by percolation of water from the tank is towards northwest, west and southwest

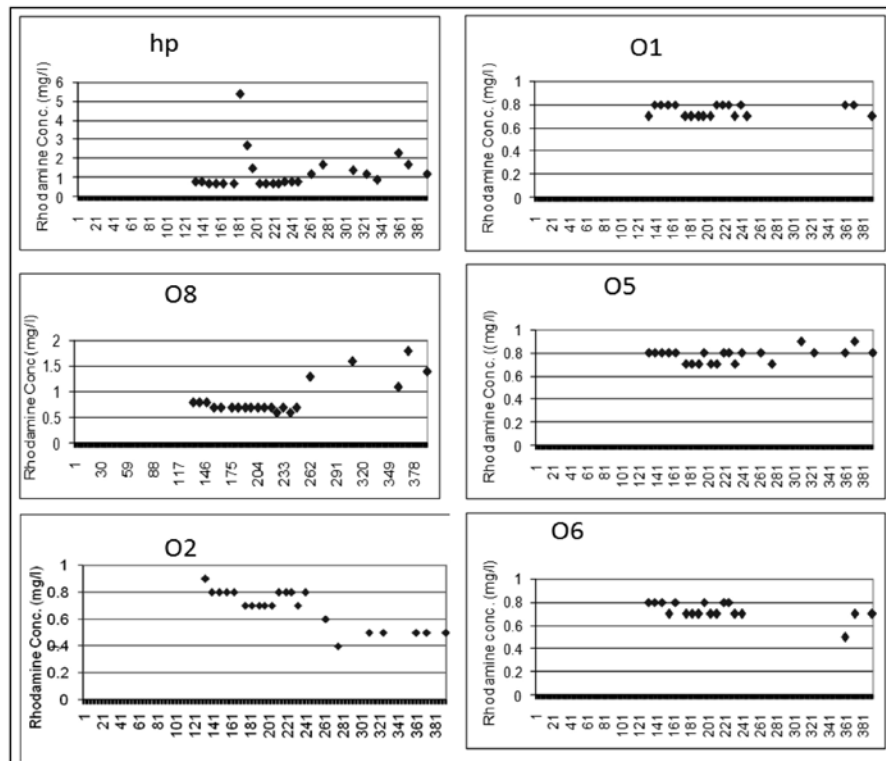


Figure 10. Rhodamine concentration in observation wells.

Table 3. Groundwater level rise in downstream and upstream during the study period.

Wells	NE monsoon (2004)	Summer shower (2005)
Downstream side (NW part)		
O1	13.3	4.09
O2	7.31	0.76
O5	6.85	1.75
O6	6.44	2.09
Average	8.5	2.2
Upstream side		
O3	4.18	0.18
O4	4.64	0.63
Average	4.4	0.4

in the downstream side of the tank. The gradient is significant along west and northwest directions compared to southwest direction (Figure 7a). The zone of influence area of percolation pond or tank can be inferred from spatial and temporal water level variations and conductivity (Muralidharan and Nair, 1998). Normally the conductivity of runoff water collected in the tank will be much lower than the natural conductivity levels of groundwater in the downstream area. When the low conductivity water in the tank travels and mixes with groundwater of the downstream area, it is expected to lower the conductivity values of water in the zone of influence. Figure 7b, shows the conductivity values of well water in the study area. The map indicated that the influence of recharge is up to

a distance of about 275 m from the tank in northwestern side. Whereas, in the southwestern side the influence is up to a distance of about 165 m from the tank and beyond which little influence is noticed.

Geo-Tracers and Recharge Estimation

The mean natural recharge computed from five rainfed sites in the study area is 18 mm for the rainfall of 374 mm and it is equivalent to 5 % of the rainfall (Table 4 and refer figure 1 for locations). Natural recharge estimated at 3 supplemental irrigation sites as 53 mm for the rainfall of 374 mm plus unknown quantity of irrigation input. All the profiles indicate clear single peak occurring within depths

Evaluation of Percolation Tank Efficiency on Groundwater Recharge:
A Case Study for Karnampettai Percolation Pond, India

Table 4. Location of the tracer injection and sample collection sites, recharge estimates and permeability measurements of soil samples.

S.No	Description	Displacement (cm)	Average volume moisture (%)	Recharge flux evaluated (mm)	Permeability (cm/d)	Silt + clay
T1	Red soil (loamy), grass land, no cultivation	11.74	20.52	24.1	373	24
T2	Red soil (loamy), ploughed, Jowar field	9.25	13.62	12.6	5.1	51
T3	Brown loamy soil, weekly water spreading land	10.29	22.35	23	452	14
T4	Soil thickness 40-50 cm, silty layer (tank bed)				9	73
T5	Hard red soil, cultivated, clay rich artificially irrigated	57.39	9.51	54.6	419	17
T6	Fallow rainfed land, hard red soil	13.64	11.21	15.3	150	31
T7	Red soil, fallow, rainfed, grass land	12.04	10.88	13.1	170	31
T8	Red soil, ploughed land, cultivated	29.14	16.74	48.8		
T9	Red soil, ploughed land, cultivated	30.8	18.24	56.2	97	40

Note: Tracer injection: 13.9.2005; Sample collection: 04 - 05.01.2006; Depth of tracer injection: 60 cm; Depth of Permeability test is: 50 cm

of 70-100 cm below ground level, this is just below the tracer injected depth of 60 cm bgl indicating low order of natural recharge (Figure 8). Grain size analysis of the soil samples shows that at most of the sites, the shallow soil zone is coarse textured, having more than 60 % of sand component. In spite of this, the natural recharge measured shows lower order of magnitude. This shows that most of the low intensity rainfall events (20-30 mm/day), which constitutes about 65 % of the rainfall of 374 mm, might have gone in contributing to lessen soil moisture deficit / evapotranspiration losses within the root zone of 60 cm and not contributed to deep percolation. The results show that higher silt having low permeability and low recharge in the area, for example the tank bed has 73% silt+clay having very low permeability and artificially irrigated area having low silt+clay(17%) having higher permeability (Table. 4). Table 4 also indicated percentage of silt has direct impact on recharge flux.

Bromide tracer was injected in O9 well (on 19.12.2004) and water samples of injection and observation wells were analyzed for bromide concentration to determine the dilution rate of tracer in injection well and arrival of tracer signal in observation wells. Figure 9 shows variation in bromide concentration of injection well (O9) and nearest observation well (O8) in the downstream side from 1.10.2004 to 30.11.2005. The initial concentration of bromide in the labeled water is calculated as 5000 mg/l. The initial bromide concentration of 5000 mg/l in the bore well water on the date of injection on 19.12.2004 reduced to background level (pre injection well) of 1-2 mg/l on 27.12.2004 (i.e. within 8 days). It indicates high dilution rate of bromide in the injection well due to faster movement of groundwater to the downstream side near to the bund. Such a hydraulic movement of 100 cm of water in the percolation tank, at the time of injection could

be due to the steep hydraulic gradient seen in the water table contour due to pumping in the command area. The filtration velocity could not be calculated based on tracer dilution as the labeled water in the well has attained background concentration within a period of 8 days. The nearest observation bore well (O8) located at a distance of 165 m from O9 shows arrival of tracer signal after 80 days of tracer injection. The water table contour maps show distinct ground water movement towards this well (refer figure 7a). Based on distance and arrival time of tracer signal, the velocity of groundwater flow in the central part of downstream area is calculated as 2 m/day. No significant concentration of bromide was observed in any of the other observation wells above the background level during the sampling period. This may be due to location of observation wells at far off distances from the injection well and / or due to dilution of tracer in the saturated zone beyond the detection level.

Rhodamine-B (dye tracer) was injected in the tank area on 22.1.2005, when the tank water was just receded. The tank received water once again in the month of April 2005 due to high intensity rainfall event occurred on 7.4.2005. Figure 10 shows Rhodamine-B concentration in the nearest observation wells (hp and O8) during the sampling period. The observation well (hp) located at a distance of 60 m from the bund of the tank has shown arrival of tracer signal pulses with maximum pulse measured on 12.4.2005. A high intensity rainfall event of 150 mm, occurred on 7.4.2005 has filled the tank to its full capacity. The observation well (O8) located at a distance of 165 m from the bund of the tank has shown first arrival of tracer signal on 1.7.2005. The experimental data indicates that the tank water is hydraulically connected with wells located in the central part of the downstream area. It is also reflected in the water table contour map, which shows predominant

groundwater flow is towards central part of the downstream area in addition to northwestern part (refer figure 7). No significant rhodamine-B concentration was observed in any of the other observation wells in the downstream area. This is because the wells are located at far off distances (> 200 m) from the tank that may indicate out of range of percolation tank influence.

CONCLUSIONS

The integrated approach of combining hydrological, hydrogeophysical and geo-tracer studies in the study area revealed clear positive impact of the percolation tank on the groundwater recharge augmentation in the command area. The most of the moderate intensity precipitation events (20-40 mm/day) that constitute 65% of the total rainfall has been lost in lessening the soil moisture deficit caused by evaporation and evapotranspiration. Only single high intensity daily rainfall events of > 100 mm/day or several moderate intensity daily rainfall events (20-60 mm/day) separated by small gaps of non-rainy days can generate runoff and cause storage in the tank with substantial groundwater percolation from the tank. The geophysical investigations, permeability and grain size analysis inferred that tank bed having more silt on the top may be causing low rate of percolation. Whereas on the other side high weathering thickness has contributed to more recharge away from the tank bed area within the tank. The average percolation rate from the tank is estimated as 32 mm/day that ranges from 47 mm/day to 15 mm/day. The percolated water from the percolation tank contributes very small quantity of percolated water to groundwater recharge, when water column is very low in the tank. Once the tank water level is above the bed level, the percolation rate is likely to be driven by the hydraulic gradient of the aquifer due to the hydraulic connection in the area. The observations also indicated that the pumping of groundwater could significantly influence the hydraulic gradient and thus contribute to the control of the artificial recharge from the tank. The natural recharge caused by rainfall in the rain fed agricultural fields of the command area of the tank is 18 mm (5 % of the rainfall) and in irrigation fields is 53 mm (14 % of the rainfall). The velocity of groundwater flow during the period of ponding is 1- 2 m/day with an influenced zone of recharge of 275 m from the tank.

ACKNOWLEDGEMENTS

CISR-National Geophysical Research Institute (NGRI), Hyderabad and Water Technology Center, Tamil Nadu Agricultural University (WTC, TNAU) have jointly undertaken a project entitled "Augmenting groundwater resource by Artificial Recharge (AGRAR)" funded by United Kingdom. The authors are thankful to the director CSIR-

NGRI for his kind permission to publish this paper. The authors gratefully acknowledge continued support, precise refinement of the manuscript through focused evaluation and apt editing by Dr.P.R.Reddy.

Compliance with Ethical Standards

The authors declare that they have no conflict of interest and adhere to copyright norms.

REFERENCES

- Abraham, M., and Mohan, S., 2015. Effectiveness of Artificial Recharge Structures in Enhancing Groundwater Storage: A Case Study. *Indian Journal of Science and Technology*, v.8, no.20, DOI: 10.17485/ijst/2015/v8i20/81596, August 2015.
- Batchelor, C.H., Rama Mohan Rao, D.V., and Manohar Rao, S., 2003. Watershed development: a solution to water shortages in semi-arid India or part of the problem? *Land Use Water Resource. Res*, v.3, pp: 1-10.
- Central Ground Water Board (CGWB), 2014. Ministry of Water Resources, River development and Ganga Rejuvenation Government of India. DYNAMIC GROUND WATER RESOURCES OF INDIA. <http://www.cgwb.gov.in/documents/Dynamic-GW-Resources-2011.pdf>
- Chandra, S., Ahmed, S., Nagaiah, E., Shashi Kant Singh., and Chandra, P.C., 2011. Geophysical exploration for lithological control of arsenic contamination in groundwater in Middle Ganga Plains, India. *Physics and Chemistry of the Earth*, 2011, v.36, no.16, pp: 1353-1362.
- Drost, W., Moser, H., Neumaier, F., and Rauert, W., 1974. Isotope methods in groundwater Hydrology, published by Eurisotop, Germany.
- Dahlin, T., 1996. 2D resistivity surveying for environmental and engineering applications. *First Break*, v.14, pp: 275-284.
- Dillon, P., Gale, I., Contreras, S., Pavelic, P., Evans, R., and Ward, J., 2009. Managing aquifer recharge and discharge to sustain irrigation livelihoods under water scarcity and climate change. *IAHS Publ*, v.330, pp: 1-12.
- Glendenning, C.J., van Ogtrop, F.F., Mishra, A.K., and Vervoort, R.W., 2012. Balancing watershed and local scale impacts of rain water harvesting in India – a review. *Agric. Water Manag.*, v.107, pp: 1-13.
- Kerr, J., Pangare, G., and Lokur Pangare, V., 2002. Watershed development projects in India – an evaluation. Research Report 127. IFPRI, Washington, DC.
- Lin, D., Jin, M., Liang, X., and Zhan, H., 2013. Estimating groundwater recharge beneath irrigated farmland using environmental tracers fluoride, chloride and sulfate. *Hydrogeology Journal*, v.21, pp: 1469-1480.
- Muralidharan, D., Rangarajan, R., Hodlur, G.K. and Sathyanarayana, U., 2005. Optimal desliting for improving the efficiency of tanks in semiarid regions. *Journal of Geological society of India*, v.65, no.1, pp: 83-88.

Evaluation of Percolation Tank Efficiency on Groundwater Recharge:
A Case Study for Karnampettai Percolation Pond, India

- Munnich, K.O., 1968. Moisture movement measured by isotope tagging, In: Guide book on Nuclear technique in Hydrology. International Atomic Energy Agency, Vienna, pp: 112-117.
- Massuel, S., Perrin, J., Mascré, C., Mohamed, W., Boisson, A., and Ahmed, S., 2014. Managed aquifer recharge in South India: What to expect from small percolation tanks in hard rock?, *Journal of Hydrology*, 2014, v.512, pp: 157-167.
- NRAA., 2011. Monitoring and Evaluation of Artificial Recharge of Ground Water Programmes/ Schemes/Projects in the Rainfed Regions of Maharashtra. Study Report 3. National Rainfed Area Authority, New Delhi, India, pp: 151.
- Pavelic, P., Patankar, U., Acharya, S., Jella, K., and Gumma, M.K., 2012. Role of groundwater in buffering irrigation production against climate variability at the basin scale in South-West India, *Agr. Water Manage.*, v.103, pp: 78-87.
- Pitrak, M., Mares, and Kobr, M., 2007. A Simple Borehole Dilution Technique in Measuring Horizontal Ground Water Flow. *GROUND WATER*, v.45, no.1, pp: 89-92, doi: 10.1111/j.1745-6584.2006.00258.x.
- Rangarajan, R., Rolland Andrade., Shankar, G.B.K., Muralidharan, D., and Peters, E., 2014. Understanding area specific recharge process from Vadoze zone resistivity variations – a case study in basalt watershed, Ujjain district, Madhya Pradesh. *J. Ind. Geophys. Union*, April 2014, v.18, no.2, pp: 211-224.
- Rangarajan, R., Mondal, N.C., Singh, V.S., and Singh, S.V., 2009. Estimation of natural recharge and its relation with aquifer parameters in and around Tuticorin town, Tamil Nadu, India. *Current Science*, v.97, no.2, pp: 25.
- Rama Prasad., 1979. Rain water harvesting in India and Middle East. Technical report by Indian Institute of Science, Bangalore, 80 pages.
- Rolland, A., Muralidharan, D., and Rangarajan, R., 2005. Evaluation of check dam recharge through water table response in the ponding area. *Current Science*, v.89, pp: 677-681.
- Sayana, V.B.M., Arunbabu E., Mahesh Kumar, L., Ravichandran, S., and Karunakaran, K., 2010. Groundwater responses to artificial recharge of rainwater in Chennai, India: A case study in an educational institution campus. *Indian Journal of Science and Technology*, v.3, no.2, pp: 124-30.
- Sukhija, B.S., Reddy, D.V., Nandakumar, M.V. and Rama., 1997. A method of evaluation of artificial recharge through percolation tanks using environmental chloride. *Ground Water*, v.35, no.1, pp: 161-165.
- Sakthivadivel, R., 2007. The ground water recharge movement in India. In: Giordano, M., Villholth, K.G. (Eds.). *The Agricultural Groundwater Revolution: Opportunities and Threats to Development*. CAB International.
- Skougstad, M.W., Fishman, M.J., Friedman, L.C., and Erdmann, D.E., 1979. Methods for determination of inorganic substances in water and fluvial sediments: U.S. Geological Survey, *Techniques of Water-Resources Investigations*, Book 5, Chapter A1, pp: 626.
- Shah, T., 2012. Community response to aquifer development: distinct patterns in India's alluvial and hard rock aquifer areas. *Irrig. Drain*; v.61, no.1, pp: 14-25.
- Sharda V.N., Kurothe R.S., Sena D.R., Pande V.C., and Tiwari S.P., 2006. Estimation of groundwater recharge from water storage structures in a semi-arid climate of India. *Journal of Hydrology*, v.329, pp: 224-243.
- Surinaidu, L., Bacon, C.G.D., Pavelic, P., 2013a. Agricultural groundwater management in the Upper Bhima Basin, India: current status and future scenarios, *Hydrology and Earth System Sciences*; v.17, no.2, pp: 507-517, doi:10.5194/hess-17-507-2013.
- Surinaidu, L., Rao, V.V.S.G., Prasad, P.R., and Sarma, V.S., 2013b. Use of Geophysical and Hydrochemical Tools to Investigate Seawater Intrusion in Coastal Alluvial Aquifer, Andhra Pradesh, India *Groundwater in the Coastal Zones of Asia-Pacific*, v.7, pp: 49-65, Springer publications.
- Surinaidu, L., Rao, V.V.S.G., Rao, G.T., Mahesh, J., Padalu, G., and Sarma, V.S., 2012. An integrated approach to investigate saline water intrusion and to identify the salinity sources in the Central Godavari delta, Andhra Pradesh, India. *Arabian Journal of Geosciences*, v. 6, no.10, pp: 3709-3724, DOI: 10.1007/s12517-012-0634-2.
- Todd, D.K., 1980. *Ground Water Hydrology*, John Wiley & Sons, Inc., USA.
- Tripathi, A., and Prasad, A.R., 2009. Agricultural Development in India since Independence: A Study on Progress, Performance, and Determinants. *Journal of Emerging Knowledge on Emerging Markets*, v.1, Art. 8, Published by Digital Commons. Kennesaw State University, 2009.
- Wang, B., Menggui Jin., John, R., Nimmo, Lei Yang., Wenfeng, Wang., 2008. Estimating groundwater recharge in Hebei Plain, China under varying land use practices using tritium and bromide tracers. *Journal of Hydrology* 2008; v.356, pp: 209-222.
- World Bank., 2010. Deep wells and prudence: Towards pragmatic action for addressing groundwater overexploitation in India, Report 51676, The International Bank for Reconstruction and Development/The World Bank 1818 H Street, NW, Washington DC, 20433, USA, pp: 100.
- Wu, Q., Wang, G., Zhang, W., Cui, H., and Zhang, W., 2016. Estimation of Groundwater Recharge Using Tracers and Numerical Modeling in the North China Plain Qinghua Water, 2016, v.8, pp: 353; doi:10.3390/w8080353.
- Zarroca, M., Bach, J., Linares, R., and Pellicer, X.M., 2011. Electrical methods (VES and ERT) for identifying, mapping and monitoring different saline domains in a coastal plain region (Alt Empordà, Northern Spain). *Journal of Hydrology*, v.409, no.1-2, pp: 407-422.

Hydrochemical Signatures for Identification of Fresh and Saline Water Resources, along Visakhapatnam-Bhimunipatnam Corridor

P. Padmavathi Devi

DST Woman Scientist, Dept. of Geophysics, Andhra University, Visakhapatnam
E-mail:padmavathidv399@gmail.com

ABSTRACT

Phenomenal increase in the demand for potable water to meet the basic needs of the ever increasing population has led to significant increase in the exploitation of groundwater, especially in many segments of our country where surface water availability is meager. One such segment includes the urban conglomeration in and around Visakhapatnam. To ensure that many localities along and across Visakhapatnam-Bhimunipatnam corridor get potable water free from saline water pollution it has been decided to first identify the patches of fresh and saline water sources and then categorize them quality wise. As a part of this important societal problem, a hydrogeochemical study has been carried out in Visakhapatnam and Bhimunipatnam district situated along the East coast of India to primarily identify the influence of saline water on fresh water aquifers and then categorize quality wise the suitability of groundwater for drinking and domestic purposes. Limited investigations in this coastal region have reported signs of seawater intrusion, pollution due to industrial effluents and natural weathering process. A total of 63 groundwater samples have been collected and analyzed for major anions and cations for post and pre-monsoon seasons of 2015. The geochemical parameters have been compared with World and Indian quality standards. The study has revealed that most of the samples are suitable for drinking purpose. Gibb's plot revealed that the mechanisms responsible for controlling the chemical composition of the groundwater include both the rock water interaction and evaporation. The correlation of laboratory analysis of different proportions (%) of seawater to freshwater and to the field electrical conductivity indicates that 84% of samples are of type I category (low salts) and are safe for drinking. Out of the remaining, 13% of samples belong to type II (medium salts) and 3% to Type III (high salts) categories, respectively. The ionic ratios show that 8% of the samples indicate the transformation of the fresh groundwater aquifer system to saline.

Key words: Groundwater, Visakhapatnam-Bhimunipatnam, hydro-geochemical study, anions and cations, weathering, seawater intrusion, electrical conductivity.

INTRODUCTION

Distribution of fresh water resources is uneven throughout the World and the fresh water availability is becoming scarce day by day owing to population growth and diverse human activities. In the absence of fresh surface water resources, groundwater is exploited to meet the demand exerted by the various sectors. Variation in the water quality of groundwater in response to local geological set-up and anthropogenic factors warrants the evaluation of the quality of the groundwater for any purposes including that for human consumption. Many researchers across the globe (Babiker and Mohamedm, 2007; Vennila et al., 2008; Shomar et al., 2010 and Magesh et al., 2013) have carried out studies with spatial technologies and interpreted the quality of groundwater.

Groundwater of an aquifer in any given area has a unique chemistry acquired as a result of chemical alteration of meteoric water recharging the system (Back, 1966; and Drever, 1982). Water is the prime natural resource for Man's survival and overall development of the country. Water is flowing in two forms, namely, surface water and groundwater. Rapid urbanization, especially in developing

countries like India, has affected the availability and quality of groundwater due to its overexploitation, improper waste disposal, irrigation return water and lack of recharge. The quality of groundwater is the function of its physical and chemical parameters, which depend on the soluble products of weathering, decomposition and the related changes that occur with respect to time and space (Bhargava and Killender 1988; Prasad et al., 1984, Srinivasamoorthy 2011). Water pollution not only affects water quality but also threatens human health, economic development and social prosperity (Milovanovic 2007). The dependence on groundwater has increased tremendously in recent years in many parts of India. Hence, physico-chemical analysis of water is important to assess the quality of groundwater that influences the suitability of water for domestic, irrigation, and industrial needs (Prasanna et al., 2011; Chidambaram et al., 2011; Singaraja et al., 2013b; Ackah et al., 2011; Sayyed and Wagh, 2011; Tripathi, 2011). Generally, groundwater quality depends on the quality of recharged water, atmospheric precipitation, inland surface water and subsurface geochemical processes (Twarakavi and Kaluarachchi 2006, Singaraja et al., 2013b). The present study pertains to the evaluation of the physico-

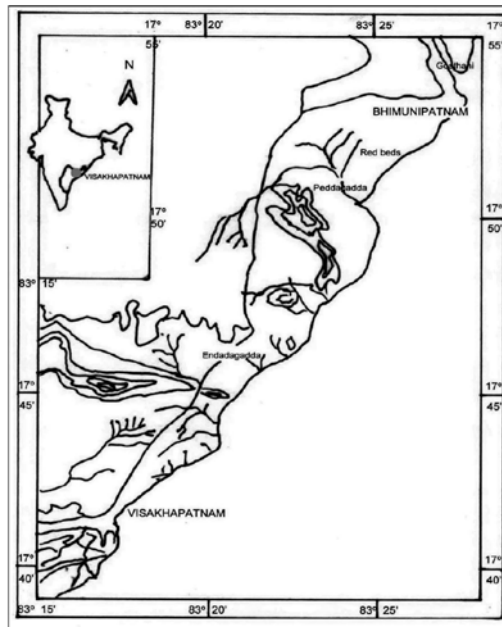


Figure 1. Map of the Study Area

chemical characteristics of the groundwater, since people are mainly dependent on the groundwater for their needs. The manuscript covers the suitability of the groundwater for drinking purposes, along and across Visakhapatnam-Bhimunipatnam corridor.

STUDY AREA

The study area, Visakhapatnam and Bhimunipatnam stretch is a 27km coastal strip situated along the East coast of India. It lies between North latitudes 17°30'- 18°0' and East longitudes 83°15'-83°30'.(Figure 1). The area under study is situated on either side of the beach road and it is characterized by Eastern Ghat mobile belt. This area is covered with denudational hills of height range between 30 to 540m above mean sea level. In the Visakhapatnam-Bhimunipatnam area, agriculture is the most important economic activity. Since agriculture depends on chemical fertilizers and pesticides that can degrade the quality of shallow aquifers through seepage of chemicals and also as the shallow aquifers in the coastal corridor under study can be affected by saline water intrusion, to ensure good quality of groundwater in the coming decades through large scale preventive measures it has been decided to take up hydro-geochemical investigations to obtain area specific groundwater chemistry. Such information, cross checked through seasonal monitoring, would help in proper planning of quality enhancement projects.

The prominent geological formations include Khondalites, Granite gneiss and Charnockites and Coastal alluvium of recent age. The major rock types exposed between Visakhapatnam and Bhimunipatnam along the

coast mainly belong to the Khondalitic group. Leptynites are found to exist in abundance. Minor quantities of Charnockites and Pegmatites occur at places. The red sediments (Rao, 1978) are found to occur as predominant land masses along the Visakhapatnam and Bhimilipatnam coast. These red sediments overlie Khondalites and Leptynites. The plain areas in the region are normally found to occur between two successive hill ranges. The plain areas mostly occupied by red sediments of varying thickness. It is further observed that one or more streams are found to flow through these plains to join the sea.

Pedda gedda, the largest stream along the coast exhibits dendritic pattern of drainage. These streams normally discharge excess rainwater from the inland areas and adjoining hills into the sea. Most of the streams discharge quickly because of the steep slope of the hills in the area.

MATERIALS AND METHODS

Groundwater samples have been collected in polyethylene bottles at 63 groundwater sampling sites during pre-monsoon and post-monsoon seasons (Figure 1) from open and bore wells. Physico-chemical parameters, such as Electrical Conductivity (EC) and pH have been measured in the field immediately after the collection of the samples using portable field meters. TDS has been calculated from EC by an empirical formula $TDS=0.64*EC$. Chloride, hardness, calcium, magnesium, carbonate and bicarbonate have been determined by titration. Flame photometer has been used to calculate the sodium and potassium. Sulphate has been determined by spectrometer. Analytical precision has been maintained throughout the experiments.

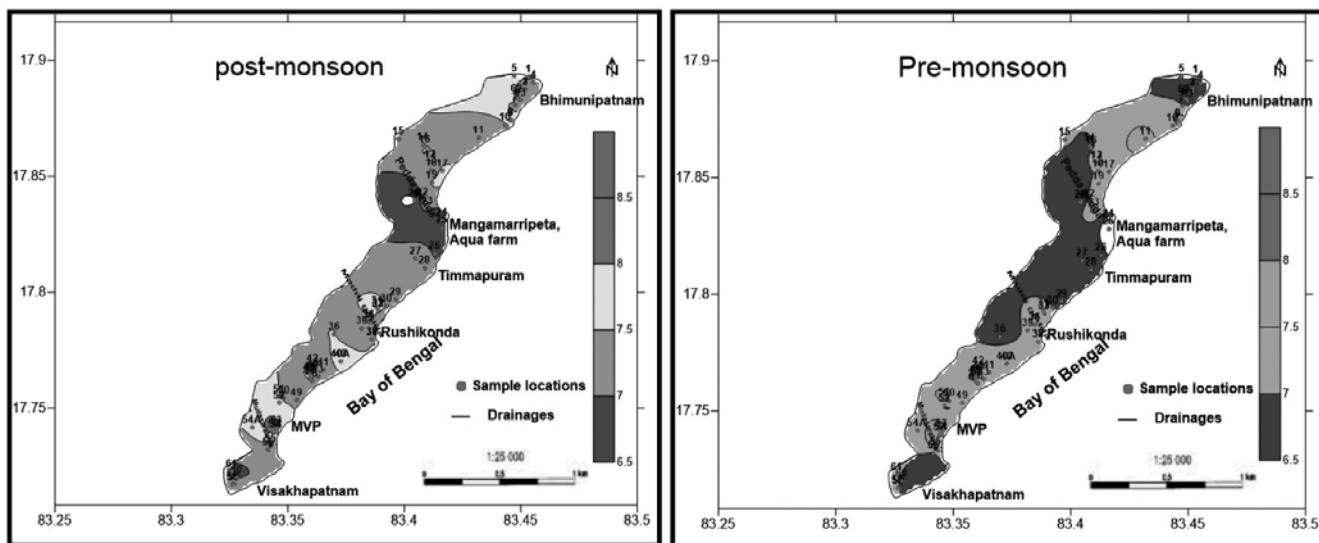


Figure 2. Distribution of pH in groundwater (Post and Pre monsoon).

Standard methods have been adopted for the analysis of the water samples (APHA 1995). The study area map has been prepared from the soft copy of the topographic map published by the Survey of India produced on a scale 1:25000.

RESULTS AND DISCUSSION

Potential Hydrogen (pH):

The pH of water is an important indicator for its quality and provides important information on geochemical equilibrium or solubility calculation (Hem 1985). The acceptable limit value for drinking water is specified as 6.5-8.5 (WHO 2011; ISI 2012). The Distribution of lesser value of pH indicates presence of CO₂ in water. The pH value of most of the groundwater samples in the study area for both post and pre-monsoon periods varies from 6.1-8.1 (Figure 2), which shows that the groundwater in the study area is slightly acidic and moderately alkaline in nature.

Electrical Conductivity

Electrical Conductance is a measure of the ability of water to conduct an electrical current-specific conductance. It is directly proportional to the saltiness (Salinity) or dissolved salt contents in water. The electrical conductivity of water is a measure of the conductance of cubic centimeter of water at 25 °C in micro-Siemens. The most desirable limit of EC in drinking water is 1,500 μs/cm (WHO 2011). Electrical Conductivity has been used as a criterion for the classification of drinking and irrigation waters (Erguvanli and Yuzer, 1987). The EC of groundwater in the study area is varying from 275-6300 μs/cm and 3970 μs/cm during post

and pre-monsoon periods, respectively (Figure 3). Higher EC in 3% of the study area indicates the enrichment of salts in the groundwater. Such higher concentration depends upon temperature, concentration and types of ions present (Hem 1985).

The EC can be classified as type I, if the enrichments of salts are low (EC < 1500 μs/cm); type II, if the enrichments of salts are medium (EC 1500 and 3000 μs/cm) and type III, if the enrichments of salts are high (EC > 3000 μs/cm). According to the above classification of EC, 84% of the total groundwater samples come under the type I (low enrichment of salts); 13% under type II (medium enrichment of salts) and 3% under type III (high enrichments of salts). While major parts of the study area come under good quality groundwater zones, the effect of saline water intrusion may be the reason for medium enrichment of EC in 13% of the study area and high percentage of salts in 3% of the study area. The conductivity of the groundwater sources varied in the total study area from 275-6300 μs/cm (post-monsoon) and 323-3970 μs/cm (pre-monsoon).

This shows that during the post-monsoon period, despite the groundwater dilution by precipitation, the EC increased significantly to 6300 μs/cm in 3% of the study area. Large variation in EC is mainly attributed to geochemical process like ion exchange, reverse exchange, evaporation, silicate weathering, rock water interaction, sulphate reductions and oxidation processes (Ramesh 2008). In the study area the enrichment of salt in groundwater, in 16% of the area, may be due to evaporation and anthropogenic activities. In general if proper precautionary measures are not taken at the earliest there is a possibility of increased salinity around such zones that are already polluted by saline water intrusion. The effect of pH may also increase the dissolution process, which eventually increases the EC value.

Hydrochemical Signatures for Identification of Fresh and Saline Water Resources, along Visakhapatnam-Bhimunipatnam Corridor

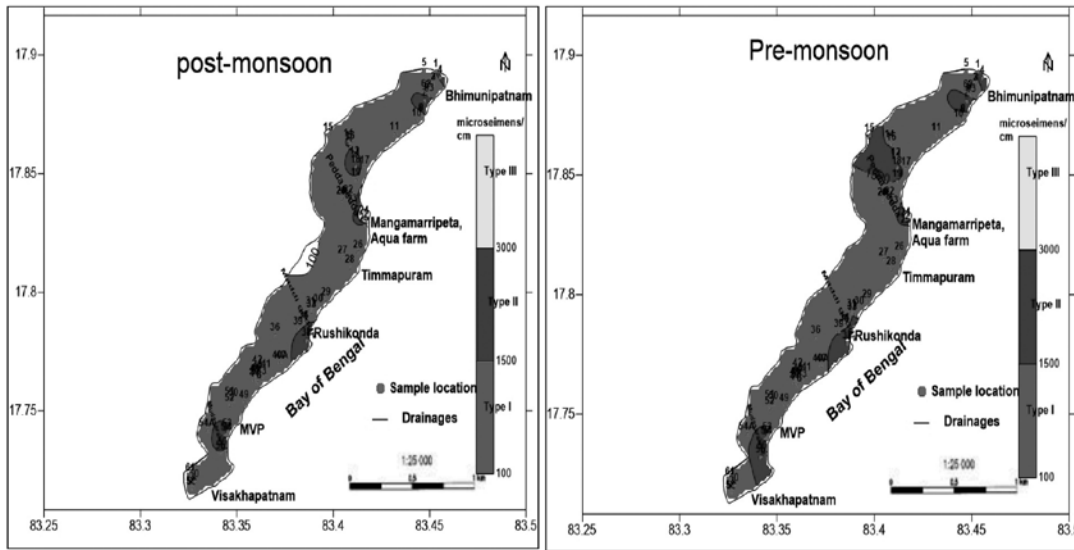


Figure 3. Distribution of EC in groundwater (Post and Pre- monsoon).

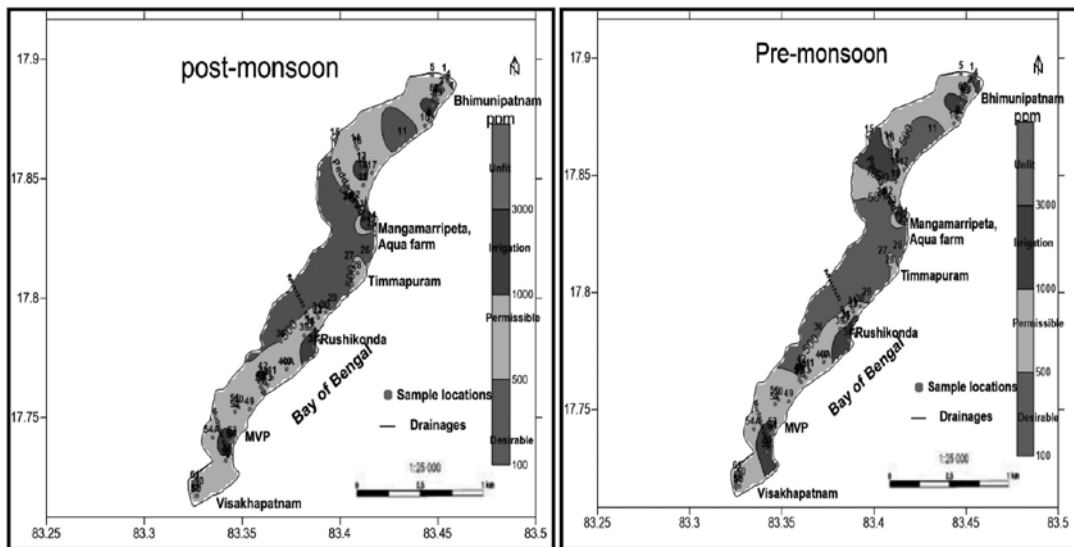


Figure 4. Distribution of TDS in Ground Water (Post and Pre Monsoon).

Total Dissolved Solids

The principal ions contributing to TDS are bicarbonate, carbonate, chloride, sulphate, nitrate, sodium, potassium, calcium and magnesium (US EPA 1983). According to (WHO, 2011) specification, TDS upto 500 mg/l is the highest desirable and upto 1000 mg/l is the maximum permissible. In the study area the TDS value varies between a minimum of 122mg/l and a maximum of 4089 mg/l (Fig 4) indicating most of the ground water samples lie within the maximum permissible limit. According to the Davis and De Wiest (1966) (Table 1) classification of groundwater based on TDS, 24% of the total groundwater samples are desirable for drinking (TDS<500mg/l), 58% permissible for

drinking (500-1000 mg/l) and 19% is suitable for irrigation purposes. High concentration of TDS in groundwater is due to leaching of salts from the soil and also domestic sewage may penetrate into the groundwater, which may lead to increase in TDS values. The spatial distribution of TDS in groundwater (pre and post monsoon) shows that major part of the study area comes under a mixed category of desirable cum permissible for drinking and good for irrigation. So, in reality even though major part of the study area comes under good quality groundwater zone, as per pH and EC values the higher TDS shows considerable impact due to anthropogenic activity. As such, even in the 84 % good quality zone it is better to distill TDS content to avoid probable ill effects due to direct drinking of groundwater.

Table 1. Classification of Groundwater samples of the study area

TDS (mg/l)	Class	Number of Samples		In Percentage	
		Post-Monsoon	Pre-Monsoon	Post-Monsoon	Pre-Monsoon
up to 500 mg/l	Desirable for drinking	15	15	24	24
500-1000 mg/l	Permissible for drinking	37	35	58	55
Up to 3000 mg/l	Useful for irrigation	10	12	16	19
Above 3000 mg/l	Unfit for drinking and irrigation	1	1	1.58	1.58

Calcium and Magnesium (Ca and Mg)

Calcium and magnesium are the most abundant elements in both surface and groundwaters. They exist mainly as bicarbonate and to a lesser degree in the form of sulphate and chloride. Calcium concentrations are varying from 141 to 2.1 mg/l. The higher concentration of calcium observed is 141 mg/l, from the groundwater samples collected from 3% of the study area. The desirable limit of calcium concentration for drinking water is specified as 75mg/l (ISI 2012). On an average in the good quality zone the percentage of calcium concentration hovers around 50 to 60 mg/l. This shows that all the groundwater samples in major part of the study area are within the permissible limit. Magnesium usually occurs in lesser concentrations in groundwater than calcium (Nilufer Arshad, 2009). Magnesium content is varying from 2.15 to 354 mg/l. The maximum permissible limit of magnesium concentration of drinking water is specified as 100mg/l (ISI 2012) and 150 mg/l (WHO 2011). Out of total 63 samples, Sample numbers 7, 15, 24, 37, 38, 56, 57 exceeds the ISI limit as they show values of 110, 106, 124, 112, 223, 354 mg/l. This shows that only about 10 % of samples are beyond permissible level.

The seawater has high Mg concentration than Ca. The ionic ratios Mg/Ca, HCO₃/Cl were plotted against the samples to evaluate the groundwater chemistry of the wells used in the present study. Fig.5 shows that 8% of the samples are showing extremely low HCO₃/Cl and variably high Mg/Ca during pre- monsoon season indicating the transformation of the fresh groundwater aquifer system to saline.

Sodium and Potassium (Na and K)

Sodium ranks sixth among the elements in order of abundance and is present in most of the natural waters. Sodium is generally found in lower concentration than calcium and magnesium in freshwater. The concentration of sodium is varied from 15 to 538mg/l. The maximum permissible limit of sodium is 200mg/l. Processed samples reveals that a few samples are exceeding the permissible limit of WHO and ISI. Since groundwater with high sodium content is not suitable for agriculture,

as it tends to deteriorate the soil, the zones that contain high concentration of sodium be left out for conventional agriculture. If experimental cultivation yields good results these patches of land could be used for growing saline resistant varieties of rice.

Potassium is a naturally occurring element; however its concentration remains quite low compared to calcium, magnesium and sodium. Its concentration in drinking water seldom reaches 20mg/l. The concentration of potassium in both post-monsoon and pre-monsoon seasons is found to vary from 0.82 to 87.2mg/l. The maximum permissible limit of potassium in the drinking water is 30mg/l. Higher concentrations are found only in 4 samples. The low concentration of potassium found in some samples is due to high resistance of potash feldspars to chemical weathering in the study area.

Bicarbonate (HCO₃)

The value of bicarbonate ranges from 57 to 765 mg/l. Bicarbonate is the dominant ion, except in the groundwater, occurs near the coast. The higher concentration of bicarbonate in the water points to the dominance of mineral dissolution (Stumm and Morgan 1996).

The plot of ionic ratio of bicarbonate/ chloride versus TDS is shown in Figure 6, for both post and pre-monsoon seasons. The plot shows that the values of HCO₃/Cl (meq/l) are <1 in the high TDS concentration (>2000) range of the analyzed samples, while its slope is positive in the low TDS concentration range (<2000mg/l). This result indicates that groundwater with high TDS concentrations is enriched with chloride due to sea water intrusion and the groundwater with low TDS concentrations is less affected by seawater. Only few samples of the study area are affected by seawater intrusion.

Sulphate (SO₄)

Sulphate is one of the major anions occurring in surface waters. A decline in a Sulphate ion frequently is associated with an increase in bicarbonate ions (Fred Bell, 1998). The upper limit for sulphate concentration for drinking water is 200mg/l (ISI 2012). The sulphate concentration in the study area ranges between 0.9 to 166 mg/l during post

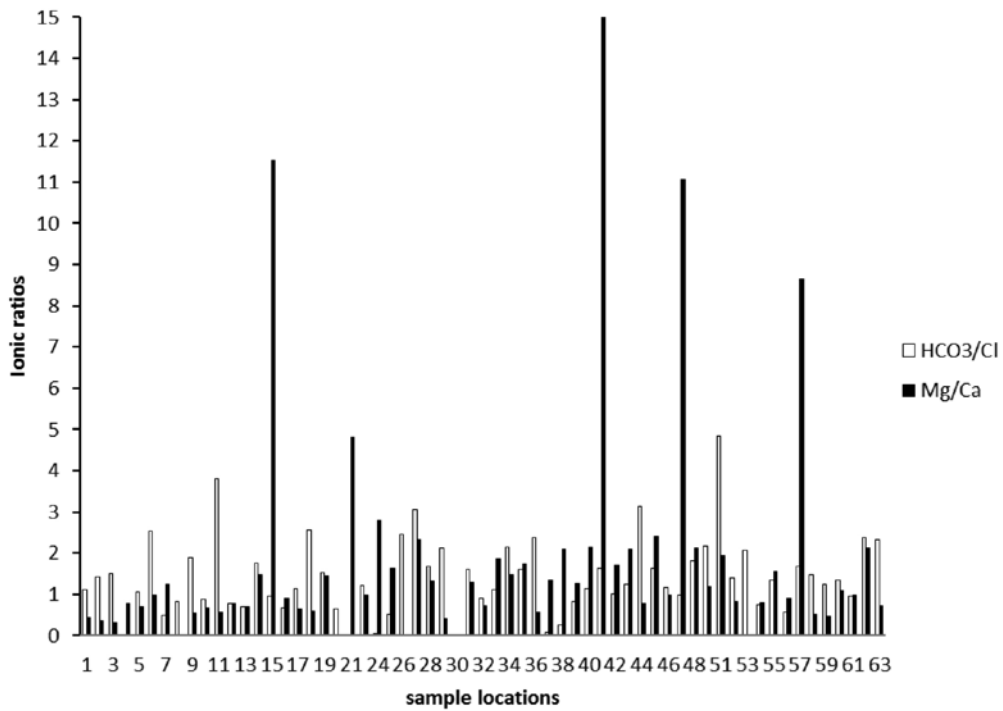


Figure 5. Ionic ratios of HCO₃/Cl and Mg/Ca.

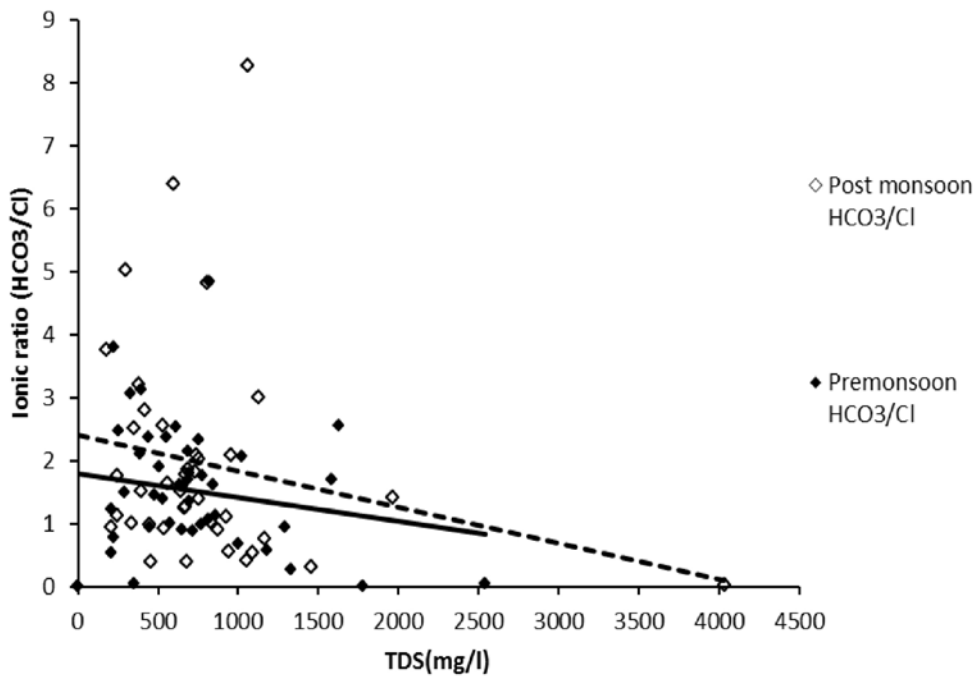


Figure 6. Cross plot of TDS versus HCO₃/Cl for post and pre monsoon seasons.

and pre-monsoon seasons. All the samples fall within the desirable limits. Higher concentration of Sulphate could cause a cathartic action on human beings and also cause respiratory problems (Maiti, 1982; Subba Rao and Prathap Reddy, 1999; and Subba Rao et al., 2002).

Chloride (Cl)

The origin of chloride in groundwater may be from diverse sources such as weathering, leaching of sedimentary rocks and soils, intrusion of saltwater, domestic and industrial

Table 2. Stuyfzand (1989) classification of groundwater

S.No	Main type	Cl(mg/l)	No. of samples
1	Oligohaline	5-30	1
2	Fresh	30-150	37
3	Fresh-Brackish	150-300	19
4	Brackish	300-1000	6

Table 3. Classification of groundwater

Percentage of seawater mixing		Type I <1500	Low salts
1%	955		
2%	1450		
4%	2910	Type II 1500-3000	Medium salts
6%	4200	Type III >3000	More salts
8%	5510		
10%	6760		
14%	9380		
18%	12000		
20%	12900		
40%	24000		
60%	34400		
100%	56000		

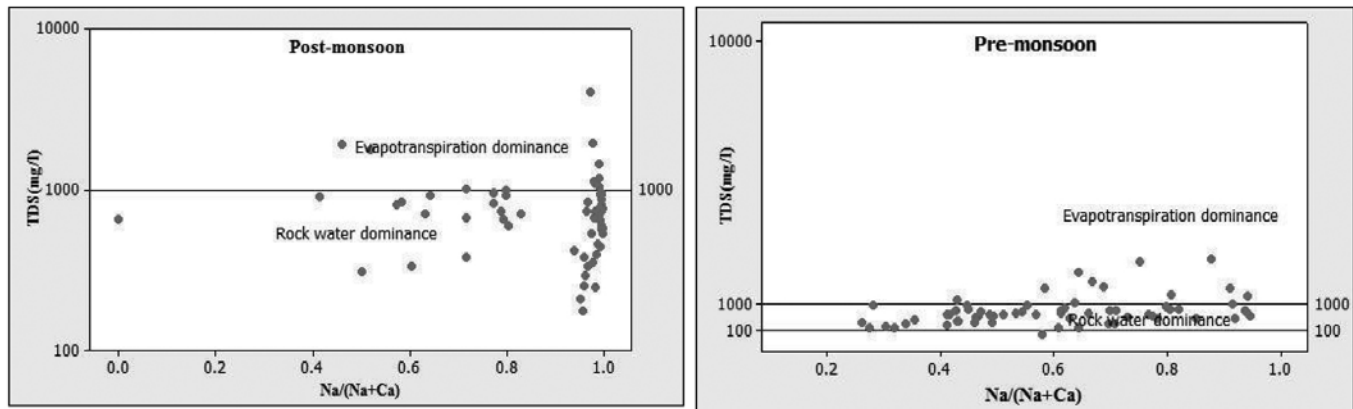


Figure 7. Gibb's diagram for post- monsoon and pre-monsoon seasons.

waste discharges, municipal effluents etc. (Karanth 1987). In the study area, the concentration of chloride is between 21 to 2769 mg/l. relatively high concentration of chloride is observed for the groundwater samples 7, 13, 15, 18, 24, 37, 38, 57. A desirable limit of chloride for drinking water is specified as 250mg/l (ISI 2012). The excess of chloride in the water is usually taken as an index of pollution and considered as tracer for groundwater contamination (Loizidou and Kapetanios 1993). In natural waters, the concentration of Cl bears strong correlation with the sodium content and specific conductance. High levels of Na and Chloride ions in coastal water may indicate a

significant effect of seawater mixing (Mondal et al., 2008). According to Stuyfzand (1989) classification (Table 2) 59% of samples are fresh waters, 30% of samples belong to a mixture of fresh and brackish waters and 10% of samples are completely brackish.

Mechanism Controlling the Ground Water Chemistry

Gibb's Diagram

The mechanism controlling chemical relationships of groundwater based on aquifer Lithology and nature of

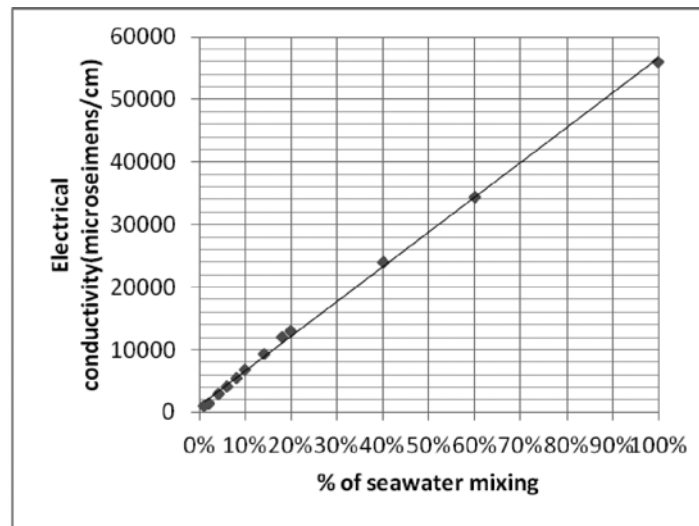


Figure 8. Plot of seawater mixing vs Electrical Conductivity.

geochemical reactions and solubility of interaction rocks has been studied following Gibbs (1970) and Viswanathaiah et al., (1978). The source of the dissolved ions in the groundwater can be understood by a Gibbs diagram (Gibbs, 1970). It is a plot of $(\text{Na}^+)/(\text{Na}^+ + \text{Ca}^{+2})$ vs. TDS. The Gibbs plot of data from the study area (Figure 7) indicates that interaction of rocks with the groundwater is the dominant process controlling the major ion composition of groundwater for both post-monsoon and pre-monsoon seasons. The plot indicates that the groundwater samples of the study area overlap in the rock-water interaction and evaporation dominance categories (Chidambaram et al., 2008; Srinivasamoorthy et al., 2008, Chowdhury and Srimanta Gupta 2011, Manikandan et al., 2011).

Laboratory studies: Mixing of seawater

Laboratory studies have been carried out to classify the groundwater based on Electrical Conductivity by mixing different proportions (%) of seawater to freshwater. The Figure 8 shows how concentration of EC is increasing for varying percentage of seawater mixing. Based on these laboratory results (Table 3) the samples of the study area are categorized as: 84 % of samples belong to type I and 13% to type II and 3% to type III.

CONCLUSIONS

The groundwater in the study area is slightly acidic and moderately alkaline in nature.

Based on EC and TDS, 84% of the total groundwater samples of the study area are desirable for drinking and good for irrigation.

Based on the hydrogeochemical parameters and their ionic ratios the seawater intrusion is noticed in few locations.

8% of the samples are showing extremely low HCO_3/Cl and variably high Mg/Ca during pre-monsoon season indicating the transformation of the fresh groundwater aquifer system into saline.

The plot of bicarbonate/ chloride versus TDS for both post and pre-monsoon seasons shows the values of HCO_3/Cl were <1 in the high TDS concentration (>2000) range of the analysed samples, while its slope was steeply negative in the low TDS concentration range ($<2000\text{mg/l}$), indicating that groundwater with high TDS concentrations was enriched with chloride due to seawater intrusion and the groundwater with low TDS concentrations is less affected by seawater.

Gibb's plot reveals that the mechanisms responsible for controlling the chemical composition of the groundwater are both rock water interaction and evaporation.

ACKNOWLEDGEMENTS

This study was carried out under the DST, Women Scientist Scheme-A (WOS-A) fellowship funded by Department of Science & Technology, Govt. of India, New Delhi (Ref No- SR/WOS-A/ES-07/2014). The author would like to thank the DST for the support and encouragement to carry out the research project. Thanks are due to Prof. P. Rajendra Prasad and Prof. P. Rama Rao, for their guidance and support. I am indebted to Dr.P.R.Reddy for his encouragement and support for the last two decades in moulding my research career. I thank him for refining and editing the manuscript.

Compliance with Ethical Standards

The author declares that she has no conflict of interest and adheres to copyright norms.

REFERENCES

- Ackah, M., Agyemang O., Anim A.K, Oseil,J., Bentil, N.O., Kpattah, L., and Gyamfil, E.T., 2011. Assessment of groundwater quality for drinking and irrigation: the case study of Teiman- Oyarifa Community, Ga East Municipality, Ghana. *Proceedings of the International Academy of Ecology and Environmental Sciences*, v.1, no.3-4, pp: 186-194.
- A.K. Chowdhury, and Srimanta Gupta., 2011. Evaluation of water quality, Hydro-geochemistry of Confined and Unconfined aquifers and irrigation water quality in Digha Coast of West Bengal, India (A case study) *International journal of environmental sciences*, v.2, no.2, pp: 576-589, ISSN 0976 – 4402.
- APHA 1995. *Standard Methods for the Examination of Water and Wastewater*, 19th Edition, American Public Health Association, Byrd Prepress Springfield Washington DC.
- Babiker, I.S. and Mohamedm. T.H., 2007. Assessing groundwater quality using GIS: *Water Resource Manage*, v.6, pp: 699-715.
- Back, W., 1966. *Hydrochemical Facies and Groundwater Flow Patterns in the Northern Part of the Atlantic Coastal Plain*. USGS pp: 498.
- Bhargava, D.S., and Killender, D.J., 1988. The technology of water resources in Industries. A rational approach. *Jr. Ind. Wat. Works Assn.*, v.20, no.1, pp: 107-112.
- Chidambaram, S., Ramanathan, A.L., Anandhan, P., Srinivasamoorthy, K., Prasanna M.V., and Vasudevan, S., 2008. A statistical approach to identify the hydrogeochemically active regimes in ground waters of Erode district, Tamilnadu. *Asian J. Water Environ Pollut*. v.5, no.3, pp:123-135.
- Chidambaram, S., Karmegam, U., Prasanna, M.V., Sasidhar, M. and Vasanthavigar, M., 2011. A study on hydrochemical elucidation of coastal groundwater in and around Kalpakkam region, Southern India. *Environ Earth Sci*. v.64, no.5, pp: 1419-1431.
- Davis, S.N., and De Wiest, R.J.M., 1966. *Hydrogeology* New York: John Wiley and Sons, v.6, pp: 463.
- Drever, J.I., 1982. *The Geochemistry of Natural Waters*, Prentice-Hall, Englewood Cliffs, NJ, USA, pp: 382.
- Erguvanli, K., and Yuzer, E., 1987. *Groundwater geology (hydrogeology)*. ITU Maden Fakültesi, Istanbul, pp: 339 (in Turkish).
- Fred Bell., 1998. *Environmental Geology: Principles and Practice / Fred G. Bell*. Bell, F.G. (Frederic Gladstone) English, Book, Illustrated edition.
- Gibbs, R.J., 1970. *Mechanism Controlling World's Water Chemistry*. *Science*, v.170, pp: 1088-1090.
- Hem, J.D., 1985. *Study and Interpretation of the Chemical Characteristics of Natural Water*. USGS Water Supply Paper, v.2254, pp: 117-120.
- IS 10500: 2012. *Indian Standard drinking water specification (Second Revision)*.
- Karant, K.R., 1987. *Groundwater assessment, development and management*. Tata McGraw Hill, New Delhi, pp: 576-657.
- Loizidou, M., and Kapetanios, E., 1993. Effect of leachate from landfills on underground water quality. *Sci. Total Environ.*, v.128, pp: 69-81.
- Magesh, N.S., Krishnakumar, S., Chandrasekhar, N., and Soundranayagam, J.P., 2013. *Groundwater quality assessment using WQI and GIS techniques, Dindigul district, Tamil Nadu, India*, *Arab J Geosciences*. DOI 10.1007/s12517-012-0673-8, pp: 4179-4189.
- Maiti, T.C., 1982. *The Dangerous Acid Rain*. *Sci Report*, v.9, no.6, pp: 360-363.
- Manikandan, S., Chidambaram, S., Prasanna, M.V., Thivya, C., and Karmegam, U., 2011. *Hydrochemical Characteristics and Groundwater Quality Assessment in Krishnagiri District, Tamilnadu, India*. *International Journal of Earth Sciences and Engineering*, v.4, no.4, pp: 623-632.
- Milovanovic, M., 2007. *Water quality assessment and determination of pollution sources along the Axios/Vardar River, Southeastern Europe*. *Desalination*, v.213, pp: 159-173.
- Mondal, N.C., Singh, V.S., Saxena, V.K., and Prasad, R.K., 2008. *Improvement of groundwater quality due to fresh water ingress in Potharlanka Island, Krishna delta, India*. *Environmental Geology*, v.55, no.3, pp: 595-603.
- Nilufer Arshad., 2009. *Environmental Management of Water Resources for Sustainable Development in Western Part of Hunsur, Karnataka, India, Using Remote Sensing and Gis.*, Ph.D. Thesis, Geology Department, Mysore University.
- Prasad, P.R., Pekdeger, A., and Ohse, W., 1984. *Geochemical and geophysical studies of saltwater intrusion in coastal regions*. In: *Proceedings of Hamburg Symposium*. IAHS publication no. 146, pp: 209-218.
- Prasanna, M.V., Chidambaram, S., Gireesh, T.V., and Jabir Ali, T.V., 2011. *A study on hydrochemical characteristics of surface and subsurface water in and around Perumal Lake, Cuddalore District, Tamil Nadu, South India*. *Environ Earth Sci*. v.64, no.5 pp: 1419- 1431.
- Ramesh, K., 2008. *Hydrochemical studies and effect of irrigation on groundwater quality Tondiar basin Tamilnadu*. Unpublished Ph.D thesis, Anna University, Chennai, Tamilnadu.
- Rao, A.T., 1978. *Red Sediments from Visakhapatnam, Andhra Pradesh*, v.19, no.2, pp: 79-82, Published: 1978-02-01.
- Sayed, M.R.G., and Wagh, G.S., 2011. *An assessment of groundwater quality for agricultural use: a case study from solid waste disposal site SE of Pune, India*. *Proceedings of the International Academy of Ecology and Environmental Sciences*, v.1, no.3-4, pp: 195-201.
- Shomar, B., Fakher, S.A., and Yahya, A., 2010. *Assessment of groundwater quality in the Gaza strip, Palestine using GIS mapping*. *J.Water Resource and Protection*, doi:10.4236/jwarp.2010.22011, pp: 93-104.
- Singaraja, C.S., Chidambaram, S., Anandhan, P., Prasanna, M.V., and Thivya, C., Thilagavathi, R., and Sarathidasan, J.,

Hydrochemical Signatures for Identification of Fresh and Saline Water Resources, along Visakhapatnam-Bhimunipatnam Corridor

2013. Hydrochemistry of groundwater in a coastal region and its repercussion on quality, a case study—Thoothukudi district. *Arabian Journal of Geosciences*. DOI: 10.1007/s12517-012-0794-0.
- Singaraja, C., Chidambaram, S., Prasanna, M.V., Thivya, C., and Thilagavathi, R., 2013b. Statistical analysis of the hydrogeochemical evolution of groundwater in hard rock coastal aquifers of Thoothukudi district in Tamil Nadu, India. *Environ Earth Sci* DOI 10.1007/s12665-013-2453-5 <http://dx.doi.org/10.1007/s12665-013-2453-5>.
- Srinivasamoorthy, K., Chidambaram, S., Prasanna, M.V., Vasanthavigar, M., John Peter, A. and Anandhan, P., 2008. Identification of major sources controlling groundwater chemistry from a hard rock terrain—a case study from Metturtaluk, Salem district, Tamilnadu India. *J Earth Syst Sci*. v.117, no.1, pp: 49–58.
- Srinivasamoorthy, K., Nanthakumar, C., Vasanthavigar, M., Vijayaraghavan, K., Rajivgandhi, R., Chidambaram, S., Anandhan, P., Manivannan, R. and Vasudevan, S., 2011. Groundwater Quality Assessment from a Hard Rock Terrain, Salem District of Tamilnadu, India. *Arab J. Geosci*, v 4, pp: 91-102.
- Stuyfzand, P.J., 1989. A new hydrochemical classification of water types, *Proc, IAHS 3 Science Association*, Baltimore, U.S.A, pp: 33-42.
- Stumm, W., and Morgan, J.J., 1996. *Aquatic chemistry*. Wiley, New York. ISBN: 978-0-471-51185-4.
- Subba Rao, N. and Prathap Reddy, R., 1999. Groundwater Prospects in a Developing Satellite Township of Andhra Pradesh, India, *J. Indian Soc Remote Sensing*, v. 27, No. 4, pp:193-203.
- Subba Rao, N., Prakasa Rao, J., John Devadas, D., Srinivasa Rao, K.V., Krishna, C., and Nagamalleswara Rao, B., 2002. Hydrogeochemistry and Groundwater Quality in a Developing Urban Environment of a Semi-Arid Region, Guntur, Andhra Pradesh, India. *Journal of the Geological Society of India*, v.59, pp: 159-166.
- Thilagavathi, R., Chidambaram, S., Prasanna, M.V., Thivya, C., and Singaraja, C., 2012. A study on groundwater geochemistry and water quality in layered aquifers system of Pondicherry region, southeast India. *Applied Water Science*, v.2, no.4, pp: 253–269.
- Tripathi, V.K., Rajput, T.B.S., Patel, N., Lata Rao, A.R., and Chandrasekharan, H., 2011. Dynamics of microorganisms under micro-irrigation system with municipal wastewater. In: *International Symposium on Water for Agriculture*, 17-19 January 2011, Nagpur, India. pp. 95.
- Twarakavi, N.K.C., and Kaluarachchi, J.J., 2006. Sustainability of groundwater quality considering land use changes and public health risks. *J. Environ. Manag.*, v.81, pp: 405-419.
- US EPA., 1983. *Methods for Chemical Analysis of Water and Waste*. EPA-600/4-79-020, US Environ, Protection Agency, Cincinnati, Ohio, USA.
- Vennila, G., Subramani, T., and Elango, L., 2008. GIS based Groundwater quality assessment of Vattamalaikarai Basib, Tamil Nadu, India. *Nat.Env. and Poll.Tech*.v.7, no.4, pp: 585-592.
- Viswanathaiah, M N., Sastri, J.C.V., and Rame Gowda, B., 1978. Mechanisms Controlling the Chemistry of Groundwater of Karnataka. *Indian Mineralogist*, v.19, pp: 65-69.
- WHO 2011. *Guidelines for Drinking-Water Quality*. ISBN: 978 92 4 154815 1, pp: 564,

Received on: 30.1.18, Revised on: 21.2.18, Accepted on: 24.2.18

Estimation of Total and Unit Stream Power along Bhagirathi River, Uttarakhand, India

Satya Prakash* and Rajesh Kumar

Centre for the Study of Regional Development, School of Social Sciences,
Jawaharlal Nehru University, New Delhi-110067, India

*Corresponding Author: satyapthakur@gmail.com

ABSTRACT

Stream power is mostly used as an indicator for investigating engineering structures along the river banks. It has a considerable influence on forms and processes of the river system. It also provides information regarding the potential of a river to move sediments. The objective of this study is to estimate the total and unit stream power of Bhagirathi River and thereby to find the relationship of average unit stream power with landslides along the river. In this study, the longitudinal profile of the Bhagirathi River has been drawn using filled ASTER DEM in GIS environment. The smoothed longitudinal profile has been further used for the computation of slope at 1 km interval. The power function relationship has been established between peak discharge and drainage area to estimate peak discharge for ungauged points along the Bhagirathi River at 1 km interval. Channel slope, the specific weight of water and discharge are vital parameters for stream power computation. Total and unit stream power have been estimated at 1 km interval along the Bhagirathi River. The slope is found to be 0.04 and 0.0014 mm^{-1} along the extreme upper and lower reaches of the Bhagirathi River, respectively. Due to the steep slope, the total and unit stream power profiles show high peaks in the mid-stream of the Bhagirathi. The fluctuations in the total stream power along the Bhagirathi River signify the variation in sub-regional slope as well as in discharge contributing areas. The unit stream power is high in the upper reaches of the river, and it shows decreasing trend in downstream. Unit stream power mainly governs the bar deposition in the active channel of the Bhagirathi River. The association between average unit stream power and number of exposures/landslides has been found to be statistically significant at the 0.01 level of significance.

Keywords: Longitudinal profile, Total stream power, Unit stream power, Bhagirathi River, ASTER DEM, GIS, Polymodal distribution.

INTRODUCTION

Stream power is a product of stream slope, discharge, and weight of water that influence sediment transport (Rhoads, 1987; Gartner, 2016). The geomorphic impacts of the running water in an open channel and sediment transportation are assessed regarding the distribution of stream power per unit channel area over time (Jain et al., 2006; Kale, 2007). River develops a broad range of channel shapes during young, mature and old stages with respect to the available energy distribution in each stage. Potential or position energy is the main force, driving the river system (Fonstad, 2003). The potential energy is gradually transformed into kinetic energy when the river flows along the slope. Thus, kinetic energy is an essential factor for erosional and transportation functions to make the fluvial system active (Knighton, 1999). The total and unit stream power are significant predictors of geomorphic response to a flood event (Yochum et al., 2017).

Rhoads (1987) argued that the stream power can be used in a conceptual context rather than specific quantitative measures of power. An actual measurement of energy expenditure is not possible in the river system (Rhoads, 1987). Hence, various alternative methods (e.g.,

total stream power and cross-sectional stream power) can be used for measuring the true stream power of the rivers (Fonstad, 2003). Bagnold (1966) termed the cross-sectional stream power as unit stream power. He applied unit stream power for calculation of sediment transport rate and for the prediction of the competence of a river. Bagnold (1966) used stream power as a theoretical basis for evaluating the bedload transport in a channel. Phillips (1989) also observed that the sediment transport capacity in a channel depends on the unit stream power. A few field studies of stream power have predicted downstream energy expenditure trends using hydraulic geometry principle (Knighton, 1999; Kale, 2007; Bawa et al., 2014; Righini et al., 2017; Wicherski et al., 2017; Yochum et al., 2017). Graf (1983, 1998) observed that the lithological dissimilarity could be responsible for the variation in stream power.

In the fluvial system, the morphology of an open channel evolves from equilibrium between the energy exerted by the running water in a channel and the resistance of sediments of the channel perimeter against entrainment (Lecce, 1997). The stream power has been studied as a vital factor that influences components of the river system, including channel shape (Mosley, 1981), sediment transport rates (Bagnold, 1966), sediment delivery

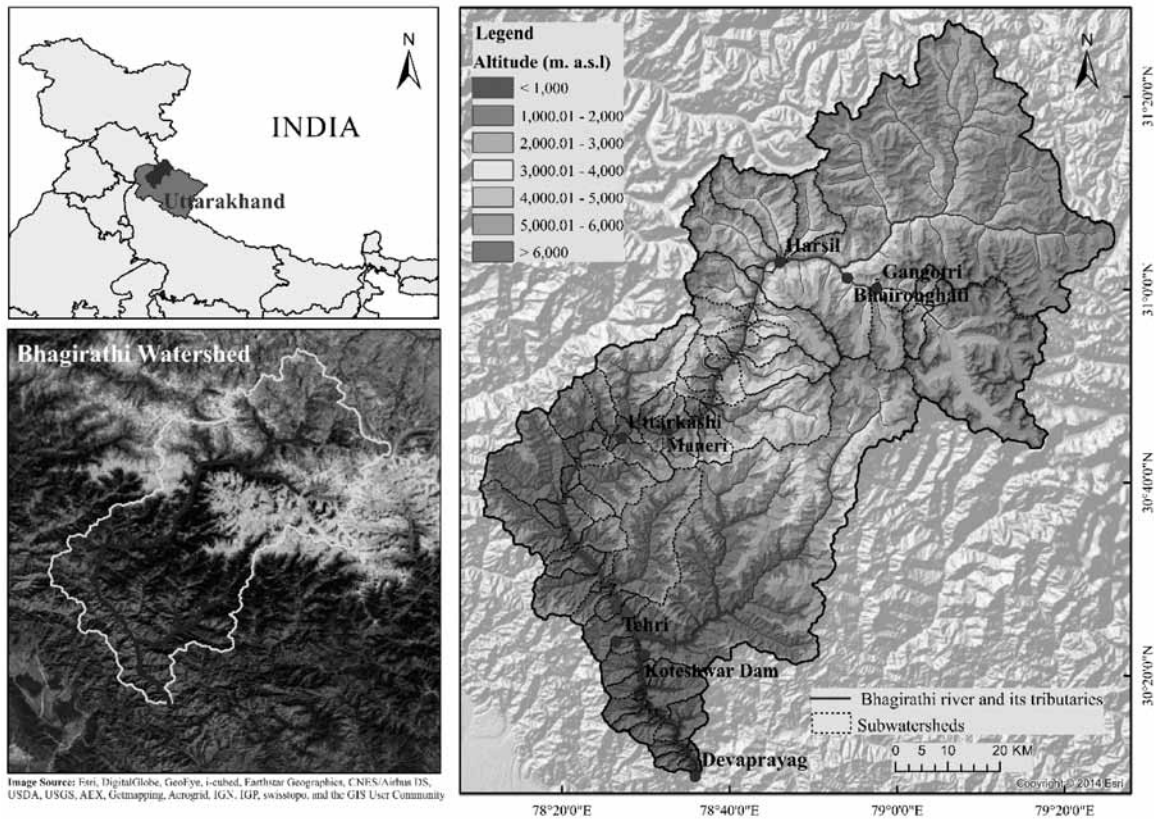


Figure 1. Location map of the study area.

ratios (Phillips and Slattery, 2006), channel migration (Nanson and Hickin, 1986; Kumar et al., 2013), channel pattern (Schumm and Khan, 1972), bedload movement (Petit et al., 2005), aggradation/ degradation threshold (Bull, 1979), riffle and pool characteristics (Wohl et al., 1993), genetic classification of floodplain (Nanson and Croke 1992), floodplain initiation processes (Jain et al., 2008) and geomorphic effectiveness of floods (Kale, 2007).

The spatial pattern of stream power expenditure has been possibly applied to correlate the longitudinal distribution of geomorphic features within a channel with stream energy. However, modeling of the river system is a challenging task because the physically-based relationship between channel geomorphic features within a channel and processes are not well established (Fonstad, 2003). The morphological structure and behavioral attributes of streams are controlled by the variables such as catchment hydrology, sediment character, degree of channel confinement, sediment supply, channel gradient, flood history, vegetation and human impact (Leopold et al., 1964; Kale, 2008; Ortega et al., 2014). Generally, in the tropical regions, the gradient decreases with an increase in discharge from upstream to downstream. Hence, channels do lateral expansion as they enter flat alluvial plains. Geological controls propel considerable local discontinuities in longitudinal profile of a river. However, the downstream variations in slope and

elevation produce a striking change in channel shape and morphology (Graf, 1983; Reinfelds et al., 2004).

Uttarakhand state is highly prone to flood and landslides. After June 2013 flood event, it became necessary to know the total and unit stream power of all Uttarakhand Rivers. Jack (2010) estimated total and unit stream power for Ganga and Yamuna River. Furthermore, he selected a small reach along the Ganga River, starting from Rishikesh to Balawali. Against the backdrop of studies mentioned above, this research is focused on the total and unit stream power estimation along the Bhagirathi River. Such a study will significantly help engineers and planners to manage and construct engineering structures along or across the Bhagirathi River.

STUDY AREA

The Bhagirathi is a major source stream of the Ganga river system in the state of Uttarakhand. The holy Bhagirathi River is a major river of the Gangetic plain of northern India. The headwater of the Bhagirathi River originates from Gamukh (snout of Gangotri glacier) at an elevation of 4255 meters a.m.s.l. Its principal tributaries join river at different locations; these are Kedar Ganga at Gangotri, Jadh Ganga at Bhaironghati, Kakora Gad, and Jalandhari Gad near Harsil, Siyan Gad near Jhala, Asi Ganga near Uttarkashi, Bhilanga River near old Tehri at an elevation of 1,750 m a.m.s.l. (Figure 1).

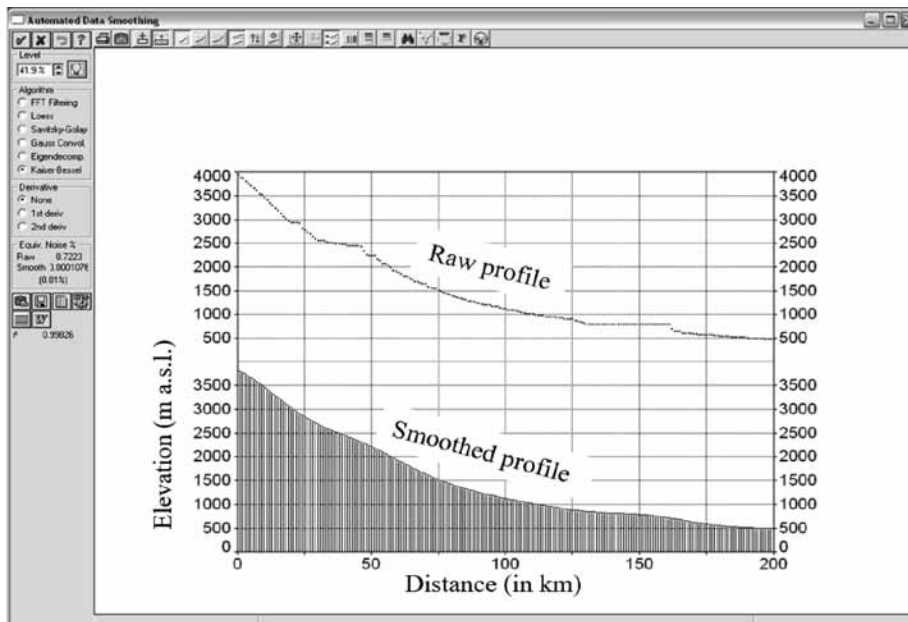


Figure 2. Raw and smoothed longitudinal profile of the Bhagirathi River.

The Bhagirathi River is 205 km long and the Alaknanda River joins it at Devprayag (elevation of 465 m, a.m.s.l.). Downstream of the confluence, the Bhagirathi is known as the holy Ganga River. In the Bhagirathi River basin, the Chaukhamba-I is the highest peak. There are several human-made dams along the Bhagirathi River, some are functional, but some are under construction or planned. The total catchment area of the Bhagirathi River is 8846.64 km², distributed in Uttarkashi and Tehri Garhwal districts of Uttarakhand.

DATA AND METHODOLOGY

Geomorphic mapping was completed using Google Earth satellite images of 2014. The Advanced Spaceborne Thermal Emission and Reflection Radiometer Digital Elevation Model (ASTER DEM), Global Digital Elevation Model Version 2 (GDEM V2) released in 2011 at 30 m spatial resolution were obtained from the USGS Global Visualization Viewer (GloVis). In this study, Spatial analyst tool (hydrology) of ESRI ArcGIS 10 was used for watershed demarcation, calculation of river profile and estimation of channel slope. ASTER DEM data were used for delineation of Bhagirathi watershed at 1 km interval and its major rivers using D-8 flow algorithm of ArcGIS 10. Subsequently, the trunk stream (Bhagirathi) was selected to extract the bed elevation values from the filled ASTER DEM using 3D Analyst of ArcGIS 10. The raw longitudinal profile contains many unrealistic kinks that are due to noise in DEM data. These unrealistic kinks were removed to compute the slope (Bawa et al., 2014). The smoothing of river profile was performed in Table 2D Curve software. In trial version of Table 2D Curve software automated data

smoothing method, 'Kaiser-Bessel' was used to eliminate the unrealistic kinks from the raw profile (Figure 2) (e.g. Thomson and Emery, 2014). The association of raw and smoothed profile is strong as the r² value is 99.82. Further, the smoothed profile was used to compute slope. A 200 km long longitudinal profile and slope (m/m) were derived for the Bhagirathi river.

Channel slope is an essential component for estimation of discharge and velocity of the river. Channel slope was computed at 1 km interval using smoothed longitudinal profile of the Bhagirathi River. Channel slope was calculated using Eq. (1):

$$S = \Delta H / \Delta L \dots\dots\dots (1)$$

S= slope, the ΔH=Height difference (m), the ΔL=Channel length between two successive points (m). The slope was calculated for 1 km interval. Step-wise flowchart of creation of longitudinal profile and slope estimation at an equal interval of 1 km are shown in Figure 3.

Hydrological data (Table 1) were obtained from the thesis of Jack (2010). These data were used to establish a power function relationship between discharge and drainage area (Eq. 2) (Jain et al., 2006). The discharge data are available for a few sites in the Bhagirathi and Alaknanda basins (Table 1).

A continuous distribution of discharge (Q) is necessary for stream power estimation, based on discharge-area relationship along the Bhagirathi River (Eq.2):

$$Q = a * A^b \dots\dots\dots (2)$$

Where A is the contribution catchment area in km², Q shows discharge (m³s⁻¹), the a and b coefficients are equal to 0.580 and 0.841, respectively. The coefficient of determination (r²) of the power function relationship is 0.893. Here, discharge is a dependent while the drainage

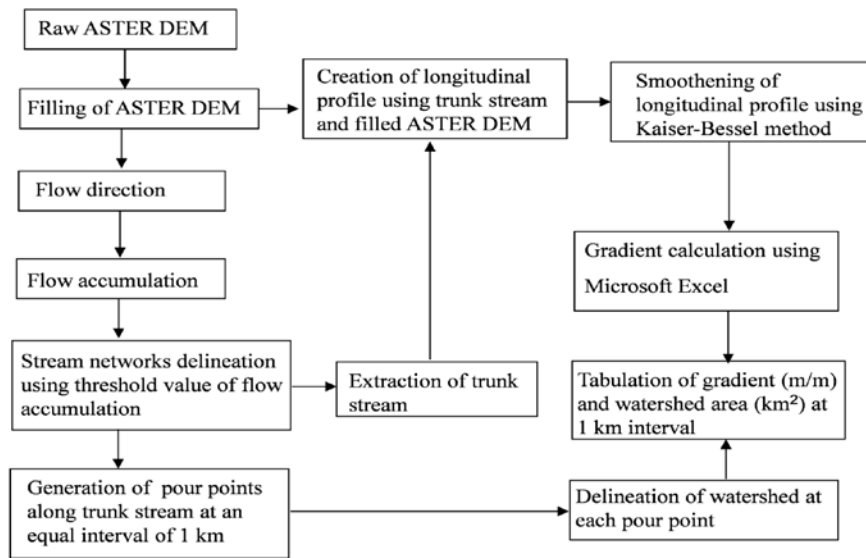


Figure 3. Flow chart depicting: a) procedures for delineation of the watershed, b) creation of the longitudinal profile, c) its smoothing and d) slope estimation at an equal interval of 1 km.

Table 1. Drainage area and peak discharge (1985-1997).

Location	Area (km ²)	Average peak monthly discharge
Rudraprayag (Alaknanda)	1647.991	287
Devaprayag (Alaknanda)	10141.81	1008
Devaprayag (Ganges)	10919.77	2269
Rishikesh (Ganges)	21467.67	2283

Source: Jack (2010).

area is an independent variable. The average peak monthly discharge data were used for the calculation of stream power because it is widely related to the river dynamics and a huge amount of sediment load is transported during the period of highest flow (Jack, 2010). Therefore, by using peak monthly discharge, a value of peak stream power was calculated and used to explain the bar formation and toe-cutting induced exposures/landslides. The mean peak discharge of the Bhagirathi watershed is 670.5 m³s⁻¹.

The total stream power was calculated using Eq. (3) (Bagnold, 1966):

$$\Omega = \gamma QS \dots\dots\dots (3)$$

Where Ω is total stream power per unit length of the channel (W m⁻¹), γ is the specific weight of water (9800 Nm⁻²), Q is discharge (m³s⁻¹), and S is the energy slope (m/m) of the flow within a given reach. We took channel slope (m/m) as a proxy for energy slope of the flow. Reinfelds et al. (2004) defined total stream power as “the total rate of energy expenditure per unit length of the channel”. Hence, it appears to be an suitable factor for longitudinal connectivity in the channel.

Unit stream power confers a measurement of the rate of energy expenditure per unit area of a river channel width. Unit stream power was calculated using Eq. (4) (Kumar et al., 2013):

$$\text{Unit stream power} = \frac{\text{Total stream power}}{\text{the width of active channel}} \dots\dots (4)$$

RESULTS AND DISCUSSION

Longitudinal River profile and channel slope

The work carried out in the badlands of Henry Mountains by Gilbert, (1877) showed that “if we draw the profile of the river on paper, we produce a curve concave upward and with the greatest curvature at the upper end.” The concavity of the longitudinal profile of rivers is mainly produced by vertical erosion and removal of bed materials, the balance between aggradation and bed subsidence, and sediment and discharge added by tributaries to the main river (Sinha and Parker, 1996). The slope of a river is primarily influenced by its discharge and sediment size distribution (Snow and Slingerland, 1987). Thus, river longitudinal profile is an outcome of its interplay with the basin topography, land cover, soil and precipitation that control the supply of water and sediment to the river.

The hierarchy of geomorphic features of the channel and valley within the Bhagirathi watershed is influenced by dissimilarity in lithology and slope. In the upstream of the river, the slope is high. It is more than 0.04 m/m at

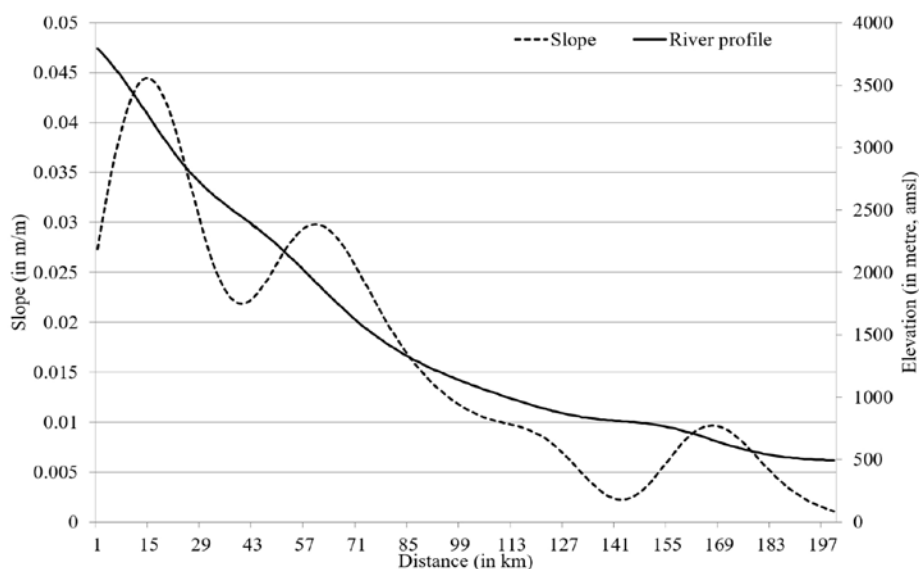


Figure 4. Longitudinal profile and slope of the Bhagirathi River.

Table 2 Overall statistics of slope, discharge, bar area, elevation, channel width, total and unit stream power

Parameters	Average	Minimum	Maximum
Slope (m/m)	0.016643	0.00106	0.04444
Discharge (cumecs)	670.46494	114	1076
Bar Area (km ²)	0.1195	0	1.147
Elevation (m)	1497.26	492.46	3793.84
Channel width(m)	156.74	11.098	1818.49
Total Stream power (wm ⁻¹)	79869.192	11169	167822
Unit stream power (wm ⁻²)	1701.86	10	9850

an elevation of 3600 m (Reach 1), and after that, it shows decreasing trend. In the middle reach, slope shows an increasing trend (0.03 m/m at an altitude of 2400m). After that altitude the slope is continuously decreasing (Figure 4). Downstream near the distance of 140 km (Reach 16), the slope is only 0.002 m/m. This lowest slope is due to the Tehri dam.

Total stream power

In Bhagirathi river, total stream power shows a direct relationship between slope and discharge. The channel slope of the entire Bhagirathi River varies between 0.00106 and 0.04444 m/m. The total stream power varies from 11169 to 167822 Wm⁻¹ with an average total stream power of 799869.2 (Wm⁻¹) (Table 2).

Along the Bhagirathi River, a high total stream power has been found in the mid-stream due to the influx of discharge by tributaries and sub-tributaries (reach 3-7) (e.g., Knighton, 1999). In the upstream, the slope is steep as a consequence; a sharp increase in the total stream power has been observed (reach 1-1). With the decrease of the slope, the total stream power also shows a decreasing

trend (Figure 5a). Overall, the total stream power mimics the slope of the channel.

At the origin point of Bhagirathi River, few tributaries debouch with it, so discharge is low in the upper reach but when Bhagirathi reaches Bhaironghati; Jadh Ganga, Jalandhri Jad near Harsil, Siyan Gad near Jhala debouch with it. Hence, a large amount of discharge has been added to the river. Thus, the influence of tributaries is visible on the downstream increase in discharge. In the downstream of middle reach of the river, no major tributary joins the Bhagirathi River. Therefore, no significant changes occur in total stream power as well as in discharge in this reach (Figure 5b). In the lower reaches, Bhilangna River joins the Bhagirathi near old Tehri and adds a considerable amount of water to Bhagirathi, resulting in an increase in the total stream power. The headwater peak of the total stream power is sharp and narrow. But in midstream and downstream of Tehri dam, the peaks in total stream power are broad and flattened. The sharp and narrow headwater peak is due to local variation in slope and addition of high discharge at one point. The significant broad and flattened peaks in the midstream and downstream of the Tehri dam is due to the diminishing slope and relatively

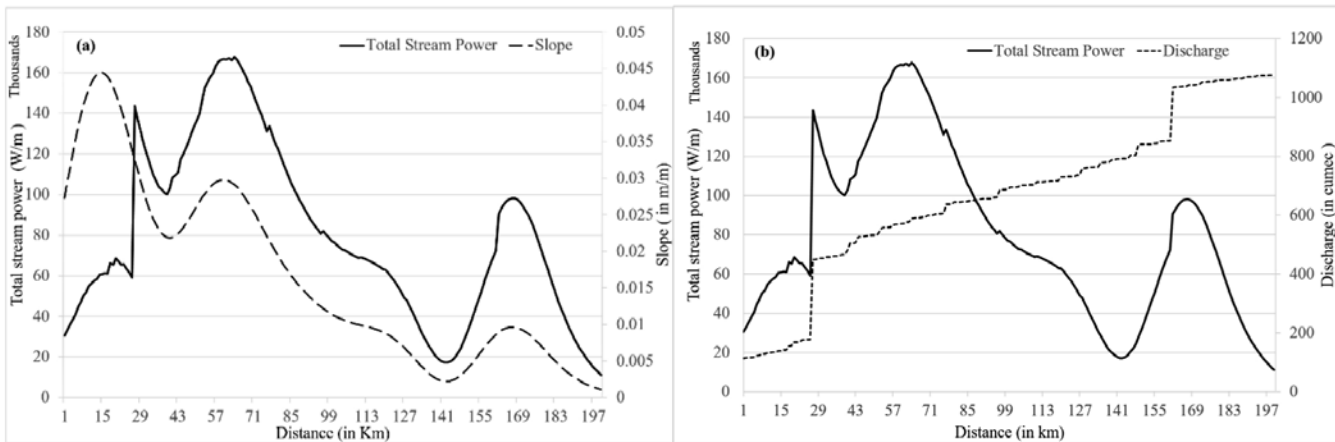


Figure 5. Relationship between (a) total stream power and slope and (b) total stream power and discharge in the Bhagirathi River.

high discharges, compared to headwater reaches. It is observed that the reach-scale variability in total stream power distribution is influenced by the discharge influxes from tributaries and change in channel slope (e.g., Fonstad, 2003; Jain et al., 2006). The river stretch between Maneri and Tehri dams is highly influenced by anthropogenic activities. Hence, the total stream power is relatively low as compared to upstream stretch. Thus, it is inferred that there are nonlinear downstream changes in the total stream power in the Bhagirathi watershed (e.g., Lecce, 1997; Jain et al., 2006). This study does not consider the stream power, estimated in the reservoirs of Maneri, Tehri, and Koteswar dams.

Unit stream power and geomorphic characterisation of the Bhagirathi River

Unit stream power has been plotted against distance and slope of the Bhagirathi River. Interactions among channel width, discharge, slope, and stream power provide a reach-wise capacity of a river to perform geomorphic work. If the channel width is wide, the relatively low amount of sediments is carried out by the river. Hence, most of the sediment would store as valley-fill deposits. It means that if channel width is more, the unit stream power will be less when other factors remain the same. In general, the trend shows a fluctuating active channel width along the longitudinal profile of the Bhagirathi basin. The active channel width is narrow in the upstream of Harsil, where the river passes through deep gorges. After that, the width of active channel begins to widen slightly. In detail, the channel width is the maximum at the upstream reach of the Tehri dam as this dam breaks the longitudinal connectivity of the Bhagirathi River. The channel width varies between 11.1 (reach-1) and 1818.5 m (reach-16) (Figure 6).

Unit stream power is also associated with bar area in the channel belt. Presence of high bar area in the channel belt signifies the low unit stream power (Harsil reach)

while the low bar area indicates (Figure 6) high unit stream power (reach 1 starting from Gomukh). Hence, bar area in the channel belt is negatively associated with the unit stream power.

The unit stream power varies from 10 (reach-16) to 9850 Wm^{-2} (upstream of Harsil). The reach-16 is a dead reach due to Tehri dam because the Bhagirathi River is not performing any geomorphic work in this reach. In the Bhagirathi watershed, unit stream power is high in the upstream, and it is decreasing in downstream due to increase in channel width (Figure 7). The reason for this high unit stream power in the upper stretch is the steep slope and narrow channel width as compared to the lower reaches. Despite a large amount of discharge added by the Bhilangana River to the Bhagirathi River near the old Tehri, the unit stream power is 1282 Wm^{-2} . But the unit stream power is not considered for the two dams namely, Maneri and Tehri dam that caused a break in longitudinal connectivity of the river as a consequence, ponding occurs in the reservoirs. On the basis of the unit stream power, the virgin stretches of the Bhagirathi river are located upstream of the Maneri dam and downstream of the Tehri and Koteswar dams. A polymodal distribution in unit stream power has been observed.

The Bhagirathi River channel was divided into twenty-one distinct reaches on the basis of the geomorphic features and valley configuration (Figure 6). Geomorphic features like confluence bar, channel lag, mid-channel bar, point bar, and side bar have been mapped (Figure 8). Seventy-four significant exposures/landslides have been mapped along Bhagirathi River. The relationship of average unit stream power with landslides shows that the high stream power is one of the primary reasons for exposures/landslides (Figure 9). The Pearson correlation coefficient (r) and coefficient of determination (r^2) between average unit stream power and number of exposures/landslides are 0.586 and 0.3447, respectively. The correlation is significant at the 0.01 level of significance. The primary

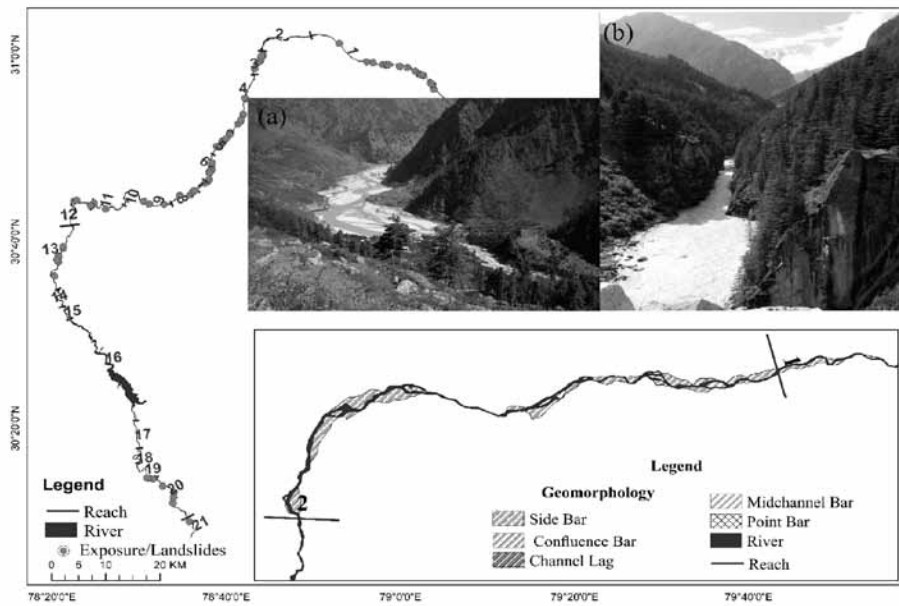


Figure 6. Bhagirathi River has been divided into twenty-one reaches and landslides have been mapped in each reach. Field photographs depict the Bhagirathi River near (a) Jhala village with a high bar area to channel ratio (b) Awe-inspiring box-shaped gorge and interlocking spurs are visible near Jangla village, and Gangotri channel is entrenched and confined. (Courtesy: Field photographs were obtained from Prof. Milap Chand Sharma, CSRD, Jawaharlal Nehru University, New Delhi). Inset: Detailed Geomorphic features of reach 2.

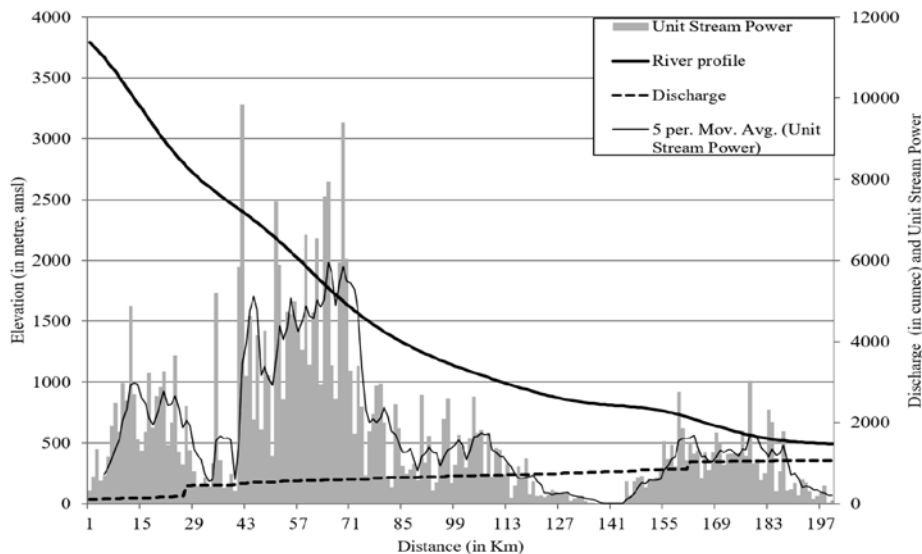


Figure 7. Unit stream power of the Bhagirathi River.

reasons behind exposures/landslide along the Bhagirathi River are down cutting, removal of basal materials and resultant slope failure. Out of seventy-four landslides, eighteen landslides (24 %) were found in part of above the average unit stream power of $5 \times 10^3 \text{ Wm}^{-2}$. Number of landslides and exposures are observed along the river with an average unit stream of $<1300 \text{ Wm}^{-2}$. Hence, along the Bhagirathi River, the highest number of exposures/landslides has been found in the reaches of the highest average unit stream power.

CONCLUSIONS

In the Bhagirathi river, tributaries provide a considerable discharge leading to increase in the upper and lower basin. The upper basin is characterised by the steep headwater slope and high peak in the total and unit stream power. But the lower basin is mostly influenced by the anthropogenic activities (damming of the river). The highest unit stream power was observed in reach 2 to reach 6. Along the dam sites, the total and unit stream power is low. The polymodal

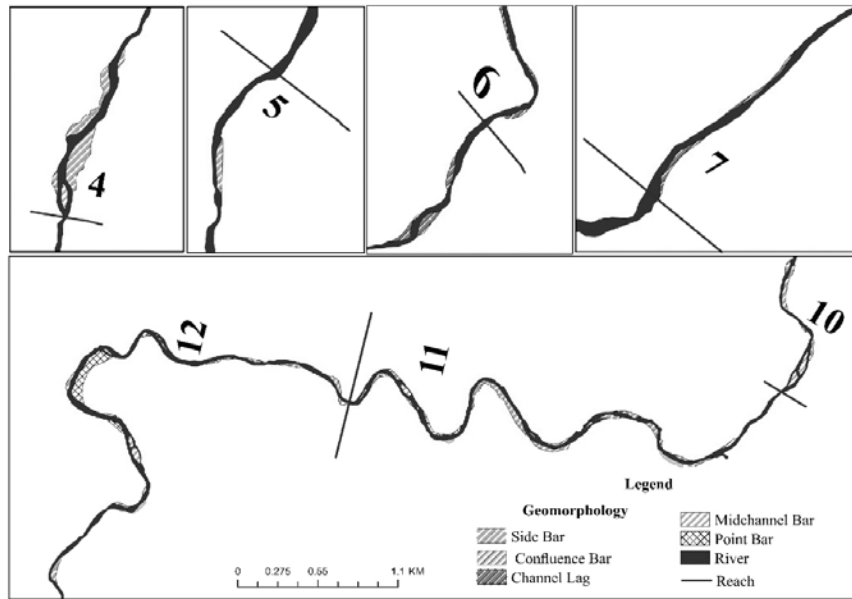


Figure 8. Geomorphic features of the Bhagirathi River in the selected reaches (4, 5, 6, 7, 10 and 11).

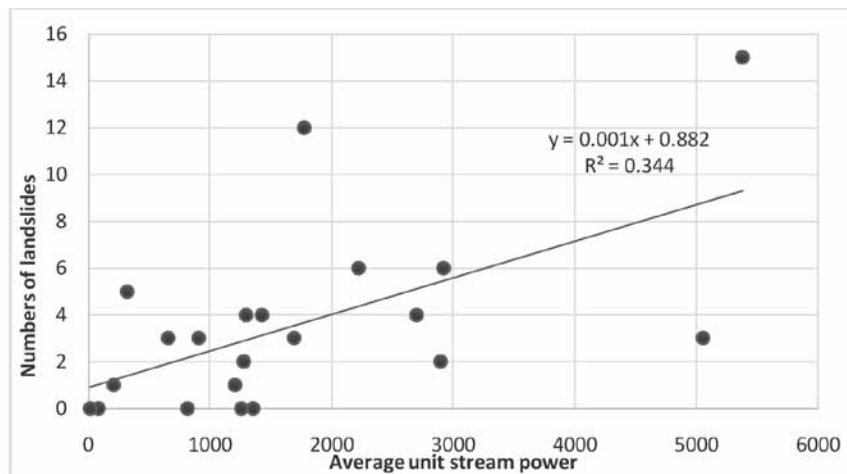


Figure 9. Relationship between exposures/landslides and average unit stream power.

distribution patterns are observed in total and unit stream power. The average unit stream power is 1701.9 Wm^{-2} that signifies downcutting without any floodplain formation along the Bhagirathi River. The presence of large boulders, cobbles, pebbles and coarse sand also signifies a high energy environment without any floodplain pocket.

ACKNOWLEDGEMENTS

The authors thank Dr.P.R.Reddy for useful suggestions, focused review process and final editing.

Compliance with Ethical Standards

The authors declare that they have no conflict of interest and adhere to copyright norms.

REFERENCES

- Bagnold, R. A., 1966. An approach to the sediment transport problem from general physics, United States Geological Survey Professional Paper. v. 422-I, pp: 1 – 37.
- Bawa, N., Jain, V., Shekhar, S., Kumar, N. and Jyani, V., 2014. Controls on morphological variability and role of stream power distribution pattern, Yamuna River, western India, *Geomorphology*, v.227, pp: 60–72.
- Bull, W. B., 1979. Threshold of critical power in streams. *Geological Society of America Bulletin*, v.90, pp: 453 – 464. doi.org/10.1130/00167606 (1979)90<453: TOCPIS>2.0.CO; 2.
- Fonstad, M.A., 2003. Spatial variation in the power of mountain streams in the Sangre de Cristo Mountains, New Mexico, *Geomorphology*, v.55, pp: 75–96. doi.org/10.1016/S0169-555X (03)00133-8.

- Gartner, J., 2016. Stream power: Origins, geomorphic applications, and GIS procedures. *Water Resources and Extension*. http://scholarworks.umass.edu/water_publications/1/. Accessed 12 Feb 2017.
- Gilbert, G.K., 1877. Report on the Geology of the Henry Mountains. Government Printing Office. Washington, DC. <https://pubs.usgs.gov/unnumbered/70039916/report.pdf>. Accessed 18 May 2017.
- Graf, W.L., 1983. Downstream changes in the stream power in the Henry Mountains, Utah, *Annals of the association of American Geographers*, v.73 pp: 337-387. DOI: 10.1111/j.1467-8306.1983.tb01423.x
- Graf, W.L., 1998. A guidance document for monitoring and assessing the physical integrity of Arizona streams, 95-0137. Phoenix, AZ: Arizona Department of Environmental Quality.
- Jack, P., 2010. Alluvial river response to active tectonics in the Dehradun region, Northwest India: A case study of the Ganga and Yamuna rivers. Durham Theses, Durham University.
- Jain, V., Fryirs, K., and Brierley, G., 2008. Where do floodplains begin? The role of total stream power and longitudinal profile form on floodplain initiation processes, *GSA Bulletin*, v.120, pp: 127-141. DOI: <https://doi.org/10.1130/B26092.1>.
- Jain, V., Preston, N., Fryirs, K., and Brierley, G., 2006. Comparative assessment of three approaches for deriving stream power plots along long profiles in the upper Hunter River catchment, New South Wales, Australia, *Geomorphology*, v.74, pp: 297-317. <https://doi.org/10.1016/j.geomorph.2005.08.012>.
- Kale, V.S., 2007. Geomorphic effectiveness of extraordinary flood on three large river of India Peninsula, *Geomorphology*, v. 85, pp: 306–316. <https://doi.org/10.1016/j.geomorph.2006.03.026>
- Kale, V.S., 2008. A half-a-century record of annual energy expenditure and geomorphic effectiveness of the monsoon-fed Narmada River, central India, *Catena*, v.75, pp: 154–163. DOI: 10.1016/j.catena.2008.05.004.
- Knighton, A.D., 1999. Downstream variation in stream power, *Geomorphology*, v.29, pp: 293-306. [doi.org/10.1016/S0169-555X\(99\)00015-X](https://doi.org/10.1016/S0169-555X(99)00015-X).
- Kumar, R., Kamal, V., and Singh, R.K., 2013. Geomorphic effects of 2011 floods on channel belt parameters of Rapti River: A remote sensing and GIS approach, *Corona Journal of Science and Technology*, v.2, pp: 4-12.
- Lecce, S.A., 1997. Nonlinear Downstream Changes in Stream Power on Wisconsin's Blue River, *Annals of the Association of American Geographers*, v.87, pp: 471-486. DOI: 10.1111/1467-8306.00064.
- Leopold, L.B., Wolman, M.G., and Miller, J.P., 1964. *Fluvial processes in geomorphology*, WH Freeman, San Francisco.
- Mosley, M.P., 1981. Semideterminate hydraulic geometry of river channels, South Island, New Zealand, *Earth surface processes and landforms*, v.6, pp: 127-137; doi: 10.1002/esp.3290060206.
- Nanson, G.C., and Croke, J.C., 1992. A genetic classification of floodplains, *Geomorphology*, v.4, pp: 459-486.
- Nanson, G.C., and Hickin, E.J., 1986. A statistical analysis of bank erosion and channel migration in western Canada, *Geological Society of America Bulletin*, v.97, pp: 497-504.
- Ortega, J.A., Razola, L., and Garzón, G., 2014. Recent human impacts and change in dynamics and morphology of ephemeral rivers, *Nat. Hazards Earth Syst. Sci.*, v.14, pp: 713-730; Doi: 10.5194/nhess-14-713-2014
- Petit, F., Gob, F., Houbrechts, G., and Assani, A.A., 2005. Critical specific stream power in gravel-bed rivers, *Geomorphology*, v.69, pp: 92-101. <https://doi.org/10.1016/j.geomorph.2004.12.004>
- Phillips, J.D., and Slattery, M.C., 2006. Sediment storage, sea level, and sediment delivery to the ocean by coastal plain rivers, *Progress in Physical Geography*, v.30, pp: 513-530.
- Phillips, J.D., 1989. Fluvial sediment storage in wetlands, *Water Resources Bulletin*, v.25, pp:867-873. DOI: 10.1111/j.1752-1688.1989.tb05402.x.
- Reinfelds, I., Cohenb, T., Battenc, P., and Brierley, G., 2004. Assessment of downstream trends in channel gradient, total and specific stream power: a GIS approach, *Geomorphology*, v.60, pp: 403-416. doi.org/10.1016/j.geomorph.2003.10.003.
- Rhoads, B.L., 1987. Stream power terminology, *Association of American Geographers*, v.39, pp: 189-195. DOI: 10.1111/j.0033-0124.1987.00189.x.
- Righini, M., Surian, N., Wohl, E., Marchi, L., Comiti, F., Amponsah, W., and Borga, M., 2017. Geomorphic response to an extreme flood in two Mediterranean rivers (northeastern Sardinia, Italy): Analysis of controlling factors, *Geomorphology*, v.290, pp: 184-199. <https://doi.org/10.1016/j.geomorph.2017.04.014>.
- Schumm, S.A., and Khan, H.R., 1972. Experimental Study of Channel Patterns, *Geological Society of America Bulletin*, [https://doi.org/10.1130/0016-7606\(1972\)83\[1755:ESOCP\]2.0.CO;2](https://doi.org/10.1130/0016-7606(1972)83[1755:ESOCP]2.0.CO;2) v.83, pp: 1755-1770.
- Sinha, S.K., and Parker, G., 1996. Causes of concavity in longitudinal profiles of rivers, *Water Resour. Res.*, v.32, pp: 1417–1428. DOI: 10.1029/95WR03819.
- Snow, R.S., and Slingerland, R.L., 1987. Mathematical modeling of graded river profiles. *J. Geol.*, v.95, pp: 15-33.
- Thomson, R.E., and Emery, W.J., 2001. *Data Analysis Methods in Physical Oceanography*, 3rd Edition, Elsevier, Amsterdam, pp: 716.
- Wicherski, W., Dethier, D.P., and Ouimet, W.B., 2017. Erosion and channel changes due to extreme flooding in the Fourmile Creek catchment, Colorado, *Geomorphology*, v.294, pp: 87-98. <https://doi.org/10.1016/j.geomorph.2017.03.030>
- Wohl, E.E., Vincent, K.R., and Merritts, D.J., 1993. Pool and riffle characteristics in relation to channel gradient, *Geomorphology*, [https://doi.org/10.1016/0169-555X\(93\)90041-Y](https://doi.org/10.1016/0169-555X(93)90041-Y), v.6, pp: 99-110.
- Yochum, S.E., Sholtes, J.S., Scott, J.A., and Bledsoe, B.P., 2017. Stream power framework for predicting geomorphic change: The 2013 Colorado Front Range flood, *Geomorphology*, <https://doi.org/10.1016/j.geomorph.2017.03.004> v.292, pp: 178-192.

Received on: 6.11.17; Revised on: 16.1.18; Re revised on: 8.2.18; Accepted on: 12.2.18

Petrology, mineral chemistry and geochemistry of the chromian muscovite bearing quartzite in the Neoproterozoic Veligallu schist belt, eastern Dharwar craton, India

Tarun C. Khanna^{1*} and V. V. Sessa Sai²

¹CSIR-National Geophysical Research Institute, Hyderabad-07, India

²Petrology Division, Geological Survey of India, Hyderabad-68, India

*Corresponding Author: khannangri@ngri.res.in

ABSTRACT

In the present study, we report on the petrography, mineral chemistry and geochemistry of the chromian muscovite bearing quartzite in the Neoproterozoic Veligallu schist belt (VSB), eastern Dharwar craton, India. The quartzites appear as greenish isolated outcrops within the metavolcanic sequences in the north-central part of the VSB. Mineralogically, the rock consists of quartz and subordinate muscovite, while zircon and rutile are noticed as accessory heavy minerals. Mineralogical composition of the muscovite indicates a maximum chrome content upto 4000 ppm. The average ($n = 5$) bulk-rock geochemical compositions consist of > 85 wt. % SiO₂, ~2.2 wt. % K₂O, ~0.21 wt. % Na₂O, ~6.3 wt. % Al₂O₃, ~0.22 wt. % TiO₂, and ~0.29 wt. % MgO contents. Archean upper continental crust normalized trace element patterns indicate positive Zr and Hf anomalies, consistent with the accumulation of zircon in the rock. Petrographic observations are inconsistent with a metamorphic origin for the enrichment of chrome in these quartzites. Geochemical attributes involving Ni-V-Th systematics suggest contribution of Ni from ultramafic rocks in the source of the protolith. Alternatively, we infer a hydrothermal origin for the enrichment of chrome in the muscovite bearing Veligallu quartzites. The geochemical compositions, for instance, high silica and the absence of Fe₂O₃ in the rocks indicate that the protolith was derived from the weathering of a felsic source, presumably an Archean granite / TTG.

Key words: Cr-muscovite, Quartzite, Neoproterozoic, Veligallu schist belt, eastern Dharwar craton, India.

INTRODUCTION

Chromian muscovite quartzite "Fuchsite" is known to occur in high and low grade metamorphosed volcano-sedimentary sequences of Meso- and Neo-Archaeon schist belts in the western Dharwar craton, India (e.g. Argast, 1995). The reference to the occurrence of such metasedimentary rocks in the Archean schist belts of the eastern Dharwar craton (EDC) is reported by GSI (Srinivasan et al., 1985). In the present study, we report on the petrography, mineral chemistry, and bulk-rock geochemistry of the chrome bearing muscovite quartzites from the Neoproterozoic Veligallu schist belt. (Figure 1).

Geological Setting

The VSB is located in the eastern Dharwar craton, and south of the Proterozoic Cuddapah basin (Figure 1A; Srinivasan et al., 1985). The belt broadly exhibits a N-S trend with an approximate strike length of ~ 60 km, and a maximum width of ~ 6 km in the central part (Figure 1B; Srinivasan, 1990). The volcano-sedimentary sequence was subjected to greenschist to lower amphibolite grade metamorphism. The metamorphism of the volcanic units is presumed to be synchronous with the first generation (F1) folds preserved in the rocks (Ramam and Murty,

1997). The metavolcanic lithologies constitute of arc basalt – high Mg-andesite – adakite suite (Khanna et al., 2015) and boninite-type ultramafic arc cumulates (Khanna et al., 2016), associated with banded iron formations (BIFs) and metasediments. The mafic-ultramafic and felsic rocks in the VSB yielded a bulk-rock Lu-Hf isochron age of 2696 ± 54 Ma (Khanna et al., 2016), which is identical to the zircon SIMS U-Pb age derived for the felsic volcanic rocks from elsewhere in the belt (2697 ± 5 Ma; Jayananda et al., 2013). Geochemically an identical suite of metavolcanic sequence is preserved in the Gadwal schist belt, which is located north of the Cuddapah basin. Recently, on the basis of identical geochemical patterns and bulk-rock Lu-Hf isotope systematics, Khanna (2017) has proposed a potential cogenetic link between the Veligallu and Gadwal schist belts. The above studies indicate that the metavolcanic rocks were produced in a subduction-related geodynamic setting in the Neoproterozoic. The focus of this study is to present a report on the petrological characteristics of chromian muscovite quartzites in the Veligallu schist belt (Figure 1C), eastern Dharwar craton, India.

Sampling and Analytical Techniques

Five representative least altered relatively fresh unweathered quartzite samples were collected from the central part

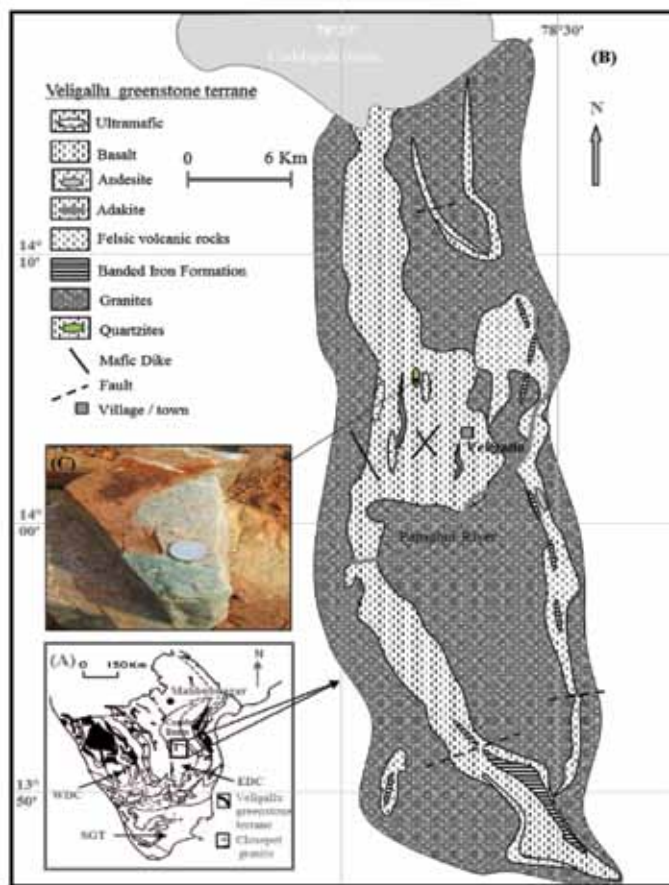


Figure 1. (A) Simplified geological map of the southern peninsular India comprising of three major tectonic blocks: the western Dharwar craton (WDC), the eastern Dharwar craton (EDC) and the southern granulite terrane (SGT). Also shown in the box is the location of Veligallu greenstone belt in the eastern Dharwar craton; (B) Generalized geological map of the Veligallu greenstone belt, modified after Srinivasan (1990); (C) Field photograph of the Veligallu quartzite that exhibits a typical green colour.

of the VSB (Figure 1). Megascopically, the rocks appear fine grained and green in color (Figure 1C). The mineral compositions (Table 1) were determined by electron probe microanalysis on a CAMECA SX-100 at the Petrology Division, Geological Survey of India, Hyderabad, India. A 20 nA beam current and an accelerating voltage of 15 keV were maintained with a focused beam. Certified natural silicate standards supplied by P&H were used for the instrument calibration. The corrections for ZAF were applied online by the instrument software.

Ten major element oxides, Cr, and Ni were analyzed using pressed powder pellets, on a Philips MagiX PRO PW2440; microprocessor controlled, wavelength dispersive sequential XRF (Table 2). The relative standard deviation for the major element oxides is < 3%. Trace elements (Table 2) including large ion lithophile elements (LILE), high field strength elements (HFSE) and rare earth elements (REE) were determined by high resolution inductively coupled plasma mass spectrometry (HR-ICP-MS; Nu Instruments Attom[®], UK). The detailed procedures relating to sample dissolution, analytical methodology and instrument

parameters are described in Khanna et al. (2015, 2016). In brief, 50 mg of finely ground sample powder was digested in a freshly prepared mixture of ultrapure grade acids (HF + HNO₃) taken in 3:1 ratio in screw top Teflon “Savillex” vessels, and heated on a hot plate at 160°C. Certified reference material GSR-4, was dissolved simultaneously following the method described above and analyzed along with the samples. Precision and accuracy are better than RSD 3% for the majority of trace elements.

RESULTS AND DISCUSSION

Field relationship

Field observations indicate that the greenish quartzite occurs as low lying “isolated” outcrops, within the mafic-ultramafic rocks in the north-central part of the VSB. To the west of Tumukunta, the quartzite occurs proximal to the shear zone (Figure 2). Two sets of structural fabric are noticed in the quartzite (i) NNE-SSW foliation is the major structural fabric in the rock, and (ii) E-W

Petrology, mineral chemistry and geochemistry of the chromian muscovite bearing quartzite in the Neoproterozoic Veligallu schist belt, eastern Dharwar craton, India

Table 1. Compositions of Cr-muscovite in the Veligallu quartzite, eastern Dharwar craton, India. Compared to Fuchsite and Mariposite in the literature.

							Average	Fuchsite [#]	Mariposite [#]
SiO ₂	46.20	45.81	46.22	46.58	46.42	45.62	46.14	45.97	56.00
TiO ₂	0.35	0.19	0.46	0.45	0.38	0.15	0.33	-	-
Al ₂ O ₃	34.97	35.05	34.31	34.86	35.25	34.75	34.87	31.67	23.52
Cr ₂ O ₃	0.17	0.12	0.13	0.10	0.08	0.39	0.16	4.81	0.78
FeO	0.43	0.33	0.41	0.34	0.36	0.32	0.36	0.53	0.51
MnO	0.00	0.02	0.01	0.01	0.02	0.03	0.01	-	-
MgO	0.67	0.52	0.69	0.58	0.45	0.61	0.59	0.31	2.12
CaO	0.00	0.03	0.00	0.00	0.00	0.04	0.01	0.15	0.37
Na ₂ O	1.27	1.28	1.20	1.32	1.34	1.15	1.26	1.03	2.72
K ₂ O	9.42	9.59	9.43	9.45	9.26	9.43	9.43	9.07	7.03
Total	93.48	92.94	92.86	93.70	93.56	92.49	93.17	93.54	93.05
<i>Number of ions on the basis of 24 oxygens</i>									
Si	6.79	6.77	6.83	6.82	6.80	6.79		7.08	8.15
Al	1.21	1.23	1.17	1.18	1.20	1.21		0.92	-0.15
Al	4.84	4.88	4.81	4.83	4.88	4.88		4.83	4.18
Ti	0.04	0.02	0.05	0.05	0.04	0.02		0.00	0.00
Fe(ii)	0.05	0.04	0.05	0.04	0.04	0.04		0.07	0.09
Mn	0.00	0.00	0.00	0.00	0.00	0.00		0.00	0.00
Mg	0.15	0.12	0.15	0.13	0.10	0.14		0.07	0.46
Ca	0.00	0.00	0.00	0.00	0.00	0.01		0.02	0.06
Na	0.36	0.37	0.34	0.38	0.38	0.33		0.31	0.77
K	1.77	1.81	1.78	1.77	1.73	1.79		1.78	1.31
Total	15.21	15.24	15.19	15.19	15.18	15.21		15.09	14.87

Whitmore et al. (1946)

Table 2. Major and trace element concentrations in the Veligallu Cr-quartzite.

	VDT-25	VDT-26	VDT-27	VDT-28	VDT-30
SiO ₂	88.34	93.44	85.83	93.20	92.75
TiO ₂	0.26	0.15	0.34	0.14	0.22
Al ₂ O ₃	8.0	4.2	9.8	4.6	4.7
Fe ₂ O ₃	nd	nd	0.06	nd	0.02
MnO	nd	nd	nd	nd	nd
MgO	0.37	0.26	0.40	0.21	0.21
CaO	0.06	0.05	0.05	0.05	0.05
Na ₂ O	0.25	0.10	0.38	0.14	0.16
K ₂ O	2.7	1.8	3.1	1.7	1.8
P ₂ O ₅	0.03	0.02	0.03	0.02	0.02
Mg#			0.93		0.95
Cr	311	323	367	344	282
Ni	78	77	90	82	82
Rb	32	19	36	17	23
Sr	23	11	27	12	14
Cs	1.55	0.90	1.22	0.59	0.91
Ba	729	345	1047	534	468
Sc	4.5	1.9	3.3	1.3	2.4
V	38	20	53	23	24
Ta	0.50	0.38	0.65	0.36	0.48
Nb	7.09	4.02	7.33	4.36	5.88
Zr	333	341	404	331	319
Hf	9	10	11	9	9
Th	12.0	9.7	9.9	12.2	11.6
U	1.9	1.7	1.7	1.4	2.0
Y	6.1	5.2	5.4	4.0	5.0
La	33.59	24.89	42.87	34.14	29.15
Ce	54.92	41.04	68.09	56.40	38.34
Pr	5.63	4.20	6.77	5.61	5.19
Nd	17.82	13.52	21.01	17.91	17.15
Sm	2.72	2.13	2.97	2.67	2.68
Eu	0.37	0.26	0.56	0.30	0.32
Gd	1.99	1.58	2.12	1.88	1.88
Tb	0.29	0.24	0.28	0.25	0.26
Dy	1.31	1.08	1.20	1.02	1.09
Ho	0.23	0.19	0.20	0.16	0.19
Er	0.59	0.51	0.51	0.37	0.47
Tm	0.10	0.09	0.08	0.06	0.07
Yb	0.63	0.56	0.53	0.37	0.46
Lu	0.11	0.10	0.10	0.07	0.09

nd = not detected

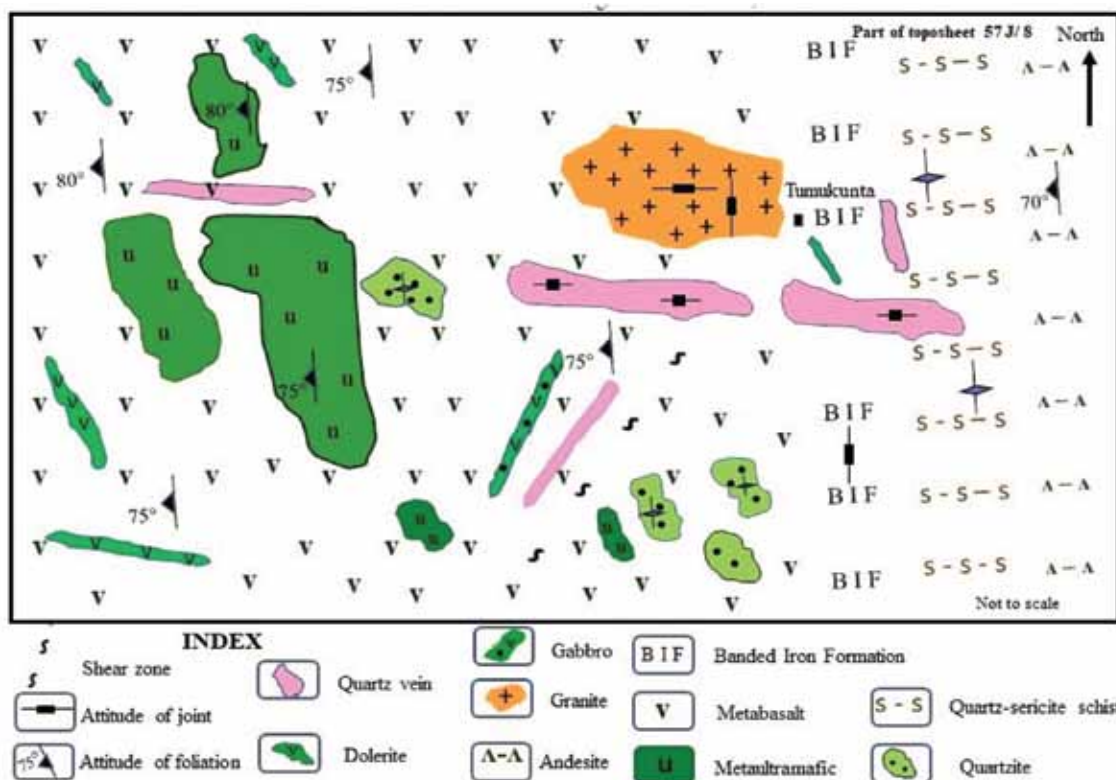


Figure 2. Geological map of the area around Thumkunta showing the disposition of the quartzite and metapelite within the metavolcanics rocks in the neoproterozoic Veligallu schist belt, eastern Dharwar craton.

warps. The structural fabric noticed in the quartzite has foliation in vertical to subvertical. The field disposition apparently indicates that the quartzites exhibit a discordant relationship with the metavolcanic sequence of the VSB. Incidentally the quartzite outcrops discussed in the present study are located to the north of Bandirevu.

Petrography

The Veligallu quartzite predominantly consist of quartz with subordinate muscovite. Rutile and zircon are noticed as accessory heavy minerals. Quartz grains are sub-rounded / sub-angular and exhibit wavy extinction. The rocks exhibit distorted cleavage in muscovite and show serrated grain boundaries in quartz, which indicates deformation. Development of planar fabric is also noticed. Muscovite occurs as large flakes as well as randomly oriented minute aggregates amidst deformed quartz grains. The planar fabric noticed in the quartzite is defined by the orientation of large muscovite flakes. Elongated quartz grains are often aligned parallel to the muscovite flakes. Under plane polarized light, muscovite appears pale green in colour (Figure 3A). It exhibits high order interference colors when observed under crossed nicols (Figure 3B and E). Rutile mostly occurs as minute oval shaped grains that range in size from ~200 μm to ~250 μm , and appears reddish brown in color. It

exhibits high relief in plane polarized light (Figure 3C), and displays straight extinction under crossed nicols (Figure 3D). Some of the rutile grains are dismembered due to microscale displacement (Figure 3F). Zircons occur as oval shaped grains (Figure 3G and F) with smooth boundaries, and range in size from 50 μm to 80 μm . It exhibits high relief in plane polarized light (Figure 3G), apart from anisotropy with high order interference colors under the crossed nicols (Figure 3H). Both, rutile and zircon are ultra stable detrital heavy minerals. Perhaps, the euhedral nature of the zircon grains suggests lesser degree of transportation and hence, proximal to the provenance. Zircon is the dominant heavy mineral in the rock with the zircon : rutile ratio of nearly 70 : 30. Morphology of the detrital zircon indicates the preservation of the elongated prismatic nature with by and large smooth grain boundary (Figure 3G, H).

Mineral chemistry and nomenclature of the muscovite

Muscovite in the Veligallu quartzite consists of ~ 46 wt. % SiO_2 , ~ 35 wt. % Al_2O_3 , ~ 1 wt. % Na_2O , ~ 9 wt. % K_2O and a maximum of ~ 0.4 wt. % (= 4000 ppm) Cr_2O_3 with minor FeO (~ 0.32 wt. %) and MgO (~ 0.6 wt. %) contents (Table 1). As such, muscovite is essentially a potassium-aluminium sheet silicate that does not commonly

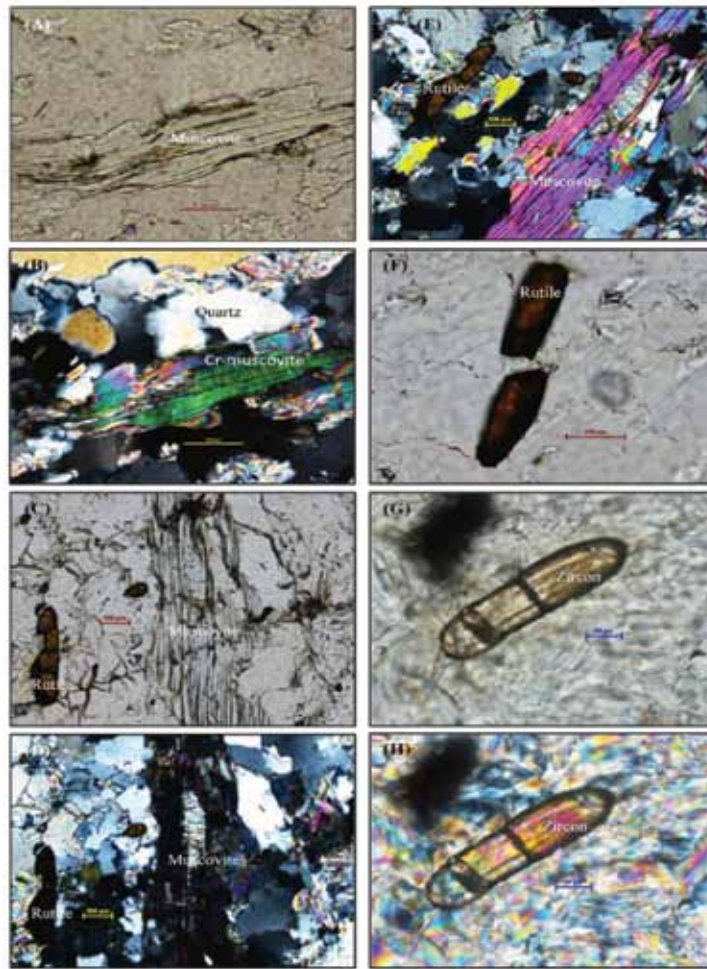


Figure 3. Photomicrograph of the Veligallu quartzite, under (A) plane polarized light, and (B) crossed nicols, showing quartz and muscovite; (C) rutile grains exhibit reddish brown pleochroism, and (D and E) straight extinction under crossed nicols; (F) dismembered grains of rutile; Oval shaped detrital zircon grains in the quartzite are shown under (G) plane polarized light, and (H) under crossed nicols. See text for details.

sequester chromium. Chrome bearing micas, where Al is partially replaced by Cr, are recognized as fuchsite and mariposite, although the varietal name “chromian muscovite” is generally preferred (Whitmore et al., 1946). The chromium contents in the fuchsite range from 8400 ppm to about 40000 ppm. Whereas, mariposite consists of relatively low concentrations of chrome ~1800 ppm to 7800 ppm. In comparison to the fuchsite, the green muscovite in the Veligallu quartzite consists of identical SiO₂, Al₂O₃, Na₂O and K₂O contents, but low chromium (Table 1). On the contrary, SiO₂, MgO and Na₂O are considerably high, and Al₂O₃ is typically low in the mariposite compared to the muscovite in the Veligallu quartzite, or a fuchsite (Table 1). On this basis, the muscovite in the veligallu quartzite does not qualify as mariposite. Alternatively, the chromium content in the muscovite is, however, not sufficiently high to be called as fuchsite either. Therefore, we only recognize the muscovite as “chromian muscovite” and hence, the name chromian muscovite quartzite for the bulk-rock samples.

Nature of chrome enrichment in the Veligallu quartzite

As noted by Heinrich et al., (1953), chrome bearing micas occur in either hydrothermal veins and replacement deposits, or regionally metamorphosed rocks e.g. schists, gneisses and quartzites. Leo et al., (1965) suggested that the probable mode of enrichment of chrome in the Serra de Jacobina quartzites, Brazil, may be due to : (1) breaking down of detrital chromite during regional metamorphism of clastic sandstones; and/or (2) hydrothermal leaching of chromium from nearby ultramafic rocks.

As such, we made an attempt to validate the above probable modes of chrome enrichment in the quartzites of VSB. Petrographic observations (Figure 3) indicate that quartz and muscovite are the only major mineral constituents, with zircon, and rutile as the predominant detrital heavy minerals. The quartzites are necessarily devoid of chromite. Therefore, breaking down of detrital

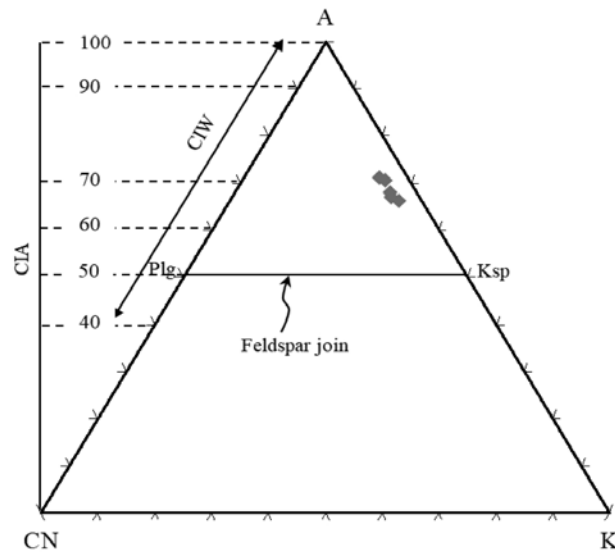


Figure 4. A-CN-K diagram of Fedo et al., (1995) plotted for the Veligallu quartzites. Also shown are the CIA values that are consistent with intermediate degree of weathering of the source rock.

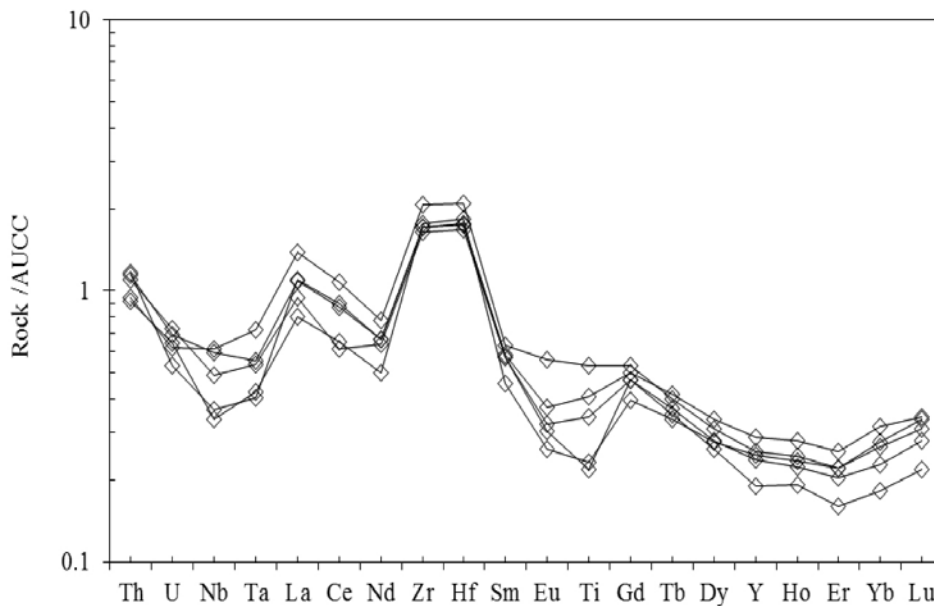


Figure 5. Archean upper continental crust (AUCC; Rudnick and Gao, 2004) normalized trace element variation diagram for the Veligallu quartzites.

chromite during regional metamorphism of the protolith cannot account for the chrome enrichment in the Veligallu quartzite. Moreover, the muscovite flakes are confined to the grain boundaries of quartz, and do not penetrate through the grains as a consequence of metamorphism, which is unlike that observed in the rocks of Montana (Heinrich, 1965), therefore, inconsistent with a metamorphic origin of the chromian muscovite in the Veligallu quartzite. Instead we infer metasomatic origin for the enrichment of chrome in the Veligallu quartzites (discussed below).

Geochemistry

The bulk-rock geochemical composition of the Veligallu quartzites is given in Table 2. The high silica contents (85 to 93 wt. %) in these quartzites indicates that the premetamorphosed rock was a siliciclastic rock. The titanium content is contributed by rutile, and K₂O and Al₂O₃ concentrations essentially reflect the presence of muscovite in these rocks. The chemical index of alteration (CIA = [molar Al₂O₃/(Al₂O₃+CaO+Na₂O+K₂O)] x 100;

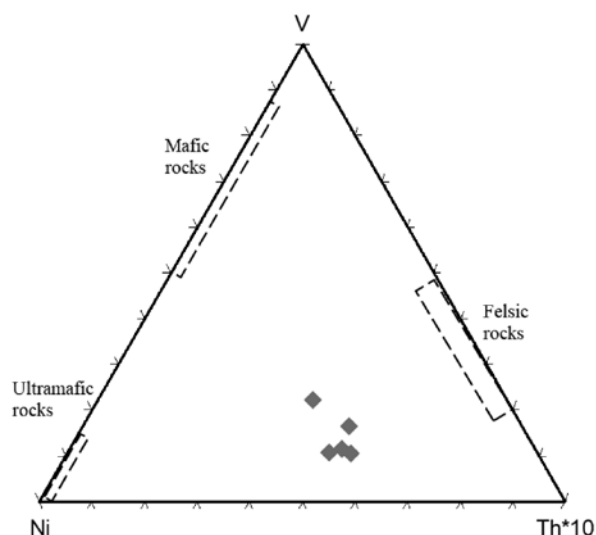


Figure 6. Ni-V-Th diagram of Bracciali et al., (2007) plotted for the Veligallu quartzites. See text for details.

Nesbitt and Young, 1982) values in the Veligallu quartzites range from 66 – 71 with an average value of 68, which indicates intermediate degree of chemical weathering of the source rock (Figure 4; cf. Fedo et al., 1995). The Veligallu quartzites exhibit prominent enrichment in their Zr/Hf relative to the Archean upper continental crust (Figure 5), which is consistent with the accumulation of detrital zircon in these rocks.

On the basis of bulk-rock geochemical concentrations, for instance, high silica contents in combination with extremely low MgO, CaO, Sc, V, and absence of Fe₂O₃, we infer that the weathered source rock must be felsic in nature, which we presume to be an Archean granite / TTG. The quartzites plot in-between the ultramafic and felsic source compositions in a triangular variation diagram involving Ni-V-Th (Figure 6; Bracciali et al., 2007), which is consistent with the regional geological setup wherein the quartzites are spatially associated with the ultramafic rocks, and that the Ni contents observed in the Veligallu quartzites were contributed from the ultramafic rocks. The chrome contents in the Veligallu ultramafics range from 2290 to 3784 ppm (Khanna et al., 2016). Therefore, it is a potential possibility that the chromium and nickel from the ultramafic rocks might have been leached by the hydrothermal solutions that precipitated it in the quartzites. Thus, hydrothermal leaching of chrome from the spatially associated ultramafics appears to be a likely hypothesis for the origin of chromian muscovite in the Veligallu quartzite.

CONCLUSION

We make a report on the field occurrence, petrography, mineral chemistry and bulk-rock geochemistry of chromian

muscovite bearing quartzite in the Veligallu greenstone belt, eastern Dharwar craton (EDC), India. The quartzites occur as pale greenish coloured isolated low lying outcrops within the Neoproterozoic mafic-ultramafic sequences in the areas to the west and south of Tumukunta in the Veligallu schist belt. The quartzites are proximally associated with the ultramafics. Petrographically the rock is composed of quartz, pale greenish muscovite with detrital zircon and rutile. In a Ni-V-Th triangular variation diagram the Veligallu quartzites plot transitional to the ultramafic and felsic sources, thus suggesting the contribution of compatible mafic elements Ni and Cr from the juxtaposed ultramafic rocks in the VSB. Therefore, we infer that leaching of these ultramafic rocks by hydrothermal solutions resulted in the enrichment of chrome in the muscovite bearing Veligallu quartzites.

ACKNOWLEDGEMENTS

We are thankful to Dr. V.M. Tiwari, the Director, NGRI, for permission to publish this work. TCK acknowledges the Department of Science and Technology, Government of India, for funding the project SR/FTP/ES-7/2012 vide letter dated 09.05.2012; in-house classification GAP-682-28 (TCK). Drs. A. Keshav Krishna and M. Satyanarayanan are thankfully acknowledged for extending the XRF and ICP-MS analytical facility, respectively. VVSS is thankful to Shri. S.T. Narahari, Senior Geologist, EPMA lab, GSI Hyderabad, for extending the analytical facility. We express our sincere thanks to Dr. Santanu Bhattacharjee, GSI, for critical review and helpful suggestions. We also thank Prof. U.V.B. Reddy for useful suggestions. Dr. P.R. Reddy, is profusely thanked for continued support, and editorial handling of the manuscript.

Compliance with Ethical Standards

The authors declare that they have no conflict of interest and adhere to copyright norms.

REFERENCES

- Argast, S., 1995. Detrital Origin of Fuchsite-bearing Quartzites in the western Dharwar craton, Karnataka, India. *Journal Geological Society of India*, v.45, pp. 559-575.
- Bracciali, L., Marroni, M., Pandolfi, L., and Rocchi, S., 2007. Geochemistry and petrography of western tethys Cretaceous sedimentary covers (Corsica and Northern Apennines): From source areas to configuration of margins. *Geological Society of America Special Paper*, v.420, pp: 73-93.
- Fedo, C.M., Nesbitt, H.W., and Young, G.M., 1995. Unraveling the effects of potassium metasomatism in sedimentary rocks and paleosols, with implications for paleoweathering conditions and provenance. *Geology*, v. 23, pp: 921-924.
- Heinrich, E. Wm., Levinson, A.A., Levandowski, D.W., and Hewitt, C.H., 1953. Studies in the natural history of micas. University of Michigan Engineering Research Institute project report M978.
- Heinrich, E. Wm., 1965. Further information on the geology of chromian muscovites. *American Mineralogist*, v.50, pp: 758-762.
- Jayananda, M., Peucat, J., Chardon, D., Krishna Rao, B., Fanning, C.M., and Corfu, F., 2013. Neoproterozoic greenstone volcanism and continental growth, Dharwar craton, southern India: constraints from SIMS U–Pb zircon geochronology and Nd isotopes. *Precambrian Research*, v.227, pp: 55-76.
- Khanna, T.C., 2017. Lutetium-hafnium isotope evidence for the co-genesis of Neoproterozoic Veligallu and Gadwal greenstone belts, eastern Dharwar craton, India. *Journal Indian Geophysical Union*, v. 21, no.3, pp: 198-206.
- Khanna, T.C., Sessa Sai, V.V., Bizimis, M., and Krishna, A.K., 2015. Petrogenesis of Basalt – high-Mg Andesite – Adakite in the Neoproterozoic Veligallu Greenstone Terrane: Geochemical evidence for a rifted back-arc crust in the eastern Dharwar craton, India. *Precambrian Research*, v.258, pp: 260-277.
- Khanna, T.C., Sessa Sai, V.V., Bizimis, M., and Krishna, A.K., 2016. Petrogenesis of ultramafics in the Neoproterozoic Veligallu greenstone terrane, eastern Dharwar craton, India: Constraints from bulk-rock geochemistry and Lu-Hf isotopes. *Precambrian Research*, v.285, pp: 186-201.
- Leo, G.W., Rose Jr. J.H., and Warr, J.J., 1965. Chromian muscovite from the Serra De Jacobina, Bahia, Brazil. *American Mineralogist*, v.50, pp: 392-402.
- Nesbitt, H.W., and Young, G.M., 1982. Early Proterozoic climate and plate motions inferred from major element chemistry of lutites. *Nature*, v.299, pp: 715-717.
- Ramam, P.K., and Murty, V.N., 1997. *Geology of Andhra Pradesh*. Geological Society of India publication, pp: 245.
- Rudnick, R.L., and Gao, S., 2004. Composition of the continental crust. *Treatise on geochemistry*, v.3, pp: 1-64.
- Srinivasan, B.V., Bansilal and Rao, K.N., 1985. Final report on large scale geological mapping and geochemical studies of Veligallu schist belt in parts of Anantapur, Chittoor and Cuddapah districts, A. P. Unpublished GSI progress report for the FS 1979-82.
- Srinivasan, K.N., 1990. Geology of the Veligallu and Gadwal schist belts. *Geological Survey of India Records*, v.5, pp: 123.
- Whitmore, D.R.E., Berry, L.G., and Hawley, J.E., 1946. Chrome Micas. *American Mineralogist*, v.31, pp. 1-21.

Received on: 29.12.17; Revised on: 21.1.18; Accepted on: 6.2.18

Long range forecast and development of a weak southwest monsoon during 2017- Pt. II: Development

Onkari Prasad^{1*}, O.P. Singh² and K. Prasad³

¹43, Ritu Apartments, A-4 Paschim Vihar, New Delhi-110063

² B44, First Floor, Parshvath Paradise, Mohan Nagar, Ghaziabad (U.P.)-201007

³ D-104, Seema Apartments, Sector 11, Dwarka, New Delhi-110085

*Corresponding Author: prasadonkari123@yahoo.in

ABSTRACT

2017 southwest monsoon was unique in several respects: (i) It was a weak monsoon, not over India alone, but over the monsoonal regions of the globe, (ii) Even with weak monsoon conditions, rainfall for India as a whole was on the higher side of normal during June by 4% (iii) Normal to above normal/excess rainfall occurred in July over different regions of India resulting in 2% above normal rainfall for the month for India as a whole, (iv) There was an intra-seasonal change in the activity of South Indian ocean Convergence Zone (SIOCZ) during the second half of the season, which was expected to bring improvement in rainfall over Central and Northwest India, but it did not happen and rainfall improved over south Peninsula, (v) Though not intense, SIOCZ remained generally active from the week ending on 5th July till the end of the season. Development of 2017 southwest monsoon has been studied with the help of OLR Total, OLR anomaly, cloudiness, daily and weekly rainfall and monthly precipitation anomaly data. It has been shown that the superimposition of intra-seasonal changes over intra-seasonal oscillation was responsible for the development of different features during 2017 monsoon as enumerated above. Further the activity of SIOCZ and rainfall distribution over India during 2017 monsoon have, once again, confirmed the validity of the results, which had formed the basis for proposing SIOCZ model of long range forecasting of monsoon rainfall in India.

Key words: Southwest monsoon, South Indian Ocean Convergence Zone model, Activity index, Intra-seasonal changes, OLR total, OLR anomaly, Monsoon Trough, Long range forecast, Updates.

INTRODUCTION

Two monsoons are never exactly the same, though the Intra-seasonal Oscillations (ISOs) and the main feature in the activity of South Indian Ocean Convergence Zone (SIOCZ), prior to the commencement of the season in two years, may be the same. This results due to superimposition of Intra-seasonal Changes (ISCs) over ISOs. The term ISO refers to variance of rainfall in the time scale of 10-15 and 30-60 days. These oscillations are well known. The features in the activity of SIOCZ corresponding to ISOs are also fairly known by now. The term ISC refers to the appearance of new features in the activity of SIOCZ, other than what had been identified as the main feature before the commencement of the season and used for preparing Long Range Forecast (LRF) of rainfall. The changes in the activity of SIOCZ cause changes in the Monsoon Trough (MT) and thereby impact the rainfall distribution. As a result of this, the forecast issued on the basis of the main feature does not get realised. During 1990 to 2016, for which LRF of rainfall based on SIOCZ model has been issued, ISCs had occurred in 1992, 1999, 2001, 2005, 2010, 2013 and 2016. The ISCs occurred in these years have been studied and documented (Onkari Prasad and Singh, 2013; Onkari Prasad et al., 2014, 2016a and 2018a). Because of the ISCs, the difference between the forecast and the realized rainfall

in some of the districts of a state, some of the subdivisions and also for India as a whole become larger than the Model Error (ME). Except for the above mentioned years (7 out of 27 (26%)), SIOCZ model's LRF was reasonably good in the remaining years. Identification of ISCs, issuing of Update, and documenting the results has been done for the years 2013 and 2016 (Onkari Prasad et al., 2016a & 2018a). ISCs had also occurred during 2017 summer monsoon. 2017 monsoon had been foreshadowed as a normal one by the operational models of India Meteorological Department (IMD). SIOCZ model had foreshadowed 2017 monsoon as a weak one with 12% below normal seasonal rainfall for India as a whole with ME of $\pm 5\%$. The performance of SIOCZ model during 2017 has been discussed in Pt.I (Onkari Prasad et al., 2018b). The verification results have shown that SIOCZ model's forecast was reasonably good in the districts of Tamilnadu, Andhra Pradesh, Telanagana, Himachal Pradesh, Maharashtra and Goa states. It was also reasonably good in meteorological subdivisions and also for the country as a whole.

The linkage between SIOCZ and Monsoon Trough (MT) had been explained by proposing a circulation model (Figure 1d) during 'break' in monsoon (Onkari Prasad, 1981). The model differs in one aspect from the earlier models (Koteswaram, 1960; Asnani, 1973 and Rao & Datta, 1975). It has an additional circulation cell close to

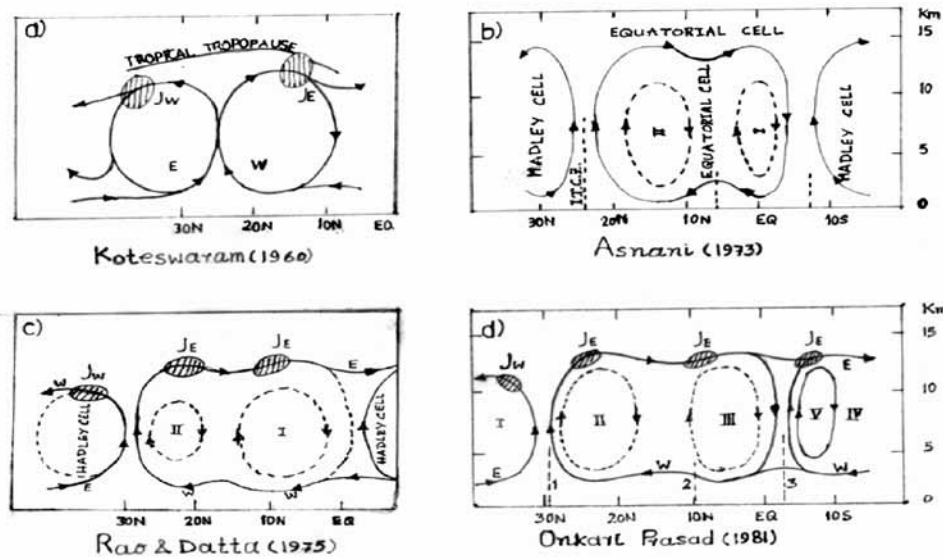


Figure 1 a): Circulation of the 'monsoon cell', b): Meridional circulation in summer monsoon over South East Asia, c): Circulation model for 'break monsoon', d): Circulation during 'break' in monsoon over India. W: Westerly, E: Easterly, Jw: Westerly Jet stream, JE: Easterly Jet stream, I.T.C.Z.: Inter Tropical Convergence Zone. In Figure 1 c): I&II: Equatorial sub-cell I & II. In Fig.1d): I: Hadley cell of Northern Hemisphere, II: Circulation cell associated with the Monsoon Trough, III: Circulation cell associated with the secondary trough, IV: Hadley cell of Southern Hemisphere, V: Circulation cell associated with South Indian Ocean Convergence Zone, 1- Monsoon Trough, 2- Secondary equatorial trough, 3- South Indian Ocean Convergence Zone.

south of equator, associated with SIOCZ. An experiment on the interaction between SIOCZ and MT using a zonal numerical model extending from South Pole to North Pole along 80°E meridian (Onkari Prasad, 1982) had shown that the revival of monsoon was associated with the weakening of SIOCZ, strengthening of the secondary trough in south Bay of Bengal around 10°N, its northward movement and establishment around 20° N latitude in the head Bay as a fresh MT. Thus it could be said that the circulation model proposed by Onkari Prasad (1981) depicts an important feature of monsoon circulation system over Southeast Asia. A reference to the circulation model is made here basically to explain the development of a weak southwest monsoon during 2017, when simultaneous existence of 3 troughs are seen a feature seen during 'break' in monsoon (Figure 1D). Such a phenomenon was seen as 3 distinct west-east oriented regions of positive precipitation anomaly, in precipitation anomaly charts for the months of July-September 2017. The charts are reproduced below.

Development of a weak summer monsoon during 2017 has been studied with the help of OLR Total, OLR anomaly, cloudiness, daily and weekly rainfall and monthly precipitation anomaly data. Salient features of these fields have been described. Changes in the features in the activity of SIOCZ have been discussed in relation to the performance of 2017 monsoon. The results of forecast verification, included in Pt. I (Onkari Prasad et al., 2018b), had shown that SIOCZ model's forecast was reasonably good in the districts of Tamilnadu, Andhra

Pradesh, Telanagana, Himachal Pradesh, Maharashtra and Goa states, in meteorological subdivisions and also for the country as a whole. However, the impact of the ISCs, which took place during 2017 monsoon, on rainfall could not be captured well in the Update issued in August. These aspects are discussed below in brief.

Salient Features of 2017 southwest monsoon

2017 Southwest Monsoon (SWM) advanced over Kerala on 30th May, around its normal date of 1st June. It covered the entire country by 19th July, i.e., 4 days after its normal date of 15th July. There were hiatuses in the progress of monsoon for 7 days in June (2nd -5th & 28th-30th) and 8 days in July (4th -11th). Cyclo-genesis was highly subdued during the season and more particularly during the second half of the season. During the first half of 2017 SWM, 11 Low Pressure Systems (LPSs) comprising Low Pressure Areas (LPAs) and Depressions, were formed. Only 3 of the Low Pressure Systems intensified into a Depression. During the second half of the season, even though 3 LPSs formed, none of them intensified into a depression. There were only 39 days of LPSs (June:11, July:12, August:10 & September:6) as against a normal of 58 days (Jun:11, July:14, August:17 & September:16). A well marked Low Pressure Area (LPA), during 11-16th July and two well marked LPAs in August, 18th - 21st and 27th Aug - 1st Sep, moved across central India and dissipated over Kutch & neighbourhood and over south Pakistan, respectively.

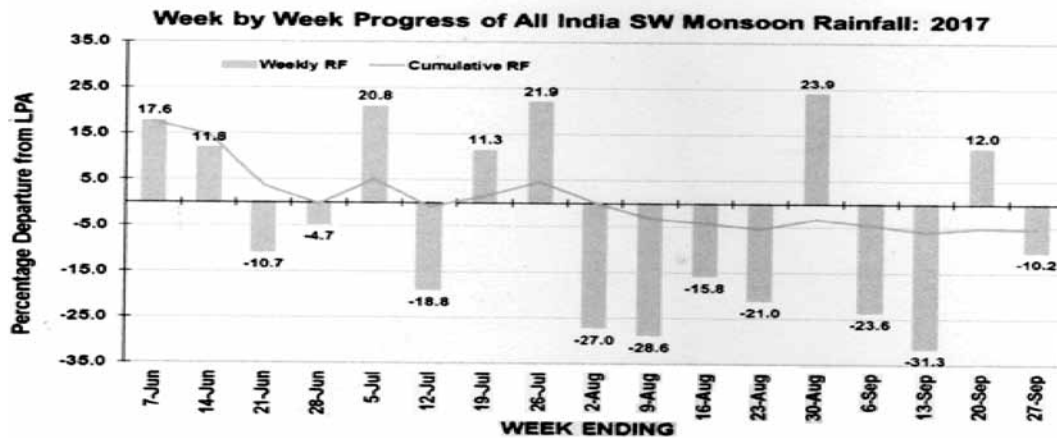


Figure 2. Week-by-week rainfall, for India as a whole, during 2017 summer monsoon. [Source: 'End of season report on 2017 southwest monsoon' by IMD].

These 3 LPAs had a southward shift in their track. The only system, which developed during 19th and 24th September was a well marked LPA. It had formed over northwest Bay of Bengal and neighbourhood and dissipated over west Uttar Pradesh and adjoining Uttarakhand. 2017 SWM started withdrawing from west Rajasthan from 27th September, i.e., much later than the normal date of 1 September. The linkage between southward shift of the track of LPSs during July -August and the location of SIOCZ is discussed below.

During the whole season, there was only one spell in July when normal to excess rainfall occurred over different regions of India: 13th -28th over Central India, 22nd -26th over Northwest India, 23rd -26th over East & Northeast India, 18th-20th over South Peninsula and 13th -25th for India as a whole, as per the daily rainfall series (www.imd.gov.in/pages/monsoon_main.php). Thus 2017 monsoon was most active over Central India during the spell. The weekly rainfall for India as a whole during 2017 monsoon is shown in Figure 2. The rainfall during this spell in July had made an important contribution in improving the seasonal rainfall scenario for India as a whole. But for this spell of good rainfall, 2017 monsoon would have slipped into a severe drought category. During this spell SIOCZ was active in a location to the south of its mean location for July, i.e. around 5° S. Spells of above normal rainfall, one each in August and September, were short lived and they did not affect the rainfall over all the four regions of India. The linkage between the spell of above normal rainfall during July and the location and intensity of SIOCZ is discussed below.

On daily basis the rainfall, for India as a whole, was on the lower side of normal on 62(51%) days (Jun:11, Jul:13, Aug:19 & Sep:19) out of 122 days of the season. The number of days with rainfall on the lower side of normal in four broad regions was: Northwest India, 75(61%) days (Jun:15, Jul:13, Aug:23 & Sep:24); East & Northeast India, 72(59%) days (20,16,17&19); Central India, 68(56%)

days (14,14,22&18),South Peninsula, 67(55%) days (16,27,14&10). On monthly basis rainfall was deficient in 7 subdivisions in June, 15 in July, 12 in August and 14 in September. The rainfall, for India as a whole was 4% and 2% above normal in June and July, 13% and 12% below normal in August and September. Severe drought like conditions prevailed over south Peninsula during July, Northwest and Central India during August and over parts of Northwest, Central, Northeast and Peninsular India during September. South Peninsula received normal-to-excess rainfall during August and September. For the season as a whole, rainfall was 5% below normal for India as a whole and it was in deficient category in 6 out of 36 subdivisions of India.

Development in equatorial Indo-Pacific region

La Nina conditions, which had prevailed over Nino 3.4 from JAS 2016-NDJ 2016/17 changed to ENSO normal, with negative anomalies up to JFM 2017 and positive anomaly thereafter. However, the positive anomalies did not reach 0.5°C, the threshold for declaring El Nino. The monthly anomaly in Nino 3.4 region was the highest in May (0.48° C) and it reduced to 0.35°C in Jul, -0.14 °C in Aug, -0.45 in Sep and Oct. In West South Indian Ocean (WSIO), the region of Indian Ocean (IO) to the west of 90°E, SST anomalies, as monitored on real time basis in weekly SST anomaly charts made available by NOAA on their website (www.esrl.noaa.gov/pst/map/clim/sst.shtml), remained positive from February 2017 till October. The 2016-17 SWIO cyclone season, 15th November 2016-30th April 2017, was a below average season. Out of five tropical storms (tropical storms as named in WSIO, are equivalent to tropical depressions in North Indian Seas- Arabian Sea and the Bay of Bengal), three intensified into tropical cyclones. Important thing to note in the development of these cyclones is that they originated south of 15°S. This is

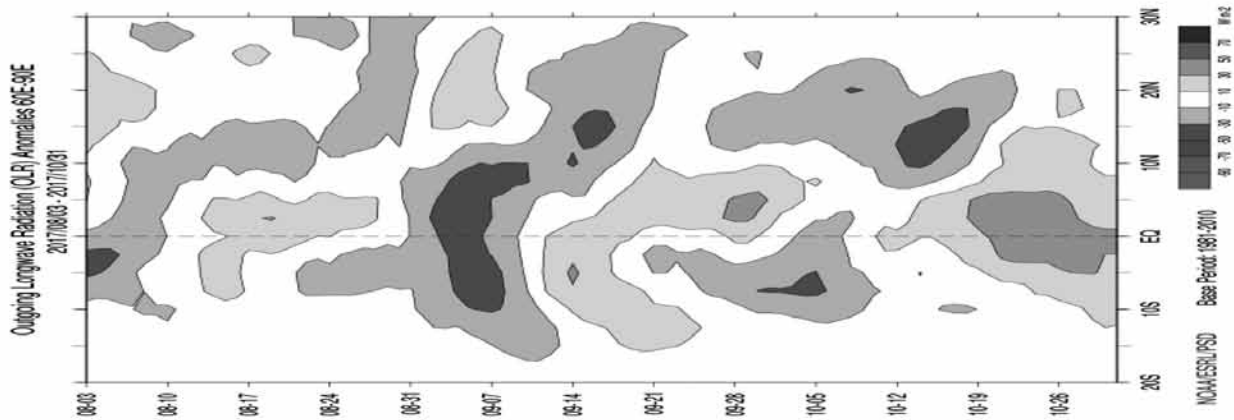


Figure 3. OLR anomaly over the region bounded by 30°N-20°S and 60°E-90°E during Aug-Oct 2017.

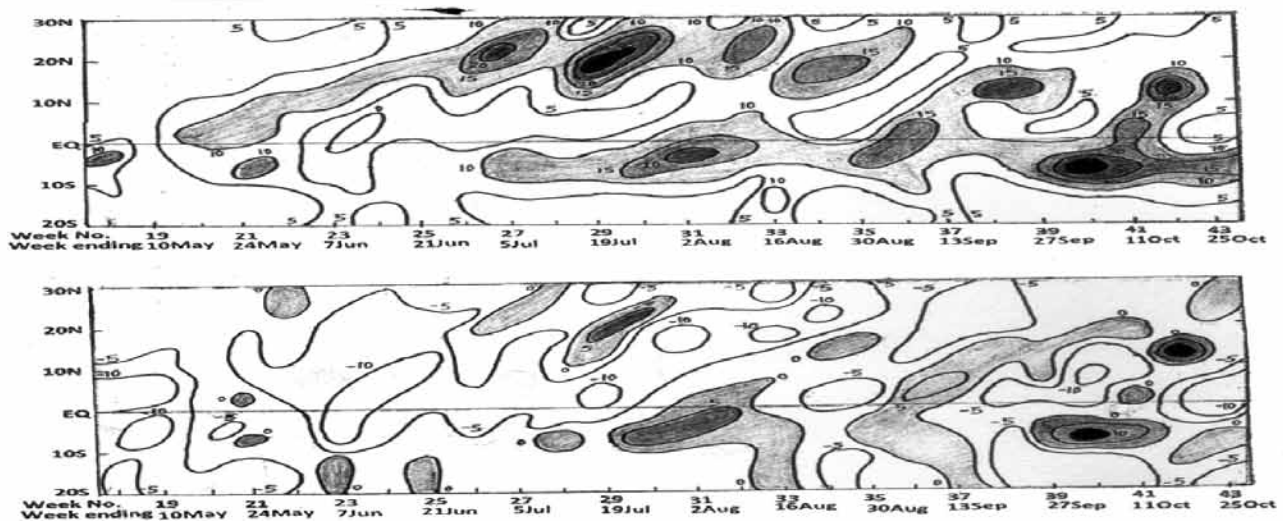


Figure 4. **Upper panel:** Zonal weekly mean cloudiness over the region bounded by 30°N-20°S and 40°E-100°E. Contours of total cloud amounts have been drawn at increments of 5%, 10%, 15%, 20%,...80%. **Lower panel:** Cloud anomaly. Contours have been drawn at increments of +/- 5%, 10%,15%, 20%, 30%, 40%, ...80%.[Base period: 1973-2012 except 1978 & there were some missing data during 1979 also]

in contrast to the cyclone season of 2015-16, when cyclogenesis took place to the north of 15°S (Onkari Prasad et al., 2018a). This implies a southward shift of the region of maximum positive SST anomaly and the location of SIOCZ- the zone of origin of tropical storms in WSIO. The implications of SIOCZ remaining active to the south of its normal position during Jul-Sep and the location of MT and distribution of rainfall over India are discussed below.

Features in the activity of SIOCZ

OLR Total, OLR anomaly, Zonal Weekly Mean Cloudiness (ZWMC) and Zonal Weekly Mean Cloud Anomaly (ZWMCA) have been used to identify the features in the activity of SIOCZ. OLR anomaly and ZWMC & ZWMCA are reproduced in Figures 3 & 4, respectively. Figure 3 shows OLR anomaly data for the period Aug-

Oct 2017. OLR anomaly data for the period Feb-Jul 2017 have been included in Pt. I (Onkari Prasad et al., 2018b). As mentioned in Pt. I, the main feature identified in the activity of SIOCZ before the commencement of 2017 monsoon season was the development of an active spell of SIOCZ for 3-4 weeks, in continuation. The other important feature was considerable reduction in the intensity of convection as seen in the dominance of positive areas in OLR anomaly and negative areas in cloud anomaly charts. These features had formed the basis for formulating SIOCZ model's LRF as discussed in Pt. I (Onkari Prasad et al., 2018b) Normally, the features in the activity of SIOCZ, which had occurred during the pre-monsoon months of April-May repeat during the season also. However, the features do change during the season in some of the years. This happened during 2017. The active spell of SIOCZ, which had started developing during the week ending on

12th April continued up to the week ending 10th May (Figure 1 of Pt. I). The next active spell of SIOCZ was expected to develop during the week ending on 14th June. However, this did not happen. An active spell of SIOCZ started developing only during the week ending on 5th July. This spell, in general, continued up to the end of October 2017. This feature is not clearly seen in OLR anomaly charts (Figure 3 and Figure 1 of Pt. I). However, in this generally active period of SIOCZ, 3 spells of intense convection developed: (i) for 4 weeks in continuation, from the week ending on 26th July to the week ending on 16th August, (ii) for 1 week only, during the week ending on 6th September, and (iii) for 3 weeks in continuation, from the week beginning from 27th September to 18th October. The interval between the development of all the 3 spells was fairly stable; around 3 weeks. The first and the third active spells lasted for 3-4 weeks, in continuation.

The features as noted in the activity of SIOCZ during the pre-monsoon months did not repeat during the season in the same manner. Additional features got superimposed over the main feature during the season and they were (i) SIOCZ remained weak for about 8 weeks during May-June, (ii) SIOCZ remained generally active for about 16 weeks, beginning from the first week of July till the end of October and (iii) convection associated with the active spell, which developed during the first week of September quickly moved to the north of equator during the next week. The implications of these changes on the performance of 2017 monsoon are discussed below.

Precipitation anomaly

The precipitation anomaly charts (<https://iridl.ldeo.columbia.edu/maproom/Global/Precipitation>) for the months of June, July, August and September-2017 are reproduced below (Figure 5). The maps show anomaly (mm/month) based upon precipitation estimates from the Climate Anomaly Monitoring System (CMAS)'s Outgoing longwave radiation Precipitation Index (OPI). The satellite precipitation estimates are based on emitted longwave radiation observed by polar-orbiting satellites. The period used for computing the climatology is 1979-2000. Green areas on the maps indicate where precipitation was above the long-term normal for the month and brown areas indicate where precipitation was below normal. Contours have been drawn at increments of +/- 10, 25, 50, 100, 200, 300, 400 and 500 mm/month. The maps are available for the Globe as well as for Asia. During the month of June, the region of reduction in precipitation extends from the Arabian Sea up to the date line and further east. The maximum reduction is seen over the Indian Seas. Reduction also occurred over parts of Northwest India, Central, East and Northeast India. A region of positive anomaly runs from Pakistan to central

Pacific. While the negative anomaly resulted due to weak monsoon conditions during the month, the positive anomaly was a result of the increased westerly influence over Northwest India and further east up to date line. In July, reduction in precipitation occurred over Peninsula, parts of Central, Northwest and Northeast India. The positive anomaly to the south of equator extending from 60°E to 90 °E is due to the presence of an active SIOCZ. During August, precipitation was deficient over a major portion of India, except over Parts of North, Northeast and south Peninsula. The 3 trough structure during 'break' in monsoon as shown in Fig. 1D, is more clearly seen in August as compared to that in July. In September, precipitation deficit occurred over Northwest, Central and parts of East and Northeast India. The 3 trough structure could be seen during September also.

DISCUSSIONS

As noted above a well marked LPA, during 11th-16th July, moved across central India and dissipated over Kutch and neighbourhood and over south Pakistan. Two well marked LPAs in August, 18th-21st and 27th Aug-1st Sep had also moved across Central India and dissipated over Kutch & neighbourhood and over south Pakistan, respectively. Normal to excess rainfall had occurred in July over Central India for 16 days (13-28 July) and for 3-5 days over the remaining 3 regions. This had resulted into rainfall becoming above normal for country as a whole for about 2 weeks (13 days, between 13-25 July) (Figure 2). Southward shift of MT and the track of LPSs during July and August and an active spell of rainfall for about two weeks over Central India during 13-28 July were linked to (i) southward shift of SIOCZ and (ii) SIOCZ remaining relatively weak as seen in convection, which remained moderate in the zone of SIOCZ. To support the above conclusions, zonal weekly mean cloud data for 4 weeks from the week beginning from 6th July till the week ending on 2nd August are reproduced below in Figure 6.

Normally, during the month of July, SIOCZ remains close to equator. But, SIOCZ remained active close to 5°S or south of it, from the week beginning 6th July till the week ending on 26th July (Figure 6a-c). It was only during the week ending on 2nd August that SIOCZ moved close to equator (Fig.6d). A southward shift in the location of SIOCZ results in a similar southward shift in MT. This gets confirmed from the existence of the Maximum Cloud Zone (MCZ) to the south of 20°N during the week, 13-19 July (Figure 6b) and between 20°N and 25°N during the week 20-26 July (Figure 6c). Central India received normal to above normal rainfall during these two weeks. This also explains the southward shift in the track of LPSs during July and increased rainfall over Gujarat in their association. With slight northward shift in MT, LPAs in

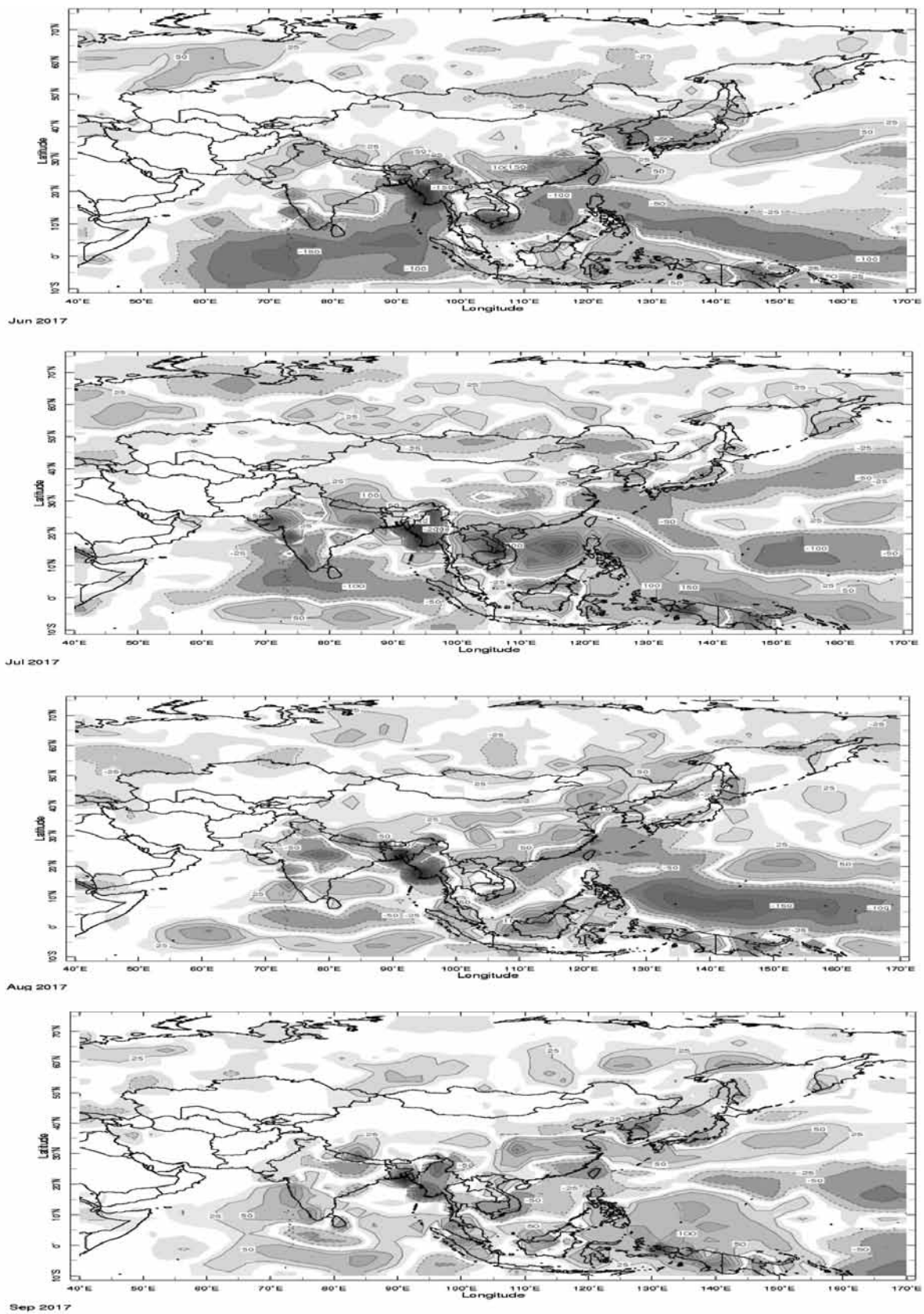


Figure 5. Monthly precipitation anomaly over Asia during Jun-Sep2017.Green- positive, brown- negative.

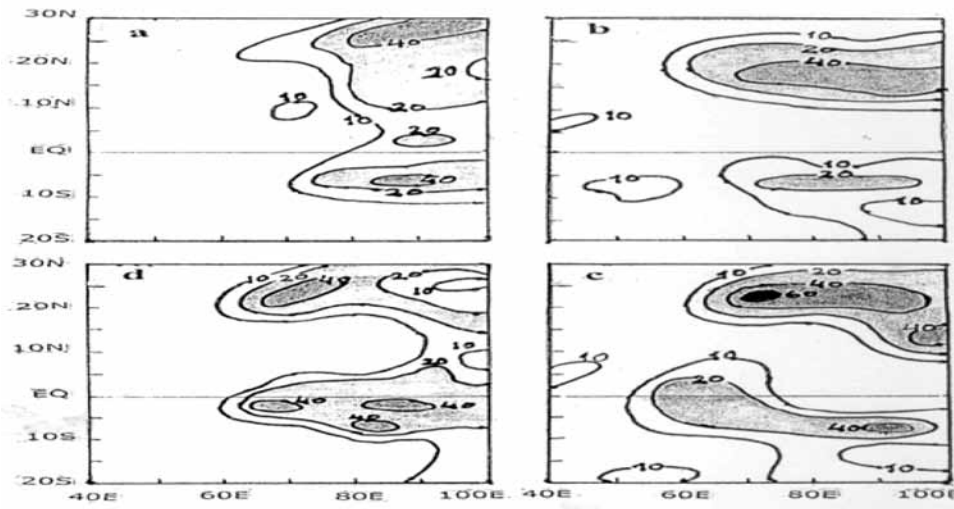


Figure 6. Zonal weekly mean cloudiness for the week (a) 6-12 July (b) 13-19 July (c) 20-26 July & (d) 27 Jul-2 August. Contours of total cloud amounts have been drawn at increment of 10%, 20%, 40%, 60% & 80%.

August moved across Central India and dissipated over Kutch and neighbourhood and south Pakistan.

The main feature as noted in the activity of SIOCZ during the pre-monsoon months, i.e., development of an active spell of SIOCZ lasting for 3-4 weeks, did repeat during August-October. But July spell was very weak. Additional features got superimposed over the main feature during the season and they were (i) SIOCZ remained weak for about 8 weeks during May-June, (ii) SIOCZ remained generally active for about 16 weeks, beginning from the first week of July till the end of October and (iii) The convection associated with the active spell of SIOCZ which began in the first week of July was not intense (iv) The convection associated with the active spell, which developed during the first week of September quickly moved to the north of equator during the next week. The MCZ associated with it could move up to 15°N only and got terminated there. As a result, this active spell could not activate/revive the MT. This also happened to the spell, which moved northward during the end of September/beginning of October. The ISC during July, which had been seen in the weakening of SIOCZ, had formed the basis for issuing an Update for improved rainfall during the second half of the season. However, that did not happen and an active spell of SIOCZ developed for 3 weeks in continuation beginning from the week ending on 26th July. August spell of active SIOCZ moved northward up to 15°N, and then to the south of equator up to 20°S. Having terminated around 15°N it could not activate the MT. In cloud anomaly field, the positive anomaly contour of 5% was confined to the areas south of 5°N. As the main feature in the activity of SIOCZ, i.e., SIOCZ developing for 3-4 weeks, reappeared during August, the improvement of rainfall during the second half remained confined to South Peninsula only. Thus the Update issued in August could not capture the

rainfall scenario during August-September. As noted earlier (Onkari Prasad et al., 2018a,b), Update/Updates could be improved, for which the information on the relationship between SST and SIOCZ and forecast SST anomaly field from SIO are required at least a month in advance. Due to various reasons this is presently not available. Need for a comprehensive study, on the relationship between SST distribution over SIO and the location and intensity of SIOCZ, is essential to obtain precise details.

CONCLUSIONS

1. Large deficiency in precipitation anomaly occurred not only over India but over the globe during 2017- a year of weak summer monsoon.
2. Prevalence of positive SST anomaly over West South Indian Ocean during the season resulted in southward shift of South Indian Ocean Convergence Zone and the track of tropical storms developing over west South Indian Ocean.
3. Southward shift of Monsoon Trough and the track of Low Pressure Systems over Indian sub-continent during July and August had occurred in response to southward shift of South Indian Ocean Convergence Zone.
4. The intra-seasonal Changes in 2017 monsoon had resulted due to changes in the location and intensity of South Indian Ocean Convergence Zone.
5. Intra-seasonal changes got superimposed over the main feature, as identified in the activity of South Indian Ocean Convergence Zone during pre-monsoon months. However, the main feature did persist and reappeared during August-October.
6. Investigations, on the relationship between SST field over South Indian Ocean and the location and intensity of South Indian Ocean Convergence

Zone, are required for a better understanding of the mechanism of development of intra-seasonal changes in summer monsoon.

7. Further improvement in SIOCZ model is possible by issuing Update/Updates incorporating the impact of intra-seasonal changes on rainfall. However, the same depends on the availability of reasonably good weekly forecast SST anomaly field from South Indian Ocean, at least a month in advance.

ACKNOWLEDGMENTS

The INSAT-3D satellite cloud imagery, available on real time basis on the web site of IMD was used for obtaining the cloud estimates information. Real time SST, OLR total and OLR anomaly charts issued by NOAA/ESRL/PSD and SST anomaly forecast charts issued by IRI, JASMTEC, ECMWF were also consulted. Monthly and seasonal rainfall data made available by IMD in their 'Southwest monsoon-2017- End of season Report' and rainfall data on daily and weekly progress of monsoon downloaded from their website have been used in the study. Thanks are due to Dr.R.S.Singh for useful suggestions. The authors gratefully acknowledge continued support, refinement and editing of the manuscript by Dr.P.R.Reddy.

Compliance with Ethical Standards

The authors declare that they have no conflict of interest and adhere to copyright norms.

REFERENCES

Asnani, G.C., 1973, Meridional circulation in summer monsoon of southeast Asia, *Ind. J. Met & Geophys.*, v.24, no.4, pp: 388-389.

IMD, 2017. 'Southwest monsoon-2017- End of season Report' Koteswaram, P., 1960. *Proc. Symp. Monsoons of the world*, New Delhi, India Met. Dept., pp: 105-110.

Onkari Prasad., 1981. Atmospheric circulation during 'break' in Indian summer monsoon, *Herald*, Moscow State University, Ser. 5, 1981, pp: 74-77. (in Russian)

Onkari Prasad., 1982, Development of Indian summer monsoon and its different phases, Ph.D. Dissertation, Moscow State University, pp: 118. (in Russian).

Onkari Prasad., and Singh, O.P., 2013. South Indian Ocean Convergence Zone model- A new approach to seasonal forecasting of summer monsoon rainfall in India Part IV: Intra-seasonal changes and long range forecast of rainfall during 2010 southwest monsoon season, *J. Ind. Geophys. Union*, v.17, no.3, pp: 289-305.

Onkari Prasad, Singh, O.P, and Prasad, K., 2014. South Indian Ocean Convergence Zone model- A new approach to long range forecasting of summer monsoon rainfall in India, Part-VI: Merits of the model and limitations in seasonal forecasting of rainfall in India, *J. Ind. Geophys. Union*, v.18, no.3, pp: 363-386.

Onkari Prasad, Singh, O.P, and Prasad, K., 2016a. Intra-seasonal changes and long range forecast of rainfall during 2013 southwest monsoon season based on South Indian Ocean Convergence Zone model, *J.Ind.Geophys.Union*,v.20, no.1, pp: 89-100.

Onkari Prasad, Singh, O.P, and Prasad, K., 2018a. 2016 southwest monsoon and its long range forecast, *J. Ind. Geophys. Union*, v.22, no.1, pp: 90-100.

Onkari Prasad, Singh, O.P, and Prasad, K., 2018b. Long range forecast and development of a weak southwest monsoon during 2017, Pt.I: Long range forecast, *J. Ind. Geophys. Union*, v.22, no.2, pp: 198-206.

Rao K., D., and Datta, R.K., 1975. Circulation during 'break' in Indian summer monsoon- a proposed model, *IJMG*, v.26, no.1&2, pp: 405-410.

Received on 4.12.17; Revised on: 25.1.18; Re revised on: 6.2.18; Accepted on: 8.2.18

Severe cyclonic storm JAL, air-sea interaction perspectives and floods along Andhra Pradesh-Tamilnadu coast

G.R. Chinthalu*, T. Dharmaraj, M.N. Patil, A.R. Dhakate, S.D. Pawar and Siingh D

Indian Institute of Tropical Meteorology,
Dr. Homi Bhabha Road, Pashan, Pune 411 008, INDIA

*Corresponding Author: chintalu@tropmet.res.in

ABSTRACT

Severe cyclonic storm JAL that devastated many Asian countries including southern east coast of India during 4-8 November 2010, evolved from a low pressure area in the South China Sea, near the eastern coast of Borneo, on 28 October 2010. Moving northwestward, the low pressure area emerged in the Bay of Bengal and concentrated in to a tropical depression on 4th November and into a severe cyclonic storm in the early morning of 6th. It produced very heavy rains causing severe floods and damage to life and property over parts of Malaysia, Thailand, Sri Lanka and India. It crossed the east-coast of India on November 7 north of Chennai, 13.3°N and 80.3°E and landfall near Nellore. The system attained a maximum intensity of T3.5. Coupled ocean-atmospheric processes have been examined to understand the unusually long track of the system and impact of floods on landfall along Andhra Pradesh- Tamil Nadu coast. Analysis of daily high resolution reanalysis data in the domain, 0-25°N, 60-130°E, during 1-8 November 2010 has revealed variation of Sea Surface Temperature (SST) between 27- 31°C, cooler SST to the left of the cyclone track and wind speed between 16 to 24 ms⁻¹. Satellite derived 3-hourly daily accumulated precipitation varied between 36 to 90 mm. Heavy rainfall was confined to the coastal hilly regions and rainfall was very low over the open ocean along the cyclone track. This had resulted in only a marginal cooling of SST, which had helped in the maintenance of sensible and latent heat fluxes. Significantly warm SST had provided continuous supply of moisture for the sustenance and unusually long travel of the system over sea.

Key words: Severe cyclonic storm JAL, Air- sea interactions, floods, damage.

INTRODUCTION

Tropical systems with maximum sustained surface winds of less than 17 ms⁻¹ are called tropical depressions. Once the surface wind speed in a tropical depression reaches the strength of at least 17 ms⁻¹ it is typically called a tropical storm or a tropical cyclone and assigned a name. When the surface winds attain the speed of 33 ms⁻¹, the storm is called a typhoon over (North Atlantic Ocean and the Northeast Pacific Oceans) and it is referred as a severe tropical cyclone in the southwest Pacific Ocean and southeast Indian Ocean (Neumann et al., 1993). Severe intensity tropical cyclones form during south-west post-monsoon period of October and November over the Bay of Bengal. Tropical cyclones (TCs) developing over the southern and central Bay of Bengal and Andaman Sea move northwestward towards the east coast of India and sometimes recurve between 15° and 18°N affecting the Bangladesh coast. Remnants of northwest Pacific typhoons moving westward develop into a low pressure system over the Andaman Sea and intensify further over the Bay of Bengal during the post-monsoon season. The life span of a severe cyclonic storm over the north Indian Ocean averages about 4 days on a yearly basis (IMD, 1979). The number of cyclones over the Bay of Bengal is 3-4 times more than those over the Arabian Sea (Obasi, 1997). The information about the

ocean response to storm forcing is one of the important factors in tropical cyclone track prediction. Monitoring of surface weather parameters and the upper ocean thermal structure from moored buoys has become a key element in the studies of tropical cyclones (Premkumar et al., 2000). Several studies have been carried out to document the ocean's response to the tropical cyclones and to understand the associated air-sea interaction processes (Stramma et al., 1986). In the case of the tropical cyclones in north Indian Ocean, earlier investigators (Gopala krishna et al., 1993; Chinthalu et al., 2001) had reported cooling of the SST after the passage of cyclones. They had noted that in the regions of weaker upper ocean stratification (southern and western Bay of Bengal) the magnitude of the SST decreases by around 2°C, due to the passage of cyclone. Tropical cyclones are more likely to intensify than weaken after an interaction with an upper-level trough when cyclones are moving over warm waters, as they continue to derive energy (Hanley et al., 2001). Emanuel (1986) had suggested that the energy from the ocean is through the transfer of moisture from the ocean to the atmosphere, which is dependent on wind speed and the difference of moisture content between the air and the saturation mixing ratio at the sea surface. The response of the upper ocean plays a major role in controlling the storm intensity through associated variability in the upper ocean conditions such



Figure 1. Track of the severe cyclonic storm JAL

Table 1. The Saffir–Simpson scale has been followed and color codes denote the wind speed of JAL.

System/Category	Wind speed
Tropical Depression	≤ 17 m/s ▲
Tropical storm	18-32 m/s ●
Category one	33-42 m/s ●
Category two	43-49 m/s ●

as SST, surface salinity, mixed layer depth, currents in the mixed layer, etc. and atmospheric conditions such as winds, atmospheric pressure, and precipitation. Recent studies indicate that generally cyclones originating from the Bay of Bengal cross the east coast of India and cause floods due to heavy rainfall. In a case study of September 1997 Andhra cyclone (Chintalu et al., 2012), the persistent southward movement of 500 hPa ridge on the eastern wedge of the system along with the steering current at 200 hPa level, has helped in maintaining the movement of the system parallel to the east coast of India. Such cyclones give rise to copious rainfall and often cause major floods, causing damage to life and property in the eastern states of India.

Track of the system

The Severe cyclonic storm JAL, 4-8 November 2010, evolved from a low pressure area in the South China Sea, near the eastern coast of Borneo on 28 October 2010. Moving northwestward the low pressure area picked up strength and emerged in the Bay of Bengal. Figure 1 shows the track of the severe cyclonic storm JAL. The wind speed criterion refers to the Saffir–Simpson scale. Different wind speeds given by color codes and symbols are shown in Table 1. IMD upgraded the system to a Depression at 0000 UTC of 4 November and to a Severe Cyclonic Storm at 2100 UTC of 5th November.

JAL lay centered over southwest Bay of Bengal at 0000 UTC of 6th November 2010 near 10.0°N, 85.5°E about 450 km east-northeast of Trincomalee (Sri Lanka). The cyclone was about 600 km east-southeast of Chennai and

about 750 km southeast of Nellore before landfall. The JAL cyclone was tracked by INSAT Kalpana-1 satellite imagery from 0600 UTC of 2 November till the time of landfall. The maximum estimated intensity of T 3.5 was reported by IMD from 2100 UTC of 5th to 0500 UTC of 7th November. The estimated lowest central pressure was 988 hPa. The estimated maximum wind speed was 30 ms⁻¹. As per Doppler Weather Radars (DWR) at Chennai and SHAR, the system started weakening from 0300 UTC of 7th November. Continuing its northwesterly track JAL crossed the coast as a deep depression between Puducherry and Nellore and very close to SHAR around 1800 UTC of 7th. The system weakened into a low pressure area over Rayalaseema and adjoining south interior Karnataka. The cloud heights were ~ 5 to 6 Km and the maximum reflectivity in the wall cloud region was about 35-45 dBz. The DWR at Chennai tracked the maximum wind, which was about 23 ms⁻¹ from 0400 to 1800 UTC on 7th November. Rainfall occurred at most places with heavy to very heavy falls at a few places over north Tamil Nadu, Puducherry, coastal Andhra Pradesh, Rayalaseema, south Interior and coastal Karnataka. JAL crossed the east-coast of India on November 7 north of Chennai near Nellore. Figure 2 shows the INSAT (Kalpana-1) satellite cloud imagery during landfall near Nellore on 7th November, at the time of land fall. The maximum intensity attained by the severe cyclonic storm JAL was T 3.5. The satellite imagery on 7th November also shows the thick and dense spiral cloud bands and overcast conditions, which has covered the major parts of the states of Andhra Pradesh and Tamil Nadu. It is further noticed that another band

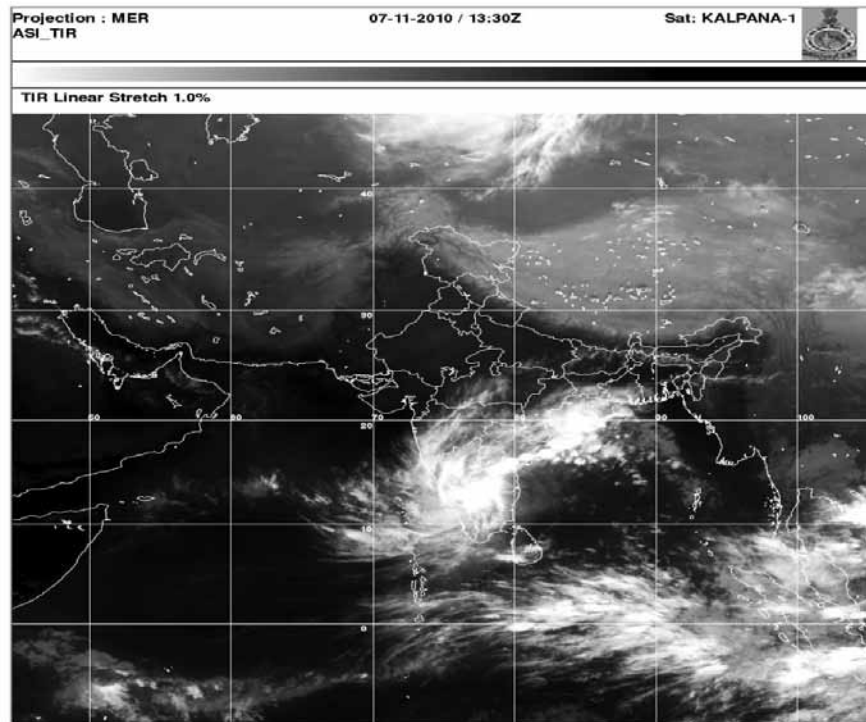


Figure 2. INSAT Kalpana-1 satellite cloud imagery of JAL during landfall on 7 November 2010.

of dense convective clouds that lay near 5° N and 82° E has crossed the Andhra Pradesh and Tamil Nadu coast in the morning hours of 8th November resulting in very heavy rainfall. This was reported by India Meteorological Department, as discussed below. The above mentioned states had suffered heavy losses in terms of life and property due to devastating floods caused by heavy rainfall.

Data and methodology

Analyses of various parameters are presented below for the period 1-8 November. The data used in the present study consist of NCEP-NCAR reanalysis and Tropical Rainfall Measuring Mission (TRMM) data products such as daily SST, winds, pressure, Outgoing Longwave Radiation (OLR), sensible and latent heat fluxes, Vertical Wind Shear (VWS) daily data with resolution of 1° lat. \times 1° long and sensible and latent heat fluxes and TRMM 3 hourly accumulated precipitation. Daily composite maps have been prepared in the domain of 0 - 25° N, 60 - 130° E. These maps have been analyzed to understand the features in air-sea interaction, which helped JAL to survive for a comparatively longer period of time.

Atmospheric pressure

Figure 3 (a-h) shows the day to day sea level pressure distribution during 1-8 November 2010. Values of atmospheric pressure, to the right of the track, varied between 1008-1018 hPa. Falling pressure to the left of the

track was an indication of gradual intensification of cyclone. The sea level pressure that initially fell slowly towards the centre of the system and later rapidly to its minimum value indicated the severity of the cyclone, with lowest pressure of 998 hPa during 5-7 November. A comparison of mean sea level pressure values with TRMM derived rainfall (Figure 9) indicates that the centre of low pressure has been associated with enhanced convective activity and heavy rainfall. There has been an increase of sea-level pressure of about 10 hPa (Fig. 3h) within a span of 2 to 6 hours after landfall. The heavy orographic rainfall has been confined to low level hills located within the cyclone track zones. They are also the potential areas of flash floods and large scale disaster. This shows that the topography along the path of the cyclone has resulted in a drastic reduction in the intensity of the system.

Sea Surface Temperature

The Sea Surface Temperature (SST) distribution is the single most important parameter in the development of tropical systems and the track followed by them (Goldernberg et al., 2001). Several studies have indicated higher SST inducing strong convection (Yu and Wang., 2009). Figure 4(a-h) depicts the daily variation of SST and 850 hPa wind field composite during 1-8 November 2010. SST was cooler (26 - 28° C) to the right as compared to the left of the cyclone track in the domain of 14 - 25° N and 110 - 130° E. The higher SST (~ 29 - 30° C) was observed to

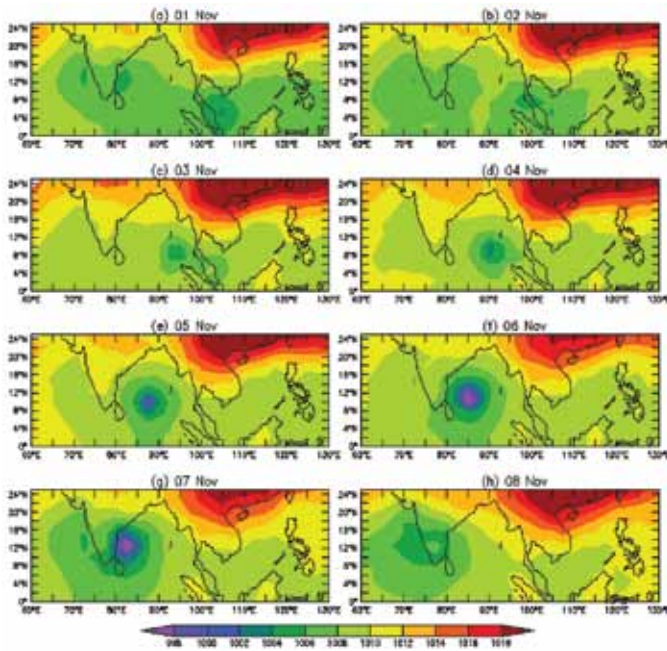


Figure 3. (a-h) Mean sea level pressure (hPa)

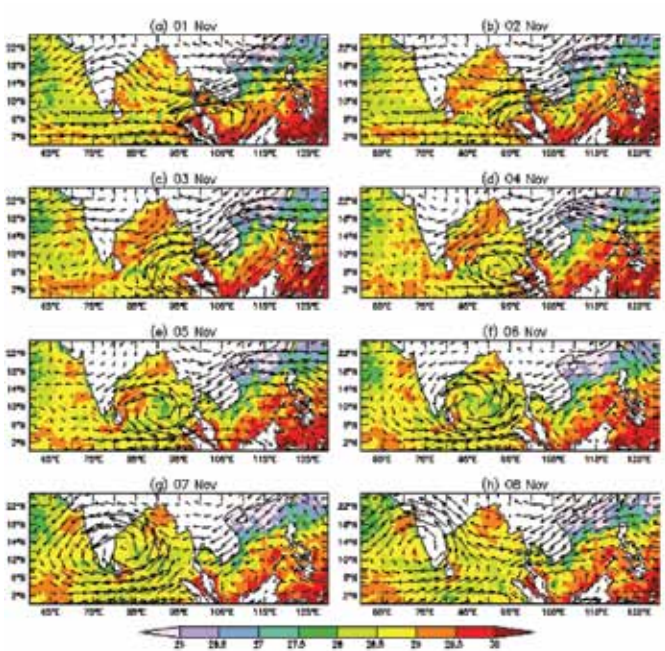


Figure 4. (a-h) Daily mean time series wind speed and direction.

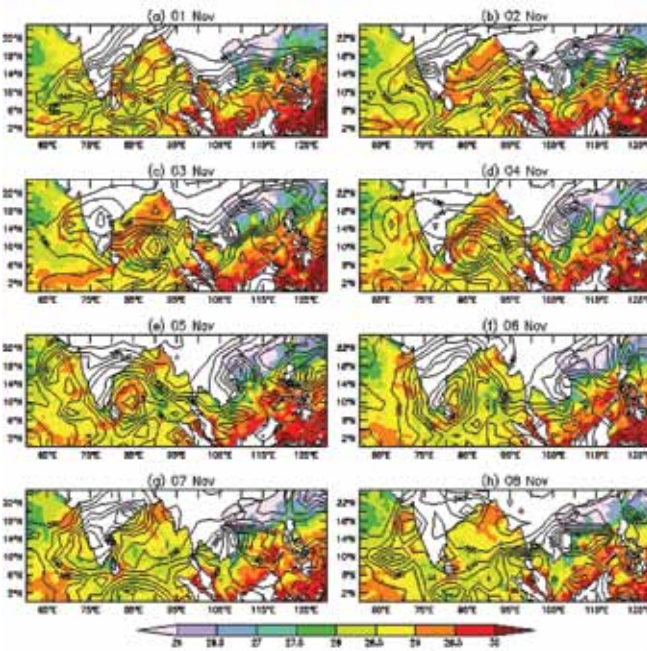


Figure 5. (a-h) Daily mean SST and OLR.

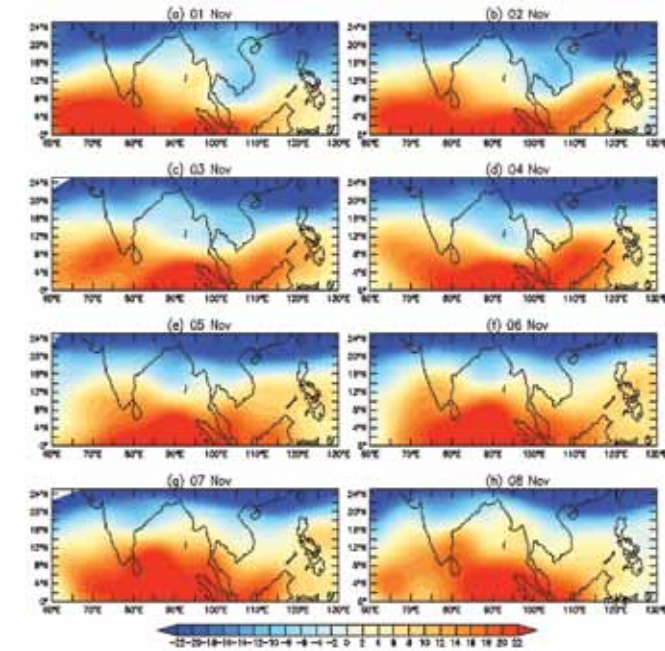


Figure 6. (a-h) Vertical Wind shear.

the left of the cyclone track. The SST was warmer by 2-4 °C to the left of the cyclone track. Fairly long survival and westward travel of the JAL could be the direct response of prevailing high SST along the track of cyclone.

Wind field

Figure 4(a-h) gives the composite of SST and wind field. The wind speed varied between 10-20 ms⁻¹ in the central

Bay of Bengal and it increased on 6th and 7th November before landfall. Similarly, the analysis of SST and wind field for 700 hPa level has shown prominent cyclonic circulation extending up to 700 hPa level during 4-7 November and system's improved organization on 5th, 6th, and 7th November. Further, analysis of wind field at 500 and 200 hPa (figures not shown) indicated that the cyclonic circulation had lost its organization above 700 hPa level, while it was still over the ocean.

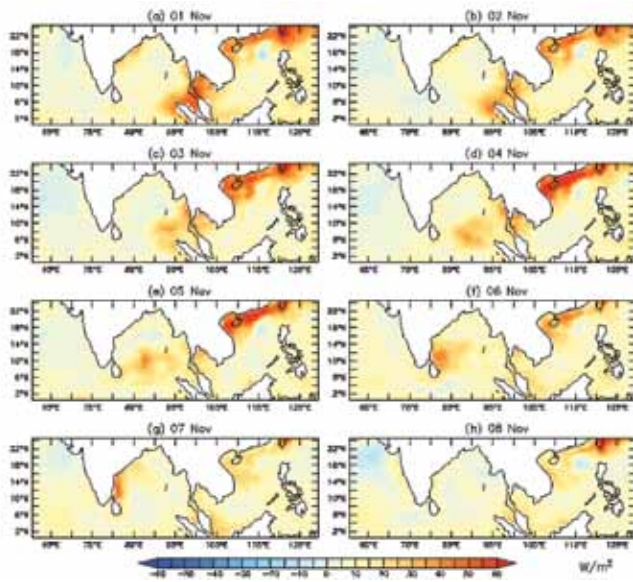


Figure 7. Sensible heat flux during 1-8 November 2010.

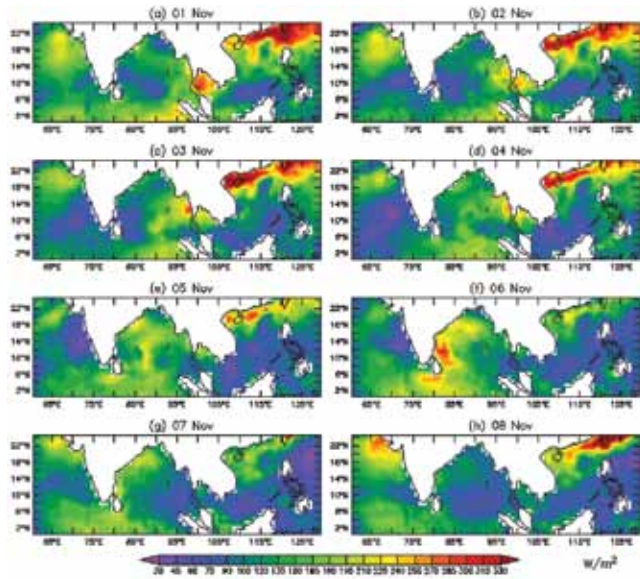


Figure 8. Latent heat flux during 1-8 November 2010.

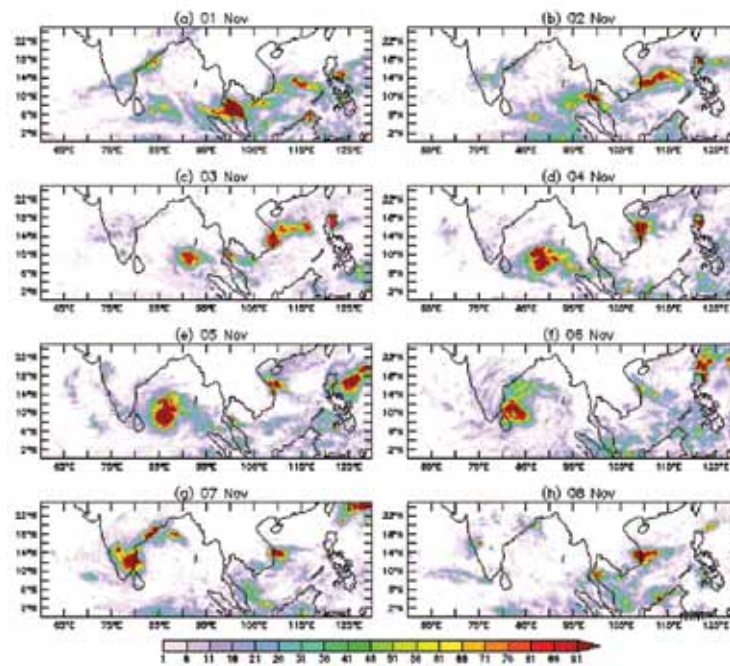


Figure 9. TRMM derived daily mean rainfall (mm).

SST and OLR

Figure 5 shows the SST and OLR composite during 1-8 November. OLR is used to locate the areas of deep tropical convection as a proxy for precipitation (Arkin and Ardanuy, 1989). The OLR values below 240 Wm^{-2} are considered to represent the convective area (Richards and Arkin, 1981). Over the land and cloud free zones (14° - 25°N , 80° - 100°E), the OLR varied between 200 - 240 Wm^{-2} . In the active

convection zone along the track of JAL (5° - 10°N , 80 - 100°E), OLR varied between 140 - 180 Wm^{-2} . It is seen that during the cyclone's active days, as shown in Figure (4d-f), the low values of OLR varying between 120 - 180 Wm^{-2} were co-located with warmer SST (~ 28 - 30°C) in the central Bay of Bengal. The large fall in OLR values indicated enhanced convective activity when JAL was approaching the east coast of India. After the landfall on 8th November, OLR values increased to 260 - 280 Wm^{-2} .

Table 2. 24 hrs accumulated rainfall (≥ 7 cm) between 0300 UTC of 7 to 0300 UTC of 8th November 2010, along Andhra Pradesh coast.

Stations	Rainfall (cm)	Stations	Rainfall (cm)
Palasa	27	Vempalli	8
Sompeta	14	Bhimunipatnam	8
Itchhapuram	12	Thambalapalli	7
Puttur	11	Madakasira	7
Kalingapatnam	10	Nellore	7
Rayacholi	10	Anakapalli	7
Kuppam	10	Mandasa	7
Tekkali	9	Kandukur	7

Table 3. Same as Table 2 but for Tamil Nadu-Puducherry coast.

Stations	Rainfall (cm)	Stations	Rainfall (cm)
Gingee	16	Vanu	9
Panruti	15	Thali	9
Ambur	13	Chengalpattu	8
Vaniyambadi	12	Polur	8
Tiruvannamalai	11	Krishnagiri	8
Alangayam	11	Dharmapuri	7
Tindivanam	10	Palacode	7
Villupuram	10	Sholingur	7
Puducherry A.P	10	Gudiyatham	7
Cuddalore	10	Vellore	7

Vertical wind shear

Figure 6(a-h) shows Vertical Wind Shear (VWS) field between 200 and 850 hPa levels during 1-8 November 2010. The VWS is an important dynamical factor affecting tropical cyclones intensity and precipitation pattern (Yu and Wang, 2009). The VWS has long been recognized to have a strong influence on the development, structure and intensity of tropical cyclones (Tang and Emanuel 2010). When VWS is low, it accelerates genesis of a system and when it increases the genesis is hampered. The low values of VWS was observed to the north of the track of JAL suggesting existence of favorable conditions for maintaining the cyclone for a relatively longer period of time.

Sensible and latent heat fluxes

Figure 7(a-h) shows the sensible heat flux during 1-8 November 2010. Warming and moistening of the boundary layer, through the sensible and latent-heat fluxes from underlying warm sea, is an efficient mechanism for convective destabilization and production of heavy precipitation. In particular, the effect of moistening the low levels is two-fold: it favors the conditional destabilization of the boundary layer, facilitating the release of convection,

and it allows a continuous replenishment of the buoyant energy, favoring the maintenance of convection. Once a favorable environment was produced, and convection developed, the latent heat released from convection further induces cyclo-genesis through diabatic heating over a deep column. This enhances the cyclone intensity and the associated surface winds, leading to greater latent-heat flux, and resulting in a hurricane-like energy engine via air-sea interaction instability. Sensible heat flux of the order of 30 - 40 Wm^{-2} was located over Thailand and adjoining sea along the track on 1st November 2010. It fell and rose as JAL approached the east coast of India. It varied between 20-30 Wm^{-2} as the system reached Andhra Pradesh-Tamil Nadu coast. It rose sharply to 30-40 Wm^{-2} on 6th and 7th November. After land fall, the sensible heat flux fell sharply to 0 to -10 Wm^{-2} . Figure 8 (a-h) shows the latent heat flux during 1-8 November. The latent heat flux was of the order of ~ 270 -300 Wm^{-2} on 1st November and was located along the track near and adjoining the Thailand sea. It varied between 75 & 180 Wm^{-2} during 2-5 November. On 6th November, there was a significant rise in latent heat flux about 100 Km away and along the Andhra Pradesh-Tamil Nadu coast. As the system approached the coast, the latent heat flux fell sharply to a low value of 120-150 Wm^{-2} .



Figure 10. Photograph showing damage and floods caused by the severe cyclonic storm JAL in the state of Andhra Pradesh (Source: Babu/Reuters)

Satellite derived rainfall

Figure 9(a-h) shows the Tropical Rainfall Measuring Mission (TRMM) derived rainfall data during the period 1-8 November 2010. On 1st November, heavy rainfall of the order of 90 mm/day was confined to a small area located around 6°N, 100°E. During 3-7 November, the system intensified and produced heavy rainfall of the order of 40-60 mm/day. These spells of heavy rainfall was for a small duration and on a smaller area. Tables 2 and 3 show the rainfall along Andhra Pradesh coast and Tamilnadu –Puducherry coast, respectively on 8th November 2010.

Damage

The severe cyclonic storm JAL caused heavy down pour in Thailand resulting in extensive flooding, which led to the demise of 59 people. The cyclone claimed four lives in Malaysia. Due to timely warnings, 70,000 people were evacuated from the villages of Andhra Pradesh where damage was expected to be the highest. Figure 10 shows the flooding and damage in Andhra Pradesh. On 9th November, the state declared that 54 people died due to the storm. The total damage estimated by the government was of the order of Rs.363 crore.

DISCUSSIONS

Cyclonic storms striking east coast of India during the south-west post-monsoon season (October-December), generally develop in the southeast Bay of Bengal. However, some of the remnants of typhoons in west Pacific Ocean/south China Sea move westward and emerge in east Bay of Bengal as a low pressure area, intensify into a cyclonic storm and cross east coast of India. JAL was one such cyclone. It formed as a weak system in South China sea on 28th October 2010 and moved across Thailand, Myanmar.

Then it emerged in the Bay of Bengal and concentrated into a Depression at 0000 UTC on 4th November 2010 over southeast Bay of Bengal near lat.8.0°N and 92.0°E. The lowest value of atmospheric pressure of 998 hPa was observed during 5-7 November. The SST was cooler to the right as compared to the left of the cyclone track in the latitude belt of 14-25°N and long. 110-130°E. The higher SST was observed to the left of the cyclone track. The wind speed varied between 10-20 ms⁻¹. Wind field showed prominent cyclonic circulation during 4-7 November in the central Bay of Bengal and increased on 6th and 7th November before making landfall on Tamilnadu-Andhra coast. The SST and wind field level shows the formation of prominent cyclonic circulation during 4-7 November, extending up to 700 hPa level. It is seen that during cyclonic active days viz. 4-7 November, the low values of OLR were co-located with warmer SST in the central Bay of Bengal. The large fall in OLR indicated enhanced convective activity as the JAL cyclone approached the east coast of India. Sensible heat flux fell and rose as the JAL cyclone approached the east coast of India and it varied between 20-30 Wm⁻²; as the system approached Andhra Pradesh - Tamilnadu coast. The sensible heat flux rose sharply to 30-40 Wm⁻² on 6th and 7th November. The latent heat flux was fluctuating between 75 and 180 Wm⁻² during 2-5 November. On 6th November there was a significant increase in the latent heat flux along the Andhra Pradesh -Tamilnadu coast and as the system approached the east coast, the latent heat flux fell sharply. Heavy rainfall occurred in the domain 110°E, 5-6°N, but it was confined to a very small area. On 2nd November, the Jal cyclone produced comparatively less rainfall. This may be attributed to the slight weakening of the cyclone. On 7th November the cyclone made land fall and caused considerable damage to life and property due to heavy rainfall. Subsequent to landfall the convective clouds dissipated and OLR rose sharply indicating dry and fair weather conditions.

CONCLUSIONS

The persistent high sea surface temperature ($> 26^{\circ}\text{C}$) along the track enabled continuous supply of moisture for long travel of JAL.

Marginal cooling of SST along the track, which had helped in the maintenance of sensible and latent heat fluxes, has aided in the longer survival of JAL.

Significant increase in latent heat, sensible heat flux and incursion of moisture, before land fall, were responsible for enhanced convective activity leading to heavy floods along Andhra Pradesh-Tamilnadu coast.

ACKNOWLEDGEMENTS

The authors thank the Director IITM Pune for the facilities and constant encouragement.

NCEP-NCAR Reanalysis data was provided by the NOAA/ESRL PSD, Boulder, Colorado, USA, from their Web site at <http://www.esrl.noaa.gov/psd/>. We thank the JAXA-USA TRMM team for providing satellite derived precipitation data. We also acknowledge Mr Babu/Reuters for the photographs reproduced in the paper. Thanks are due to Dr.Onkari Prasad for reviewing the manuscript and suggesting useful changes to the text. The authors thank Dr.P.R.Reddy for continued support and final editing.

Compliance with Ethical Standards

The authors declare that they have no conflict of interest and adhere to copyright norms.

REFERENCES

Arkin and Ardanuy, 1989. Estimating Climatic-Scale Precipitation from space: A review, *Journal of Climate*, v.2, pp: 1229-1238.

Chinthalu, G.R., Seetaramayya, P., Ravichandran, M., and Mahajan, P.N., 2001. *Current Science*, v.81, no.3, 10 August.

Chinthalu, G.R., Dharmaraj, T., Dhakate, A.R., and Devara, P.C.S., 2012. Salient features of Andhra Pradesh cyclonic

storm in the Bay of Bengal during September 1997 *Nat Hazards* 62:613–633 DOI 10.1007/s11069-012-0097-5.

Cyclonic disturbances over north Indian Ocean during 2010. A Report, Cyclone warning division New Delhi, report No. 5/2011, India Meteorological Department, January 2011.

Emanuel, K.A., 1986. An air–sea interaction theory for tropical cyclones. Part I: Steady-state maintenance. *J. Atmos. Sci.*, v.43, pp: 585–604.

Gopala krishna Murty, V.V.V.S. N., Sarma, M.S.S., and Sastry, J.S., 1993. Thermal response of upper layers of Bay of Bengal to forcing of a severe cyclonic storm: A case study, *Indian J. Mar. Sci.*, v.22, pp: 8–11.

Hanley, D., Molinari, J., and Keyser, D., 2001. A composite study of the interactions between tropical cyclones and upper-tropospheric troughs. *Mon. Wea. Rev.*, v.129, pp: 2570-2584.

India Meteorological Department, 1979. Tracks of storms and depressions in the Bay of Bengal and the Arabian sea, 1877–1970, 186 maps, pp: 26.

Neumann, C.J., Jarvinen, B.R., McAdie, C.J., and Elms, J.D., 1993. Tropical cyclones of the North Atlantic Ocean, 1871-1992. NOAA Historical Climatology Series 6-2, Asheville, pp: 193.

Obasi, G.O.P., 1997. WMO's programme on tropical cyclone, *Mausam*, v.48, pp: 103–112.

Premkumar, K., Ravichandran, M., Kalsi, S.R., Sengupta, D., and Gadgil, S., 2000. First results from a new observational system over the Indian seas, *Curr. Sci.* v.78, no.3, p: 323–330.

Richards, F., Arkin, P.A., 1981. On the relationship between satellite-observed cloud and precipitation. *Mon. Wea. Rev.* v.109, pp: 1081-1093.

Stramma, L., Cornillon, P., and Price, J.F., 1986. Satellite observations of sea surface cooling by hurricanes. *Journal of Geophysical Research*, v.91, no.C4, pp: 5031-5035.

Tang, B., Emanuel, K., 2010. Midlevel ventilation's constraint on tropical cyclone intensity. *J. Atmos. Sci.*, v.67, pp: 1817-1830.

Jinhua, Y., and Yuqing Wang, 2009. Response of tropical cyclone potential intensity over the north Indian Ocean to global warming *Geophysical Research Letters*, v.36, L03709, doi:10.1029/2008GL036742,

Received on: 27.12.17, Revised on: 19.1.18; Re revised on: 22.1.18; Accepted on: 2.2.18

Meteorological conditions for development of heat wave over Coastal Andhra Pradesh and Telangana

Charan Singh* and S. V. J. Kumar

India Meteorological Department, Mausam Bhavan, Lodi Road, New Delhi-110003

*Corresponding Author: csingh1964@gmail.com

ABSTRACT

Heat waves are one of the weather hazards affecting different regions of India with varying intensity. Beforehand knowledge of the meteorological conditions favorable for the occurrence of heat wave/severe heat wave conditions over a given region/state is required for issuing warnings. Reasonably accurate meteorological conditions are now available from dynamical models, several days in advance, and the same could be used for issuing warnings about likely development of heat wave/severe heat wave condition. In the recent past, Andhra Pradesh and Telangana had been affected by severe heat wave conditions for several days in continuation. In the present study meteorological conditions associated with the heat waves over coastal Andhra Pradesh and Telangana during May 2015 have been detailed. The analysis of meteorological conditions has shown that the severe heat wave conditions during the year had resulted due to advection of dry air from northwest over a prolonged period of time when skies were cloud-free, soil moisture was low and there was an absence of development of strong sea breeze in the afternoons.

Key words: Meteorological conditions, Heat waves, Sea breeze, Soil moisture, Warnings about heat waves.

INTRODUCTION

WMO statement on the status of the global climate has indicated a rise in temperatures over various parts of the globe (WMO Tech No.1085). According to the 'Synthesis report-climate change 2014' (IPCC- AR5), each of the past 3 decades has been warmer than any other preceding decades since 1850. Over northern hemisphere, the period from 1983 to 2012 was the warmest 30-year period of the past 1400 years (Fifth Assessment Report AR5, 2014). The global averaged combined land and ocean surface temperature data, as calculated by a linear trend, has shown a warming of 0.85 (0.65 to 1.06°C) over the period 1880 to 2012. These reports (Fifth Assessment Report AR5, 2014) have thus indicated an increasing propensity of occurrence of heat waves over different countries of the globe. A heat wave is a condition of excessively hot weather, for a few days or for a prolonged period of time in some cases, which may be accompanied by dry hot winds and high humidity. There is no universal definition of heat wave as temperature ranges have wide variance over different continental and maritime regions. One range of temperature may be easily adaptable in one region, but may cause discomfort in another region, because of different levels of endurance to these climatic conditions. In India, the intense heat days commence in the month of March over the extreme south peninsular India and subsequently affect the central and northern parts of the country till mid-July by which time the southwest monsoon establishes over the entire country. While most parts of the country including Andhra Pradesh and Telangana experience heat waves in the month of April and May, the northern states

experience heat waves mainly during May-June. Advection of heat fluxes causes the spread of heat from one area to the neighboring areas. If a heat wave forms over an area and remains confined there only, the heat wave is called an in-situ type of heat wave. If the heat wave conditions spread over the neighboring areas, then this type of heat wave is called an advection type of heat wave. In India, most of the heat waves are of the advection type.

India Meteorological Department (IMD) defined heat wave in terms of the departure of maximum temperature from the normal maximum temperature of a station (Table 1). Subbaramayya and Rao (1976) have described, in detail, the heat and cold wave days in different states of India. Bedekar et al., (1974) and Chaudhary et al., (2000) have analyzed heat and cold waves and their impact. Jenamani (2005) analysed Ocean and atmospheric features associated with extreme temperature variation over east coast of India during 1998. Ray et al., (2013) have analysed the cause of extreme high temperatures over Gujarat state. Pai et al., (2004) concluded that there is a significant increasing trend in the heat wave days over Telangana and Andhra Pradesh. The study by Bhadram et al., (2005) has shown increase in the frequency of severe heat waves and also their duration. The authors noted that the highest maximum temperatures which hitherto used to be recorded over Telangana are shifting to the coastal districts of the state in recent years. Pai et al., (2013) found that both Andhra Pradesh and Telangana experienced 8 or more number of heat wave days during the 5 months period of March-July in the study period of 1961-2010. These studies have addressed some aspects of the heat wave. Analysis of synoptic, dynamic and thermodynamic conditions helps in understanding the



Figure 1. Map of meteorological sub-divisions of India including the shaded sub-divisions Telangana and coastal Andhra Pradesh.

Table 1. IMD criteria of heatwaves, severe heatwaves and hot days

S.No.	Criteria	Departure from normal	Intensity of the Heat wave
1	Heat wave is considered if maximum temperature of a station reaches at least 40.0 °C or more for plains.	Between 4.5 to 6.4 °C	Heat wave
		≥ 6.4 °C	Severe Heat wave
2	When the absolute/actual maximum temperature of the day is 45.0 °C or more.	Absolute/actual maximum temperature of the day is 45.0 °C or more.	Heat wave
		Absolute/actual maximum temperature of the day is ≥ 47.0 °C.	Severe Heat Wave
3	Warm night should be considered only when maximum temperature remains 40 °C or more. It may be defined based on departures or actual minimum temperatures.	minimum temperature departure is 4.5 °C to 6.4 °C	Warm night:
		minimum temperature departure is >6.4 °C	Very warm night:
4	When maximum temperature departure is 4.5 °C or more from normal, Heat Wave may be described provided actual maximum temperature is 37 °C or more.	Maximum temperature departure is 4.5 °C or more.	Heat wave for coastal stations

various physical processes involved in the development of heat wave conditions. The heat waves during the summer of 1998, 2002, 2003 and 2015 had a profound impact on the lives of the people over various regions of India. A large number of deaths were reported from different parts of the two states during May-June 2003, more particularly from the coastal districts. According to the state government reports, 3054 persons died in the states of Andhra Pradesh

and Telangana in 2003 (Bhadram et al., 2005).The heat wave during May 2015 swept across the states of Andhra Pradesh and Telangana and resulted in a lot of discomfort and the death toll reached an alarmingly high number of 1910 human lives (Press Information Bureau, Govt. of India, 5th August 2014). Meteorological conditions that prevailed over Andhra Pradesh and Telangana during the severe heatwave of May 2015 have been analyzed in this study.

METHOD OF ANALYSIS

Favorable conditions for the occurrence of heat waves:

(a) Synoptic conditions

- (i) A large amplitude high / anti-cyclonic flow that promotes subsidence and stagnation over the heat wave region.
- (ii) High geo-potential thickness values.
- (iii) High positive vertical velocity and
- (iv) Warm-air-advection over the region or hot and dry wind flow over the region from northwest.
- (v) Jet-streams to prevail over northern parts of the country

(b) Dynamic and thermodynamic conditions

- (i) Maximum insolation
- (ii) Scanty clouds or cloudless days
- (iii) Near dry adiabatic lapse rate over the region and
- (iv) Lesser moisture up to a deep layer aloft

DATA USED IN HEAT WAVE ANALYSIS

IMD daily station data for the study period in respect of maximum temperature (T_{max}) recorded across the states of Andhra Pradesh and Telangana have been utilized. Analysis using the temperature metrics (the values of Threshold Maximum Temperatures or intensity of temperature) in respect of mean monthly Maximum Temperature, mean diurnal range, Maximum Temperature equal to or above 40°C ($T-40$) and Maximum Temperature equal to or above 45°C ($T-45$), heat wave & severe heat wave days are identified and analyzed in this section. Several metrics in respect of temperature are computed and analyzed. The departure of day maximum temperature of May 2015 from the pentad normal maximum temperature for the climatological period 1981-2010 is calculated. The composite mean, climatology and anomaly of the geopotential height thickness on daily and monthly time-scales and the targeted period are plotted and analyzed. The National Centers for Environmental Prediction/National Center for Atmospheric Research (NCEP/NCAR) reanalysis data of daily/ monthly average fields in respect of 500 hPa geo-potential height (Z_{500}), winds at surface, 850 hPa & 200 hPa, temperature at 2-m level is used. The NCEP/NCAR reanalysis data is used to draw graphics for visualization and quick analysis and evaluation of the prevailed conditions during the heat wave period (Kalnay et al., 1996). The National Oceanic and Atmospheric Administration (NOAA) Outgoing Long-wave Radiation (OLR) NOAA data is used to study the OLR & OLR anomalies, sensible and latent heat regimes that affected the region.

RESULTS AND DISCUSSIONS

Analysis of synoptic, physical and dynamical conditions have been carried out to find the meteorological conditions favorable for rise of temperature up to the threshold of heat wave/severe heat wave conditions over Telangana and Andhra Pradesh during May 2015. The results of analysis of different parameters have been discussed, in brief, in the following paragraphs.

Surface air temperature: The area of maximum values of mean air temperature is seen in central India and the contiguous areas of Telangana and Coastal Andhra Pradesh. The areal extent of $T-40$ contour (line passing through mean temperatures of 40°C or more) is larger during 15-31 May than during 01-31 May, 2015. It implies that there is an increase in the intensity of air temperature over the areas around Andhra Pradesh and Telangana. The advection of heat from Arabian mainland and Gulf to southeastwards upto Coastal Andhra Pradesh through Afghanistan, Pakistan, Rajasthan, Madhya Pradesh, Vidarbha, Telangana and adjoining area is evident (Figure 2). The intense heat fluxes concentrated over Madhya Pradesh, Chhattisgarh, Odisha, Telangana, and Andhra Pradesh are also shown in Figure 2. The advection of hot dry air does not indicate the area of maximum temperature because the parameter in use here is for mean temperature. The propagation and advection of heat takes place from Arabian area to the interior parts of India. The image clearly indicates that the advection is more pronounced under conducive synoptic conditions during the latter half than during the first half of May 2015. The Figure 3 shows the maximum temperature distribution over the country. The image shows a pronounced change in the areal extent of increased temperatures in the second half of May than in the first half. The figures 2 and 3 indicate a significant change in the intense heat conditions over central and adjoining parts of India. Absolute maximum temperatures alone cannot be construed as heat-waves. The term 'heat-wave' is a relative condition with respect to the normal maximum temperature of an area. The normal maximum temperatures of Andhra Pradesh and Telangana are lower than central parts of the country. This gives an indication that heat-wave conditions did exist in second half of May 2015 over Coastal Andhra Pradesh and Telangana.

Distribution of Prevailing winds

Wind flow pattern at 850 hPa level (Figure 4) shows an anti-cyclonic flow with incursion of northwesterly winds deep to the south upto latitude 5.0°N near Java Islands. At 700 hPa level, the anti-cyclone lies over northeast Arabian Sea with the ridge line extending up to Malaysia

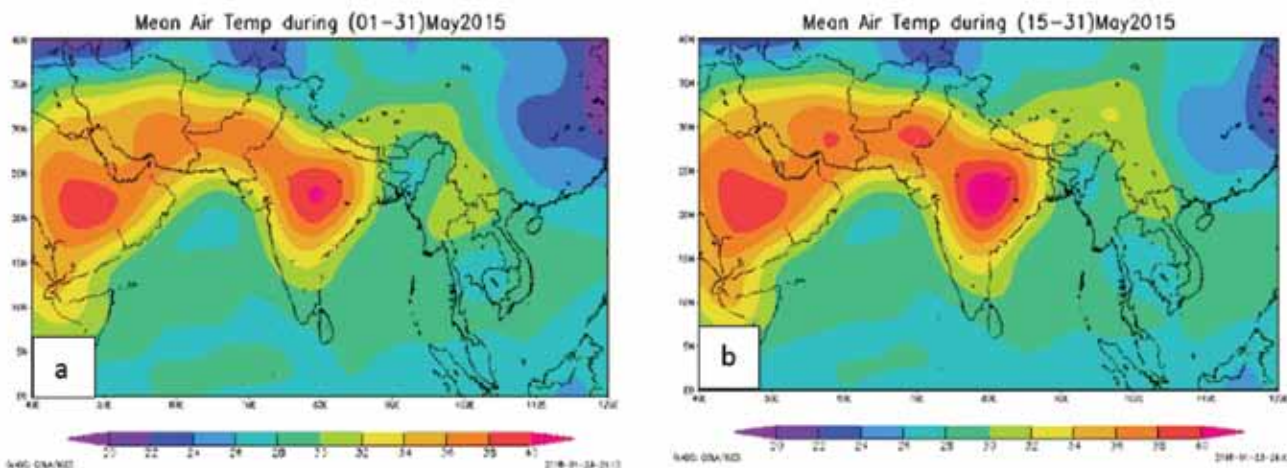


Figure 2. Advection of dry hot air from the Arabian continent and adjoining areas over to parts of the country during (a) May 01-31 and (b) during May 15-31, 2015.

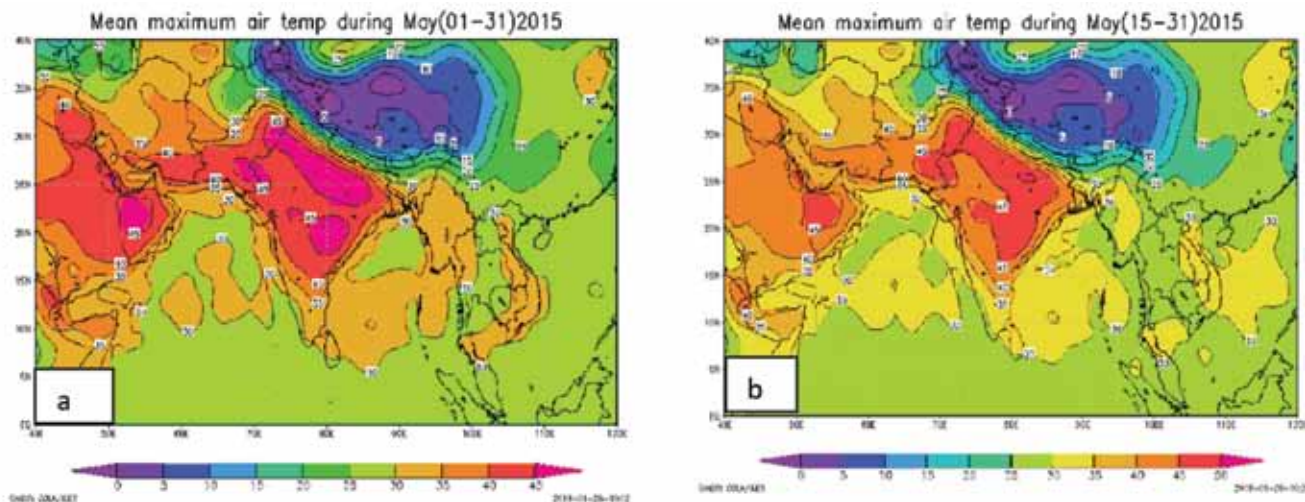


Figure 3. Mean maximum temperature ($^{\circ}\text{C}$) distribution over the country during (a) May 01-31 and (b) May 15-31, 2015.

with southward tilt. There is a pronounced, strong, sustained, stagnant ridge at 500 hPa level running along latitude 20.0°N over the Indian region with an elongated ridge line extended east-southeastwards upto the South China Sea. The composite wind pattern from surface to 500 hPa indicates the position of the ridge line delineating the westerly/ northwesterly flow to the north and north/northeasterly flow to the south during first half of the May. Westerly to northwesterly winds prevailed over the major parts of the country with an anti-cyclonic flow at around 5.0°S in the Sumatra over the surface during the second half of May 2015. The anti-cyclonic flow at 700 hPa and 500 hPa shows reinforcement in the second half of May than in the first half. There is also a strong clock-wise flow of winds over the west central parts of Bay of Bengal and Coastal Andhra Pradesh in the period 15-31 May than during the period 01-31 May.

Position of Sub-Tropical Westerly Jetstream

At 200 hPa level the mean position of Sub-Tropical Westerly Jetstream (STWJ) is located at 25.0°N . The STWJ defines northern limit of the Hadley Cell (Chandler, 1979). This STWJ is the place to the south of which maximum subsidence takes place. This contributes to the formation of stagnant high pressure area and hence to the persistence of higher temperature on the surface. The upper tropospheric winds (Figure 5) show strong convergence upto 100 hPa level indicating lower level strong divergence, in concurrence with the Dines Compensation principle.

Geopotential height thickness

The geopotential height thickness analysis as a prognostic tool provides an inkling of an idea as to the probability of

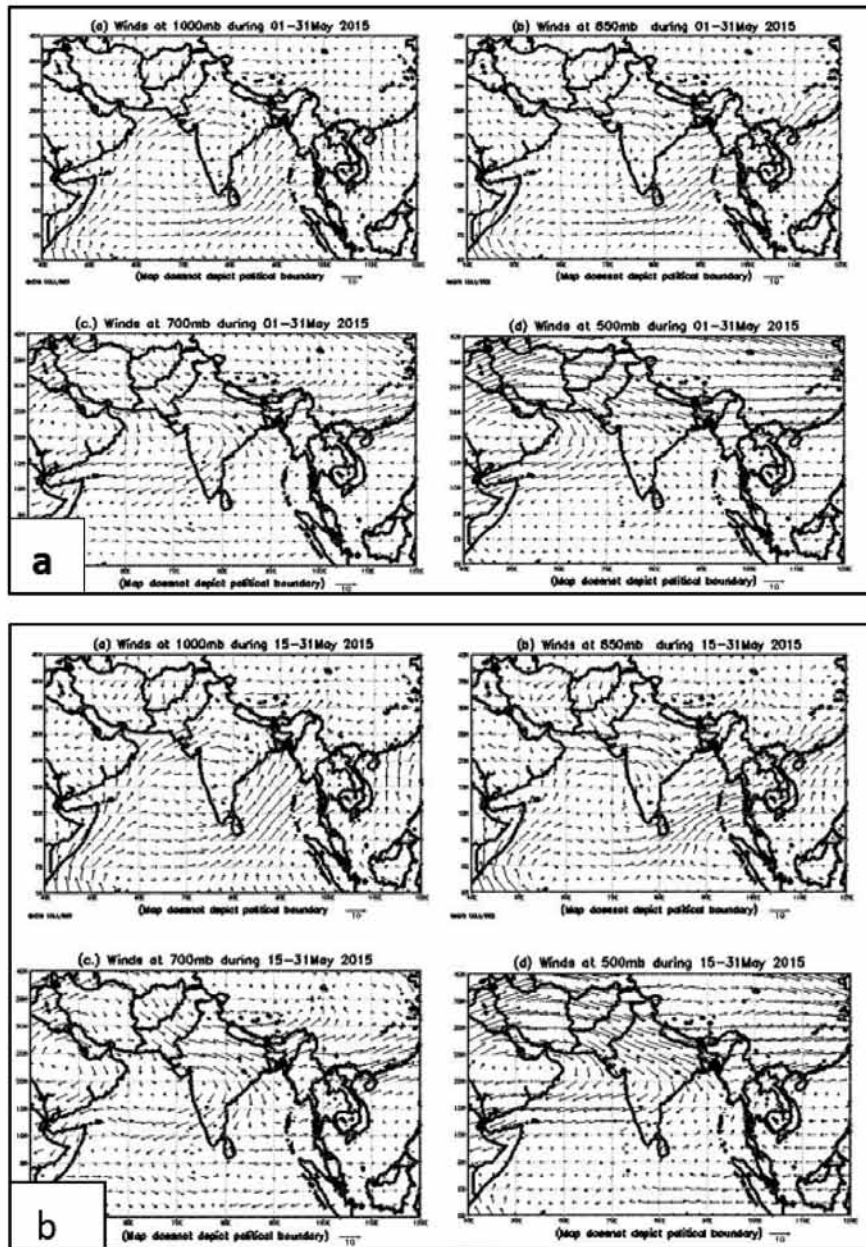


Figure 4. Prevailing winds during (a) May 1-31 May and (b) 15-31 May, 2015 at 1000, 850, 700 and 500 hPa levels.

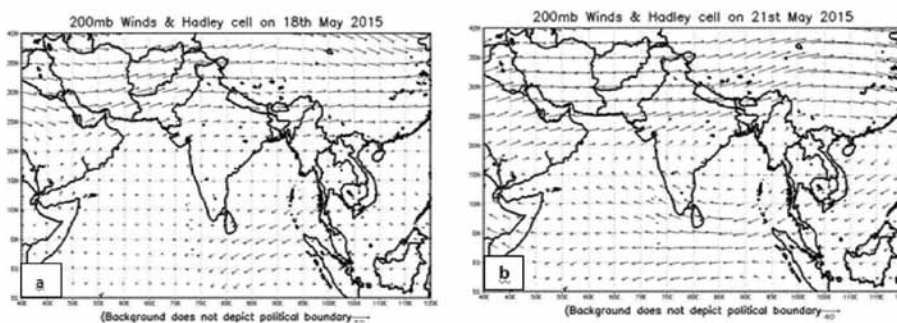


Figure 5. Transition of Upper Tropospheric circulation strengthening in to sub-tropical Westerly Jet stream (a) on May 18 and (b) May 21.

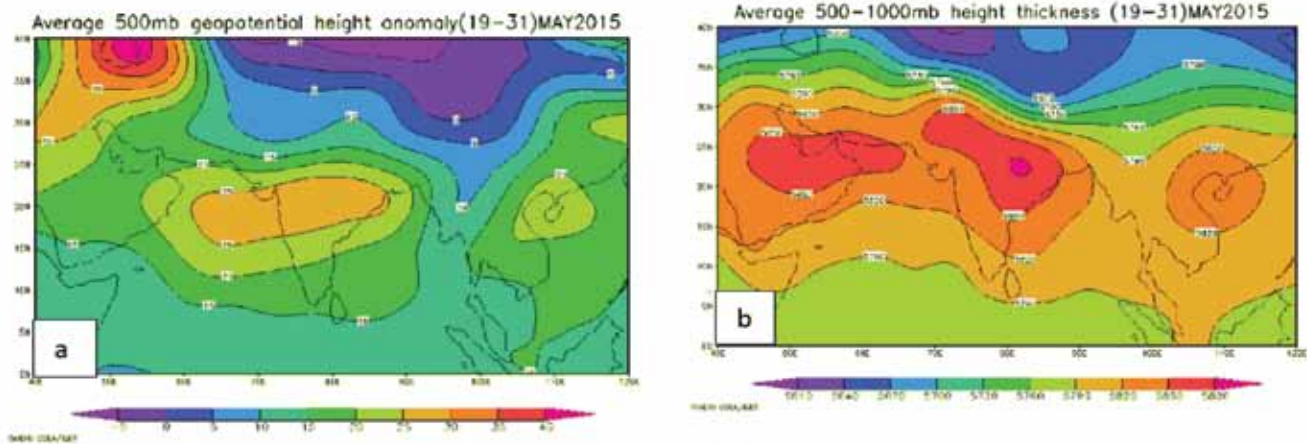


Figure 6. (a) 500 hPa Geopotential anomaly and (b) 500-1000 hPa thickness during 19-31 May, 2015.

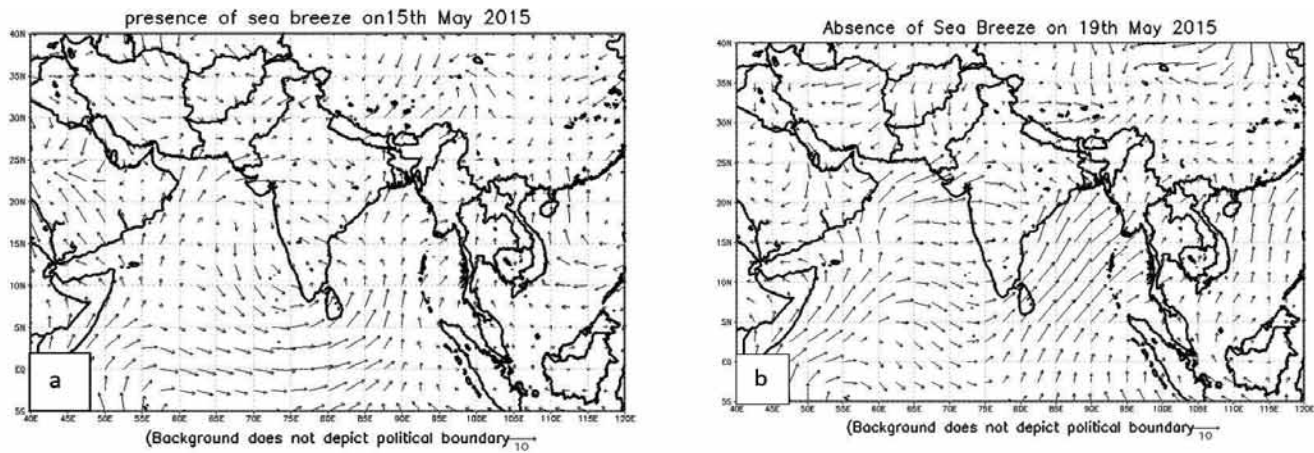


Figure 7. Winds indicating (a) presence of Sea Breeze on May 15 and (b) absence of sea breeze on May 19, 2015.

occurrence of heatwaves. The geopotential height thickness (z) is a function of air temperature and moisture between the levels for which the z is computed. The increase in thickness (z) results in warm air advection (WAA) or diabatic heating. This implies that the solar heating is concentrated in to the area where the maximum z is found. Mcqueen and Cadesman (1957) have shown the correlation of heatwaves with thickness of the air-mass between 1000 and 500 hPa levels. It is obvious that the larger average height thickness and positive anomaly of thickness between the levels 1000 and 500 hPa are indicative of the warmer regions (Figure 6(b)). Hence, it shows the zone of maximum heatwaves or severe heatwaves.

The contour/ isoline of maximum geo-potential (Z_{500}) thickness is observed around the area of Rajasthan, Haryana, Chandigarh & Delhi, Uttar Pradesh, Madhya Pradesh, Chhattisgarh, Odisha, Coastal Andhra Pradesh, Telangana and Vidarbha (Figure 6(a)). This promoted maximum flux over this area and resulted in an intense negative vorticity advection in the mid-troposphere and

warm air advection over the surface area enclosed by the maximum Z_{500} contour. The warm air advection is more conspicuous / evident at 700 hPa. The clockwise flow contributes to the incursion of warm, dry air over the larger contour of Z_{700} .

Late onset of sea-breeze

The coastal areas of Andhra Pradesh, generally, experience during the afternoon sea breezes that alleviate the impact of heat. The prevailing wind and synoptic conditions upto 17 May 2015 were supportive of a breeze from the sea along the coastal areas. The southerly and southeasterly winds prevailed over Bay of Bengal on most of the days from May 1-17, 2015 (Figure 7). The anti-clockwise flow was located over southeast peninsula & Comorin till 15 May, produced south easterly flow and sea breeze over the southeast peninsula south of south coastal Andhra Pradesh. The winds over the Bay of Bengal off Coastal Andhra Pradesh were from southeasterly/south-southwesterly direction

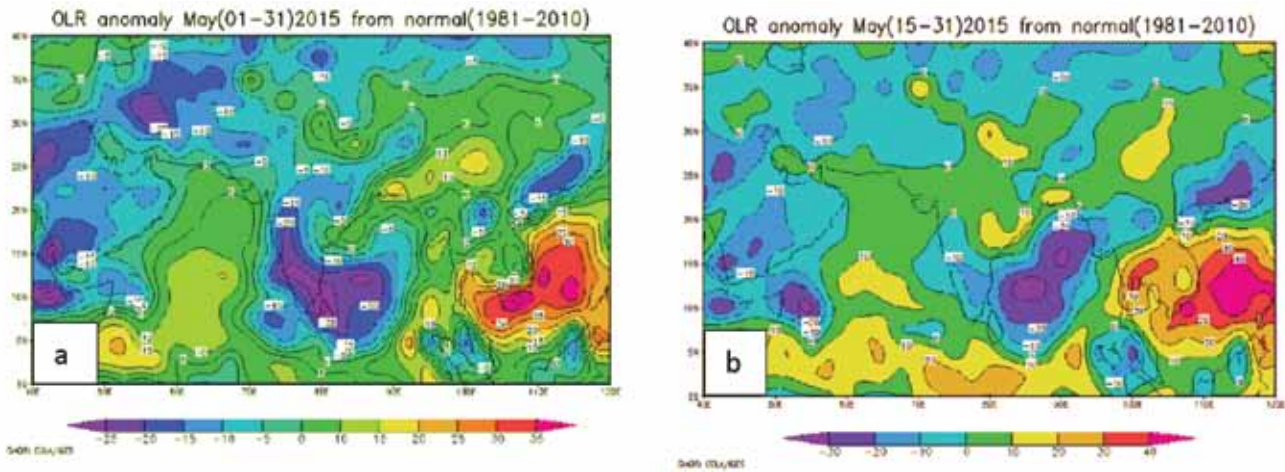


Figure 8. Outgoing Longwave Radiation Anomaly during (a) 1-31 May and (b) 15-31 May 2015.

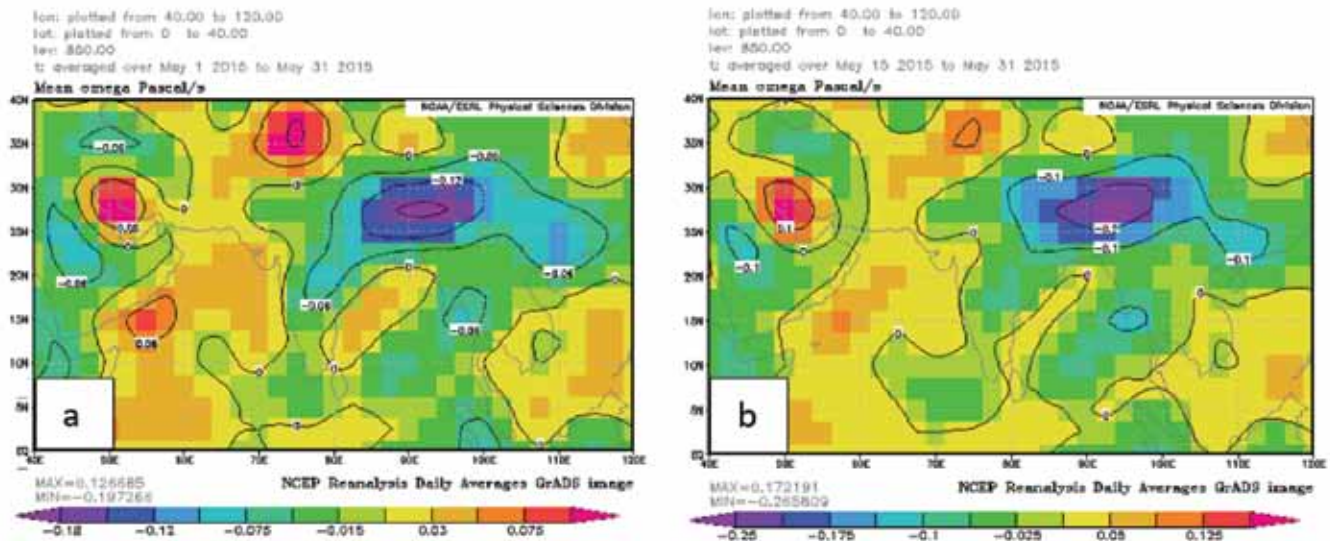


Figure 9. Mean omega indicates the stagnant air and subsidence over the area under study at (a) 850 hPa during May (1-31) and (b) during May (15-31), 2015.

during the middle of May and did become south-westerly from 19th May and exhibit/delay of sea breeze setting. Resulted dry/hot winds from northwest continued to prevail over Andhra Pradesh. Details pertaining to the prevailing winds and the sea breeze on (a) 15th May and (b) on 19th May are shown in Figure 7 (a & b).

Relative humidity (RH) and moisture

Relative humidity over the northwest, central and adjoining peninsular India was very less. The maximum and minimum RH was of the order of 40-50 and 20-30 in general. Such lesser RH contributes to rapid rise in day temperature as the duration of day is quite longer in the month of May; the night could not cool so much. As a

result, the higher temperature cycle was lasting for many days over the study area.

Outgoing long wave radiation and Cloudiness

Outgoing long wave radiation was used as proxy to measure the amount of clouds, particularly over the heat wave region. The Outgoing long wave radiation value during 19-31 May was more than 250 w/m². This indicates that the cloud was practically absent over the region. The OLR anomaly is positive over the region. It allows incoming radiation during day time and outgoing during night time. This has resulted in more insolation heating over the region (Figure 8). Resulted increase in temperatures maintained the temperature up to heat wave level.

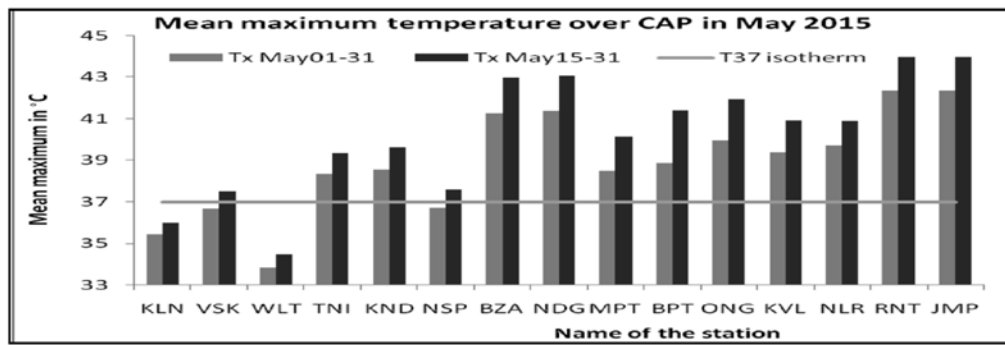


Figure 10(a). Mean maximum temperature over the sub-divisions namely of Coastal Andhra Pradesh during May 1-31 and May 15-31, 2015.

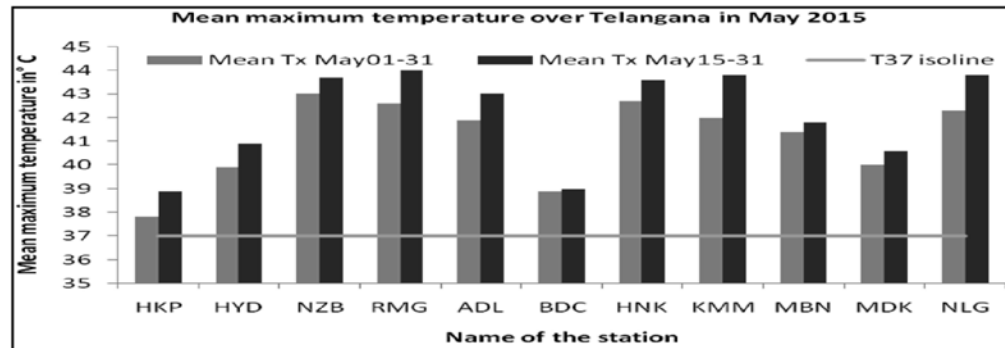


Figure 10(b). Mean maximum temperature over the sub-divisions of Telangana during May 1-31 and May 15-31, 2015.

Observed Temperatures

The metrics derived from the Maximum temperatures and diurnal ranges have been analyzed and the final output is presented. It can be seen that the mean Tx is conspicuously more in May 15-31 period than from May 01-31 (Figure 10, Red spike is higher than blue spike) over coastal Andhra Pradesh, little higher in Telangana and more or less the same/ lesser in Rayalaseema. Most stations in Telangana and Rayalaseema had experienced more than 19 days of T40 days in May. Whereas, only 50% stations in coastal Andhra Pradesh have recorded 10 or more T40 days. Station-wise analysis indicates that Rentachintala & Gannavaram (10 days), Bapatla (8 days), Nandigama (7 days), Machilipattanam (6 days), Ongole (5 days) and Kavali (4 days) in south coastal Andhra Pradesh experienced more cumulative heatwave days as compared to north coastal Andhra Pradesh stations, where only Kakinada (4 days) experienced more number of heat wave days.

It is obvious that there is more number of severe heat waves over coastal Andhra Pradesh, with Gannavaram experiencing 8 severe heatwave days. No station in Rayalaseema experienced heatwave days. In Telangana, Ramagundam & Nalgonda (12 days each), Hanumkonda (10 days), Nizamabad & Khammam (9 each) and Adilabad (6 days) experienced cumulative heatwave days. It is also evident that there is less number of Severe Heatwave days

over Telangana than over the coastal Andhra Pradesh. This explains the severity of heat wave intensity over coastal Andhra Pradesh compared to Telangana. This also explains the distinctively higher mortality rate over coastal Andhra Pradesh than over the state of Telangana. The continental sub-divisions of Telangana and Rayalaseema have larger normal maximum temperatures than over the coastal Andhra Pradesh where most of the stations have maritime climate (Figures 10, 11&12).

During the climatological span of 50 years from 1961 to 2010, Nellore had experienced 18 years of prolonged, persistent heat wave spells of 15 days or more with an exceptionally long spell of 35 days from 6th May to 9th June, 1996 (Pai et al., 2013). Contrary to the record spells that it experienced, Nellore did not record any heatwave days in May 2015. Ramagundam (1984) and Kakinada (1998), the stations from Telangana and coastal Andhra Pradesh experienced once i.e., the former in 1984 and later in 1998 recorded climatological instances of 16 days (>15 days) of heat wave spells. They also observed that no station in Andhra Pradesh or Telangana experienced spells of Severe Heat Wave (SHW) of 7 days or more during the above climatological period. It is quite noticeable that more stations in coastal Andhra Pradesh recorded SHW days than in Telangana during May 2015. In fact, Machilipattnam and Bapatla recorded 5 days each of SHW days. The stations in coastal Andhra Pradesh aggregate

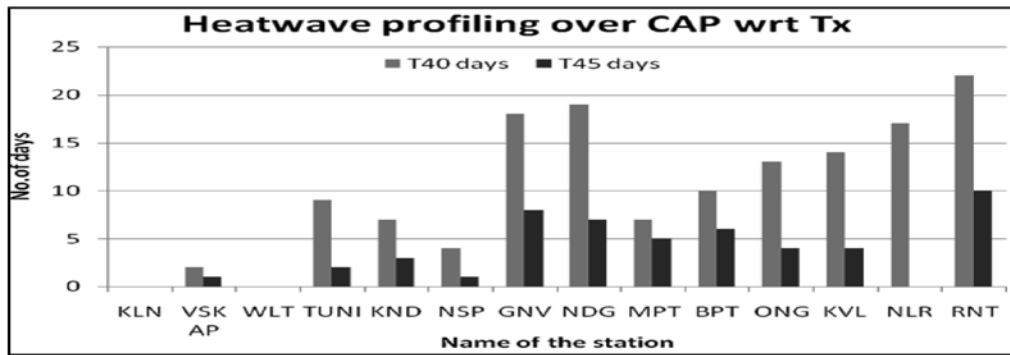


Figure 11(a). Heat wave profiling over the sub-divisions of Coastal Andhra Pradesh during May 2015.

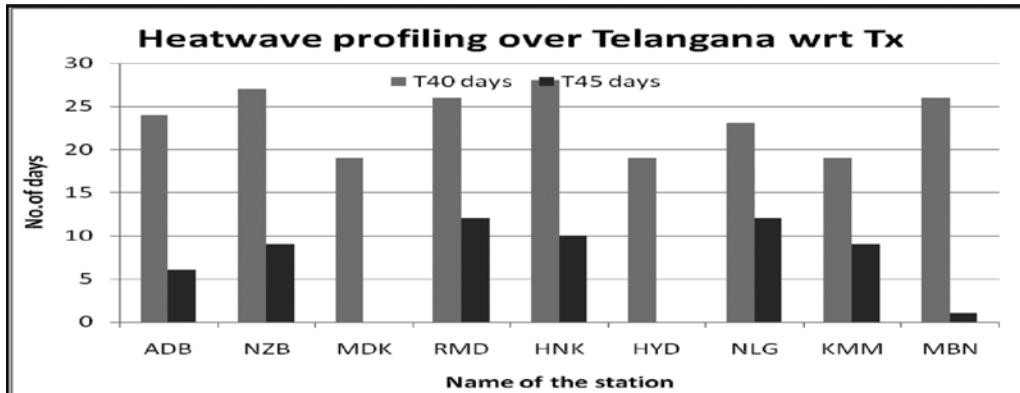


Figure 11(b). Heat wave profiling over the sub-divisions of Telangana during May 2015.

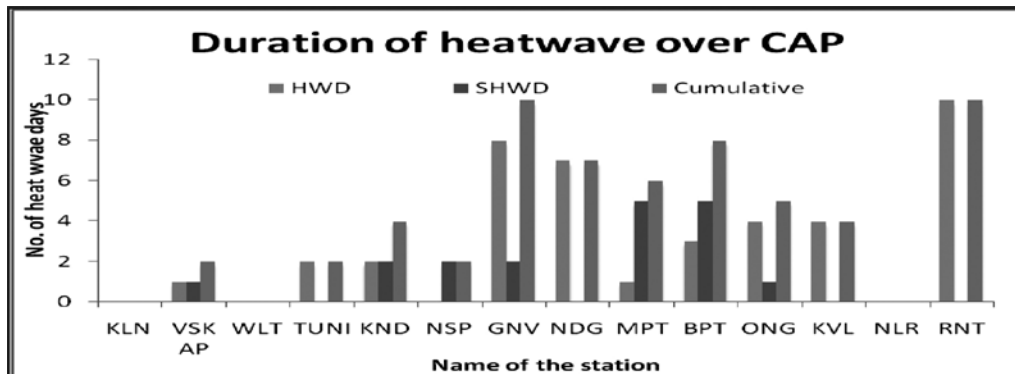


Figure 12(a). Duration of heat-wave over the sub-divisions of Coastal Andhra Pradesh during May 2015.

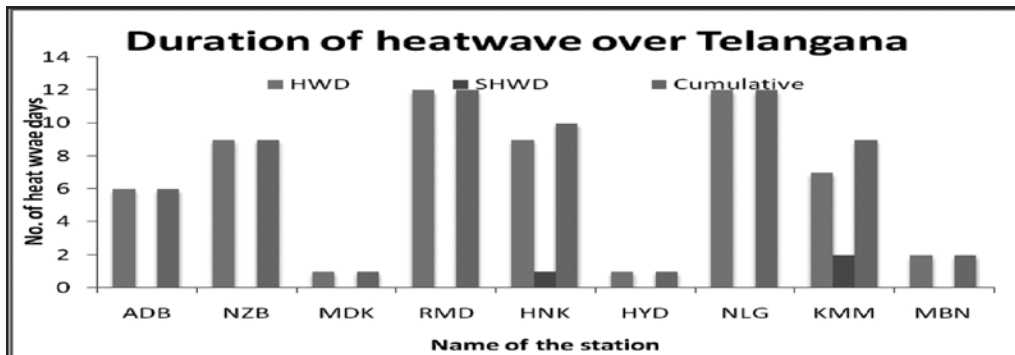


Figure 12(b). Duration of heat-wave over the sub-divisions of Telangana during May 2015.

18 days of SHW days while Telangana stations account for only 3 days of SHW days.

CONCLUSIONS

It is noticed from the study that the heat wave condition developed over Telangana prior to Andhra Pradesh. The period of heat wave over Telangana was 12 days from 19th May onwards; bout of heat wave like conditions was developed from 3rd May 2015 onwards. The heat wave spell continued over coastal Andhra Pradesh for 9 days from 21st to 28th and on 31st after an interruption/hiatus of 2 days. The number of severe heat wave days is more over coastal Andhra Pradesh than over Telangana. Khammam in Telangana recorded the highest maximum temperature of 47.6^o C on 23rd and it is the highest Tx of the season. Visakhapatnam in coastal Andhra Pradesh recorded the highest ever recorded Tx of 45.0^oC on 25th May. There are no heat wave days over Rayalaseema.

On the basis of analysis of synoptic, thermodynamic and dynamic aspects of the heat-waves it is inferred that various parameters like prevailing wind, advection of dry air, absence of sea breeze or late setting of sea breeze, high insolation and cloud-free atmosphere are the causes of such a long spell of heat wave/ severe heat wave over Telangana and Andhra Pradesh during May 2015.

Since heat wave recurrence every summer is expected as a normal feature as suggested by Reddy (Nov, 2017) in his editorial we need to take various precautionary and curative measures, especially by senior citizens and children to lessen the negative impact. Quoting global studies he pointed out that "The 500-hPa height anomalies are most strongly related to positive warm season precipitation anomalies over the Indian monsoon region and associated positive convective heating anomalies that drive mid-latitude teleconnection patterns in response to anomalous tropical convective heating in future climate. Thus, areas already experiencing strong heat waves could experience even more intense heat waves in the future. But other areas could see increases of heat wave intensity that could have more serious ramifications/impacts because these areas are not currently as well adapted to heat waves." So, it is needed to study this phenomenon more closely in the near future.

ACKNOWLEDGEMENTS

The authors express their sincere gratitude to the Director General of Meteorology, IMD for his support and permission to carry out the work. The authors Thank Dr. Onkari Prasad for valuable suggestions to enhance quality of the study. Thanks are also due to Dr.P.R.Reddy, for useful suggestions and final editing.

Compliance with Ethical Standards

The authors declare that they have no conflict of interest and adhere to copyright norms.

REFERENCES

- Bedekar, V.C., Dekate M.V., and Banerjee, A.K., 1974. "Heat and cold waves in India", Forecasting Manual-Part-IV-6, India Meteorological Department.
- Bhadram, C.V.V., Amatya, C.V.V., Pant, G.B., and Krishna Kumar, K., 2005. "Heatwave over Andhra Pradesh: A case study of summer 2003", MAUSAM, v.56, no.2, pp: 385-394.
- Chaudhary, S.K., Gore, J.M., and Sinha Ray, K.C., 2000. "Impact of heat waves over India", Current Science, v.79, no.2, pp: 153-155.
- Fifth Assessment Report AR5 2014. "A Report of the intergovernmental Panel on Climate Change, WMO.
- IMD, 2002 and 2015. "Recommendation regarding the revised criteria for declaring heat wave/ cold wave", DDGM (WF). UOI. No. W-969/1304 to 1365 dated February 2002 and DDGM (WF) Forecasting Circular No. 5/2015 (3.7), India Meteorological Department.
- Jenamani, R.K., 2005. Analysis of Ocean Atmospheric feature associated with extreme temperature variation over east coast of India- A special emphasis to Orissa heat wave of 1998 and 2005, by MAUSAM, v.63, no.3, pp: 401-422.
- Kalnay, E., Kanamitsu, M., Kistler, R., Collins, W., Deaven, D., Gandin, L., Iredell, M., Saha, S., White, G., Woollen, J., Zhu, Y., Chelliah, M., Ebisuzaki, M., Higgins, W., Janowiak, J., Mo, K. C., Ropelewski, C., Wang, J., Leetmaa, A., Reynolds, R., Jenne, R., and Joseph, D., 1996. The NMC/NCAR 40-Year Reanalysis Project". Bull. Amer. Meteor. Soc., v.77, pp: 437-471.
- Pai, D.S., Thapliyal, V., and Kokate P.D., 2004. "Decadal Variation in the heat waves over India during 1971-2000, MAUSAM, v.55, no.2, pp: 281-292.
- Pai, D.S., Smitha Anil Nair, and Ramanathan A.N., 2013. "Longterm climatology and trends of heat waves over India during the recent 50 years 1961-2010", MAUSAM, v.64, no.4, pp: 585-604.
- Ray, K., Chincholikar, J.R., and Manorama M., 2013. "Analysis of extreme high temperature conditions over Gujarat", by MAUSAM, v.64, no.3, pp: 467-474.
- Reddy, P.R., 2017 Editorial, JIGU, v.21, no.5.
- Subbaramayya, I., and Surya Rao, D.A., 1976. "Heat wave and cold wave days in different states of India", Indian J. Meteorol. Hydrol. Geophys, v.27, pp: 436-440.
- WMO, 2012. "WMO Statement on the Status of the Global Climate in 2011", WMO No. 1085, Geneva: World Meteorological Organization.
- Website: www.imd.gov.in.

Received on: 1.12.17; Revised on: 30.1.18; Re revised on: 7.2.18; Accepted on: 10.2.18

FORTRAN code to convert resistivity Vertical Electrical Sounding data to RES2DINV format

R. Rajesh* and R.K.Tiwari

CSIR-NGRI, Hyderabad, India,

* Corresponding Author: rekapalli@gmail.com

ABSTRACT

We present the conversion of multiple vertical electrical resistivity sounding data measured at equal intervals along a profile into '*.DAT' 2D data file, which is compatible with Res2D.INV to obtain 2D resistivity inverse model. For this, we have developed a FORTRAN code. We applied the code on real time resistivity sounding data acquired using Dipole-Dipole array and obtained the 2D data file. Finally, we have inverted the converted 2D data using Res2D.INV program to obtain the 2D resistivity subsurface model. Thus, the code helps to generate the 2D resistivity model of the subsurface from sounding data obtained using four electrode setup (Wenner, Dipole-Dipole, Schlumberger arrays), where the usage of advanced equipment and financial supports are limited, to provide two dimensional interpretation on groundwater resources, soil pollution etc. The conversion and analysis of available past resistivity data helps to study the time-lapse resistivity changes through the comparison of present data within the limits of data errors and resolutions. The weathered water bearing zone and fractures identified on the 2D resistivity inverse model obtained from the converted 1D sounding data from Boneikela village, Sundargarh district, Orissa clearly matches with regional hydrogeology.

Key words: Vertical Electrical Sounding, Res2D.INV, 2D inverse model, FORTRAN code, Groundwater, Time lapse resistivity.

INTRODUCTION

Electrical resistivity tomography is a non-invasive geophysical technique, which researchers have been practicing rigorously for the investigations of groundwater, environmental pollution, and site characterization (Loke et al., 2013), since past five decades. Although the researchers have been employing advanced multi electrode systems to carryout 2D, 3D and 4D resistivity studies, the basic electrode configurations used in the data acquisition are the same conventional arrays commonly used for vertical electrical sounding (VES) and profiling techniques (Griffiths and Barker 1993; Loke and Barker, 1996; Dahlin, 2001; Loke, 2010; Loke et al., 2013). However, the quality of data acquired using such automatic multi electrode systems is adequate because of the stacking procedure employed in the acquisition (Loke et al., 2013). In view of the cost involved in the purchase, maintenance and depth of investigation limitations of high-resolution electrical resistivity data acquisition systems, researchers are still using the conventional four-electrode operation for ground water mapping, bed rock detection, pollution studies etc., where the input of economic resources is limited.

Hence, the main objective of this study is to present a FORTRAN code that converts the sounding data to '*.DAT' file, compatible with Res2D.INV (Loke, 2010) inversion software. Since the 2D resistivity imaging is a robust geophysical tool, the conversion of multiple VES

data acquired along a profile with fixed traverse interval will help the research community, where the availability of the economic resources is limited. Apart from this, the research organizations and academic institutions have acquired sounding /profiling data since late seventies. Archiving such an enormous data has become difficult and time consuming. Therefore, the proper conversion of such large amount of sounding /profiling data into a format in which it can be processed using advanced resistivity tomography software (Res2D.Inv) will help to obtain the resistivity inverse model from the available past data. This also helps to compare the 2D cross section obtained from the data acquired now with the 2D cross sections obtained from the converted data to assess the temporal variations in the subsurface resistivity. This enhances precision of data interpretation as well as facilitates to study the time-lapse resistivity imaging up to decadal scales. We present an example of format conversion of VES data acquired using Dipole-Dipole array to '*.DAT' along with its inverse 2D resistivity model.

Development and application of FORTRAN code

Following the file format information provided by Loke (2010), the following FORTRAN code is developed and presented to convert the multiple sounding data acquired using Wenner, Dipole-Dipole (Inline) and Schlumberger electrode arrays into '*. DAT' file.

Table 1. Sample input data file of Dipole –Dipole.

Location % Name of the Survey File or area%			
Array type	Center location(m)	na (m)	Apparent Resistivity (ohm-m)
Dipole-Dipole	0	10	223.8359 First data point
Dipole-Dipole	0	20	219.2669
Dipole-Dipole	0	30	200.4101
-	-	-	-
-	-	-	-
Dipole-Dipole	240	110	1434.010 Last data point

Code:

```

!*PROGRAM TO COVERT SOUNDING DATA TO 2D
RESISTIVITY DATA FILE *!
!-----!
      IMPLICIT NONE
      REAL::A,X,R,L,LN,N1,N2,LT
CHARACTER :: HEAD
CHARACTER(Len = 20) :: FNI,FNO,LOC
INTEGER :: I,N,SP,SPN, AT
!-----!
WRITE(*,*) 'ENTER INPUT FILE NAME (CASE
SENSITIVE):'
READ(*,*) FNI
WRITE(*,*) 'ENTER OUTPUT FILE NAME:'
READ(*,*) FNO
WRITE(*,*)'For Wenner=1;Dipole-
Dipole=3,Schlumberger=7'
WRITE(*,*)'ENTER ARRAY TYPE:'
READ(*,*) AT
WRITE(*,*) 'ENTER NO OF DATA POINTS:'
READ(*,*) N
WRITE(*,*) 'ENTER MINIMUM SPACING:'
READ(*,*) A
      OPEN (1,FILE=FNI,STATUS='OLD')
      OPEN(2,FILE=FNO,STATUS='NEW')
      READ(1,'(A)') LOC
      WRITE(2,*) LOC
      READ(1,'(A)') HEAD
      WRITE(2,*) A
      WRITE(2,*) AT
      WRITE(2,*) N
      WRITE(2,*) '1'
      WRITE(2,*) '0'
      SP=0
      N2=0
      DO 10 I=1,N
      READ (1,*) LT,LN,X,R
      N1=X/A
      IF (N1.LT.N2) THEN
      SP=SP+1
      ENDIF

```

```

      L=SP*A
      N2=N1
      IF (AT.EQ.1) THEN
      WRITE(2,*) L,A,R
      ENDIF
      IF (AT.GT.1) THEN
      WRITE(2,*) L,A,N2,R
      ENDIF
      10 CONTINUE
      WRITE(2,*) '0'
      WRITE(2,*) '0'
      WRITE(2,*) '0'
      CLOSE(1)
      CLOSE(2)
      END
!-----!

```

Vertical Electrical Sounding data from Boneikela village, Sundargarh district, Orissa acquired using Dipole-Dipole array configuration are saved as a text file in the prescribed format as shown in the Table 1.

The first column of the file is 'Array type', second column is 'x co-ordinate of the array center', third column is the 'dipole separation factor (n)', and the last column is the apparent resistivity value. Table 1 depicts an example of input file format.

When we run the FORTRAN code, it takes the user input parameter like input file name, output file name, array type (1 for Wenner, 3 for Dipole Dipole, 7 for Schlumberger), number of data points, and minimum electrode separation (a). The successful execution of the program converts the VES data into the 2D file in format as shown bellow and writes to the output file with the given output file name. A sample output of the program is given bellow.

Output file format

```

Location | Location or survey file name
10.0000 | Minimum electrode separation 'a'
3        | Type of the electrode array (1 for Wenner, 3
          | for Dipole Dipole, 7 for Schlumberger)
275     | Total number of data points

```

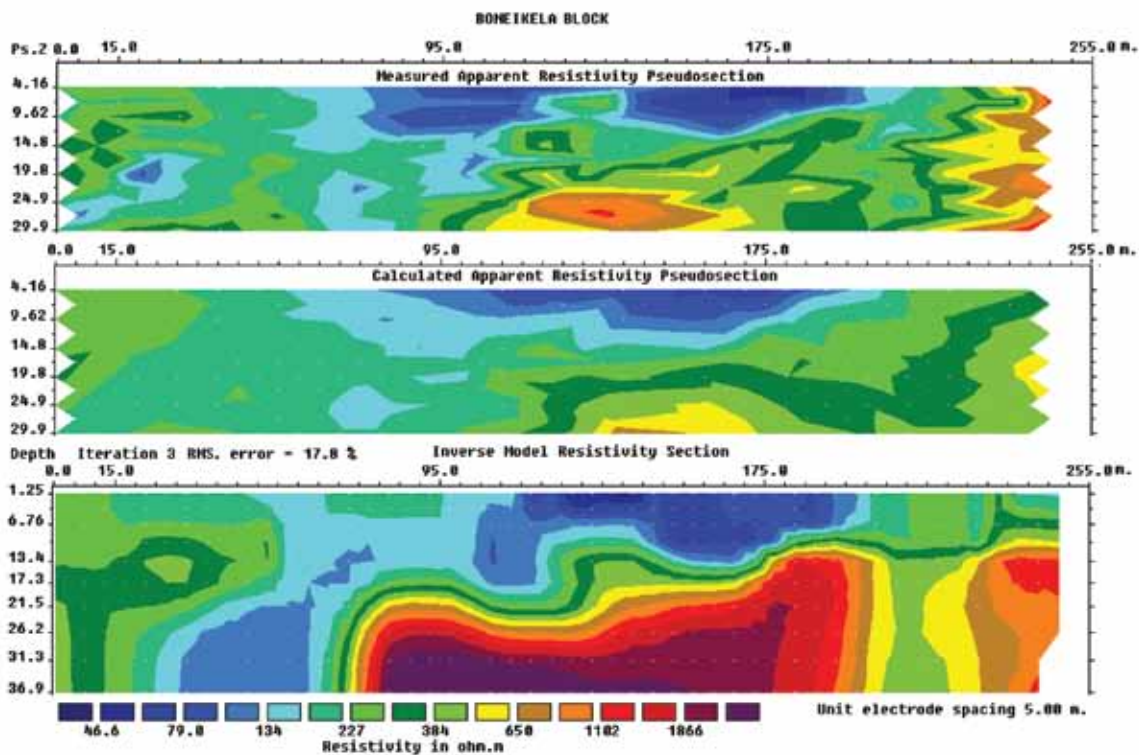


Figure 1. Dipole-Dipole 2D cross section image obtained from the converted data of multiple soundings from the Boneikela village, Sundargarh district, Orissa.

```

1      | 1 Formidpointlocation; 0 for starting electrode
      | location
0      | 0 For apparent resistivity data

0.00000 10.0000 1.00000 223.836 | First data point
      | (x location,
0.00000 10.0000 2.00000 219.267 | minimum
      | electrode
0.00000 10.0000 3.00000 200.410 | n and apparent
      | resistivity)
0.00000 10.0000 4.00000 269.916
0.00000 10.0000 5.00000 334.812
-
-
240.000 10.0000 10.0000 1081.10
240.000 10.0000 11.0000 1434.01 | Last data point
0      | Three zeros
      | indicating enf of
      | file

0
    
```

The output file was processed using Res2D.INV software (trail version) to get the 2D resistivity model of the subsurface. The processed output of least square inversion after 3 iterations is shown in Figure 1. The model refinement ($a=5m$) is used in the processing to reduce the misfit due to huge resistivity variation near the

shallow depth. Although the output has shown 17.8 RMS error, processing the data using Res2D.INV software full version with statistical filtering and more iterations will reduces the error.

The groundwater availability varies from place to place depending upon nature of broad category of hydrological units like consolidated, semi consolidated and unconsolidated formations with high heterogeneity in character, showing both vertical and lateral variations in Sundargarh district, Orissa (CGWB Repot, 2013). Highly weathered mica schist, highly jointed and well foliated carbonaceous phyllites, highly jointed metabasic rocks (Amphibolites), Lime stone, Dolomite, Granite, Granite gneiss, Quartzites are the major water bearing litho units within 4 to 18m depth. The recharge occurs mainly in the secondary porosity resulting from weathering and fracturing of the rocks in the consolidated formations comprising Precambrian metasediments of Gangpur series and Iron ore series and also granite gneiss, metasediments like amphibolite, epidiorite. CGWB report (2013) clearly indicated two to four water bearing fracture zones down to a depth of 100 m bgl. The sand stone, shales, conglomerates, grits belonging to Talcher, Barakar and Kamthis of lower Gondwana are the semi consolidated formations in this region. Among them the Barakar formations are the potential aquifer rocks in the area with water level depth varying between 7 to 18m (CGWB report, 2013).

Laterites and alluvium of Sub-recent to Recent age form the unconsolidated formations in this region. Laterites occurring as capping over older formations are highly porous in nature and form good aquifers to be tapped through dug wells. The limited alluvial deposit strips of recent origin along the prominent drainage channels are also the potential aquifers of unconfined to semi-confined condition. The shallow low resistivity zone between spatial location 100 to 200m and depth range 4 to 14m is the water bearing weathered formation (Bottom panel of Figure 1). We can also notice a high resistive rock formation beyond 14m with a fracture around spatial location at 45m.

CONCLUSION

We present a FORTRAN code to convert multiple vertical electrical sounding data recorded along a profile into '*.DAT' file. The conversion allows us to process the data in Res2D.INV to generate inverse resistivity model of the subsurface. The code developed here helps the research community to generate the 2D resistivity model cross section images for the 2D interpretation of ground water, environmental pollution, bedrock studies etc., from sounding (Deep resistivity sounding) data, where the operational cost and advanced instrumentation facilities are limited. The conversion of the past sounding data that is available from late seventies will allow estimating the temporal variability (even up to decadal scales) by comparing with the present data. We have clearly identified the weathered aquifer zone within 4m to 13m depth in the 2D section of selected example data from Boneikela village, Sundargarh district, Orissa. The deep fracture in the high

resistive rock formation is also clearly visible in the 2D section. The aquifer identified in the 2D section obtained from the multiple 1D soundings using the code is agreeing well with regional geology of the study area.

ACKNOWLEDGEMENTS

The authors thank Director, CSIR-NGRI for his permission to publish this work. The authors thank Dr.P.R.Reddy for reviewing and final editing of the manuscript. First author thank CSIR for RA fellowship and second author thank DAE for Rajaramanna Fellowship.

REFERENCES

- Dahlin, T., 2001. The development of DC resistivity imaging techniques. *Computers & Geosciences*, v.27, no.9, pp: 1019-1029.
- Griffiths, D.H., and Barker, R.D., 1993. Two-dimensional resistivity imaging and modelling in areas of complex geology. *Journal of Applied Geophysics*, v.29, no.3, pp: 211-226.
- Loke, M.H., and Barker, R.D., 1996. Rapid least-squares inversion of apparent resistivity pseudosections by a quasi-Newton method. *Geophysical prospecting*, v.44, no.1, pp: 131-152.
- Loke, M.H., 2010. Res2DInv ver. 3.59.102 Geoelectrical imaging 2D and 3D. Instruction manual. Geotomo Software. www.geoelectrical.com.
- Loke, M.H., Chambers, J.E., Rucker, D.F., Kuras, O., and Wilkinson, P.B., 2013. Recent developments in the direct-current geoelectrical imaging method. *Journal of Applied Geophysics*, v.95, pp: 135-156.
- CGWB Report, 2013, Central Ground Water Board, South Eastern Region, Bhubaneswar.

Received on: 15.2.18; Revised on: 27.2.18; Accepted on: 1.3.18

Endeavours in seismic monitoring of oceans through drifting network with development of a New Generation Mobile Earthquake Recorder in Marine Areas by Independent Divers---The Son-O-MERMAID

Raja Acharya

Indian Meteorological Department, Regional Meteorological Centre, Kolkata (Ministry of Earth science)
raja.acharya2011@gmail.com

INTRODUCTION

Our understanding of the internal dynamics of the Earth is to a significant extent based on images of seismic velocity variations in the earth's mantle obtained through global seismic tomography (Sukhovich et al., 2015). While the land is covered by a dense network of seismic stations, the coverage in the Oceans is inadequate mainly due to the high cost of installation and recovery of the conventionally used sensors such as Ocean Bottom Seismometers (OBS) and moored hydrophones. This unequal seismic data coverage fundamentally limits the quality of tomographic representations of seismic wave speeds in the earth's interior (FJ Simons et al., EOS v.87, no.31 1st Aug 2006). To overcome this problem some important measures have been taken in the recent past. Some specifics are given below to highlight the efficacy of such techniques and recording instruments.

NEW INITIATIVES

A) Requirement of floating seismic stations or MERMAID (Mobile Earthquake Recorder in Marine Areas by Independent Divers)

A remedial solution includes apt observation of seismic waves in the oceans to obtain adequate data coverage in oceans using a prototype of a mobile receiver that will function as a floating seismometer (developed by Prof Dr. Guust Nolet of Geoazur in France). This prototype was nicknamed "MERMAID", which stands for Mobile Earthquake Recorder in Marine Areas by Independent Divers. The Mermaid is an autonomous freely drifting underwater robot, which by changing its buoyancy can dive up to and remain at a programmed depth. A seismic wave (i.e. P wave) arriving at the ocean bottom refracts into the water and generates acoustic wave, which propagates vertically. Whenever an acoustic wave generated by teleseismic P wave is detected by the MERMAID, it moves up to the ocean surface as quick as possible to transmit via satellite the recorded signal and information

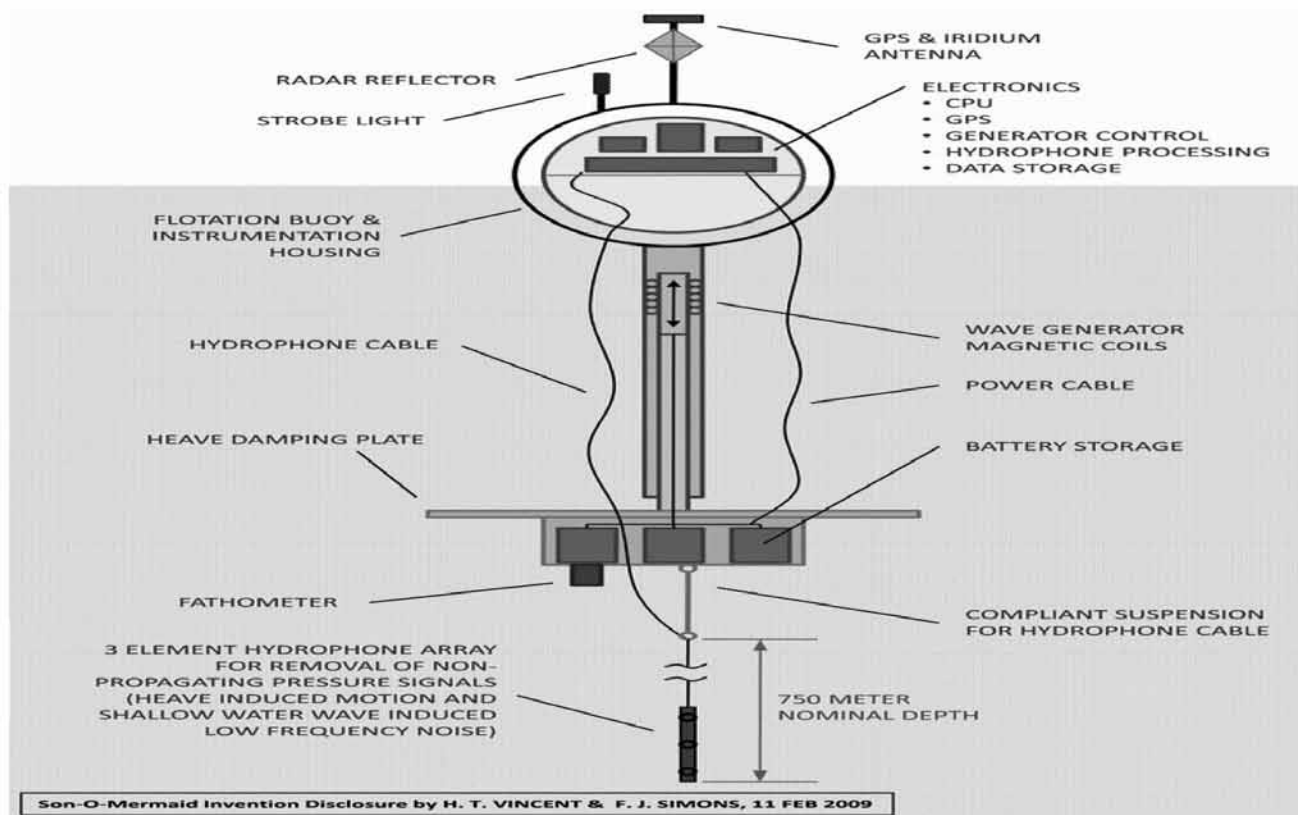
such as time of arrival of the signal, depth of the robot at the moment of detection etc. The principal advantage of the MERMAID over Ocean Bottom Seismometer and Moored Hydrophones is its lower operational costs. The Mermaid was first tested on 4-6 Nov 2003.

B) Development of Son-O-Mermaid--the New Generation Mobile Earthquake Recorder in Marine Areas by Independent Divers

The Son-O-MERMAID instrument is a next generation drifting prototype, jointly developed at the University of Rhode Island (URI) by Prof. Harold Vincent and at Princeton University by Prof. Frederik Simons. It combines a surface buoy with instruments dangling from an untethered cable. Son-O-Mermaid was initially deployed at off the coast of Bahamas on October 9th, 2012.

B-1) System Description and working of Son-O-Mermaid

Son-O-Mermaid operates at a water depth of about 1500 meters, while a drifting buoy stays at the surface and allows the continuous contact with a satellite. The surface unit enables the GPS and IRIDIUM capabilities to be always engaged. Son-O-MERMAID can be divided in to three subcomponents: **First**, a surface component that receives and stores the acoustic data sent from the submerged unit for further analysis. This unit is accurately time synchronized with a GPS receiver and used to time stamp the acoustic data. **Second**, a submerged component immersed at a depth of ~750 meters. It collects, digitizes and samples acoustic data. The submerged component includes the following parts: (I) a three-hydrophone array, spaced about 70 cm apart at the end of a 750 m long cable attached to a surface buoy that houses electronics, communications, and a GPS location package(ii)an analog to digital converter (ADC), (iii) a central processing unit (CPU) and one RS-485 adapter. All these parts with the exception of the hydrophones are placed inside a pressure vessel. **Third** is the interface that connects the submerged and surface components.



Son-O-Mermaid: Picture Courtesy: Princeton University
 (<http://geoweb.princeton.edu/people/simons/MERMAID.html>).

B-2) Technical Advancement of Son-O-Mermaid over its predecessors and advantages over OBS (Ocean Bottom Seismometers)

Son-O-Mermaid is a freely drifting buoy that (a) derives energy from wave action, enough to power (b) a vertical array of hydrophones suspended from a compliant cable connected to a damping plate below the waves, (c) a full-ocean-depth echo sounder, (d) GPS for location and timing accuracy, (e) an IRIDIUM satellite communication unit for near real-time data transfer, and an (f) on-board digitizing and processing unit. The predecessor instrument, MERMAID, does not have facilities mentioned under (a), (c) and array aspect of (b). The Son-O-Mermaid can be deployed even by untrained personnel. This gives it an extra advantage over conventional approaches e.g., ocean-bottom seismometers, tethered, moored hydrophones. Unlike traditional ocean-bottom seismometers, which are placed in stationary locations and must be retrieved to obtain their data, Son-O-Mermaid drifts with ocean currents and regularly reports data back to scientists using wireless technology. Several of these recorders can be deployed for the same cost as one ocean-bottom seismometer.

Compared to its progenitor MERMAID, the new float (Son-O-Mermaid) has better real-time communication capabilities because part of the instrument is always above water, and, in addition to batteries, has solar panels that power a vertical array of hydrophones. Energy harvesting technology will give Son-O-Mermaid great operational independence and the possibility to take payload for ocean-based observations not limited to hydroacoustics for seismic tomography. The hydrophone array configuration eliminates non-propagating noise and suppresses surface multiples. The fathometer helps in determining the travel time of teleseismic waves with maximum accuracy. It will also deliver data for the high-resolution study of Earth's global bathymetry. As Son-O-Mermaid is a drifting instrument it helps to generate data on sea surface currents. (https://www.nsf.gov/awardsearch/showAward?AWD_ID=1318416).

B-3) LIMITATIONS

Son-O-Mermaid does have drawbacks. Since the buoy is at the surface, in the waves, it can get run over by ships — or be hit by a hurricane.

FUTURE STRATEGIES

- a. Keeping in view the tremendous capability of the Son-O-Mermaid to detect teleseismic waves in the ocean, and transmit the information to land centres in near realtime, there is a need for deployment of a large array of Son-O-Mermaids mainly in the southern Oceans (For ex Indian Ocean), which are not adequately covered by seismic sensors. Such a deployment helps to provide a denser tomographic data; a useful input for better imaging of deeper structures.
- b. There should be networking between various sensors (Son-O-Mermaids, Ocean Bottom Seismometers, Tsunami Bouys, Moored hydrophones), as exchange of data ultimately results in better scanning of structures present at shallower to deeper depths.
- c. Moreover, in the near future the Son-O-Mermaid will be fitted with multiple instruments like meteorological and oceanographic becoming multipurpose and multidisciplinary platforms for all types of scientific research in the oceans. (Simon J.D et al AGU 2014, Nolet G et al; AGU Dec 2014, Dec 2017 issue of IASPEI News letter) ultimately paving the future vision for a large array of drifting Geophysical observatories (Multidisciplinary Mermaids)in the ocean.(Hello Y et al; AGU Dec 2013), (Nolet G et al; AGU Dec 2014)

CONCLUSION

The Son-O-Mermaid will help to revolutionize seismic data collection in the oceans, by better detection of signals and near real time transmission of collected data. The Son-O-Mermaid will help to revolutionize seismic data collection in the oceans, by better detection of signals and near real time transmission of collected data. (Simon J.D et al AGU 2014), (Frederik J. Simons et al; Journal of Geophysical Research 23rd May 2009).

ACKNOWLEDGEMENTS

This technical Note has been compiled using internet information and other sources, basically to propagate the importance of Son-O-Mermaid the new generation drifting seismic tool. I unequivocally state that the technical details given above have not been developed by me either directly or indirectly. I thank Dr.P.R.Reddy for apt editing and recommending its publication as a Technical Note. The views expressed in the article are solely the views of myself and not of my organisation.

BIBLIOGRAPHY AND REFERENCES

- Simon J.D. et al., AGU 2014. Data and Analysis Methods of the Son-O-Mermaid and MERMAID Experiments.
- Donaldo Guevara, 2014. Delete and insert Data Collection and Telemetry System Design For Marine Instrumentation: The Son-O-Mermaid.
- Award Abstract #1318416 Phased Testing at Sea of the Son-O-Mermaid Prototype (Reference: https://www.nsf.gov/awardsearch/showAward?AWD_ID=1318416).
- Picture Courtesy: Princeton University (<http://geoweb.princeton.edu/people/simons/MERMAID.html>)
- Frederik J. Simons et al., the potential of recording earthquakes for global seismic tomography by low-cost autonomous instruments in the oceans; Journal of Geophysical Research 23rd May 2009.
- F.J., Simon et al., 2006. EOS, v.87, no.31. A future for drifting seismic networks.
- Sukhovich et al., 2015. Nature:Seismic Monitoring in the Oceans by Autonomous floats. DOI:10.1038/ncomms9027, pp:1-6.
- Hello, et al., AGU Dec 2013. MULTIMERMAID: A dedicated multichannel seismic/weather/zoological float for monitoring of the oceans.
- Nolet et al., AGU Dec 2014. Mariscope: Observing P Waves (and much more) everywhere in the Oceans.
- Dec 2017. Issue of International Association of Seismology and Physics of the Earth's Interior (IASPEI) News letter; article Seismology in Oceans by Guust Nolet Geoazur France.

GUIDE LINES TO AUTHORS

The Journal of Indian Geophysical Union (J-IGU), published bimonthly by the Indian Geophysical Union (IGU), is an interdisciplinary journal from India that publishes high-quality research in earth sciences with special emphasis on the topics pertaining to the Indian subcontinent and the surrounding Indian Ocean region. The journal covers several disciplines of earth sciences such as the Geosphere, its watery and gaseous envelopes (the Hydrosphere, the Cryosphere and the Atmosphere), and life (the Biosphere). It also publishes articles on Space and Planetary sciences. J-IGU welcomes contributions under the following categories:

- Research papers reporting development of new theoretical methods, new techniques of data processing, development of area specific models, new experimental findings and results.
- Review articles providing comprehensive overview of a significant research field related to earth system sciences

In addition, J-IGU also welcomes short communications on opinion and report on scientific activity, personal information, book reviews, news and views, etc.

The manuscript should be submitted electronically as a single word format (.doc file) including the main text, figures, tables, and any other supplementary information along with the signed "Declaration Letter". The manuscript should be submitted by email (jigu1963@gmail.com) to the Editor.

After acceptance of the manuscript the corresponding author would be required to submit all source files (text and Tables in word format) and figures in high resolution standard (*.jpg, *.tiff, *.bmp) format. These files may be submitted to the Editor as a single *.zip file along with the "Copyright Transfer Statement".

IMPORTANT INFORMATION

Ethics in publishing

J-IGU is committed to ensuring ethics in publication and takes a serious view of plagiarism including self-plagiarism in manuscripts submitted to the journal. Authors are advised to ensure ethical values by submitting only their original work and due acknowledgement to the work of others in case used the manuscript. Authors must also refrain from submitting the same manuscript to more than one journal concurrently or publish the same piece of research work in more than one journal which is unethical and unacceptable. Editor of J-IGU is committed to make every reasonable effort to investigate any allegations of plagiarism brought to his attention, as well as instances that come up during the peer review process and has full authority to retract any plagiarized publication from the journal and take appropriate action against such authors if it is proven that such a misconduct was intentional.

Similarly, Editor and Reviewers are also expected to follow ethical norms of publishing by ensuring that they don't use any unpublished information, communicated to them for editorial or review purpose, in their own research without the explicit written consent of the author. They are also expected to keep manuscript/ data/ observations/ any other information related to the peer review confidential to protect the interest of the authors. Reviewers should refrain from reviewing the manuscripts in which they have conflicts of interest resulting from competitive, collaborative, or other relationships or connections with any of the authors, companies, or institutions connected to the manuscript.

Conflict of interest

All authors are requested to disclose any actual or potential conflict of interest including any financial, personal or other relationships with other people or organizations within three years of beginning the submitted work that could inappropriately influence, or be perceived to influence, their work.

Submission declaration

Submission of a manuscript implies that the work has not been published previously and it is not under consideration for publication elsewhere, and that if accepted it will not be published elsewhere in the same or any other form, in English or in any other language, without the written consent of the publisher. It also implies that the authors have taken necessary approval from the competent authority of the institute/organization where the work was carried out.

Copyright

After acceptance of the manuscript the corresponding author would be required to sign and submit the "Copyright Transfer Statement".

MANUSCRIPT PREPARATION

The corresponding author should be identified (include E-mail address, Phone/Mobile number). Full affiliation and postal address must be given for all co-authors.

Abstract:

An abstract of not more than 300 words must be included.

Text:

The manuscript should be structured to include a front page containing the title, Author(s) name, affiliation and address of the institute where the work was carried out, a short title, and 5-to-6 index terms/Key words. Author(s) present address, if different from the above mentioned

address, may be given in the footnote. The corresponding author should be identified with an asterisk and his/her email ID should be provided. This page should be followed by the main text consisting of Abstract, Introduction, Methods/ Techniques/ Area description, Results, Discussion, Conclusions, Acknowledgements, and References. Tables and Figures with captions should be inserted in the main text of the manuscript at appropriate places.

Figures/ Illustrations:

All figures should be provided in camera-ready form, suitable for reproduction (which may include reduction) without retouching. Figures in high-resolution (at least 300 dpi) standard formats (*.jpg, *.tiff, *.bmp) are acceptable. Figures should be numbered according to their sequence in the text. References should be made in the text to each figure. Each figure should have a suitable caption.

Tables:

Authors should take note of the limitations set by the size and layout of the journal. Table should not exceed the printed area of the page. They should be typed on separate sheets and details about the tables should be given in the text. Heading should be brief. Large tables should be avoided and may be provided as supplementary information, if required.

Equations:

Equations should be numbered sequentially with Arabic numerals and cited in the text. Subscripts and Superscripts should be set off clearly. Equation writing software that presents each equation as an object in MS Word will be accepted. Style and convention adopted for the equations should be uniform throughout the paper.

References:

All references to publications cited in the main text should be presented as a list of references following the text and all references in the list must be cited in the text. References should be arranged chronologically, in the text. The list of references should be arranged alphabetically at the end of the paper.

References should be given in the following form:

Kaila, K.L., Reddy P.R., Mall D.M., Venkateswarlu, N., Krishna V.G. and Prasad, A.S.S.R.S., 1992. Crustal structure of the west Bengal Basin from deep seismic sounding investigations, Geophys. J. Int., v.111,no., pp:45-66.

REVIEW PROCESS:

All manuscripts submitted to the journal are peer-reviewed. It is advisable to send the contact details of **4 potential reviewers** along with the manuscript to expedite the review process. Editor has the option to select reviewers from the list or choose different reviewers. The review process usually takes about 3 months. All enquiries regarding the manuscript may be addressed to the Editor. It is helpful to have the list of several potential reviewers covering various research topics/themes/ sub themes, to avoid delay in choosing the right persons. Authors and learned experts may help in developing a reference manual, which could be updated from time to time.

GALLEY PROOF:

Technical editing of manuscripts is performed by the editorial board. The author is asked to check the galley proof for typographical errors and to answer queries from the editor. Authors are requested to return the corrected proof **within two days** of its receipt to ensure uninterrupted processing. The editor will not accept new material in proof unless permission from the editorial board has been obtained for the addition of a "note added in proof". Authors are liable for the cost of excessive alterations to galley proof.

PUBLICATION CHARGES:

There are no page charges for publication and printing charges for b/w figures, provided length of **printed manuscript is not more than 10 pages. For every additional page Rs.3000/ is charged**, basically to meet publication costs. Also, in view of substantial cost involved in printing of color figures, author will be charged for printing of pages containing color figures @ Rs.2,500/- per page. The charges may be revised at any time based on cost of printing and production. Author will receive an estimate/ invoice of the additional page charges, color figures reproduction cost along with the galley proof. It is the responsibility of the author to remit the additional page charges and/ or color figures reproduction cost **within one month** of the receipt of the estimate/invoice.

The corresponding author will receive a soft copy (pdf format) of his/her published article. Should the author desire to purchase reprints of his/her publication, he/she must send the duly signed Reprint Order Form (accompanies the galley proof and contains price details) along with the corrected galley proof to the Editor. The reprint charges must be paid **within one month** of sending the Reprint Order Form.

Any payment related to additional page charges, printing of color figures and/ or purchase of reprints should be made in the form of a Demand Draft in the name of **Treasurer, Indian Geophysical Union**, payable at **Hyderabad**.

You may download the pdf file from: <http://www.j-igu.in/IGU-Guide-forAuthors.pdf>